Rico Melgoza, J. Jesús. (1997) *Steady state modelling of non-linear power plant components.* PhD thesis.

http://theses.gla.ac.uk/5319/

Copyright and moral rights for this thesis are retained by the author

A copy can be downloaded for personal non-commercial research or study, without prior permission or charge

This thesis cannot be reproduced or quoted extensively from without first obtaining permission in writing from the Author

The content must not be changed in any way or sold commercially in any format or medium without the formal permission of the Author

When referring to this work, full bibliographic details including the author, title, awarding institution and date of the thesis must be given

Glasgow Theses Service
http://theses.gla.ac.uk/
theses@gla.ac.uk

Steady State Modelling of Non-linear Power Plant Components

By
J. Jesús Rico Melgoza

A Thesis
Submitted to
the Department of Electronics and Electrical Engineering of
the University of Glasgow
for the Degree of Doctor of Philosophy

December, 1996

The University of Glasgow

©, J. Jesús Rico Melgoza, 1997

To Rachel,
my mother and
all my silent partners from pop-mobility

Abstract

This thesis studies the problem of periodic, waveform distortion in electric power systems. A general framework is formulated in the Hilbert domain to account for any given orthogonal basis such as complex Fourier, real Fourier, Hartley and Walsh. Particular applications of this generalised framework result in unified frames of reference. These domains are unified frameworks in the sense that they accommodate all the nodes, phases and the full spectrum of coefficients of the orthogonal basis. Linear and linearised, non-linear elements can be combined in the same frame of reference for a unified solution.

In rigorous waveform distortion analysis, accurate representation of non-linear characteristics for all power plant components is essential. In this thesis several analytical forms are studied which provide accurate representations of non-linearities and which are suitable for efficient, repetitive waveform distortion studies.

Several harmonic domain approaches are also presented. To date most frequency domain techniques in power systems have used the Complex Fourier expansion but more efficient solutions can be obtained when using formulations which do not require complex algebra. With this in mind, two real harmonic domain frames of references are presented: the real Fourier harmonic domain and the Hartley domain. The solutions exhibit quadratic rate of convergence. Also, discrete convolutions are proposed as a means for free-aliasing harmonic domain evaluations; a fact which aids convergence greatly.

Two new models in the harmonic domain are presented: the Three Phase Thyristor Controlled Reactor model and the Multi-limb Three Phase Transformer model. The former uses switching functions and discrete convolutions. It yields efficient solutions with strong characteristics of convergence. The latter is based on the principle of duality and takes account of the non-linear electromagnetic effects involving iron core, transformer tank and return air paths. The algorithm exhibits quadratic convergence. Real data is used to validate both models.

Harmonic distortion can be evaluated by using true Newton-Raphson techniques which exhibit quadratic convergence. However, these methods can be made to produce faster solutions by using relaxation techniques. Several alternative relaxation techniques are presented. An algorithm which uses diagonal relaxation has shown good characteristics of convergence plus the possibility of parallelisation.

The Walsh series are a set of orthogonal functions with rectangular waveforms. They are used in this thesis to study switching circuits which are quite common in modern power systems. They have switching functions which resemble Walsh functions substantially. Accordingly, switching functions may be represented exactly by a finite number of Walsh functions, whilst a large number of Fourier coefficients may be required to achieve the

same result. Evaluation of waveform distortion of power networks is a non-linear problem which is solved by linearisation about an operation point. In this thesis the Walsh domain is used to study this phenomenon. It has deep theoretical strengths which helps greatly in understanding waveform distortion and which allows its qualitative assessment.

Traditionally, the problem of finding waveform distortion levels in power networks has been solved by the use of repetitive linearisation of the problem about an operation point. In this thesis a step towards a true non-linear solution is made. A new approach, which uses bi-linearisations as opposed to linearisations, is presented. Bi-linear systems are a class of simple, non-linear systems which are amenable to analytical solutions. Also, a new method, based on Taylor series expansions, is used to approximate generic, non-linear systems using a bi-linear system. It is shown that when using repetitive bi-linearisations, as opposed to linearisations, solutions show super-quadratic rate of convergence.

Finally, several power system applications using the Walsh approach are presented. A model of a single phase TCR, a model of three phase bank of transformers and a model of frequency dependent transmission lines are developed.

Acknowledgments

The completation of this modest work would not be possible without a combinations of efforts. Now I sincerely whish to acknowledge the help, support and advice received from many people during this process.

Firstly, I want to extend my most honest thanks and gratitude to my supervisor, Dr. Enrique Acha, for his wise supervision, encouragement in some very critical moments of this work; and for his sincere friendship. I also wish to thank him for giving me freedom to explore the areas I thought useful and still keeping the research into perspective. His help during the preparation of this document is greatly appreciated.

Thanks to my friends and colleagues, Manuel Madrigal and Dr. Salvador Acha. Their active cooperation overcome geographical limitations. Their help made possible practical use of collective ideas.

I whish to thank Dr. Francisco de León for kindly helping me to increase my understanding in many important aspects relating multi-limb, three phase transformer modelling. His help facilitated the development of the harmonic domain transformer model presented in this thesis.

Thanks to Mrs Monica Derrington. Her suggestions for improving the English of important parts of the thesis are sincerely appreciated.

I would also like to thank to my postgraduate colleagues. Thanks to Claudio Fuerte and his wife Monica for lightening the last two years of my research with their kind friendship. Some of the long discussions with Claudio give me insight to many concepts I thought I knew well. I wish also to extend my gratitude to Henrik Gollee and Gary Gray for their honest friendship and advice in many computational aspects.

I want to express a word of gratitude to my friends in Mexico. Thanks to Isidro Lazaro and J.Juan Rincon Pasaye, for their support and for helping me so many times, via e-mail, with all legal matters related to my study leave. Thanks to Marcelino Madrigal for all support offered.

I wish to thank to the Consejo Nacional de Ciencia y Tecnología and the Faculty of Electrical Engineering of the U.M.S.N.H. in México for granted me the study leave and financial support during the course of my doctoral studies.

Finally, I want to thank to my mother and family for their love and unconditional support through all my life. Thanks to my dear friend Martha Maciel for all her support, encouragement and friendship.

Contents

Acknowledgments v

Abbrevations xv

Part I General Theory 1

1. Introduction 2
1.1 Description of the Power System Harmonic Problem 2
1.2 Research Line of this Work 3
1.3 Techniques for Periodic Steady State Analysis of NLS 3
1.4 Purpose and Objectives of the Present Work 5
1.5 Publications 6
1.6 Contributions 6
1.7 Outline of the Thesis 7

2. Analytical Representation of Non-linear Characteristics 9
2.1 Introduction 9
2.2 Non-linear Circuits Elements 10
2.3 The Black Box Approach 11
2.4 Representation of Smooth Non-linear Characteristics 11
2.4.1 Linear Interpolation 13
2.4.2 Piecewise linear 13
2.4.3 Polynomial approximation 15
2.4.4 Cubic splines 17
2.4.5 Orthogonal expansions 18
2.4.6 Rational-fraction polynomials 19
2.4.7 Hyperbolic functions 20
2.4.8 Representation of Hysteresis Effects 21
2.4.9 Validation of hysteresis models 23
2.5 Non-smooth characteristics 25
2.6 Conclusions 26

3. Generalised Analysis of Periodic Steady State Responses of NLS 28
3.1 Introduction 28
3.2 State Variable Description of Electric Power Networks 29
3.2.1 Linearisation of dynamical equations 30
3.2.2 Forms of solution of periodic LTVS 31

3.3 Analysis of Periodic LTVS Via Orthogonal Expansions 32
3.3.1 A general representation of orthogonal basis 32
3.3.2 Operational matrix P for integration of $\gamma_{(m)}(t)$ 33
3.3.3 Operational matrix D for differentiation of $\gamma_{(m)}(t)$ 33
3.3.4 Transformation operational matrix W 33
3.3.5 Product and coefficients matrices 34
3.3.6 Analysis of LTVS 34
3.4 Tableau Analysis in the Generalised Domain 37
3.4.1 Tableau analysis for invariant linear systems 38
3.4.2 STM for LTIS 38
3.4.3 Tableau analysis for LTVS 40
3.5 Generalised Hybrid Methods 40
3.6 Modified Nodal Analysis (MNA) 41
3.7 Conclusions 43

Part II Harmonic Domain Modelling 44

4. Harmonic Domain Modelling of Electric Power Circuits 45
4.1 Introduction 45
4.2 Direct Frequency Domain Evaluations 46
4.3 Harmonic Domain Evaluations Using Complex Fourier Series Expansions 46
4.3.1 Dynamic elements 48
4.3.2 Numerical example 48
4.4 Efficient Polynomial Evaluation 49
4.4.1 Recursive Evaluation 49
4.4.2 Exponentiation 50
4.5 Harmonic Domain Evaluations Using Real Fourier Series 50
4.5.1 Dynamic elements 52
4.5.2 Numeric example 53
4.6 Harmonic Domain Evaluations Using Hartley Series Expansions 54
4.6.1 Dynamic elements 56
4.6.2 Numeric example 57
4.7 Harmonic Domain Newton-Raphson Techniques 58
4.7.1 Newton-Raphson in Real Fourier Harmonic Domain 59
4.7.2 Newton-Raphson in Complex Fourier Harmonic Domain 60
4.7.3 Newton-Raphson in Hartley Harmonic Domain 60
4.8 Harmonic Domain Computations 61
4.9 Case Studies 62
4.10 Conclusions 64

5. Three-Phase Thyristor Controlled Reactors 65
5.1 Introduction 65
5.2 Single Phase Modelling of Thyristor Controlled Reactors 67
5.2.1 TCR Harmonic current vector 68
5.2.2 Harmonic switching functions 69
5.3 Firing Control Systems 70

5.3.1 Voltage zero crossing evaluation 71
5.3.2 Firing angle evaluation 71
5.3.3 Turn-off time evaluation 72
5.4 Three Phase TCR Modelling 73
5.5 Case Studies 74
5.5.1 Six pulse, three phase TCR 75
5.5.2 Twelve pulse, three phase TCR 77
5.6 Conclusions 78

6. Duality-Based Three-Phase Multi-limb Transformers 79
6.1 Introduction 79
6.2 Magnetic Behaviour of Three Phase Transformers 81
6.3 Harmonic Electro-Magnetic Models 84
6.3.1 Transformation from primitive to nodal parameters 85
6.4 Harmonic Thevenin Equivalent 85
6.5 Harmonic Norton Equivalent 89
6.6 Harmonic Domain Solutions Via Newton-Rapshon Method 89
6.7 Case Study 90
6.7.1 Voltage supply 91
6.7.2 Multiple saturation levels 91
6.8 Conclusions 91

7. Analysis of Convergence and Relaxation Methods 94
7.1 Introduction 94
7.2 The Non-linear Inductor in Harmonic Domain 95
7.2.1 Test cases 96
7.2.2 Full Newton-Raphson Method 98
7.3 Single-valued Newton-Raphson method 99
7.3.1 Gauss-Seidel scheme 99
7.3.2 Diagonal relaxation 99
7.4 Conclusions 100

Part III Sequency Domain Modelling 102

8. Sequency Domain Modelling of Linear Time-Invariant Electric Power Networks 103
8.1 Introduction 103
8.2 Theory of Walsh Functions 104
8.2.1 Rademacher Functions 104
8.2.2 Walsh Functions 105
8.3 Fundamental Properties of Walsh Functions 109
8.3.1 Multiplications 109
8.3.2 Trigonometric functions 109
8.3.3 Orthonormality 109
8.4 Walsh Series 109
8.4.1 Walsh series of a ramp function 109
8.4.2 Discrete formulation 110

8.4.3 Convergence 110
8.4.4 Walsh Series Versus Fourier Series 111
8.4.5 Numeric examples 111
8.4.6 Integrals of Walsh functions 114
8.4.7 Integral representation of differential functions 115
8.5 Case Studies 117
8.5.1 Response to step functions with Walsh approach 118
8.5.2 Response to periodic inputs 120
8.6 Conclusions 122

9. Analysis of Linear Time Varying Power Plant Components Via Walsh Functions 123
9.1 Introduction 123
9.2 Product Operational Matrix 124
9.3 Solution of Time-varying Systems 125
9.3.1 Numeric Example 129
9.4 Conclusions 134

10. Steady State Analysis of Non-linear Systems 135
10.1 Introduction 135
10.1.1 Bilinear Systems 135
10.1.2 Polynomial systems 136
10.2 Analysis of Bilinear Systems in Walsh Domain 136
10.3 Numeric Example 139
10.4 Bi-linearisations of non-linear systems 139
10.5 The n-Product Operational Matrix 141
10.6 Analysis of Hammerstein Model 142
10.6.1 Solution and Analysis 143
10.6.2 Numeric example: Polynomial systems 144
10.7 Numeric example: Bi-linear systems 144
10.7.1 Time domain solutions 147
10.7.2 First order Newton-Raphson solution 147
10.7.3 Newton-Raphson retaining non-linearity 148
10.7.4 Effect of bi-linearisations in the convergence region 151
10.8 Conclusions 151

11. Applications of Walsh Functions to Power Systems Distortion 152
11.1 Introduction 152
11.2 Single Phase TCRs 153
11.2.1 The TCR and Power Systems Equations 153
11.3 Modelling of Single Core Three Phase Transformers 159
11.3.1 Newton-Raphson in the Sequency Domain 159
11.3.2 Effect of Non-Linear Operations on Walsh Series 160
11.3.3 Response of a non-linear element to a Walsh series 161
11.3.4 Product of Walsh Series 162
11.3.5 Effect of Trigonometric Transformations 163
11.3.6 Transformer Equivalent Circuit 165

11.3.7 Test Case 166
11.4 Transmission Line Representation in Walsh Series 166
11.5 Conclusions 169

12. Conclusions and Suggestions for Future Research Work 170
12.1 General Conclusions 170
12.2 Future Research Work 171

A. Parameters of the South Island Reduced System 182
A.1 Transmission lines: 182
A.1.1 Invercagill220-Manapouri220 182
A.1.2 Manapouri220-Tiwai220. 182
A.1.3 Invercagill220-Tiwai220. 182
A.2 Generators: 183
A.3 Transformers: 183
A.4 Loads: 183
A.5 System parameters: 183

B. Parameters of the Jaguara Taquaril System 184
B.1 System data 184
B.2 Transformers 184
B.3 Generators 184
B.4 Shunt reactor 184
B.5 Transmission line 184

C. Power-Invariant Transformation for Transformer Connections 185

List of Figures

2.1 Common non-linear characteristics in electric devices 10
2.2 Non-linear inductances for 3- and 5-limb transformers 13
2.3 Continuous, one-dimensional piecewise-linear function 14
2.4 Piecewise-linear approximation 15
2.5 Polynomial approximation 16
2.6 Cubic spline approximation 17
2.7 Orthogonal approximation 18
2.8 (a) Non-linear characteristic (b)Equivalent transfer characteristic 19
2.9 Polynomial rational-fraction approximation 20
2.10 Hyperbolic approximation 21
2.11 Non-linear element represented as a 'black box' with flux $x(t)$ as input and $y(t)$ as output 22
2.12 Hysteresis loop 22
2.13 Ferromagnetic inductor (a) non-linear inductor with hysteresis (b) equivalent circuit 24
2.14 Qualitative properties of the hysteretic representation 24
2.15 Minor hysteresis loops 25
2.16 TCR input-output characteristics with Fourier Series 26
2.17 Voltage-current characteristics in ACDC Converters 27

3.1 Block diagram representation of electric networks 29
3.2 Block diagram of linear, time-varying electric circuits 30
3.3 RLC circuit 38
3.4 Single phase transmission system 42

4.1 General procedure for harmonic domain calculations 61
4.2 Simplified Jaguara-Taquaril transmission system 62
4.3 Voltages at Jaguara bus bar with voltage excitation of 1.1 [p.u.] 63
4.4 Voltages at Jaguara bus bar with an excitation voltage of 1.15 [p.u.] . . 63

5.1 (a)Schematic representation of a Single phase TCR (b)instantaneous $\psi - i_R$ characteristic 67
5.2 (a)Excitation voltage and output current source, (b) switching function and (c) product of input and switching function 68
5.3 Switching function 70
5.4 Harmonic currents versus Conduction angle 71
5.5 South Island Test System 74
5.6 Frequency scan 75
5.7 Voltages at Tiwai bus bar with $\sigma = 140^o$ 76

5.8 Voltages at Tiwai bus bar with $\sigma = 70^o$ 76
5.9 Voltages at Tiwai bus bar with $\sigma = 140^o$ 77
5.10 Voltages at Tiwai bus bar 77

6.1 Commonly used Iron Cores 81
6.2 Magnetic fields in a three-legged transformer 82
6.3 Magnetic circuit in a three-legged transformer 82
6.4 Magnetic field distribution in a five-legged transformer 83
6.5 Magnetic circuit associated to the 5-legged transformer 83
6.6 12-terminal Primitive Network of a three-legged Transformer 84
6.7 Electric Dual of the three-legged transformer 86
6.8 Structure of linearised impedance matrix of the transformer 88
6.9 Unified harmonic domain solution 89
6.10 jaguara Taquaril transmission system 90
6.11 Magnetisation curves of a power transformer 91
6.12 Voltages at Jaguara busbar with 1.1 p.u. of voltage supply 92
6.13 Voltages at Jaguara busbar with 1.2 p.u. of voltage supply 92
6.14 Voltages at Jaguara busbar with 1.2 p.u. of voltage supply 92

7.1 Non-linear inductor excited from a periodic voltage source 95
7.2 Harmonic Norton equivalent of the non-linear inductor and periodic voltage source. 96
7.3 Harmonic Norton equivalent of the ideal, non-linear inductor in series with leakage admittance. 97
7.4 Jaguara-Taquaril transmission system 97
7.5 Convergence of full Newton-Raphson 98
7.6 Convergence of single-valued Newton-Raphson 98
7.7 Convergence characteristics of Gauss-Seidel methods 99
7.8 Convergence characteristics of the NR with diagonal relaxation 100
7.9 Convergence characteristics of the various methods 101

8.1 Rademacher functions 105
8.2 A set of 2^3 Walsh functions 106
8.3 Comparison of Walsh and Fourier spectra 111
8.4 Triangular function 112
8.5 Double triangular function 113
8.6 Alternating triangular function 113
8.7 Integral of Walsh functions 114
8.8 Six order circuit 118
8.9 Runge-Kutta's solution 118
8.10 Phase plane analysis 119
8.11 Solution with 8 Walsh coefficients 119
8.12 Comparison of time domain solution and the Walsh solution 120
8.13 Input waveform 121
8.14 Comparison of Walsh and Time domain solutions 121
8.15 Limit Cycles 121

9.1 Periodic circuit 129

9.2 Response of a time-varying circuit 130
9.3 Response of a time-varying circuit in the Walsh domain, (a)-(b) solution with 32 Walsh coefficients, (d)-(f) solution with 64 Walsh coefficients, (h)-(i) solution with 128 Walsh coefficients 131
9.4 Solution with 512 Walsh coefficients 132
9.5 Approximation of limit cycle 133
9.6 Solution with 256 Walsh coefficients and a good guess of the initial condition 133
9.7 Structure of transfer matrix where 32 Walsh coefficients are considered 134

10.1 Bilinear system state diagram 137
10.2 Time response of a simple bilinear system 140
10.3 Hammerstein model 142
10.4 Products of Walsh series 145
10.5 Non-linear characteristics, – $f_1(q_i)$ –$f_3(q_3)$ and –$f_2(\varphi_2)$ 146
10.6 Steady state solution for an input of $1.1\sin(t)$ 147
10.7 Steady state solution for an input of $1.2\sin(t)$ 148
10.8 Newton-Raphson Iterative process,— Walsh solution, - - Time Domain solution 149
10.9 Iterative process using a third order Newton-Raphson retaining non-linearity via bilinear terms 150

11.1 Piecewise-linear approximation 154
11.2 The reduced equivalent system 155
11.3 Time domain solution for $\sigma_1 = \sigma_2 = 30^o$ 155
11.4 Walsh domain solution $\sigma_1 = \sigma_2 = 30^o$ 157
11.5 TCR, Terminal voltage waveform 158
11.6 Walsh domain solution for $\sigma_1 = 30^o$ and $\sigma_2 = 45^o$ 158
11.7 Sequence currents Vs conduction angles 159
11.8 Response of a non-linear element to a Walsh series 161
11.9 Jaguara-Taquaril transmission system 166
11.10 Voltages at Jaguara bus bars 166

List of Tables

2.1 Magnetising curve parameters 12
2.2 Correspondence between transformer core branches and magnetising curves in Figure 2.2 12
2.3 Piecewise approximation data 15
2.4 Polynomial approximation data 17
2.5 Polynomial rational-fraction approximation data 19

3.1 Literature on operational matrices 32

4.1 Polynomial evaluations 50

8.1 Ordering of relationship between Walsh-Hadamard and Hadamard matrices 108

Abbrevations

PSS	Periodic Steady State
NLS	Non-Linear Systems
HVDC	High Voltage Direct Current
VAR	Voltage Amper Reactive power
SVC	Static VAR Compensator
AC	Alternating Current
FACTS	Flexible AC Transmissions Systems
FFT	Fast Fourier Transform
TCR	Thyristor Controlled Reactor
AC/DC	Alternate Current/Direct Current
STM	Sparse Tableau Method
MNA	Modified Nodal Analysis
LTIS	Linear Time Invariant Systems
LTVS	Linear Time-Varying Systems
BLS	Bi-Linear Systems
KCL	Kirchoff's Current Law
KVL	Kirchoff's Voltage Law
NA	Nodal Analysis
IPC	Idividual Phase Control
PFC	Pulse Frequency Control
PPC	Pulse Phase Control
DC	Direct Current
EMTP	Electro Magnetic Transient Program
EMTDC	Electro Megnetic Transient and Direct Current transmission systems program
CCM	Component Connection Model
GCBC	Gray Code Binary Conversion
BLS	Bi-Linear Systems

Part I

General Theory

Chapter 1

Introduction

1.1 Description of the Power System Harmonic Problem

Under ideal operating conditions all power system waveforms are sinusoidal and balanced. A unique operating frequency is expected throughout the system. In practice, such ideal conditions are difficult to meet. Physical systems are, to a greater or lesser extent, non-linear. They possess the undesirable characteristic of distorting ideal, periodic operating conditions. In terms of Fourier analysis, these waveforms can be expressed as fundamental frequency sinusoids and higher frequency sinusoids, i.e. *harmonics*. The study of steady state distorted waveforms is traditionally known as *Harmonic Analysis of Power Systems*. However, Fourier series are not the only alternative for analysing distorted, periodic waveforms in power networks. In fact, they are not the best choice for cases when the periodic waveforms are rectangular. This may be the case in power systems containing a substantial component of power electronic-based devices.

The concept of harmonics is only related to Fourier transform-like expansions, Hartley transforms included. However, other orthogonal expansions exist which may contain a more general idea of frequency. For instance, the Walsh domain uses the concept of sequency. Other transforms exist where the basis functions may not have zero crossings, e.g. block-pulse expansions. In this work, the distorted waveforms are not just expressed in terms of Fourier series. Other orthogonal basis are used, depending on the class of waveforms under analysis. Accordingly, the term *harmonic analysis* or *harmonic distortion* is deemed not general enough to express the overall ideas presented in this thesis. Other terms, such as Periodic Steady State (PSS) analysis of non-linear systems (NLS) and non-linear distortion, are preferred.

Non-linear distortion in power systems is not a new phenomenon. In the early days of power systems, non-linear distortion caused by magnetic saturation of transforms and rotating machinery was recognised by power engineers. Nowadays, the use of power electronic-based devices in bulk power transmission systems has exacerbated the risks of non-linear distortion. These devices achieve their main operating state at the expense of distorting power network waveforms. It is generally accepted that if the problem is left unchecked it could easily get out of hand. In the early days of this technology, most applications were in the area of HVDC transmission. However, the last 15 years have seen a substantial number of Static VAR compensators (SVCs) being incorporated into existing AC transmission systems to provide voltage support and reactive power control. Many utilities worldwide now consider the deployment of the newest and most advanced generation of power electronic-based plant components, Flexible AC

Transmission Systems (FACTS) devices, a real alternative to the traditional devices based on electro-mechanical technologies.

Many adverse technical and economic problems have been traced to the existence of non-linear distortion and many countries have regulated on permissible levels of harmonic distortion. Adverse problems include insulation failures, maloperation of protective devices and communication interference. Economic repercussions include transmission line losses and watt-hour meter errors, which are causing great concern to electric utilities and consumers alike.

1.2 Research Line of this Work

Over the years, increased levels of waveform distortion have led utilities worldwide to seek action against this unwanted phenomenon. Corrective and predictive actions are being adopted by utilities to limit waveform distortion. Corrective actions involve repairs or replacements of existing equipment. In general, they are expensive and therefore avoided whenever possible. Preventive actions are cheaper to implement and are preferred.

As part of preventive actions, two main areas of development can be identified, namely measuring and simulation. Significant progress has been made in the development of accurate instrumentation to monitor waveforms distortion at the point of measurements but in planning and systems analysis the problem must be approached differently because the network may not even exist. In such cases, digital simulation based on mathematical modelling provides an alternative to actual measurement. This work represents an effort to produce new models to predict non-linear distortion in power systems.

In the past, time and frequency domain solutions have been used for purposes of predicting non-linear distortion. To date, most frequency domain techniques have made use of Fourier series in spite of strong indications that alternative basis such as Hartley, Walsh, Wavelets etc. can provide more efficient solutions. The methodology developed in this work is domain independent. Solutions in Fourier, Walsh and Hartley domains are presented.

1.3 Techniques for Periodic Steady State Analysis of NLS

Integral transforms are a means for the solution of boundary-value and initial value problems in physics and engineering. In particular, use of the Laplace transform in the analysis and synthesis of time-invariant systems has proved very popular. For instance, the periodic solution of linear circuits can easily be obtained with the use of the Laplace transform. However, this technique cannot be applied to non-linear circuits.

Arguably, a straightforward solution of a Non-Linear System (NLS), though not the most efficient, is to start the solution from a given initial condition and to integrate the state equations until the transient disappears. Two major problems are found with this approach. Firstly, it is not easy to establish, from visual inspection, whether or not the transient response has died out and secondly, the periodic response is reached at a high computational cost for cases of poorly damped systems.

Determining the PSS response of NLS is not a trivial matter. The large number of

publications devoted to this problem seems endless, especially in the areas of circuits and systems. Various time and frequency domain methods have been developed. Each has its advantages and drawbacks. The fundamental problem that all methods must address is the fact that most NLS are represented by equations containing a mixture of linear and non-linear operators. Linear operators are efficiently handled in the frequency domain and non-linear operators are easily evaluated in the time domain. In the past, some methods have used hybrid time-frequency domain approaches.

Single shooting methods [1] were used first to solve this problem. The methods can be applied to circuits of any kind, even those containing strong non-linearities. However, they require substantial computational effort since the numerical integration is rather time consuming. Even modified versions of these methods have proved very costly in terms of computing time [2, 3, 4]. Alternative methods make use of extrapolation [5] or gradient-based iterations [6], but the computational overheads are still a problem. In a recent paper [7], a multiple shooting method has been presented which claims to be more efficient. The authors have also reported on substantial improvements in the rate of convergence. The attraction of this new approach is that it can easily be parallelised.

Also, there are frequency domain methods which make use of Volterra series. A rather large number of publications has been devoted to the solution of non-linear circuits [8, 9] via Volterra series approach. Early publications such as references [10, 11, 12] give good examples of this theory. However, the multidimensional structure of Volterra series and difficulties in identifying Volterra Kernels have rendered Volterra series unattractive among engineers.

Power series representation provides another useful frequency approach [13, 14]. Similarly to Volterra series, this method provides analytical solutions for periodic responses. The non-linear characteristics are represented by a power series. It can deal with stronger non-linearities than Volterra series but the method is not general.

In an attempt to improve on the efficiency of the solution algorithms, frequency-only or frequency-time domain methods have been developed. These methods assume a solution in the form of generalised Fourier series and can be grouped in a family of algorithms knows as Harmonic Balance techniques. These algorithms have gained acceptance among electric and electronic engineers because they can be written to take advantage of the fact that large portions of most electric circuits are linear [15]. It is interesting to note that according to open literature, after reference [15] was published, power systems researchers have developed their own harmonic balance techniques [16, 17, 18]. In the power systems camp two approaches are now clearly identified, the Gauss-Seidel approach [16] and the Newton-Raphson approach [17]. The latter approach yields better characteristics of convergence and has become widely accepted.

In the early stages of the harmonic balance technique, most algorithms used to alternate between time domain and frequency domain in order to evaluate individual non-linear element responses. Here, the Fourier coefficients of the series are transformed to the time domain for evaluating the non-linearity. Subsequently, the resulting waveforms are transformed back into the frequency domain. These operations impose unnecessary overheads on the analysis. Furthermore, the method of transforming between time and frequency domains via Fast Fourier Transform (FFT) is not necessarily accurate. In fact, it may introduce aliasing at each iteration, compromising accuracy and convergence of the solution.

In reference[18], a harmonic balance method where the operations are performed entirely in the frequency domain has been put forward. In this method, round-off errors are minimised since there is no need to transform harmonic information into time domain information and vice-versa. Furthermore, the overheads are reduced by using discrete convolutions. The method described in [18] uses polynomial equations to represent the non-linearity. However, the method should also be valid for cases when polynomial rational fraction are used to represent the non-linearity.

The method proposed in this work follows the overall line of harmonic balance methods but it is more general, orthogonal expansions, other than complex Fourier series, are used. Similarly to reference [19], the iterative process employed is not cyclical in the fixed point iteration [16, 17].

The calculation of steady state currents and voltages $v(t)$ at each non-linear plant component takes place via an iterative process. This computation can be carried out very efficiently by taking into account that in the neighbourhood of a limit cycle the cycle's dynamic is almost linear. The authors in reference [19] have used this concept. However, they extrapolate the limit cycle using time domain calculations. In this work, the extrapolation of the limit cycle is carried out more efficiently using orthogonal expansions and an iterative method. It is also shown that a sufficiently large number of terms in the series is used then the limit cycle can be reached in one iteration.

1.4 Purpose and Objectives of the Present Work

- It was recognised early in the project that the waveforms involved in power system analysis are always real and that there was no need for a framework of analysis requiring complex algebra. Accordingly, one of the main purposes of this work was to investigate the use of real frames of reference were solutions could be carried out more efficiently.

- To investigate the adequacy of orthogonal transforms, which have not been widely used in power systems, to model non-linear plant components. These include, Real Fourier, Hartley and Walsh orthogonal series.

- To developed a general framework where both linear and non-linear power plant components can be modelled irrespective of the orthogonal basis selected for modelling individual plant components.

- To realise a unified framework in the sequency domain where non-linear and linear, time-varying power plant components can be combined together for an efficient solution.

- To develop frequency dependent transmission line models in the sequency domain.

- To develop models for single phase and three phase Thyristor Controlled Reactor (TCR) which do not require time-frequency domain transformations.

- To develop a multi-limb, three phase power transformer model based on the principle of duality.

- To investigate efficient solution algorithms with reduced storage and cpu requirements but without compromising significantly the convergence characteristics of the full Newton-Raphson method.

- To investigate the properties of a class of non-linear systems known as bi-linear systems, their ability to approximate more general NLS. The aim of this action is twofold: to make a step forward towards understanding true non-linear methods of analysis and to use non-linear approximations in the iterative solution of NLS.

1.5 Publications

The following publications were generated during the course of this research.

Transaction-graded papers

- J.J. Rico and E. Acha *'Harmonic Domain Modelling of Three Phase Thyristor Controlled Reactors by Means of Switching Vectors and Discrete Convolutions,"* IEEE Transactions on Power Delivery, Vol. 11, No. 3, pp. 1678-1684, July, 1996.

- E.Acha, J.J. Rico, S.Acha and M.Madrigal *"Harmonic Domain Modelling in Hartley's Domain with Particular Reference to Three Phase Thyristor-Controlled Reactors"*, To be presented at IEEE PES Winter Meeting, 2-5 of February, New York, 1997.

- C.R. Fuerte-Esquivel, E. Acha, SG. Tan and J.J. Rico *"Efficient Object Oriented PowerSystems Software for the Analysis of Large-Scale Networks Containing FACTS-Controlled Branches"*, To be presented at IEEE PES Summer Meeting, 20-24 of July, Berlin, Germany, 1997.

Conference papers

- E. Acha and J.J. Rico *" Harmonic Domain Modelling of Non-linear Power Plant Components,"* Proceedings of the IEEE ICHPS VI, Bologna, Italy, September 21-23, 1994.

1.6 Contributions

The main contributions of this research work are discussed below:

- A general framework for determining the steady-state response of power networks has been presented. The framework is general, it acommodates linear and non-linear elements. It is not restricted to anyone orthogonal basis. Particular cases of this framework are Real Fourier, Hartley and Walsh domains.

- A unified frame of reference in the sequency domain has been highly developed. In this frame of reference linear and non-linear power plant components can be represented together. Frequency dependent transmission lines are also represented in the sequency domain. This avoids the need for evaluating non-linear elements in the sequency domain and linear elements in the frequency domain.

- Analytical expressions for the response of linear and linear, time-varying power plant components in the sequency domain are given. It is shown how static, non-linear elements are handled in the sequency domain. Given an input expressed by a Walsh series, expressions for calculating the coefficients of the output are given in terms of the coefficients of the input.

- It is shown that quasi-linearisations as opposed to linearisations avoids the need for Norton or Thevenin equivalents. With quasi-linearisations, the non-linear element is represented as a time varying element. In cases of linear, time-varying elements the solution is reached in one iteration.

- An important class of non-linear systems, namely bi-linear systems, are analysed and used to approximate more complex non-linear systems. Non-linear approximations, as opposed to linear approximations, are a step towards non-iterative solutions of waveform distortion in power systems. The use of bi-linearisations provides a means for obtaining super-quadratically convergent algorithms.

- It is shown that discrete convolutions are a means for performing harmonic domain operations in a free-aliasing fashion. Also, it is shown that not only devices with polynomial characteristics are amenable to evaluations via discrete convolutions but also devices having characteristics exhibiting dead-band zones. A new and efficient three phase TCR model based on switching vectors and discrete convolutions has been put forward. The TCR equations are solved using a Newton-Raphson technique which exhibits quadratic convergence.

- A comprehensive steady state model for multi-limb power transformers based on the principle of duality has been developed.

- Complete first order Newton-Raphson or Newton-Raphson methods retaining non-linearity via bi-linearisations produce solutions with strong characteristics of convergence, however, alternative formulations that speed up the solutions can be obtained. Such alternatives are also presented in this work.

1.7 Outline of the Thesis

The research generated during the course of this PhD project can be divided into three main parts: General theory, Harmonic Domain analysis and Sequency Domain analysis.

Practical applications of software-based tools to predict non-linear distortion have been limited by their huge storage requirements and their heavy computational load. One objective of this work is the search for more efficient solution techniques which ease the computational burden. Several concepts have emerged as being critical to this endeavour, non-linear characteristic representation, the frame of reference and the numeric solution. Accordingly, the research generated is presented as follows

- Chapter 2 investigates possible representations of various non-linear characteristics present in power systems. Both single-valued characteristics and characteristics which include hysteretic behaviour are considered. It is shown in this

chapter that elements exhibiting hysteresis can be represented by an equivalent resistance and inductance which are amenable to single valued representations.

- Chapter 3 develops a generalised framework where all non-linear power plant components can be represented. The framework allows the inclusion of any orthogonal expansion.

- In Chapter 4 various orthogonal basis are used to predict non-linear distortion via iterative techniques. These orthogonal expansions lead to harmonic methods since they are based on trigonometric expansions. It is also shown in this chapter that, for studies where all signals are real, the framework based on Complex Fourier series [17] is redundant and more efficient solutions can be obtained using series with real coefficients. Real Fourier series and Hartley series are used for this purpose.

- In Chapter 5, a model for three phase TCRs is presented. The model takes advantage of switching functions and the iterative solution is performed entirely in the frequency domain.

- In Chapter 6, three phase multi-limb power transformers are modelled using the principle of duality. The model makes use of a first order Newton-Raphson methods. For a given voltage at the transformer terminals, the limit cycle of the currents is accurately extrapolated using another first order Newton-Raphson iterative process.

- Chapter 7 deals with the search for an alternative iterative process that can be used to solve efficiently most practical problems of non-linear distortion. The alternative algorithms proposed range from algorithms with weak convergence characteristics but which require a lower number of operations to methods with strong convergence characteristics which require a larger number of operations.

- Chapter 8 presents a sequency domain framework for studying linear, time-invariant power plant components.

- Chapter 9 presents the main characteristics of Walsh series-based solutions of linear, time varying systems. It is shown that closed form solutions can be obtained by using these methods. The theory described is also valid for any other orthogonal expansion.

- Chapter 10 addresses the calculation of the steady state response of non-linear electric circuits. Bi-linear systems are analysed in detailed. Polynomial systems and Hammerstain systems are also studied.

- In Chapter 11, several applications concerning the use of Walsh series to plant components modelling are presented. In this chapter a new model of single phase TCRs in the sequence domain is presented. Frequency dependent transmission lines and three phase bank trasformers are also modelled in the Walsh Domain.

- General Conclusions and suggestions for future research can be found in Chapter 12.

Chapter 2

Analytical Representation of Non-linear Characteristics

Non-linear elements are responsible for distorting the sinusoidal waveforms expected during idealised operating conditions of electric power systems. Thus, in the study of undesirable effects that such distortion may cause, an accurate representation of all non-linear characteristics is critically required.
In principle, experimental input-output set of points could be used for PSS studies of NLS, however, this is not efficient for cases where the systems equations must be evaluated repeatedly. Instead, analytical representations are preferred since they provide a more efficient alternative than working with input-output set of points.
This chapter presents various alternatives for the analytical representation of non-linear characteristics normally encountered in non-linear circuits. The accuracy of these methods are tested by using actual saturation characteristics corresponding to multi-limb transformers.

2.1 Introduction

Most electric circuits consist of three basic elements: resistors, inductors and capacitors. All possible non-linearities involved in electric circuit analysis are limited to the possible non-linear behavior of such basic elements. A detailed discussion of theses non-linearities and their analytical representation is provided in this Chapter.

Mathematical representations of NLS can be classified as either implicit or explicit. Implicit models are those in which the system response is expressed by implicit operations on the system input. Explicit models are those in which the system response is expressed by explicit operations on the system input.

The study of electric circuits PSS is concerned with evaluating levels of waveform distortion. Traditionally, waveform distortion has been expressed in terms of the steady-state response's frequency spectrum to a periodic input. In open literature, explicit methods have been preferred to solve this problem, since basic electric elements are well characterised by their explicit input-output characteristics. Very often information relating to non-linear power plant components is only available as a set of measurements of the input and the output and explicit methods become the best solution alternative. The class of explicit, non-linear systems is exceptionally large and no single analytical approach is applicable to all of them. However, by considering the class of non-linear input-output characteristics, solution procedures may be found for specific subclasses. Non-linear systems can be classified according

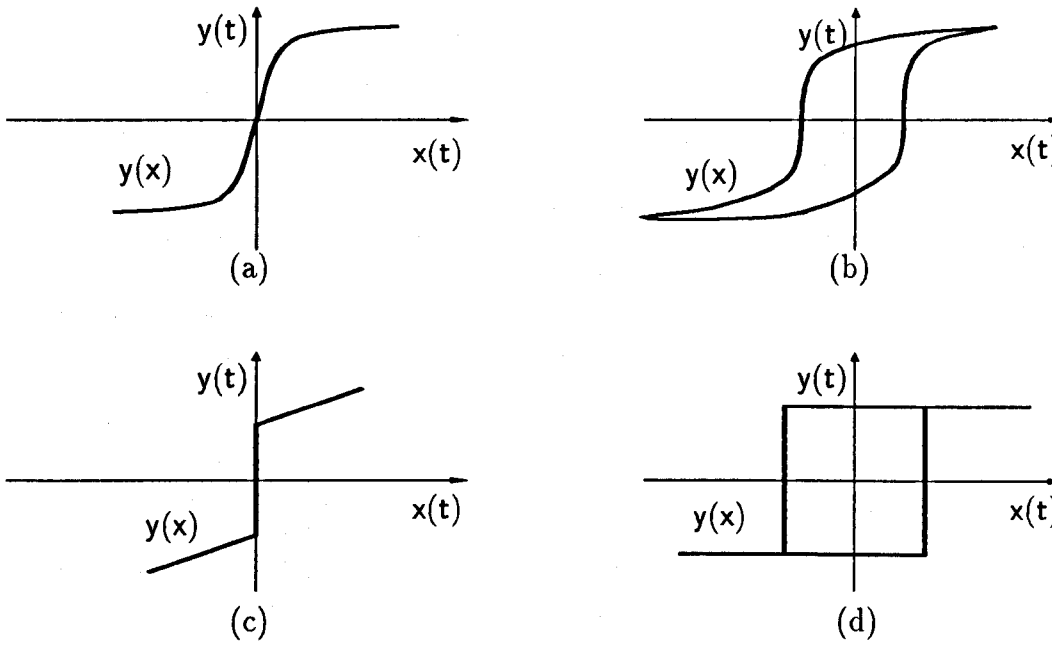

Fig. 2.1: Common non-linear characteristics in electric devices

to their non-linearities as *inherent* and *intentional.* Inherent non-linearities are those which naturally come with the system. Examples of these non-linearities include saturation and hysteresis effects. Usually, such non-linearities produce undesirable effects. Intentional non-linearities, on the other hand, are artificially introduced by the designer. AC/DC Converters and static VAR compensators are typical examples of such non-linearities. Non-linearities can also be classified in terms of their mathematical properties, *continuous, discontinuous, explicit, implicit* and *static.*

2.2 Non-linear Circuits Elements

Combinations of the three basic elements, resistors, inductors and capacitors should suffice to model most non-linear circuits encountered in the real world. These basic elements are two terminal devices described by their functional characteristic in the input-output plane. The input and output signals can be currents, voltages, fluxes and electric charges. Mathematically, these input-output relationships can be described by continuous, single valued functions, Figure 2.1(a), or multi-valued functions as shown in Figure 2.1(b). A similar description exists for discontinuous input-output characteristics. For a 2-terminal element the pair $\{x(t), y(t)\}$ can be either $\{v(t), i(t)\}$ or $\{i(t), v(t)\}$, where $v(t)$ and $i(t)$ are the voltage across and the current through the non-linear element, respectively. If $\{x(t), y(t)\}$ is $\{v(t), i(t)\}$ the input-output characteristic represents a voltage-controlled admittance. If, on the another hand, $\{x(t), y(t)\}$ is $\{i(t), v(t)\}$ the characteristic represents a current-controlled impedance. Note that since $x(t)$ can be either $v(t)$ or $i(t)$ and $y(t)$ can be $v(t)$ or $i(t)$, the non-linear characteristics in Figure 2.1 are general representations, where $x(t)$ is the controlling variable and $y(t)$ is the controlled variable. Accordingly, it is possible to have six types of non-linear elements since the three basic elements may be either current-controlled or voltage-controlled.

2.3 The Black Box Approach

A basic rule in mathematical modelling is that one should use as much knowledge and physical insight as possible of the system being modelled. Approaches which use this rule are most appealing because, if carried out properly, the model could be quite realistic. Unfortunately, the principles governing most physical phenomena are not well understood. Alternatively, postulating suitable mathematical representations which can be made to exhibit the same response as the system being modelled offer a more practical alternative. The later approach is known in open literature as the **black box approach**. Earlier literature on the subject concentrated on global basis function expansions, such as Volterra expansions [8, 9]. These representations were not very popular since finding the Volterra kernels is complicated process and their multi-dimensional nature causes computational overheads. The topic only revived until alternatives techniques such as neural network, fuzzy models and Wavelets started to take off. In power systems, physical modelling and the black box approach have been used in the past. In this research the black box approach is used extensively. In terms of this approach the problem of modelling non-linear and linear systems can be established as follows.

Let us consider two set of signals, the inputs $x(t)$ and the outputs $y(t)$ of a dynamic system:

$$u(t)^t = [x(1), x(2), \ldots, x(t)] \tag{2.1}$$

$$y(t)^t = [y(1), y(2), \ldots, y(t)] \tag{2.2}$$

then, we start by looking at a relationship between past $[x^{t-1}, y^{t-1}]$ values and future outputs, $y(t)$,

$$y(t) = g(x^{t-1}, y^{t-1}) + O(t) \tag{2.3}$$

Where the additive function $O(t)$ accounts for the fact that the next output will not be an exact function of past data. However, the aim is that $O(t)$ is small, so that we may think of $g(x^{t-1}, y^{t-1})$ as a good prediction of $y(t)$. A difficult issue to resolve is how to find function g in equation (2.3). For linear systems this may be an easy problem but in non-linear systems the problem is much more difficult since a very rich spectrum of possible model descriptions must be taken into account. In this chapter, some representations are reviewed. In particular, representations which have shown promising results in powers systems are described.

Parameterising function g with a finite dimensional vector θ gives,

$$y(t) = g(x^{t-1}, y^{t-1}, \theta) \tag{2.4}$$

This model is still too general. Indeed, a major topic is finding good parametric representation of non-linear relations. Once a decision has been taken about the parametric structure and the data set $[x^N, y^N]$ has been collected then the quality of the representation can be assessed by comparing fitted model results and record data:

$$\sum_{t=1}^{N} ||y(t) - g(x^{t-1}, y^{t-1}, \theta)||^2 \tag{2.5}$$

2.4 Representation of Smooth Non-linear Characteristics

In practice, non-linear characteristics are obtained as a set of recorded points $x(t)$ and $y(t)$. However, their use in digital studies is avoided whenever possible due to the high number of points that are required for an accurate solution and to the increasing computational effort caused by these representations when the systems equations are evaluated repeatedly.

Curve	M_{linear}	$M_{saturation}$	Knee Flux	Knee Current	b_1	b_2
1	292.38	0.67	1.037	0.0035	0.0	1.03
2	292.38	1.67	1.037	0.0035	0.0	1.03
3	6.00	1.44	0.290	0.050	0.0	0.22
4	173.33	1.48	0.504	0.0030	0.0	0.50
5	173.33	1.67	0.505	0.0030	0.0	0.50

Tab. 2.1: Magnetising curve parameters

3ϕ-3limb		3ϕ-5limb	
Branch	Curve	Branch	Curve
Main	1	Main	1
Yoke	2	Yoke	5
Leakage	3	Leakage outside phase	4
		Leakage central phase	3

Tab. 2.2: Correspondence between transformer core branches and magnetising curves in Figure 2.2

Alternatively, experimental curves can be analytically approximated thus reducing storage requirements and computational burden. Analytical representations also provide a way of classifying non-linear systems into classes that could include say, non-linear systems with polynomial representation, hyperbolic representation, piecewise linear representation etc. Furthermore, in this thesis emphasis is placed on analytical representations as they will dictate, in general, the most efficient procedure to determine the response of non-linear elements.

There is a wide range of possible analytical representations. Extensive research, has been devoted to the development of adequate analytical models to represent magnetic core saturation. In this chapter they are reviewed in detail. It is shown that arbitrary accuracy can be achieved when fitting magnetising characteristics but, in electric power networks, non-linearities due to magnetic elements are not the only possibility. Often, non-linear characteristics due to dead-band zones of some devices such static VAR compensator or power converters are difficult to fit with methods that have proven useful for magnetising characteristics. From the analysis of this section it is expected that one can decide which analytical representation can embody the largest possible classes of non-linear systems without loosing accuracy or efficiency in the computations. To show the advantages and disadvantages of the various alternatives, the magnetization curves measured by Dick and Watson in [20] are used. Multi-limb core transformers have different cross sections and therefore for detailed studies this fact must be take into account. Data for the non-linear characteristics corresponding to the different sections of a five-legged, three phase transformer is given in Table 2.1. All values in this chapter are given in p.u. related to a base of 25 MVA and 110 kV.

Table 2.2 gives the correspondence between cross sections in 3-limb and 5-limb transformers and the measured magnetising characteristics shown in Figure 2.2. It is evident that considering all transformer sections to have the same non-linear characteristic would lead to serious errors, especially when operation takes place in the saturation region.

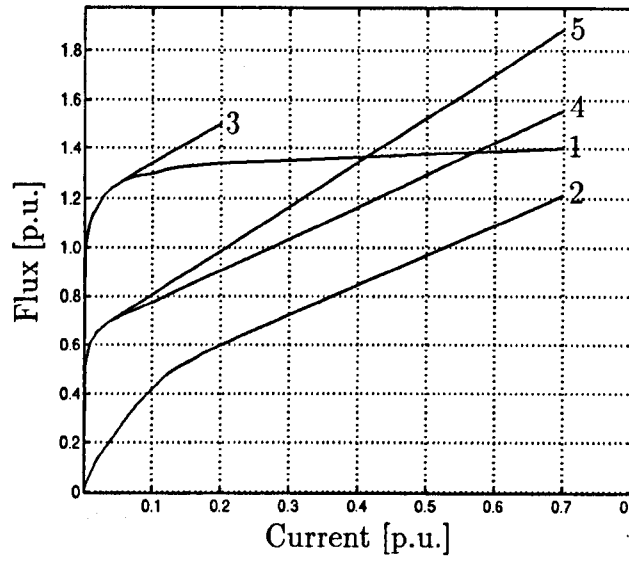

Fig. 2.2: Non-linear inductances for 3- and 5-limb transformers

2.4.1 Linear Interpolation

Most physical phenomena are deemed to be continuous, even though we measure them in discrete form. From such discrete information, we attempt to reconstruct continuity in order to learn about the phenomena's behaviour. The accuracy with which such phenomena can be assured to be reconstructed depends on the separation of consecutive samples. Non-linear characteristics, such as those shown in Figure 2.2, are obtained in the laboratory and then for the benefit of simulations they are provided as a set of input-output pairs. The behavior of the analysed system between consecutive samples can be considered as either linear or non-linear. Provided that enough number of samples is considered, systems are usually considered linear from one sample to the next. This facilitates the calculations and yields good accuracy. Algorithms using this idea have succeeded in representing magnetising characteristics [21, 17]. However, the computational effort increases with the number of non-linear elements and with the number of pairs considered for each non-linear characteristic.

For most physical systems, these drawbacks may be overcome by representing the discrete data by its best analytical approximation. Moreover, having an analytical description of the problem may have other advantages, it can be subjected to mathematical manipulations such as differentiation or integration.

2.4.2 Piecewise linear

Piecewise linear representations have also been used in the past. In publication [22] the authors have modelled magnetising characteristics with two independent equations and have reported a reasonable match with the actual response of the non-linear elements has been reported. Two regions are well defined in magnetic characteristics, namely linear and saturating regions. This piecewise linear representation, however, incur substantial errors when the operating point is about the knee point. The use of independent straight lines introduces computational overheads in the algorithm [23]. In this section, a piecewise linear representation with arbitrary accuracy is analysed. The approach produces a single equation. Because of its analytical nature, this representation allows algebraic manipulations such as derivation and integration. This is a fact from which waveform distortion analysis can benefit. Ow-

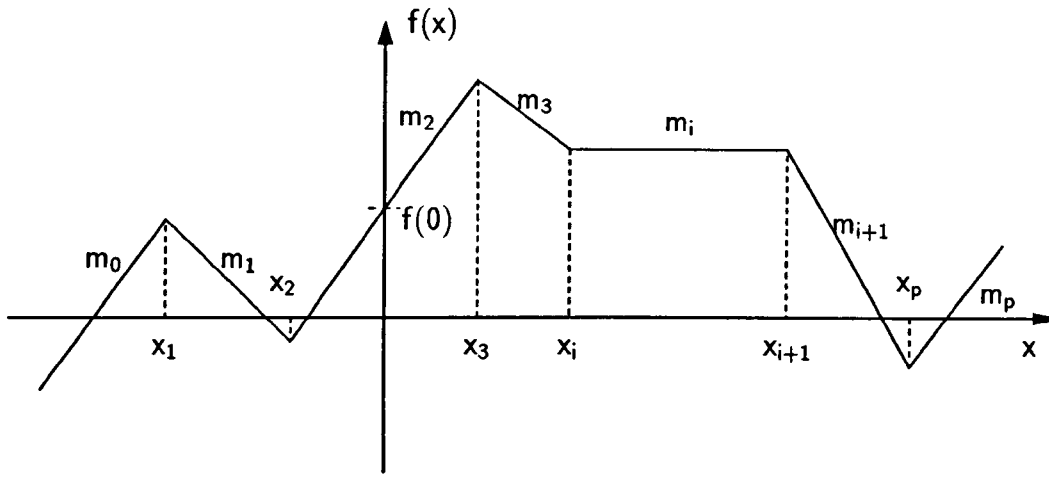

Fig. 2.3: Continuous, one-dimensional piecewise-linear function

ing to the simplicity and flexibility of this method, it can be used to represent a wide class of non-linearities. A fairly generalised canonical representation, where multiple-input and multiple-output cases are taken into account, has been published in [24]. A comprehensive analysis of single variable piecewise linear functions can be found in references [25] and [26].

Most single variable, non-linear functions can be approximated, with acceptable accuracy, by a single piecewise linear equation in canonical form,

$$f(x) = a + bx + \sum_{i=1}^{p} c_i|x - x_i| \tag{2.6}$$

An added advantage of the canonical form is that the parameters a, b and c_i can be calculated explicitly.

A function $f : \mathbb{R}^1 \to \mathbb{R}^1$ is said to be continuous, piecewise linear if it is composed of a finite number of linear segments. Points common to two segments with different slopes are called *break points.*

Let us consider a continuous, piecewise-linear function f with p breakpoints $x_1 < x_2 < \ldots < x_p$, as shown in Figure 2.3. Let m_i, $i = 0, 1, 2, \ldots, p$ denote the slope of each segment. Coefficients a, b and c_i can be explicitly calculated [26] by

$$b = \frac{1}{2}(m_o + m_p) \tag{2.7}$$

$$c_i = \frac{1}{2}(m_i - m_{i-1}) \tag{2.8}$$

$$a = f(0) - \sum_{i=1}^{p} c_i|x_i| \tag{2.9}$$

The canonical, piecewise representation was used to fit the experimental data shown in Figure 2.2 and the results are presented in Figure 2.4(a). The fitting errors are shown in Figure 2.4(b) and the number of segments used in the fittings regions is presented in Table 2.3. The errors in this chapter are calculated as the difference of measured data and calculated points.

Equation 2.6 shows the simplicity of the canonical form, a definitive advantage when repetitive use of the equation is required. Normally, saturating regions can be represented with

Curve number	Number of linear sections
1	6
2	3
3	5
4	5
5	4

Tab. 2.3: Piecewise approximation data

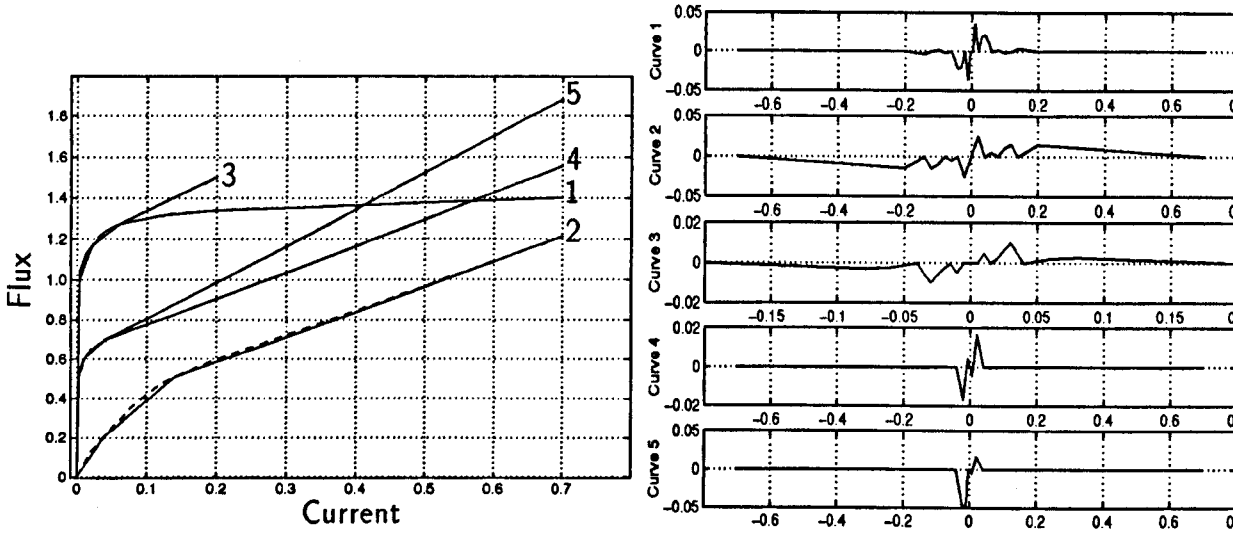

(a) Curve fitting

(b) Current Vs Error

Fig. 2.4: Piecewise-linear approximation

few segments and the evaluations involve simple operations which do not require high computational effort. Furthermore, it facilitates some algebraic manipulation such as derivation, an operation from which PSS analysis may benefit. It is proven in [27] that the derivative of a single-valued, non-linear function is,

$$f'(x) = b + \sum_{i=1}^{p} c_i J(x - x_i) \tag{2.10}$$

where $J(\cdot)$ is the jump function,

$$J(x) = \begin{cases} -1 & x < 0 \\ 1 & x \geq 0 \end{cases} \tag{2.11}$$

No further derivatives exist for this representation. This can be a limitation for some applications. It is important to say that piecewise linear functions are a particular case of a more general family of fitting methods called *splines*.

2.4.3 Polynomial approximation

Perhaps polynomial functions were the first class of functions which were used for the purpose of curve fitting non-linear characteristics. In power system analysis, polynomial series

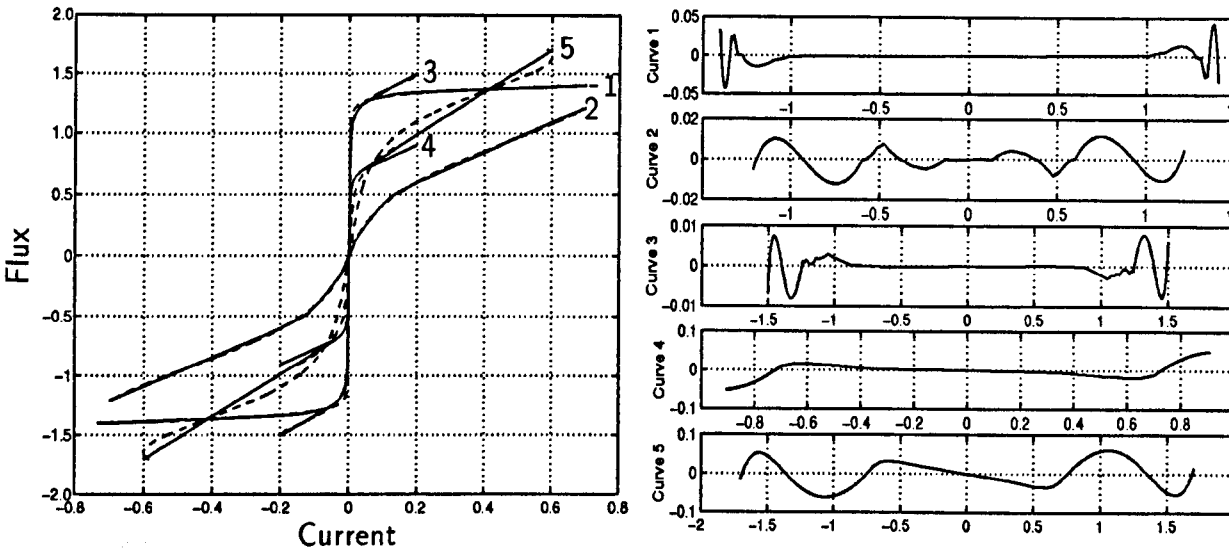

(a) Curve fitting

(b) Current Vs Error

Fig. 2.5: Polynomial approximation

approximation has won acceptance because of its simplicity formulation [28, 17] and because its analytical representation allows mathematical manipulations in the frequency domain [18]. Good approximations have been achieved using this approach but there has also been evidence of problems. For instance, accurate polynomial fitting is obtained by high order polynomial but this is at the risk of severe oscillations. A trade off between oscillations and accuracy has been achieved by using truncated polynomial series with two [28, 17] and three [18] terms,

$$i = a\varphi + b\varphi^n \tag{2.12}$$

$$i = a\varphi + b\varphi^n + c\varphi^m \tag{2.13}$$

Fitted polynomial responses and errors incurred in fitting the magnetising characteristics of Figure 2.2 are presented in Figure 2.5. It can be seen that good approximations have been found for cases with rounded knee regions and low slopes in the saturation region, e.g. curves 1 and 3. Difficulties arouse when fitting characteristics with high slopes in the saturation region. These may be the case of saturation characteristics of synchronous machines and some of the core sections in multi-limb transformers, e.g. curves 4 and 5. The error of the fitting is shown in Figure 2.5(b). The relevant data for the calculated polynomials is given in Table 2.4.

Apart from the poor results that sometimes are obtained with polynomial fittings, their importance in distortion analysis is considerable. They are amenable to easy harmonic domain calculations. Evaluation at a point, addition, multiplication, differentiation and integration are operations easily carried out. For evaluation at a point, it is only necessary to multiply and add real numbers together.

There may be ways of circumventing poor accuracy problems inherent in direct polynomial fittings and yet keeping the above advantages. Two variants of polynomial fitting are considered in this chapter, namely rational-fraction polynomials and spline techniques.

Curve number	a	b	c	m	n
1	0.002434	0.000071	0.000006	27	29
2	0.146267	0.590694	-0.204350	3	5
3	0.003072	0.002638	-0.000065	13	21
4	0.014620	0.249270	-0.037242	5	9
5	0.060934	0.094885	-0.007289	5	9

Tab. 2.4: Polynomial approximation data

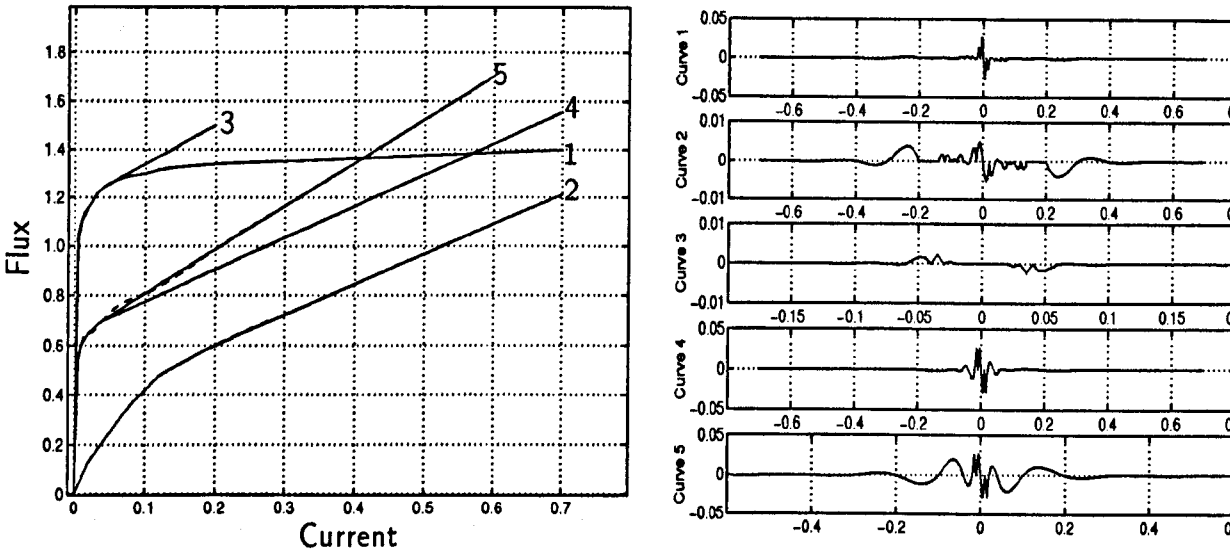

(a) Curve fitting

(b) Current Vs Error

Fig. 2.6: Cubic spline approximation

2.4.4 Cubic splines

One way of avoiding high-degree polynomials is to join adjacent pairs of data points with polynomials of low degree, ensuring that smoothness at joint points. Splines and other piecewise polynomial interpolation offer such a possibility. Splines are very popular owing to their accuracy and well established identification procedures. There are several ways of carrying out piecewise polynomial fittings, however, open literature indicates that cubic splines are the most widely used [27]. A cubic spline $S(x)$ has the following structure,

$$S(x) = \frac{1}{3}Ax^3 + \frac{1}{2}x^2 + D + \frac{1}{6}\sum_{i=1}^{n-1}|x - k_i|^3 \tag{2.14}$$

This is a cubic polynomial in each subinterval, $[k_0, k_1], [k_1, k_2], \ldots, [k_{n-1}, k_n]$. The cubic segments of the function (2.14) are joined together at the interior knots $k_1, k_2, \ldots, k_{n-1}$ in such a way that $S(x)$ has two continuous derivatives within the interval of interest. When cubic splines are used to approximate the data of Figure 2.2, the results shown in Figure 2.6(a) are obtained with the error shown in Figure 2.6(b).

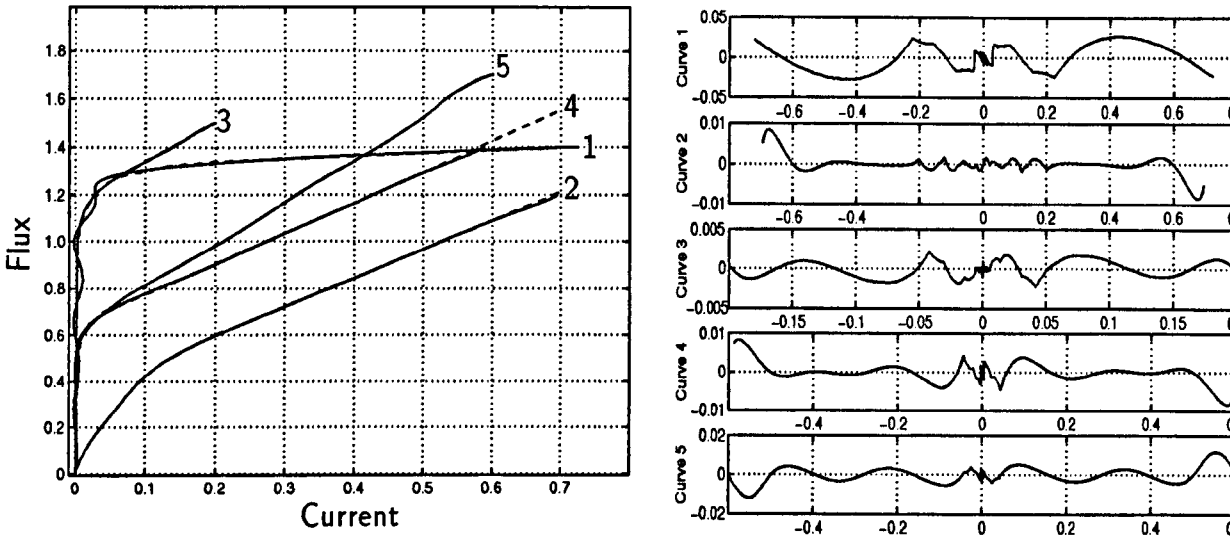

(a) Curve fitting

(b) Current Vs Error

Fig. 2.7: Orthogonal approximation

2.4.5 Orthogonal expansions

Orthogonal series such as Fourier, Hartley, Walsh, Haar or Wavelet can also be used to approximate non-linear characteristics. In this section, the non-linear characteristics are approximated using Fourier series only but the ideas can be extrapolated to other orthogonal basis. Fourier series have been used in many areas, powers systems included [29, 30, 31, 32]. They are simple in structure but may be time consuming since their evaluation requires special functions. Figure 2.7(a) shows the approximation achieved using trigonometric Fourier series. It can be seen that in some cases the truncated series with 14 terms are enough to obtain small errors, curves 2,3,4 and 5 in Figure 2.7. In other cases accuracy is poor, curve 1, and additional terms may be required.

The identification procedure is as follows. Consider the non-linear characteristic shown in Figure 2.8(a). In a real system, the input will have a finite maximum amplitude A. Hence, for $|x| > A$, the non-linear characteristic can be arbitrarily approximated without affecting the output. This is illustrated in Figure 2.8(b).

From the theory of Fourier series the equivalent transfer characteristic may be written as follows,

$$y = \sum_{n=1}^{N} b_n \sin\left(\frac{n\pi}{A}x\right) \tag{2.15}$$

where

$$b_n = \frac{1}{A}\int_{-A}^{A} f(x)\sin\left(\frac{n\pi}{A}x\right)dx \tag{2.16}$$

When using orthogonal expansions the error decreases as the number of terms in the series increases. However, a problem present in Fourier series is that when the number of terms increases, high oscillations can be introduced in the approximating function. By way of example, curve 1 has been badly approximated to show that effect. Oscillations are in fact a

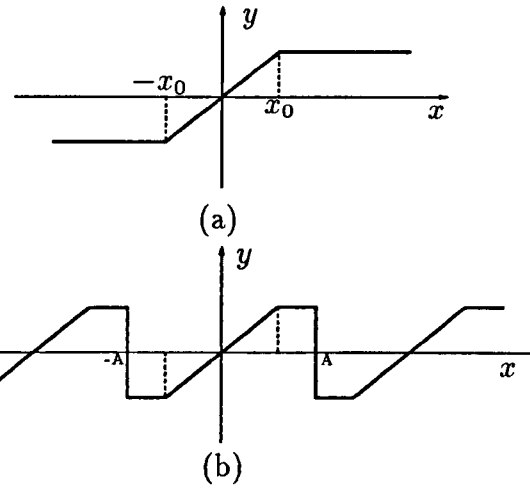

Fig. 2.8: (a) Non-linear characteristic (b)Equivalent transfer characteristic

common problem in orthogonal expansions. This problem can be controlled to a certain extent using windowing methods, widely used in signal processing. An example of this enhancement is given later on in this chapter when piecewise continuous characteristics are considered in Section 2.5.

2.4.6 Rational-fraction polynomials

Polynomials provide adequate fittings for short ranges of independent variables. Unfortunately, they are inadequate for large ranges, as shown in Section 2.4.3.

On the other hand, rational-fraction polynomials of the form,

$$f(x) = \frac{P_n(x)}{Q_m(x)} = \frac{p_0 + p_1 x + \ldots + p_n x^n}{q_0 + q_1 x + \ldots + q_m x^m} \tag{2.17}$$

have proven accurate [33] for the purpose of polynomial fitting. In this section, the characteristics of Figure 2.2 were modelled using this formulation. The results show good fitting along all the range of interest and for all cases. The fitted polynomials are presented in Figure 2.9(a) whereas Figure 2.9(b) illustrates the error in the range of interest. Data relevant to the order of the different polynomials is given in Table 2.5.

Curve number	m	n
1	11	11
2	7	7
3	5	5
4	5	9
5	17	17

Tab. 2.5: Polynomial rational-fraction approximation data

In general, rational-fractions are of lower order than their polynomial counterpart. They have also the nice characteristic of minimising oscillations, a problem commonly encountered with polynomial approximations. Sometimes, the problem of identification can be non-linear in which case an iterative method of solution is required, or a linearised formulation can be

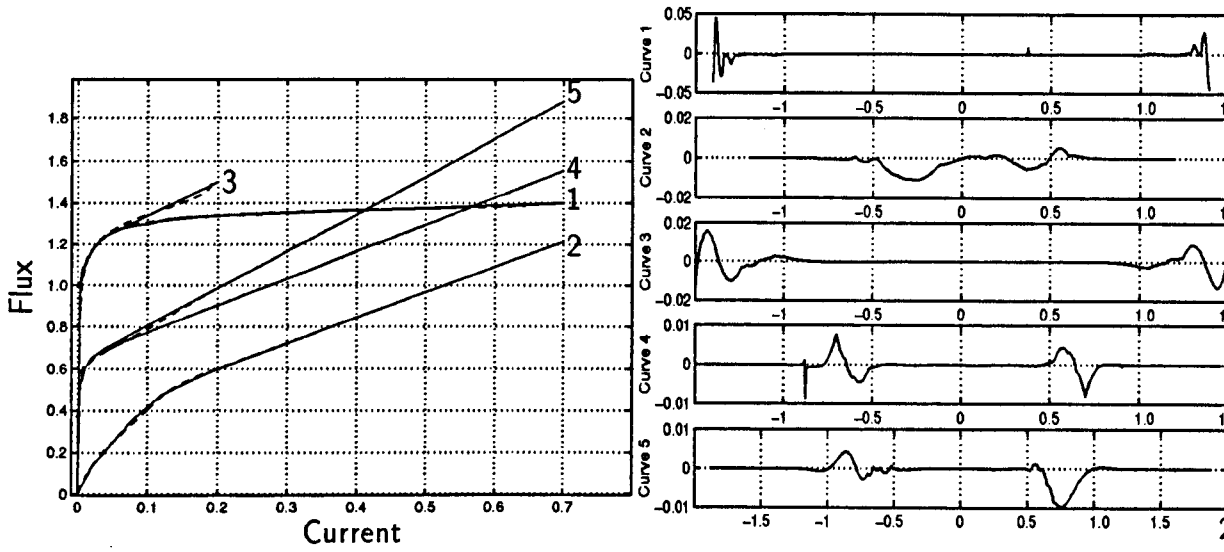

(a) Curve fitting (b) Current Vs Error

Fig. 2.9: Polynomial rational-fraction approximation

used [33]. In the latter case, an artificial error function is proposed and the parameters can be calculated directly using a generalised least square algorithm.

2.4.7 Hyperbolic functions

Approximation of magnetising characteristics has also been carried out using hyperbolic functions [34]. This approach can be quite accurate, as shown in Figure 2.10(a). The hyperbolic formulation has won acceptance because the identification of the required parameters can be performed with only a few hand calculations. If higher accuracy is required in the knee region, the calculation process becomes iterative. The procedure is based on the following equation,

$$F(i,\varphi) = (m_1 i + b_1 - \varphi)(m_2 i + b_2 - \varphi) - b_1 b_2 = \xi\varphi \tag{2.18}$$

where

m_1, m_2 are the slopes of the unsaturated and saturated regions.

b_1, b_2 are the ordinates to the origin of the asymptotes to m_1 and m_2

$\xi\varphi$ is the correction term

The correction term $\xi\varphi$ modulates the knee region. If modulation is not required $\xi\varphi$ can be set an arbitrary value or zero. The solution of the hyperbolic function in the first quadrant leads to the following expression for the magnetising current,

$$i = \frac{-B - \sqrt{(B^2 - 4AC)}}{2A} \tag{2.19}$$

where

$$\begin{aligned} A &= m_1 m_2 \\ B &= m_1(b_2 - \varphi) + m_2(b_1 - \varphi) \\ C &= \varphi_2 - \varphi(b_1 + b_2 + \xi) \end{aligned}$$

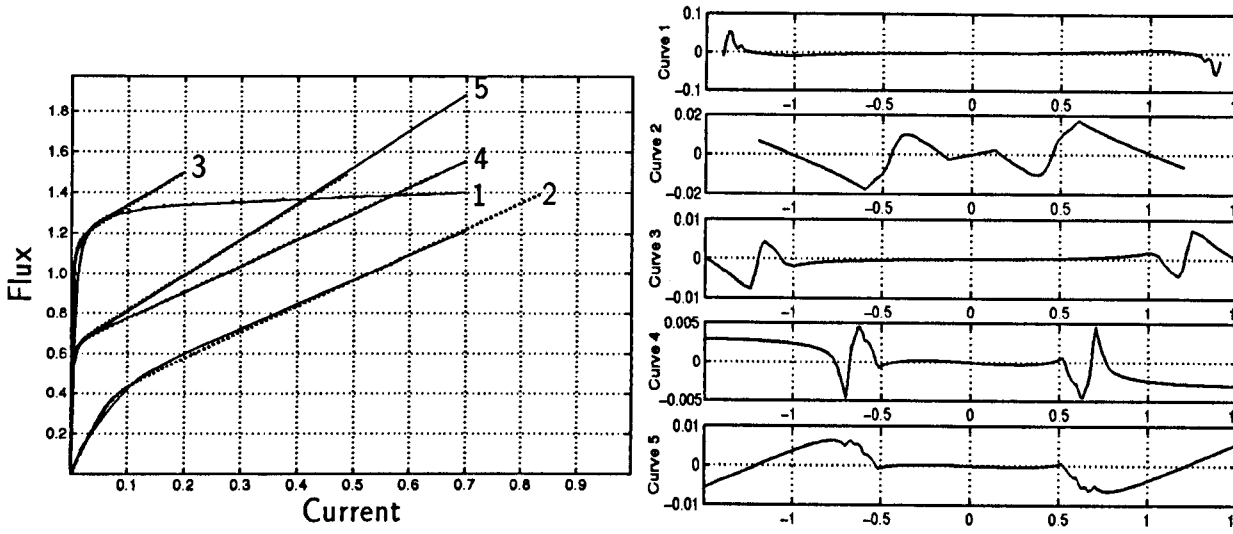

(a) Curve fitting

(b) Current Vs Error

Fig. 2.10: Hyperbolic approximation

This alternative is a good option for modelling magnetising characteristics.

2.4.8 Representation of Hysteresis Effects

Hysteresis is observed in many different materials and processes. Perhaps, the most familiar examples are the hysteretic effects observed in ferromagnetic materials. However, hysteresis is also observed in many other processes such as stress-strain relationship of materials that undergo plastic deformation, dielectric stress or the human respiratory system [35].

Basically, two approaches can be used to model hysteresis. One approach uses the differential equations that describe the principles governing the system. The second approach is based on postulating suitable mathematical representations which exhibit hysteresis [35, 36, 37] but which do not take into account the physics of the device. Considering that sometimes the principles governing most hysteretic phenomena are not well known, the latter approach is preferred. Furthermore, the analyses of non-linear circuits containing hysteretic elements can be very difficult. They are normally described by partial differential equations.

In this research, the hysteretic effects are modelled in terms of their input-output relationships. An advantage of this method is that the a double-valued problem can be mapped into two, single valued problems. For instance, a non-linear inductor exhibiting hysteresis can be represented as an equivalent resistor and a non-linear inductor without hysteresis loop. One attraction of this approach is that the equivalent circuit can be realised from measured hysteresis data [38]. Also, this method correctly reproduces the property observed in ferromagnetic materials of increasing loop areas with increasing operating frequencies.

Let us assume that a non-linear element can be represented by the 'black box' shown in Figure 2.11. The $x - y$ relationship has been obtained experimentally and plotted in Figure 2.12. The hysteresis loop can be firstly expressed as the summation of two functions,

$$y(x) = f_o(x) + g(x) \tag{2.20}$$

Fig. 2.11: Non-linear element represented as a 'black box' with flux $x(t)$ as input and $y(t)$ as output

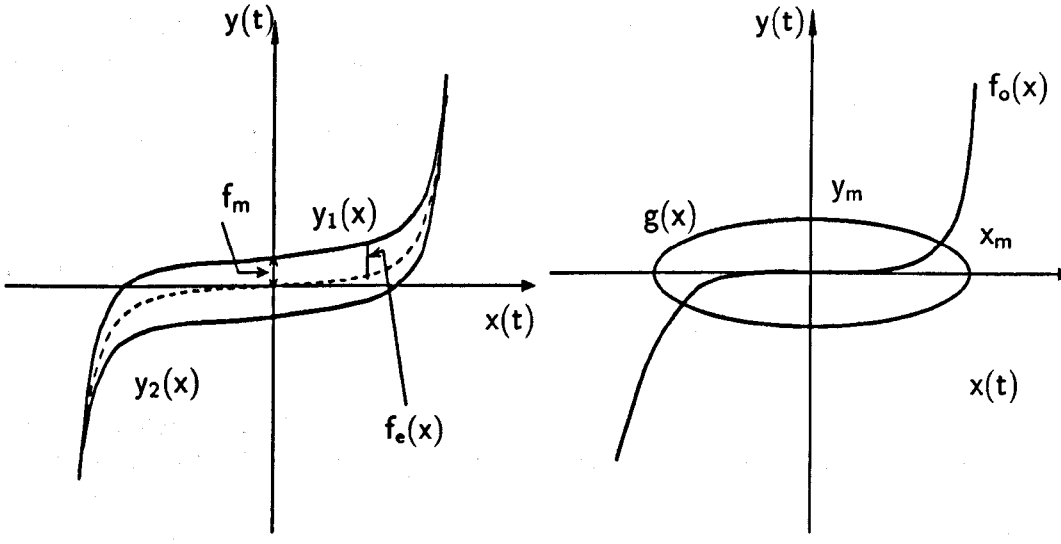

(a) Hysteresis loop in inverted position

(b) Hysteresis loop decomposed into two polynomials

Fig. 2.12: Hysteresis loop

where,

$$f_o(x) = \frac{y_1(x) + y_2(x)}{2} \tag{2.21}$$

and $g(x)$ is the equation of the ellipse,

$$g(x) = \pm\sqrt{y_m^2 - \frac{y_m^2}{x_m^2}x} \tag{2.22}$$

so that equation (2.20) can be rewritten as,

$$y(x) = f_o(x) \pm \sqrt{y_m^2 - \frac{y_m^2}{x_m^2}x} \tag{2.23}$$

Equation (2.23) is troublesome because of the double sign before the square root. If a sinusoidal input of the form,

$$x(t) = x_m \cos(\omega t) \tag{2.24}$$

is assumed then it is possible to find an alternative expression for the output which uses the derivative,

$$\frac{dx}{dt} = -\omega x_m \sin(\omega t) \tag{2.25}$$

It is not difficult to see that $y(t)$ can be expressed in terms of the function $f_0(x)$ and another function $f_e(x)$ which characterises the distance between f_0 and the periphery of the hysteresis loop. The function $f_e(x)$ as seen in Figure 2.12 is the reverse function to the input $x(t)$. It reaches a maximum value when $x(t) = 0$ and a minimum value when $x(t) = x_m$. It has also negative and positive values. Accordingly one can write,

$$y(x) = f_o(x) + f_e(x) \tag{2.26}$$

Here the function f_e is expressed as,

$$f_e(x) = \frac{1}{\omega x_m} f_m \frac{dx}{dt} \tag{2.27}$$

where the derivative determines the sign of the function f_e.

Equation (2.26) is interesting in the sense that it has physical interpretation. For instance, if the non-linear element is a non-linear inductor then $f_o(x)$ can be taken to be a current flowing through a lossless, non-linear inductance while the second term corresponds to a current flowing through a non-linear resistance. This allows the use of the equivalent circuit shown in Figure 2.13.

2.4.9 Validation of hysteresis models

In general, systems which exhibit hysteresis are non-linear and their representations must be non-linear be necessity. In these cases, there are problems with establishing the validity of models. Superposition is not applicable and the validation of a non-linear model requires an infinite set of measurements corresponding to all excitation signals. Hence, the validity of these models can only be established qualitatively.

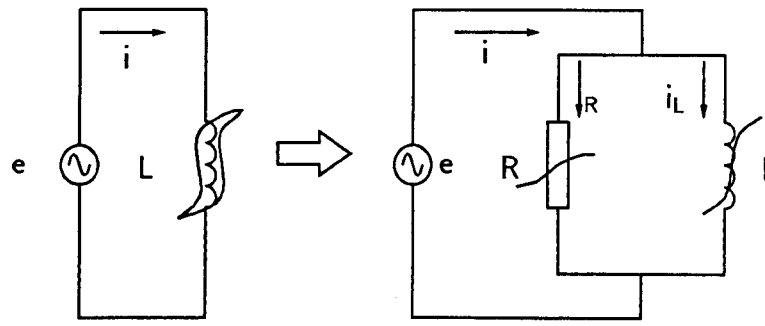

(a) (b)

Fig. 2.13: Ferromagnetic inductor (a) non-linear inductor with hysteresis (b) equivalent circuit

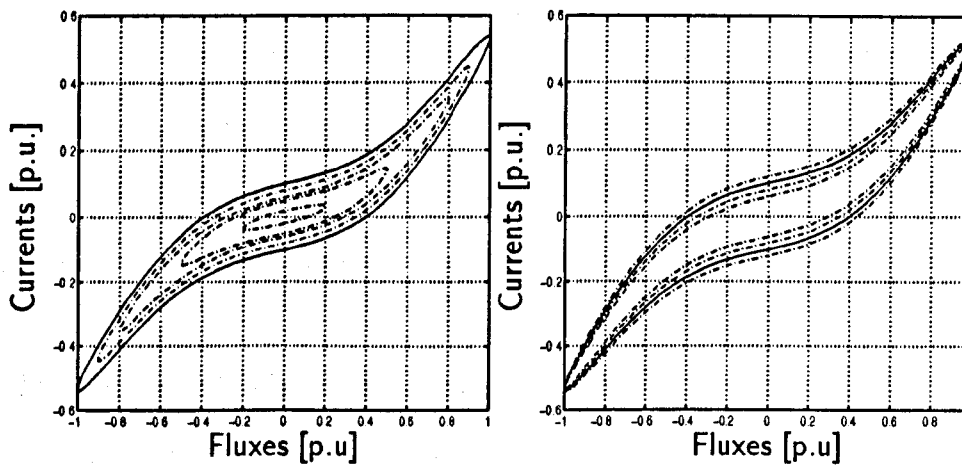

(a) (b)

Fig. 2.14: Qualitative properties of the hysteretic representation

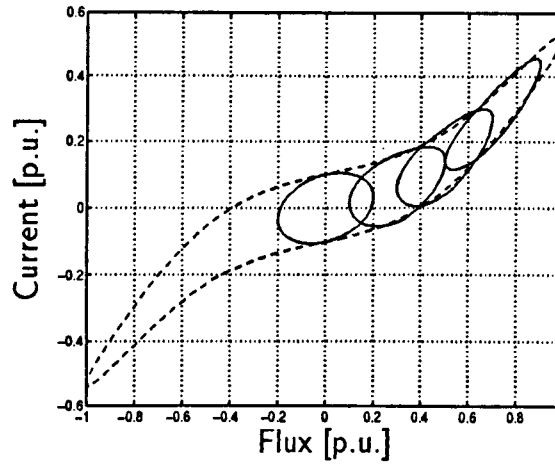

Fig. 2.15: Minor hysteresis loops

In this particular case, one must show that the postulated mathematical model exhibits the same significant properties and features of the hysteretic element. Among these properties is expansion of the loop with frequency and the presence of minor loops observed in hysteretic non-linear inductors. The model is constructed using appropriate parameters so that it would yield realistic responses to one on more test signals. To show that the mathematical representations adopted to model hysteresis reproduce the most important properties of non-linear inductors, Figure 2.14(a) illustrates the effect of sinusoidal excitation at various amplitudes and constant frequency. Figure 2.14(b) shows a family of hysteresis loops corresponding to sinusoidal excitations with constant amplitude but different frequencies.

Magnetisation history will cause the presence of minor loops [20]. A good model for hysteresis loops must reproduce this phenomena since some studies such as ferro-resonance analysis depend on the ability to reproduce these results accurately. Results obtained with the model used in this research are illustrated in Figure 2.15. The results were obtained considering small sinusoidal excitation in the presence of remanent flux. This was simulated as a DC flux component,

$$\varphi = k + a\sin(\omega t) \tag{2.28}$$

where k is the DC component of the flux and a is the amplitude of the sinusoidal component.

2.5 Non-smooth characteristics

Smooth non-linearities are not the only possibility in power systems. The use of power electronics in modern power systems control is on the increase leading to the presence of non-linearities characterised by dead-band zones. As opposed to smooth non-linearities, non-smooth or *hard non-linearities* are piecewise linear functions where most of the approximating approaches described before are likely to fail in producing accurate representations. In this case, piecewise linear functions are the most suitable representation since they render mathematical representation with no errors. However, orthogonal expansion such Fourier series or Walsh series still provide a way to represent such non-linearities with good accuracy.

A typical example of this class of non-linearities is that observed in Static VAR compensators, relays and AC/DC power converters. Figure 2.5(a) shows a flux-current characteristic

present in thyristor controlled reactors, plotted together with a Fourier series approximation. The error is illustrated in Figure 2.5(b). In this case a Hamming window was used to reduce oscillations. A more complex characteristic is that shown in Figure 2.17, observed

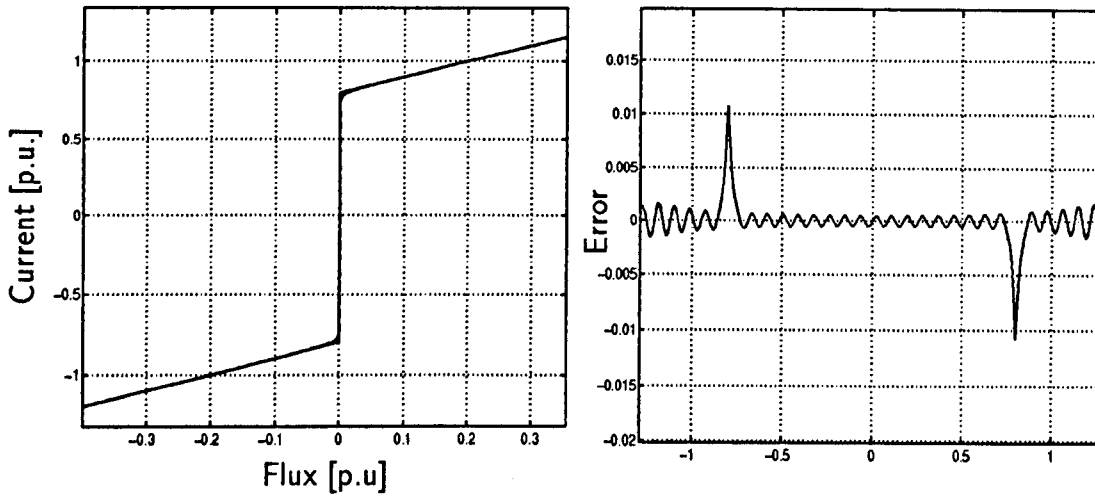

(a) Approximation (b) Error

Fig. 2.16: TCR input-output characteristics with Fourier Series

in AC/DC converters. These characteristics are piecewise polynomials rather than piecewise linear. Their piecewise nature presents difficulties for most approximating approaches. However, good approximations can be found by using linear splines and Fourier series.

2.6 Conclusions

This chapter has addressed a major problem in the analysis of power systems distortion, namely representation of non-linear characteristics. Various mathematical representations have been analysed in terms of their ability to approximate experimental data relating to the input-output response of non-linear power plant components. Both smooth and non-smooth representations have been considered.

It has been seen that a unified representation capable of modelling both smooth and non-smooth characteristics can be obtained by using orthogonal expansions or splines. Polynomial and rational fraction representations are also efficient alternatives for modelling smooth, non-linear characteristics while piecewise, linear functions are the natural option for representing characteristics showing dead-band zones.

It was also shown that elements showing hysteretic behaviour, such as iron core transformers, can be modelled with two single valued, non-linear characteristics. An important feature of this equivalent circuit is the fact that it can be realised purely by electric elements, a resistor and a inductor. Hence, the model can be made easily to interact with other models of the power network. It has been shown that these equivalents reproduce some important phenomena present in hysteretic materials such as frequency dependence and the formation of minor loops.

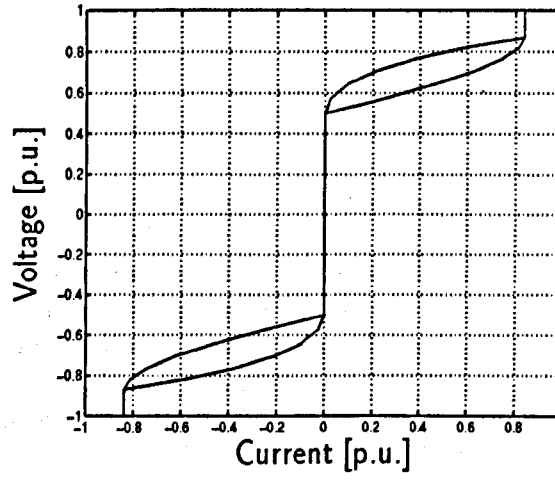

Fig. 2.17: Voltage-current characteristics in ACDC Converters

Chapter 3

Generalised Analysis of Periodic Steady State Responses of NLS

This chapter presents a generalised frame of reference for the solution of the periodic steady state response of non-linear circuits. The frame of reference is based on orthogonal expansions of the non-linear dynamic equations which govern the circuit. The description is carried out without making reference to any particular set of orthogonal functions. This generalised frame of reference embodies unified frameworks based on Fourier series or the unified Walsh framework introduced in this Thesis. In each particular application, a choice of frame work is made on the basis of the characteristics of the system waveforms being studied. The best choice is always the one which requires the minimum number of coefficients to represent all waveforms within a prescribed error.
This generalised frame of reference allows to investigate efficient numerical solutions for studying waveform distortion effects in power systems containing power electronic-based plant components.
Two alternative methods for writing non-linear equations of power networks are investigated, namely the Sparse Tableau Method (STM) and the Modified Nodal Analysis (MNA).
STM is proposed as a better alternative to nodal analysis-based methods for writing the equations of an electric power network. In the generalised domain, the orthogonal set of equations representing the dynamic equations are transformed into algebraic equations by the use of orthogonal functions. It is shown in this chapter that the STM is a powerful tool which separates Kirchhoffs' laws and branch equations. It can be used to formulate hybrid frameworks were different plant components are represented by different sets of orthogonal functions.

3.1 Introduction

Integral transforms provide a means for the solution of boundary-value and initial value problems in physics and engineering. In particular, the use of Laplace transform in the analysis and synthesis of linear, time-invariant systems (LTIS) has proved very popular. This transform converts the problem into a linear, algebraic one where the solution is obtained more easily. For instance, it provides a means for obtaining the periodic response of a linear, time-invariant circuit by a simple multiplication of the input and the system's transfer

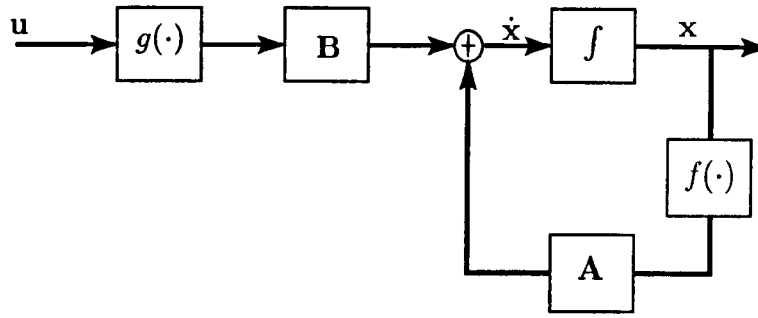

Fig. 3.1: Block diagram representation of electric networks

function. However, this technique cannot be applied to non-linear systems or linear, time varying systems (LTVS). In the latter case, Laplace transform methods yield a differential equation as opposed to an algebraic equation. The case of NLS is even more complicated since the resulting equations are non-linear algebraic or non-linear differential. Accordingly, a different approach is required. The one researched in this Thesis consists on expanding the dynamic, non-linear equations into a set of orthogonal sequence of functions. In this case, time-varying differential equations are transformed into either linear algebraic or non-linear algebraic equations. These equations can be solved analytically for linear systems or iteratively if the set of algebraic equations is non-linear.

Subclasses of orthogonal basis functions include orthogonal functions, orthogonal polynomials, Wavelets, etc. Any one of these basis series can be used to transform differential equations into algebraic equations. No given rules exist for selecting a class of orthogonal basis series. In power systems harmonic studies, for instance, orthogonal expansions in the form of Fourier series have been used since they resemble more the sinusoidal waveforms existing in the power system under ideal operating conditions. However, the increasing use of power electronic-based power plant components characterised by rectangular waveforms suggest that other orthogonal basis series could produce better results.

In this chapter, a frame of reference based on orthogonal functions is presented. The motivation of this generalised frame of reference is to investigate more efficient solutions for power systems subjected to periodic excitations.

3.2 State Variable Description of Electric Power Networks

Electric power systems are an important class of electric circuits. Power systems are, to a greater or lesser extent, non-linear circuits. Accordingly, if a formulation is valid for power systems then it is valid for non-linear circuits in general. It is assumed in this Thesis that these networks are described by a canonical equation of the form,

$$\dot{\mathbf{x}} = \mathbf{A}f(\mathbf{x}) + \mathbf{B}g(\mathbf{u}) \tag{3.1}$$

where $\mathbf{A} \in \mathbb{R}^{n\times n}$ and $\mathbf{B} \in \mathbb{R}^{n\times q}$. The state variable $\mathbf{x}$ is an n-vector and $\mathbf{u}$ is a q-vector. The functions $f(\cdot)$ and $g(\cdot)$ are n-vectors of non-linear functions of x_i and u_j, respectively. Equation (3.1) can be represented in block form as shown in Figure 3.1. A problem when analysing equation (3.1) is that few methods are available for studying the PSS response of NLS. The first alternative that springs to mind is the use of numerical integration. However, the computation process may be very slow in cases of lightly damped circuits. Alternatively, if the system operates about a fixed point, then steady state techniques can be used for solving the PSS response can be calculated more efficiently.

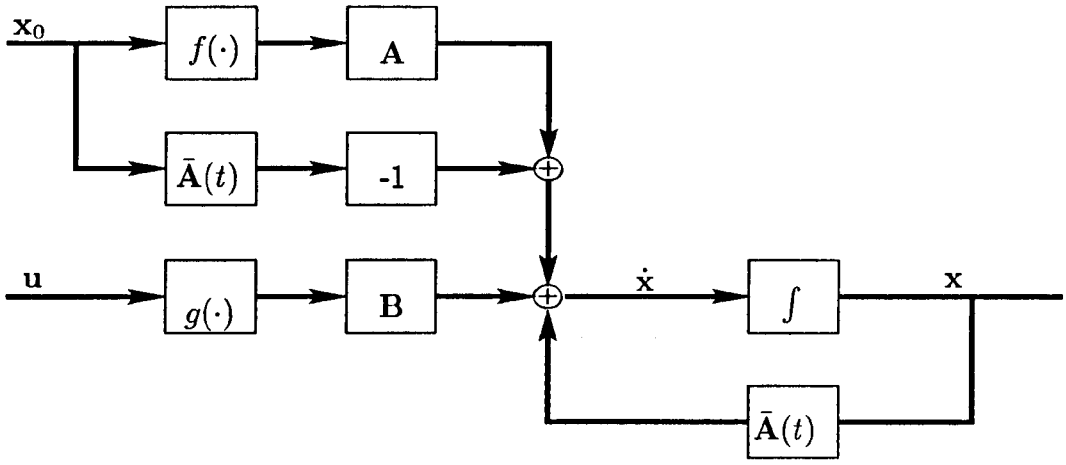

Fig. 3.2: Block diagram of linear, time-varying electric circuits

3.2.1 Linearisation of dynamical equations

Linearisation about a base point $\mathbf{x}_0$ and $\mathbf{u}_0$ yields,

$$\dot{\mathbf{x}} = \mathbf{A}\left(f(\mathbf{x}_0) + \left.\frac{df(\mathbf{x})}{d\mathbf{x}}\right|_{\mathbf{x}_0} \Delta\mathbf{x}\right) + \mathbf{B}g(\mathbf{u}) \tag{3.2}$$

or

$$\dot{\mathbf{x}} = \mathbf{A}\left(\left.\frac{df(\mathbf{x})}{d\mathbf{x}}\right|_{\mathbf{x}_0} \mathbf{x}\right) + \mathbf{A}\left(f(\mathbf{x}_0) - \left.\frac{df(\mathbf{x})}{d\mathbf{x}}\right|_{\mathbf{x}_0} \mathbf{x}_0\right) + \mathbf{B}g(\mathbf{u}) \tag{3.3}$$

In PSS, if $\mathbf{x}$ and $\mathbf{u}$ are periodic then the linear functions $f(\cdot)$, $g(\cdot)$ and $f'(\mathbf{x})$ are also periodic.

If one defines,

$$J = \begin{bmatrix} f_1'(x_1) & & & \\ & f_2'(x_2) & & \\ & & \ddots & \\ & & & f_n'(x_n) \end{bmatrix} \tag{3.4}$$

and

$$\bar{\mathbf{A}}(t) = \mathbf{A}J(t) \tag{3.5}$$

then

$$\dot{\mathbf{x}} = \bar{\mathbf{A}}(t)\mathbf{x} - \bar{\mathbf{A}}(t)\mathbf{x}_0 + \mathbf{B}g(\mathbf{u}) + \mathbf{A}f(\mathbf{x}_0) \tag{3.6}$$

The NLS in equation (3.1) may be approximated, about an operating point , by the linear, time varying circuit shown in Figure 3.2. The structure of equation 3.6 can be further simplified by defining,

$$\bar{f}(\mathbf{x}_0) = \mathbf{A}f(\mathbf{x}_0) - \bar{\mathbf{A}}(t)\mathbf{x}_0 \tag{3.7}$$

and

$$\bar{\mathbf{B}}(t) = \left[\begin{array}{c|cccc} & 1 & & & \\ \mathbf{B} & & 1 & & \\ & & & \ddots & \\ & & & & 1 \end{array}\right] \tag{3.8}$$

so that,

$$\dot{\mathbf{x}} = \bar{\mathbf{A}}(t)\mathbf{x} + \bar{\mathbf{B}}(t)\bar{g}(\bar{\mathbf{u}}) \tag{3.9}$$

where

$$\bar{g}(\bar{\mathbf{u}}) = [\ g(\mathbf{u})^t \mid \bar{f}(\mathbf{x}_0)^t\ ]^t \tag{3.10}$$

For the sake of simplicity, the bar notation is dropped from equation (3.9),

$$\dot{\mathbf{x}} = \mathbf{A}(t)\mathbf{x} + \mathbf{B}(t)\mathbf{u} \tag{3.11}$$

LTVS are a significant class of problem in their own right.

3.2.2 Forms of solution of periodic LTVS

Systems with parameters that vary periodically are an special class of LTVS. Here,

$$\begin{aligned} \mathbf{A}(t+T) &= \mathbf{A}(t) \\ \mathbf{B}(t+T) &= \mathbf{B}(t) \end{aligned} \tag{3.12}$$

where T is the fundamental period.

These systems are characterised by linear equations with periodic coefficients. Because of the periodicity of the coefficients, there are important response properties which are unique to these systems. These properties simplify their analysis and synthesis. The solution becomes simple and several methods can be used.

It can be proved that the general solution of equation (3.11) is [39],

$$\mathbf{x}(t) = \Phi(t, t_0)\mathbf{x}_0 + \int_0^t \Phi(t, \tau)\mathbf{B}(\tau)\mathbf{u}(\tau)d\tau \tag{3.13}$$

where $\Phi(\cdot)$ is a matrix called the state-transition matrix. A major problem with the solution of (3.13) is that the transition matrix $\Phi(\cdot)$ must be known in order to determine $\mathbf{x}(t)$. This is difficult for general LTVS. There is not a unified approach to achieve this task. However, for periodic piecewise constant cases this can be achieved by using Floquet theory [40]. As a concrete example, the analysis of power networks with TCRs has been conducted using this approach [41]. Although this solution does not necessarily apply to the more general case of periodic LTVS, it can be used to approximate smooth transition matrices [39]. Additional ideas and contributions on approximations to transition matrices have been presented in [19, 42]. Transition matrices are approximated in this chapter by using generalised orthogonal expansions.

Method	Linear Time-invariant	Linear Time-Varying	Bilinear
Piecewise orthogonal Functions			
Fourier	[44],[45],[46, 47],	[48],[49, 50]	[48]
Hartley			
Smooth orthogonal Functions			
Walsh	[43],[51, 52, 53, 54] [59, 60, 61] [66],[67],[68],[69]		[55],[56],[57],[58] [62],[63],[64], [65] [70],[71]
Block-Pulse	[72],[73],[74],[75]	[76],[77]	[78],[78]
Haar Wavelets	[79]		
Orthogonal polynomials			
Laguerre	[80, 81, 82]	[83],	[84]
Legendre	[85, 86]	[83],	[84]
Chebyshev (first kind)	[87]	[87],[83],	[84]
Chebyshev (second kind)		[88],[89],[83]	[88],[89],[84]
Jacobi Series	[90]		
Non-orthogonal polynomials			
Taylor Series		[91]	[84],[91]

Tab. 3.1: Literature on operational matrices

3.3 Analysis of Periodic LTVS Via Orthogonal Expansions

Approximation of functions as linear combinations of sets of orthogonal functions is a standard tool in numerical analysis and signal processing. Since Walsh functions were first used by Corrington [43] in 1975 to solve differential and integral equations, orthogonal polynomials and other orthogonal functions have received considerable attention. A summary of methods, applications and references is presented in Table 3.1.

The main advantage of these methods is that they reduce the problem to a system of algebraic equations which can be solved efficiently using computer algorithms. This is achieved by using the concept of operational matrices, a useful tool for solving the problem using matrix algebra. In the following sections these operational matrices are defined in a generalised fashion. Particular applications are presented throughout the Thesis.

3.3.1 A general representation of orthogonal basis

If $\{\gamma_i\}$ is a complete system of orthogonal functions in $t \in [t_i, t_f]$ and f(t) is any function integrable in the interval $t \in [t_i, t_f]$ then,

$$f(t) = \sum_{i=0}^{\infty} f_i \gamma_i(t) \simeq \sum_{i=0}^{m-1} = \mathbf{f}_{(m)}^t \gamma_{(m)} \tag{3.14}$$

with

$$f_i = k \int_{t_i}^{t_f} f(t) \gamma_i dt \tag{3.15}$$

where k is a constant which is different for different set of orthogonal sets $\{f_i\}$. In general, the coefficients are the spectrum components of a given basis. For instance, the coefficients could be the Fourier coefficients and the spectra would be the frequency spectra.

3.3.2 Operational matrix P for integration of $\gamma_{(m)}(t)$

An important feature of the orthogonal basis which is used in the study of TILS and TVLS, is that the integral of basis functions can also be expanded in terms of the same basis. If,

$$\gamma_{(m)}(t) = \begin{bmatrix} \gamma_0(t) \\ \gamma_1(t) \\ \vdots \\ \gamma_{m-1}(t) \end{bmatrix} \tag{3.16}$$

then

$$\int_{ti}^{t} \gamma_{(m)}(t)d(t) = P \begin{bmatrix} \gamma_0(t) \\ \gamma_1(t) \\ \vdots \\ \gamma_{m-1}(t) \end{bmatrix} \tag{3.17}$$

where P is the operational matrix of integration which has different values for different orthogonal basis.

3.3.3 Operational matrix D for differentiation of $\gamma_{(m)}(t)$

Similarly to the operational matrix of integration, it is possible to show that,

$$\frac{d\gamma_{(m)}(t)}{dt} = D\gamma_{(m)}(t) \tag{3.18}$$

or, for higher order derivatives,

$$\frac{d^i\gamma_{(m)}(t)}{dt} = D^i\gamma_{(m)}(t) \tag{3.19}$$

where D is the $m \times m$ differentiation operational matrix. In general, D may be obtained as the inverse of P. However, care must be taken when using this concept to calculate the derivatives of $\gamma_{(m)}$(t) if the application involves piecewise basis. This is the case of Walsh, Haar and block-pulse series. It was pointed out by Corrington [43] that the derivatives of such series result in series of delta-Dirac impulses, one for each discontinuity. Accordingly, the use of these series is not recommended for the study of differential equations. For instance, the Walsh expansion of the derivative of a Walsh function is, usually, a divergent Walsh series.

3.3.4 Transformation operational matrix W

Consider a signal $f(t)$ represented in a particular orthogonal basis as,

$$f(t) = \mathbf{c}_1^t\gamma_{(m)}^1(t) \tag{3.20}$$

and the same signal represented by a different orthogonal basis,

$$f(t) = \mathbf{c}_2^t\gamma_{(m)}^2(t) \tag{3.21}$$

Both coefficient vectors $\mathbf{c}_1$ and $\mathbf{c}_2$ are components of a Hilbert space representing the same signal over the interval $(0, T)$. Each vector can be expressed as linear combination of components of the other vector,

$$\mathbf{c}_1 = W\mathbf{c}_2 \tag{3.22}$$

If W represent an orthogonal transformation, i.e. a rotation of the Hilbert space coordinates system, then the inverse transformation, W^{-1}, equals the transposed transformation W^t,

$$\mathbf{c}_2 = W^t\mathbf{c}_1 = W^{-1}\mathbf{c}1 \tag{3.23}$$

3.3.5 Product and coefficients matrices

The product of a vector of orthogonal functions, $\gamma_{(m)}(t)$, and its transposed, $\gamma^t_{(m)}(t)$, is called the product matrix $\Gamma_{(m\times m)}(t)$. That is,

$$\gamma_{(m)}(t)\gamma^t_{(m)}(t) = \Gamma_{(m\times m)}(t) \tag{3.24}$$

For some orthogonal basis this matrix can be formed, in a systematic way, by using a computer algorithm. Several examples are presented in this Thesis. Product matrices for Fourier, Walsh and Hartley domains are provided.

Similarly, the coefficient matrix $\mathbf{C}$ corresponding to the coefficient vector $\mathbf{c}_{(m)}$ is defined as follows,

$$\mathbf{C} = \mathbf{c}_{(m)}\mathbf{c}^t_{(m)} \tag{3.25}$$

An important property of product and coefficient matrices is that they facilitate LTVS computations [56, 55],

$$\Gamma_{(m\times m)}\mathbf{c}_{(m)} = \mathbf{C}\gamma_{(m)} \tag{3.26}$$

3.3.6 Analysis of LTVS

Consider equation (3.11) where $\mathbf{x}_0$ is specified. Let $a_{ij}(t)$ and $b_{ij}(t)$ be the elements of $\mathbf{A}(t)$ and $\mathbf{B}(t)$. Assume that all elements are absolutely integrable in the time interval [0,T) then the generalised series approximation of all elements of $\mathbf{A}(t)$ and $\mathbf{B}(t)$ become,

$$a_{ij}(t) \approxeq \mathbf{A}^t_{ij}\gamma_{(m)}(t) \tag{3.27}$$

$$b_{ij}(t) \approxeq \mathbf{B}^t_{ij}\gamma_{(m)}(t) \tag{3.28}$$

where

$$\mathbf{A}^t_{ij} = [\ \mathbf{A}_{ij,0}\ \ \mathbf{A}_{ij,1}\ \ \ldots\ \ \mathbf{A}_{ij,m}\ ] \tag{3.29}$$

$$\mathbf{B}^t_{ij} = [\ \mathbf{B}_{ij,0}\ \ \mathbf{B}_{ij,1}\ \ \ldots\ \ \mathbf{B}_{ij,m}\ ] \tag{3.30}$$

Similarly, $\mathbf{x}(t)$ and $\mathbf{u}(t)$ may be expanded as,

$$x_i(t) \approxeq \mathbf{X}^t_i\gamma_{(m)}(t) \tag{3.31}$$

$$u_i(t) \approxeq \mathbf{U}^t_i\gamma_{(m)}(t) \tag{3.32}$$

where

$$\mathbf{X}_i^t = [\ \mathbf{X}_{i,0}\ \ \mathbf{X}_{i,1}\ \ \ldots\ \ \mathbf{X}_{i,m}\ ] \tag{3.33}$$
$$\mathbf{U}_i^t = [\ \mathbf{U}_{i,0}\ \ \mathbf{U}_{i,1}\ \ \ldots\ \ \mathbf{U}_{i,m}\ ] \tag{3.34}$$

Therefore, the following relations can be derived,

$$\mathbf{A}(t) \approxeq \begin{bmatrix} \mathbf{A}_{11}^t\gamma_{(m)}(t) & \mathbf{A}_{12}^t\gamma_{(m)}(t) & \ldots & \mathbf{A}_{1n}\gamma_{(m)}(t) \\ \mathbf{A}_{21}^t\gamma_{(m)}(t) & \mathbf{A}_{22}^t\gamma_{(m)}(t) & \ldots & \mathbf{A}_{2n}\gamma_{(m)}(t) \\ \vdots & \vdots & \ddots & \vdots \\ \mathbf{A}_{n1}^t\gamma_{(m)}(t) & \mathbf{A}_{n2}^t\gamma_{(m)}(t) & \ldots & \mathbf{A}_{nn}\gamma_{(m)}(t) \end{bmatrix}_{(n\times n)} \tag{3.35}$$

$$\approxeq \begin{bmatrix} \mathbf{A}_{11}^t & \mathbf{A}_{12}^t & \ldots & \mathbf{A}_{1n} \\ \mathbf{A}_{21}^t & \mathbf{A}_{22}^t & \ldots & \mathbf{A}_{2n} \\ \vdots & \vdots & \ddots & \vdots \\ \mathbf{A}_{n1}^t & \mathbf{A}_{n2}^t) & \ldots & \mathbf{A}_{nn} \end{bmatrix} \begin{bmatrix} \gamma_{(m)}(t) & 0 & \ldots & 0 \\ 0 & \gamma_{(m)}(t) & \ldots & 0 \\ \vdots & \vdots & \ddots & \vdots \\ 0 & 0 & \ldots & \gamma_{(m)}(t) \end{bmatrix} \tag{3.36}$$

$$\approxeq \widehat{A}\,\widehat{\Gamma}(t) \tag{3.37}$$

and

$$\begin{bmatrix} x_1(t) \\ x_2(t) \\ \vdots \\ x_n(t) \end{bmatrix} \approxeq \begin{bmatrix} \mathbf{X}_1^t\gamma_{(m)}(t) \\ \mathbf{X}_2^t\gamma_{(m)}(t) \\ \vdots \\ \mathbf{X}_n^t\gamma_{(m)}(t) \end{bmatrix} = \begin{bmatrix} \mathbf{X}_1^t \\ \mathbf{X}_2^t \\ \vdots \\ \mathbf{X}_n^t \end{bmatrix} \gamma_{(m)}(t) = \mathbf{X}\gamma_{(m)}(t) \tag{3.38}$$

The product $\mathbf{A}(t)\mathbf{x}(t)$ can be expressed as follows,

$$\mathbf{A}(t)\mathbf{x}(t) \approxeq \begin{bmatrix} \mathbf{A}_{11}\gamma_{(m)}(t)\mathbf{X}_1^t\gamma_{(m)}(t) + \mathbf{A}_{12}\gamma_{(m)}(t)\mathbf{X}_2^t\gamma_{(m)}(t) + \ldots + \mathbf{A}_{1n}\gamma_{(m)}(t)\mathbf{X}_n^t\gamma_{(m)}(t) \\ \mathbf{A}_{21}\gamma_{(m)}(t)\mathbf{X}_1^t\gamma_{(m)}(t) + \mathbf{A}_{22}\gamma_{(m)}(t)\mathbf{X}_2^t\gamma_{(m)}(t) + \ldots + \mathbf{A}_{2n}\gamma_{(m)}(t)\mathbf{X}_n^t\gamma_{(m)}(t) \\ \vdots \\ \mathbf{A}_{n1}\gamma_{(m)}(t)\mathbf{X}_1^t\gamma_{(m)}(t) + \mathbf{A}_{n2}\gamma_{(m)}(t)\mathbf{X}_2^t\gamma_{(m)}(t) + \ldots + \mathbf{A}_{nn}\gamma_{(m)}(t)\mathbf{X}_n^t\gamma_{(m)}(t) \end{bmatrix}$$

$$\approxeq \begin{bmatrix} \mathbf{X}_1\mathbf{C}_{\mathbf{A}_{11}}\gamma_{(m)}(t) + \mathbf{X}_2^t\mathbf{C}_{\mathbf{A}_{12}}\gamma_{(m)}(t) + \ldots + \mathbf{X}_n^t\mathbf{C}_{\mathbf{A}_{1n}}\gamma_{(m)}(t) \\ \mathbf{X}_1\mathbf{C}_{\mathbf{A}_{21}}\gamma_{(m)}(t) + \mathbf{X}_2^t\mathbf{C}_{\mathbf{A}_{22}}\gamma_{(m)}(t) + \ldots + \mathbf{X}_n^t\mathbf{C}_{\mathbf{A}_{2n}}\gamma_{(m)}(t) \\ \vdots \\ \mathbf{X}_1\mathbf{C}_{\mathbf{A}_{n1}}\gamma_{(m)}(t) + \mathbf{X}_2^t\mathbf{C}_{\mathbf{A}_{n2}}\gamma_{(m)}(t) + \ldots + \mathbf{X}_n^t\mathbf{C}_{\mathbf{A}_{nn}}\gamma_{(m)}(t) \end{bmatrix} \tag{3.39}$$

$$\approxeq \begin{bmatrix} \mathbf{A}_1 \\ \mathbf{A}_2 \\ \vdots\mathbf{A}_n \end{bmatrix} \gamma_{(m)}(t) \tag{3.40}$$

where the use of product and coefficient matrices allow us to write,

$$\mathbf{A}_{ij}^t\gamma_{(m)}(t)\mathbf{X}_j\gamma_{(m)}(t) = \mathbf{X}_j\gamma_{(m)}(t)\gamma_{(m)}^t(t)\mathbf{A}_{ij} = \mathbf{X}_j^t\mathbf{C}_{\mathbf{A}_{ij}} \tag{3.41}$$

and

$$\mathbf{A}_i = \sum_{j=1}^{n} \mathbf{X}_j\mathbf{C}_{\mathbf{A}_{ij}} \tag{3.42}$$

Where $\mathbf{X}_j\mathbf{C}_{\mathbf{A}_{ij}}$ is the coefficient matrix corresponding to vector $\mathbf{A}_{ij}$.

Now it is possible to reconstruct the product $\mathbf{A}(t)\mathbf{x}(t)$ in a more convenient form,

$$\begin{aligned}
\left[\ \mathbf{A}_1 \quad \mathbf{A}_2 \quad \dots \quad \mathbf{A}_n\ \right]\widehat{\Gamma}(t) &= \left[\ \mathbf{X}_1^t \quad \mathbf{X}_2^t \quad \dots \quad \mathbf{X}_n^t\ \right]\begin{bmatrix} \mathbf{C}_{\mathbf{A}_{11}} & \mathbf{C}_{\mathbf{A}_{12}} & \dots & \mathbf{C}_{\mathbf{A}_{1n}} \\ \mathbf{C}_{\mathbf{A}_{21}} & \mathbf{C}_{\mathbf{A}_{22}} & \dots & \mathbf{C}_{\mathbf{A}_{2n}} \\ \vdots & \vdots & \ddots & \vdots \\ \mathbf{C}_{\mathbf{A}_{n1}} & \mathbf{C}_{\mathbf{A}_{n2}} & \dots & \mathbf{C}_{\mathbf{A}_{nn}} \end{bmatrix}\widehat{\Gamma}(t) \\
&= \mathbf{X}\mathbb{A}\bar{\Gamma}(t) \qquad (3.43)
\end{aligned}$$

In the same way, we can expand $\mathbf{B}(t)$ and $\mathbf{u}(t)$ as follows,

$$\mathbf{B}(t) \approxeq \begin{bmatrix} \mathbf{B}_{11}^t\gamma_{(m)}(t) & \mathbf{B}_{12}^t\gamma_{(m)}(t) & \dots & \mathbf{B}_{1q}\gamma_{(m)}(t) \\ \mathbf{B}_{21}^t\gamma_{(m)}(t) & \mathbf{B}_{22}^t\gamma_{(m)}(t) & \dots & \mathbf{B}_{2q}\gamma_{(m)}(t) \\ \vdots & \vdots & \ddots & \vdots \\ \mathbf{B}_{n1}^t\gamma_{(m)}(t) & \mathbf{B}_{n2}^t\gamma_{(m)}(t) & \dots & \mathbf{B}_{nq}\gamma_{(m)}(t) \end{bmatrix}_{(n\times q)} \qquad (3.44)$$

$$\approxeq \begin{bmatrix} \mathbf{B}_{11}^t & \mathbf{B}_{12}^t & \dots & \mathbf{B}_{1q} \\ \mathbf{B}_{21}^t & \mathbf{B}_{22}^t & \dots & \mathbf{B}_{2q} \\ \vdots & \vdots & \ddots & \vdots \\ \mathbf{B}_{n1}^t & \mathbf{B}_{n2}^t) & \dots & \mathbf{B}_{nq} \end{bmatrix}\begin{bmatrix} \gamma_{(m)}(t) & 0 & \dots & 0 \\ 0 & \gamma_{(m)}(t) & \dots & 0 \\ \vdots & \vdots & \ddots & \vdots \\ 0 & 0 & \dots & \gamma_{(m)}(t) \end{bmatrix} \qquad (3.45)$$

$$\approxeq \widehat{B}\,\widehat{\Gamma}(t) \qquad (3.46)$$

and

$$\begin{bmatrix} u_1(t) \\ u_2(t) \\ \vdots \\ u_n(t) \end{bmatrix} \approxeq \begin{bmatrix} \mathbf{U}_1^t\gamma_{(m)}(t) \\ \mathbf{U}_2^t\gamma_{(m)}(t) \\ \vdots \\ \mathbf{U}_n^t\gamma_{(m)}(t) \end{bmatrix} = \begin{bmatrix} \mathbf{U}_1^t \\ \mathbf{U}_2^t \\ \vdots \\ \mathbf{U}_n^t \end{bmatrix}\gamma_{(m)}(t) = \mathbf{U}\gamma_{(m)}(t) \qquad (3.47)$$

to express the product $\mathbf{B}(t)\mathbf{u}(t)$ as,

$$\begin{aligned}
\left[\ \mathbf{B}_1 \quad \mathbf{B}_2 \quad \dots \quad \mathbf{B}_n\ \right]\widehat{\Gamma}(t) &= \left[\ \mathbf{U}_1^t \quad \mathbf{U}_2^t \quad \dots \quad \mathbf{U}_n^t\ \right]\begin{bmatrix} \mathbf{C}_{\mathbf{B}_{11}} & \mathbf{C}_{\mathbf{B}_{12}} & \dots & \mathbf{C}_{\mathbf{B}_{1n}} \\ \mathbf{C}_{\mathbf{B}_{21}} & \mathbf{C}_{\mathbf{B}_{22}} & \dots & \mathbf{C}_{\mathbf{B}_{2n}} \\ \vdots & \vdots & \ddots & \vdots \\ \mathbf{C}_{\mathbf{B}_{n1}} & \mathbf{C}_{\mathbf{B}_{n2}} & \dots & \mathbf{C}_{\mathbf{B}_{nn}} \end{bmatrix}\widehat{\Gamma}(t) \\
&= \mathbf{X}\mathbb{B}\bar{\Gamma}(t) \qquad (3.48)
\end{aligned}$$

where

$$\mathbf{B}_i = \sum_{j=1}^{q}\mathbf{U}_j\mathbf{C}_{\mathbf{B}_{ij}} \qquad (3.49)$$

Now, integration of equation (3.11) from 0 to t yields,

$$\mathbf{x} - \mathbf{x}_0 = \int_0^t \mathbf{A}(\tau)\mathbf{x}(\tau)d\tau + \int_0^t \mathbf{B}(\tau)\mathbf{u}(t\tau)d\tau \qquad (3.50)$$

Substitution of equations (3.43) and (3.48) into equation (3.50) yields,

$$\mathbf{X}\bar{\Gamma}(t) - \mathbf{X}_0\bar{\Gamma}(t) = \int_0^t \mathbf{X}\mathbb{A}\bar{\Gamma}(\tau)d\tau + \int_0^t \mathbf{U}\mathbb{B}\bar{\Gamma}(\tau)d\tau \qquad (3.51)$$

or

$$\mathbf{X}\bar{\Gamma}(t) - \mathbf{X}_0\bar{\Gamma}(t) = \mathbf{XA}\int_0^t \bar{\Gamma}(\tau)d\tau + \mathbf{UB}\int_0^t \bar{\Gamma}(\tau)d\tau \tag{3.52}$$

Using the operational matrix of integration, we have that,

$$\begin{aligned}\int_0^t \bar{\Gamma}(\tau)d\tau &= \begin{bmatrix} \int_0^t \gamma_{(m)}(\tau)d\tau & 0 & \dots & 0 \\ 0 & \int_0^t \gamma_{(m)}(\tau)d\tau & \dots & 0 \\ \vdots & \vdots & \ddots & \vdots \\ 0 & 0 & \dots & \int_0^t \gamma_{(m)}(\tau)d\tau \end{bmatrix} \\ &= \begin{bmatrix} P & 0\dots & 0 & \\ 0 & P & \dots & 0 \\ \vdots & \vdots & \ddots & \vdots \\ 0 & 0 & \dots & P \end{bmatrix} \bar{\Gamma}(t) = \mathbb{P}\bar{\Gamma}(t)\end{aligned} \tag{3.53}$$

Then equation (3.52) can be expressed in compact form as,

$$\mathbf{X}\bar{\Gamma}(t) - \mathbf{X}_0\bar{\Gamma}(t) = \mathbf{XA}\mathbb{P}\bar{\Gamma}(t) + \mathbf{UB}\mathbb{P}\bar{\Gamma}(t) \tag{3.54}$$

Equation (3.54) represent as set of nm linear algebraic equations that can be solved as follows,

$$\mathbf{X}(\mathbf{I} - \mathbf{A}\mathbb{P}) = \mathbf{UB}\mathbb{P} + \mathbf{X}_0 \tag{3.55}$$

or

$$\mathbf{X} = (\mathbf{UB}\mathbb{P} + \mathbf{X}_0)(\mathbf{I} - \mathbf{A}\mathbb{P})^{-1} \tag{3.56}$$

where $\mathbf{I}$ is a $nm \times nm$ identity matrix and

$$\mathbf{X}_0 = [\ x_1(0)\ \ 0\ \ \dots\ \ 0\ \vdots\ x_2(0)\ \ 0\ \ \dots\ \ 0\ \vdots\ \dots\ \vdots\ x_r(0)\ \ 0\ \ \dots\ \ 0\ ] \tag{3.57}$$

3.4 Tableau Analysis in the Generalised Domain

In order to take advantage of operational matrices of integration, product and coefficients, the electric circuits under analysis are expressed in their state variable form i.e. Equation 3.1. Such representation can be obtained by inspection of the electric network structure and by proper selection of the state variables. Inspection methods can be easily applied to generate the state variable equations of a given network, however, developing computer algorithms capable of generating the state variables equations, can be a difficult task. It must be remarked that several state descriptions of the system are possible, since the circuit can be described by different sets of state variables [92]. However, more general methods are possible. They can be efficiently implemented in computer algorithms. Two methods of analysis that can be applied to any dynamic circuits are Sparse Tableau Method (STM) and the Modified Nodal Analysis (MNA) [93]. The two alternative can easily be combined with the use of operational matrices. The salient characteristics of the STM method are presented below.

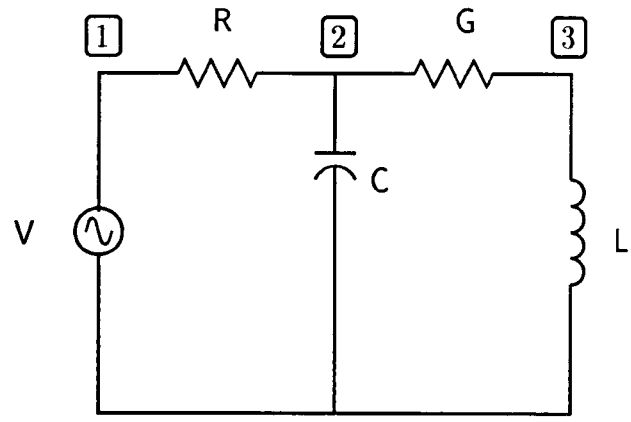

Fig. 3.3: RLC circuit

3.4.1 Tableau analysis for invariant linear systems

When formulating equations for hand solutions, an obvious objective is to write as few equations as possible. However, the opposite is true for the STM, where as many equations as possible are written. The Tableau involves many more equations than alternative approaches such as MNA. Fortunately, STM is extremely sparse. In fact, the analysis of circuits using STM yields a set of equations which is more sparse than any other approach. The STM is a powerful analytical tool for studying general purpose circuits. It segregates Kirchhoffs' laws from branch equations. STM is considered an excellent tool for studying distortion in power systems where each power plant component can have a very particular description. It is shown in this chapter, that the above characteristic of STM allows us to formulate generalised hybrid methods.

3.4.2 STM for LTIS

The STM is a conceptually simple method. It consists of writing out a complete list of linearly independent KCL and KVL equations and branch equations. By collecting these three conditions into a unique matrix relation we have that,

$$\begin{bmatrix} \mathbf{A} & \mathbf{0} & \mathbf{0} \\ \mathbf{0} & \mathbf{I} & \mathbf{A}^t \\ \mathbf{M}_i \int & \mathbf{N}_v \int & \mathbf{0} \end{bmatrix} \begin{bmatrix} i \\ v \\ v_n \end{bmatrix} = \begin{bmatrix} \mathbf{0} \\ \mathbf{0} \\ \mathbf{u} \end{bmatrix} \tag{3.58}$$

where $\mathbf{A}$ is the incidence matrix of the circuit and $\mathbf{N}$ and $\mathbf{M}$ are branch operators which can be in differential or integral form. Some orthogonal expansions such as Walsh and Haar series are difficult to operate since they generate trains of pulses when differentiated. Hence, the integral form of $\mathbf{N}$ and $\mathbf{M}$ are preferred. The salient features of STM can be demonstrated by example. Consider the circuit in Figure 3.3. The incidence matrix is,

$$\mathbf{A} = \begin{array}{c} \overbrace{\begin{array}{ccccc} V & R & C & G & L \end{array}} \\ \begin{bmatrix} \mathbf{I} & \mathbf{I} & \mathbf{0} & \mathbf{0} & \mathbf{0} \\ \mathbf{0} & -\mathbf{I} & \mathbf{I} & \mathbf{I} & \mathbf{0} \\ \mathbf{0} & \mathbf{0} & \mathbf{0} & -\mathbf{I} & \mathbf{I} \end{bmatrix} \end{array} \begin{array}{c} \\ \boxed{1} \\ \boxed{2} \\ \boxed{3} \end{array}$$

The static and dynamic elements are modeled independently, with the following relations:

Inductor

$$i_L = \frac{1}{L}\int_0^t v_L(t)dt + i_L(0) \tag{3.59}$$

Capacitor

$$v_c = \frac{1}{C}\int_0^t i_c(t)dt + v_c(0) \tag{3.60}$$

Resistor

$$v_R = Ri_R \tag{3.61}$$

Conductance

$$i_G = Gv_G \tag{3.62}$$

Using the operational matrix of integration we have that,

Inductor

$$\begin{bmatrix} I_{L_0} \\ I_{L-1} \\ \vdots \\ I_{L_{m-1}} \end{bmatrix} = \frac{1}{L}P^t \begin{bmatrix} V_{L_0} \\ V_{L-1} \\ \vdots \\ V_{L_{m-1}} \end{bmatrix} + \begin{bmatrix} i_L(0) \\ 0 \\ \vdots \\ 0 \end{bmatrix} = \frac{1}{L}P^t\mathbf{v}_L + \mathbf{i}_L(0) \tag{3.63}$$

Capacitor

$$\begin{bmatrix} V_{C_0} \\ V_{C_1} \\ \vdots \\ V_{C_{m-1}} \end{bmatrix} = \frac{1}{L}P^t \begin{bmatrix} I_{C_0} \\ I_{C-1} \\ \vdots \\ I_{C_{m-1}} \end{bmatrix} + \begin{bmatrix} v_c(0) \\ 0 \\ \vdots \\ 0 \end{bmatrix} = \frac{1}{L}P^t\mathbf{I}_C + \mathbf{v}_C(0) \tag{3.64}$$

Resistor

$$\begin{bmatrix} V_{R_0} \\ V_{R_1} \\ \vdots \\ V_{R_{m-1}} \end{bmatrix} = R\mathbf{I} \begin{bmatrix} I_{R_0} \\ I_{R-1} \\ \vdots \\ I_{R_{m-1}} \end{bmatrix} = R\mathbf{I}\mathbf{i}_R \tag{3.65}$$

Conductance

$$\begin{bmatrix} I_{G_0} \\ I_{G_1} \\ \vdots \\ I_{G_{m-1}} \end{bmatrix} = GP^t \begin{bmatrix} V_{G_0} \\ V_{G_1} \\ \vdots \\ V_{G_{m-1}} \end{bmatrix} = G\mathbf{I}\mathbf{v}_G \tag{3.66}$$

Collecting expressions (3.63) to (3.66) into a single equation we have that,

$$\left[\begin{array}{cccccccccccc|cc}
I & I & 0 & 0 & 0 & 0 & 0 & 0 & 0 & 0 & 0 & 0 & 0 & 0 \\
0 & -I & I & I & 0 & 0 & 0 & 0 & 0 & 0 & 0 & 0 & 0 & 0 \\
0 & 0 & 0 & -I & I & 0 & 0 & 0 & 0 & 0 & 0 & 0 & 0 & 0 \\
0 & 0 & 0 & 0 & 0 & I & 0 & 0 & 0 & 0 & -I & 0 & 0 & 0 \\
0 & 0 & 0 & 0 & 0 & 0 & I & 0 & 0 & 0 & -I & I & 0 & 0 \\
0 & 0 & 0 & 0 & 0 & 0 & 0 & I & 0 & 0 & 0 & -I & 0 & 0 \\
0 & 0 & 0 & 0 & 0 & 0 & 0 & 0 & I & 0 & 0 & -I & I & 0 \\
0 & 0 & 0 & 0 & 0 & 0 & 0 & 0 & 0 & I & 0 & 0 & I & 0 \\
0 & 0 & 0 & 0 & 0 & I & 0 & 0 & 0 & 0 & 0 & 0 & 0 & 0 \\
0 & R & 0 & 0 & 0 & 0 & -I & 0 & 0 & 0 & 0 & 0 & 0 & 0 \\
0 & 0 & I & 0 & 0 & 0 & 0 & \frac{1}{L}P^t & 0 & 0 & 0 & 0 & 0 & 1 \\
0 & 0 & 0 & I & 0 & 0 & 0 & 0 & G & 0 & 0 & 0 & 0 & 0 \\
0 & 0 & 0 & 0 & -\frac{1}{C}P^t & 0 & 0 & 0 & 0 & -I & 0 & 0 & 0 & 1 \\
\hline
0 & 0 & 0 & 0 & \phi(1) & 0 & 0 & 0 & 0 & 0 & 0 & 0 & 0 & -1 \\
0 & 0 & 0 & 0 & 0 & 0 & 0 & \phi(1) & 0 & 0 & 0 & 0 & 0 & -1
\end{array}\right]
\begin{bmatrix} i_V \\ i_R \\ i_C \\ i_G \\ i_L \\ V_V \\ V_R \\ V_C \\ V_G \\ V_L \\ V_1 \\ V_2 \\ V_3 \\ i_L(0) \\ v_C(0) \end{bmatrix}
=
\begin{bmatrix} 0 \\ 0 \\ 0 \\ 0 \\ 0 \\ 0 \\ 0 \\ \mathbf{V} \\ 0 \\ 0 \\ 0 \\ 0 \\ 0 \\ 0 \end{bmatrix}$$

or, in compact form,

$$\mathbf{T}\mathbf{x} = d \tag{3.67}$$

The initial conditions are given as,

$$[\ \phi_0(1)\ \ \phi_1(1)\ \ \ldots\ \ \phi_{m-1}(1)\ ]\mathbf{b} = b(0) = \phi\mathbf{b}$$

3.4.3 Tableau analysis for LTVS

If the circuit elements are time-varying capacitances or inductances, the tableau equation can be rewritten as follows,

$$\begin{bmatrix} \mathbf{A} & \mathbf{0} & \mathbf{0} \\ \mathbf{0} & \mathbf{I} & \mathbf{A}^t \\ \mathbf{M}_i(t)\int & \mathbf{N}_v(t)\int & \mathbf{0} \end{bmatrix} \begin{bmatrix} i \\ v \\ v_n \end{bmatrix} = \begin{bmatrix} \mathbf{0} \\ \mathbf{0} \\ \mathbf{u} \end{bmatrix} \tag{3.68}$$

or, in compact form,

$$\mathbf{A}(t)\mathbf{x}(t) = d \tag{3.69}$$

Then, by using the representation of the product $\mathbf{A}(t)\mathbf{x}(t)$ in equation (3.48), the solution can be expressed as follows,

$$\mathbf{X}\mathbf{A} = \mathbf{d}^t \tag{3.70}$$

where vector $\mathbf{d}$ contains the coefficients resulting from the expansion of each term in d.

3.5 Generalised Hybrid Methods

The STM formulation relates a group of voltages and currents waveforms to another group of voltages and currents waveforms. Therefore, matrix $\mathbf{A}$ in equation (3.69) is closely related to the generalised concept of immittance [69]. The fact that the STM segregates Kirchhoffs' laws and branch equations allows this method to relate different variables and to enclose any hybrid method [17, 19]. The method can take advantage of the fact that particular power

plant components can be modelled more efficiently in a particular domain. By way of example, lets assume that in the example in section 3.4.2 the capacitor is modelled using a different domain than the rest of the system. If one were to represent the set of orthogonal functions relating the capacitor by $\chi_m(t)$ and W the operational matrix for transforming variables from the domain of $\chi_m(t)$ to the base domain of W, then the hybrid STM is expressed as,

$$\left[\begin{array}{cccccccccccc|cc}
I & I & 0 & 0 & 0 & 0 & 0 & 0 & 0 & 0 & 0 & 0 & 0 & 0 \\
0 & -I & W & I & 0 & 0 & 0 & 0 & 0 & 0 & 0 & 0 & 0 & 0 \\
0 & 0 & 0 & -I & I & 0 & 0 & 0 & 0 & 0 & 0 & 0 & 0 & 0 \\
0 & 0 & 0 & 0 & 0 & I & 0 & 0 & 0 & 0 & -I & 0 & 0 & 0 \\
0 & 0 & 0 & 0 & 0 & 0 & I & 0 & 0 & 0 & -I & I & 0 & 0 \\
0 & 0 & 0 & 0 & 0 & 0 & 0 & W & 0 & 0 & 0 & -I & 0 & 0 \\
0 & 0 & 0 & 0 & 0 & 0 & 0 & 0 & I & 0 & 0 & -I & I & 0 \\
0 & 0 & 0 & 0 & 0 & 0 & 0 & 0 & 0 & I & 0 & 0 & I & 0 \\
0 & 0 & 0 & 0 & 0 & I & 0 & 0 & 0 & 0 & 0 & 0 & 0 & 0 \\
0 & R & 0 & 0 & 0 & 0 & -I & 0 & 0 & 0 & 0 & 0 & 0 & 0 \\
0 & 0 & I & 0 & 0 & 0 & 0 & \frac{1}{L}P^t & 0 & 0 & 0 & 0 & 0 & 1 \\
0 & 0 & 0 & I & 0 & 0 & 0 & 0 & G & 0 & 0 & 0 & 0 & 0 \\
0 & 0 & 0 & 0 & -\frac{1}{C}P_W^t & 0 & 0 & 0 & 0 & -I & 0 & 0 & 0 & 1 \\
\hline
0 & 0 & 0 & 0 & \phi(1) & 0 & 0 & 0 & 0 & 0 & 0 & 0 & 0 & -1 \\
0 & 0 & 0 & 0 & 0 & 0 & 0 & \phi(1) & 0 & 0 & 0 & 0 & 0 & -1
\end{array}\right]
\begin{bmatrix} i_V \\ i_R \\ i_C \\ i_G \\ i_L \\ V_V \\ V_R \\ V_C \\ V_G \\ V_L \\ V_1 \\ V_2 \\ V_3 \\ i_L(0) \\ v_C(0) \end{bmatrix}
=
\begin{bmatrix} 0 \\ 0 \\ 0 \\ 0 \\ 0 \\ 0 \\ 0 \\ 0 \\ \mathbf{V} \\ 0 \\ 0 \\ 0 \\ 0 \\ 0 \\ 0 \end{bmatrix}$$

In this way, it is shown that matrix A in the STM is not just an immittance matrix relating a group of variables to another group of variables of the same kind but rather this immittance matrix can also group variables represented in different domains.

3.6 Modified Nodal Analysis (MNA)

Nodal Analysis (NA) for the study of electric power systems has proved very popular. The nodal matrix in this formulation can be efficiently handled in the computer. In general, the admittance matrix is very sparse and solution algorithm can be designed to take advantage of this feature where the equation for a given circuit can be easily written by inspection. Furthermore, the number of equations is always smaller than that generated by using STM. NA has been extended to incorporate the dynamic equations of a the network. Such extension has been termed the Modified Nodal Analysis (MNA) method. The dynamic equations can be generated by inspection but since they contain information about the network interconnection as well as information about the nature of the branches, the equations may not have the clarity observed in STM where this information is clearly segregated. Owing to this, the degree of generalisation obtained with STM may not be easily achieved with MNA.

The Underlying ideas of the MNA are: (1) Write the NA equations using nodal voltages and (2) whenever an element is not voltage-controlled, new variables are introduced to the node variables vector and the the branch equation is added to the nodal matrix.

To show the salient characteristics of MNA the single phase network of Figure 3.4 is analysed.

Node equations

$$-i_1 + i_6 = 0 \tag{3.71}$$

$$i_1 - i_2 - C_L\frac{dv_2}{dt} - i_4 = 0 \tag{3.72}$$

$$i_4 - C_L\frac{dv_3}{dt} = 0 \tag{3.73}$$

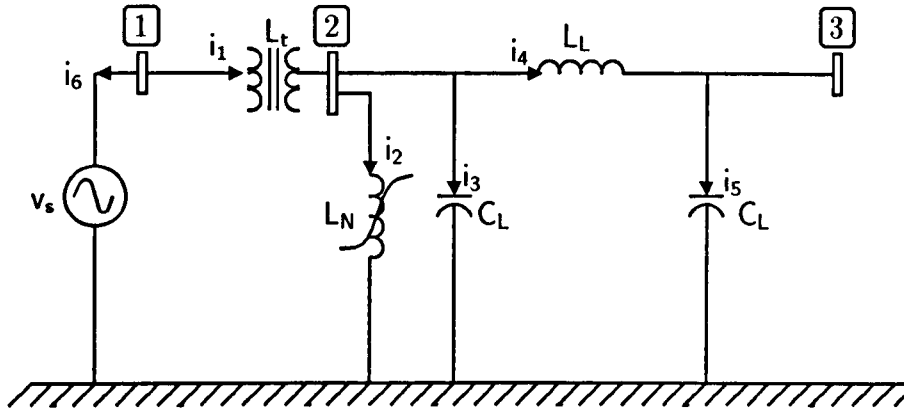

Fig. 3.4: Single phase transmission system

Linear Inductor

$$v_2 - v_1 - L_t \frac{di_1}{dt} = 0 \tag{3.74}$$

$$v_3 - v_2 - L_L \frac{di_4}{dt} = 0 \tag{3.75}$$

Non-Linear inductor

$$v_2 - L_N(i_2)\frac{di_2}{dt} = 0 \tag{3.76}$$

where

$$\frac{1}{L_N}(i_2) = \frac{di_4}{d\varphi} \tag{3.77}$$

and

$$i = f(\varphi) = a\varphi + b\varphi^n \tag{3.78}$$

$$v = \frac{d\varphi}{dt} \tag{3.79}$$

Voltage source

$$v_1 = v_s \tag{3.80}$$

Then MNA, in matrix form, is

$$\begin{bmatrix} v_s \\ 0 \\ 0 \\ 0 \\ 0 \\ 0 \end{bmatrix} = \begin{bmatrix} 1 & & & & & \\ & -C_L\frac{d}{dt} & & 1 & -1 & -1 \\ & & -C_L\frac{d}{dt} & & & 1 \\ -1 & 1 & & -L_t\frac{d}{dt} & & \\ & -1 & 1 & & & -L_L\frac{d}{dt} \\ & 1 & & & -L_N(i_4)\frac{d}{dt} & \end{bmatrix} \begin{bmatrix} v_1 \\ v_2 \\ v_3 \\ i_1 \\ i_2 \\ i_4 \end{bmatrix} \tag{3.81}$$

By using the operational matrix of derivation, D, and approximating voltages and currents as,

$$v_i(t) \approxeq V^t_{(m)}\gamma_{(m)}(t), \qquad i = 1,2,3 \tag{3.82}$$

$$i_i(t) \approxeq I^t_{(m)}\gamma_{(m)}(t), \qquad i = 1,2,4 \tag{3.83}$$

$$\tag{3.84}$$

Equation (3.81) becomes,

$$\begin{bmatrix} V_s \\ \hline 0 \\ \hline 0 \\ \hline 0 \\ \hline 0 \\ \hline 0 \end{bmatrix} = \left[\begin{array}{c|c|c|c|c|c} 1 & & & & & \\ \hline & -C_L D & & 1 & -1 & -1 \\ \hline & & -C_L D & & & 1 \\ \hline -1 & 1 & & -L_t D & & \\ \hline & -1 & 1 & & & -L_L D \\ \hline & 1 & & & -L_N(i_4)D & \end{array}\right] \begin{bmatrix} V_1 \\ \hline V_2 \\ \hline V_3 \\ \hline I_1 \\ \hline I_2 \\ \hline I_4 \end{bmatrix} \tag{3.85}$$

3.7 Conclusions

In this chapter a generalised frame of reference for solving PSS responses of power networks has been introduced. The frame of reference was presented in a such a way that it is independent of any particular orthogonal basis function. The motivation for this representation has been to search for more efficient algorithms for predicting waveform distortion in power networks.

Two algorithms, the STM and the MNA were investigated in order to write the dynamical equations of any power network. They were also extended so that they can be combined with the concepts of operational matrices described in this chapter. However, it was shown that STM is a powerful analysis tool which provides more flexibility than the MNA. Owing to its characteristic of separating the Kirchhoffs laws and the branch equations, it is capable of relating a heterogeneous group of variables to another group of variables with the same characteristics. It also allows to formulate solutions for cases when different elements are modelled in different domains.

Part II

Harmonic Domain Modelling

Chapter 4

Harmonic Domain Modelling of Electric Power Circuits

To date, research efforts worldwide have produced accurate model for predicting power systems harmonic distortion. Time and frequency domain solutions have been used for such purpose. Fourier's transform has been used for most frequency domain purpose. In this and next chapters, more efficient numerical solutions are explored. Harmonic analysis methods based on Hartley transform and real Fourier transform are presented. Also, discrete convolution operations are intruduced to improve frequency domain calculations since they provide clean harmonic domain evaluations.

4.1 Introduction

The Complex Fourier formulation uses complex algebra, however, the signals to be encountered in waveform distortion analysis are always real, hence there is a fundamental asymmetry between the data domain and the Fourier transform domain. This fact can be better understood by looking back at the choice made in favour of the familiar complex formulation of the Fourier approach. After the initial work of Fourier, two main streams of analysis, whose boundaries are not clear, took place. On the one hand, Fourier introduced his theory in terms of sines and cosines. This permitted him to analyse terms which were harmonically related using trigonometric functions. This analysis leads to separate lists a_n and b_n for the cosines and sines terms, respectively. Both lists are real. On the other hand, the theory of the integral of Fourier with more general purposes (no restricted to periodic analysis) was also developed. This analysis is required to be in terms of complex variables. The ability of working with complex algebra was done by packing the two real lists a_n and b_n into a complex term of the form $a_n - jb_n$. An interesting feature of the Hartley transform is that both sines and cosines are packed in a way which does not require complex algebra leading to more efficient to instruction to the computer, since real operations are less time consuming than the complex ones.

With this in mind, this chapter harmonic domain addresses formulations which rely solely on the use of real algebra, i.e. real harmonic domain and Hartley harmonic domain. Each of these formulations provides an elegant and powerful frame of reference where both nonlinear and linear elements can be combined together for a unified, iterative solution via Newton-Raphson methods exhibiting quadratic convergence. Solutions to voltage tolerances of 1e-6 for the fundamental and harmonic frequencies are obtained in less than five iterations. Discrete convolutions are used to achieve frequency domain evaluations. Thus, avoiding time

domain excursions and the use of aliasing-prone FFT.

4.2 Direct Frequency Domain Evaluations

The dynamic equations representing LTIS can be transformed into a linear set of algebraic equations by using operational matrices of integration. Another operational matrix that facilitates the solution of LTVS, together with the operational matrix of integration, is the operational matrix of direct product. The operational matrix of direct product is a powerful tool for analysing a class of nonlinear systems, termed bilinear systems, and non-linear systems that can be represented by polynomial equations,

$$y = b_0 + b_1 x + b_2 x^2 + \ldots + b_n x^n \tag{4.1}$$

$$y = \frac{a_0 + a_1 x + a_2 x^2 + \ldots + a_n}{b_0 + b_1 x + b_2 + \ldots + b_m x^m} \tag{4.2}$$

The product operational matrix for various domains are presented in this chapter. The methods presented are frequency domain methods as opposed to sequency domain methods.

Equations (4.1) and (4.2) are amenable to direct frequency domain evaluations via discrete convolutions. Discrete convolutions are central to these methods and they provide a means for clean harmonic domain evaluations, a fact which aids convergence significantly. To date, most frequency domain methods have made use of Fourier's transform, in spite of strong indications that alternative transformations such as Hartley [94], Walsh [69], Wavelets [95] can provide more efficient solutions.

This chapter presents frequency domain representations of non-linear elements. Equations (4.1) and (4.2) can be evaluated in the harmonic domain by performing a series of self-convolutions, e.g.

$$x^2(t) = x(t)x(t) = X \circledast X = Y \tag{4.3}$$

and mutual convolutions, e.g.

$$y(t) = s(t)x(t) = S \circledast X = Y \tag{4.4}$$

where $x(t)$, $y(t)$ and $s(t)$ are periodic functions; X, Y and S are harmonic vectors and $\circledast$ is the convolution operator. Several harmonic transforms can be used for carrying out operational products. In this chapter, Complex Fourier, Real Fourier and Hartley transforms are used.

4.3 Harmonic Domain Evaluations Using Complex Fourier Series Expansions

To date, most power harmonic analysis tools [17] have been developed with inputs $x(t)$ and outputs $y(t)$ expanded in the Complex Fourier domain, i.e.

$$x(t) = \sum_{i=-\infty}^{\infty} X_i e^{ji\omega t} \tag{4.5}$$

and

$$y(t) = \sum_{h=-\infty}^{\infty} Y_h e^{jh\omega t} \tag{4.6}$$

The product $x(t)$ of $y(t)$ can also be expressed in the same basis, i.e.

$$\sum_{k=-\infty}^{\infty} Z_k e^{jk\omega t} = \left(\sum_{i=-\infty}^{\infty} X_i e^{ji\omega t}\right)\left(\sum_{h=-\infty}^{\infty} Y_h e^{jh\omega t}\right) \tag{4.7}$$

Direct evaluation of equation (4.7) confirms that Z is the result of convolving vectors X and Y.

$$Z = X \circledast Y \tag{4.8}$$

where

$$\begin{aligned} X &= [\ldots, X_{-i}, \ldots, X_{-2}, X_{-1}, X_0, X_1, X_2, \ldots, X_i, \ldots]^t \\ Y &= [\ldots, Y_{-j}, \ldots, Y_{-2}, Y_{-1}, Y_0, Y_1, Y_2, \ldots, Y_j, \ldots]^t \\ Z &= [\ldots, Z_{-k}, \ldots, Z_{-2}, Z_{-1}, Z_0, Z_1, Z_2, \ldots, Z_k, \ldots]^t \end{aligned} \tag{4.9}$$

Equation (4.8) can also be written in matrix form,

$$Z = [X]Y = \begin{pmatrix} X_0 & X_{-1} & X_{-2} & \cdots & X_{-i} & & & & \\ \ddots & \ddots & \ddots & \ddots & \cdots & \ddots & & & \\ X_2 & X_1 & X_0 & X_{-1} & X_{-2} & \cdots & X_{-i} & & \\ \cdots & X_2 & X_1 & X_0 & X_{-1} & X_{-2} & \cdots & X_{-i} & \\ X_i & \cdots & X_2 & X_1 & X_0 & X_{-1} & X_{-2} & \cdots & X_{-i} \\ & X_i & \cdots & X_2 & X_1 & X_0 & X_{-1} & X_{-2} & \cdots \\ & & X_i & \cdots & X_2 & X_1 & X_0 & X_{-1} & X_{-2} \\ & & & \ddots & \cdots & \ddots & \ddots & \ddots & \ddots \\ & & & & X_i & \cdots & X_2 & X_1 & X_0 \end{pmatrix} \begin{pmatrix} Y_{-i} \\ \vdots \\ Y_{-2} \\ Y_{-1} \\ Y_0 \\ Y_1 \\ Y_2 \\ \vdots \\ Y_i \end{pmatrix} \tag{4.10}$$

where the matrix $[X]$ is a Hermitian matrix with Toeplitz structure. The elements of $[X]$ can be identified by taking one term at the time in the variable $Y(t)$,

$$\sum_{k=-\infty}^{\infty} Z_k e^{jk\omega t} = \left(\sum_{i=-\infty}^{\infty} e^{j(i+h)\omega t}\right) Y_h$$

or in vector form,

$$\begin{pmatrix} Z_{-i} \\ \vdots \\ Z_{-2} \\ Z_{-1} \\ Z_0 \\ Z_1 \\ Z_2 \\ \vdots \\ Z_i \end{pmatrix} = \begin{pmatrix} X_{-i-h} \\ \vdots \\ X_{-2-h} \\ X_{-1-h} \\ Y_0 \\ Y_{1-h} \\ Y_{2-h} \\ \vdots \\ Y_{i-h} \end{pmatrix} \tag{4.11}$$

4.3.1 Dynamic elements

The integral of Complex Fourier series can also be written in terms of the Complex Fourier coefficients as follows,

$$\sum_{i=-\infty}^{\infty} \int_{o}^{t} Y_i e^{ji\omega t} dt = \int_{0}^{t} \left(\sum_{i=-\infty}^{\infty} X_i e^{ji\omega t} \right) dt = \sum_{i=-\infty}^{\infty} \frac{1}{ji\omega} X_i e^{ji\omega t} \tag{4.12}$$

or in matrix form

$$\begin{pmatrix} -ji\omega & & & & & & & & \\ & \ddots & & & & & & & \\ & & -j2\omega & & & & & & \\ & & & -j\omega & & & & & \\ & & & & 0 & & & & \\ & & & & & j\omega & & & \\ & & & & & & j2\omega & & \\ & & & & & & & \ddots & \\ & & & & & & & & ji\omega \end{pmatrix}^{-1} \begin{pmatrix} X_{-i} \\ \vdots \\ X_{-2} \\ X_{-1} \\ X_0 \\ X_1 \\ X_2 \\ \vdots \\ X_i \end{pmatrix} = \begin{pmatrix} -\frac{1}{ji\omega} X_{-i} \\ \vdots \\ -\frac{1}{j2\omega} X_{-2} \\ -\frac{1}{j\omega} X_{-1} \\ 0 \\ \frac{1}{j\omega} X_1 \\ \frac{1}{j2\omega} X_2 \\ \vdots \\ \frac{1}{ji\omega} X_i \end{pmatrix} \tag{4.13}$$

4.3.2 Numerical example

Harmonic evaluations are better understood with a numerical example. Let us consider the polynomial equation,

$$i = f(\psi) = 0.001\psi + 0.074\psi^4 \tag{4.14}$$

subjected to the excitation,

$$\psi = \sin(\omega t) = \frac{e^{j\omega t} - e^{-j\omega t}}{2j} = \frac{j}{2} \begin{pmatrix} 0 \\ 1 \\ 0 \\ -1 \\ 0 \end{pmatrix} \begin{matrix} -2 \\ -1 \\ 0 \\ 1 \\ 2 \end{matrix} \tag{4.15}$$

The harmonic evaluation is carried out as follows,

$$\psi^2 = \psi \cdot \psi = \frac{j}{2} \begin{pmatrix} 0 \\ 1 \\ 0 \\ -1 \\ 0 \end{pmatrix} \begin{matrix} -2 \\ -1 \\ 0 \\ 1 \\ 2 \end{matrix} \circledast \frac{j}{2} \begin{pmatrix} 0 \\ 1 \\ 0 \\ -1 \\ 0 \end{pmatrix} \begin{matrix} -2 \\ -1 \\ 0 \\ 1 \\ 2 \end{matrix} \tag{4.16}$$

which in matrix form becomes,

$$\psi^2 = \frac{j}{2} \begin{pmatrix} 0 & 1 & & & \\ -1 & 0 & 1 & & \\ & -1 & 0 & 1 & \\ & & -1 & 0 & 1 \\ & & & -1 & 0 \end{pmatrix} \times \frac{j}{2} \begin{pmatrix} 0 \\ 1 \\ 0 \\ -1 \\ 0 \end{pmatrix} \begin{matrix} -2 \\ -1 \\ 0 \\ 1 \\ 2 \end{matrix} = \frac{1}{4} \begin{pmatrix} 1 \\ 0 \\ 2 \\ 0 \\ -1 \end{pmatrix} \tag{4.17}$$

Also,

$$\psi^3 = \psi^2 \cdot \psi = \frac{1}{4}\begin{pmatrix} 0 \\ 1 \\ 0 \\ 2 \\ 0 \\ -1 \\ 0 \end{pmatrix}\begin{matrix} -3 \\ -2 \\ -1 \\ 0 \\ 1 \\ 2 \\ 3 \end{matrix} \circledast \frac{j}{2}\begin{pmatrix} 0 \\ 0 \\ 1 \\ 0 \\ -1 \\ 0 \\ 0 \end{pmatrix}\begin{matrix} -3 \\ -2 \\ -1 \\ 0 \\ 1 \\ 2 \\ 3 \end{matrix} \tag{4.18}$$

or in matrix form

$$\psi^3 = \frac{1}{4}\begin{pmatrix} 2 & & -1 & & & & \\ & 2 & & -1 & & & \\ -1 & & 2 & & -1 & & \\ & -1 & & 2 & & 1 & \\ & & -1 & & 2 & & 1 \\ & & & -1 & & 2 & \\ & & & & -1 & & 2 \end{pmatrix}\begin{matrix} -3 \\ -2 \\ -1 \\ 0 \\ 1 \\ 2 \\ 3 \end{matrix} \times \frac{j}{2}\begin{pmatrix} 0 \\ 0 \\ 1 \\ 0 \\ -1 \\ 0 \\ 0 \end{pmatrix}\begin{matrix} -3 \\ -2 \\ -1 \\ 0 \\ 1 \\ 2 \\ 3 \end{matrix} = \frac{j}{8}\begin{pmatrix} -1 \\ 0 \\ 3 \\ 0 \\ -3 \\ 0 \\ 1 \end{pmatrix}\begin{matrix} -3 \\ -2 \\ -1 \\ 0 \\ 1 \\ 2 \\ 3 \end{matrix} \tag{4.19}$$

The cubic polynomial is the evaluated in the complex Fourier domain

$$\begin{pmatrix} I_{-3} \\ I_{-2} \\ I_{-1} \\ I_0 \\ I_1 \\ I_2 \\ I_3 \end{pmatrix} = j\frac{0.001}{2}\begin{pmatrix} 0 \\ 0 \\ 1 \\ 0 \\ -1 \\ 0 \\ 0 \end{pmatrix}\begin{matrix} -3 \\ -2 \\ -1 \\ 0 \\ 1 \\ 2 \\ 3 \end{matrix} + j\frac{0.0743}{8}\begin{pmatrix} -1 \\ 0 \\ 3 \\ 0 \\ -3 \\ 0 \\ 1 \end{pmatrix}\begin{matrix} -3 \\ -2 \\ -1 \\ 0 \\ 1 \\ 2 \\ 3 \end{matrix} = \begin{pmatrix} -j0.0093 \\ 0 \\ j0.0284 \\ 0 \\ -j0.0284 \\ 0 \\ j0.0093 \end{pmatrix}\begin{matrix} -3 \\ -2 \\ -1 \\ 0 \\ 1 \\ 2 \\ 3 \end{matrix} \tag{4.20}$$

or

$$i = 0.0568\sin(\omega t) - 0.0186\sin(3\omega t) \tag{4.21}$$

4.4 Efficient Polynomial Evaluation

The mechanics of polynomial evaluation is a straightforward, though cumbersome process. The number of algebraic operations grows rapidly with the polynomial degree and the harmonic order of the excitation. Therefore, suitable algorithms for polynomial evaluation must be developed for practical harmonic domain calculations.

4.4.1 Recursive Evaluation

Many applications in power harmonic analysis require evaluations of power series of the form,

$$y = a_0 + a_1 x + a_2 x^2 + \ldots + a_n x^n \tag{4.22}$$

Evaluations of this structure would require many multiplications (convolutions) if brute force is used. However, operations are minimised if the structure of the polynomial is re-arranged. *Synthetic devision* can be used to achieve this aim. For example, consider the polynomial,

$$y = a_0 + a_1 x + a_2 x^2 + a_3 x^3 + a_4 x^4 \tag{4.23}$$

Using brute force evaluations would requires 7 multiplications, but the the same polynomial can be represented as,

$$y = a_0 + x(a_1 + x(a_2 + x(a_3 + a_4 x))) \tag{4.24}$$

which only requires 4 multiplications in order to be evaluated.

Similarly, polynomials with more specific structure,

$$y = a_1 x + a_n x^n + a_m x^m \tag{4.25}$$

can be rewritten as,

$$y = x(a_1 + x^{n-1}(a_n + a_m x^{m-n})) \tag{4.26}$$

for more efficient evaluations.

4.4.2 Exponentiation

Equation (4.26) requires that a factor x^q be evaluated. This can be carried out quite efficiently for large numbers of q. The sequence of convolutions required to evaluate x^q can be guided by the integer q expressed as a binary number [18]. For instance, consider the evaluation of the factor x^{19}. Table 4.1 shows the binary number corresponding to q. Both sequences, self-convolutions and mutual convolution are shown. It can be seen that the number of bits required to represent the decimal number guides the sequence of self-convolutions whereas non-zero bits guides the mutual convolutions.

Decimal number	19				
Significant bits	4	3	2	1	0
Binary number	1	0	1	0	1
Self Convolutions	x^{16}	x^8	x^4	x^2	x
Mutual Convolutions	x^{16}			x^2	x

Tab. 4.1: Polynomial evaluations

4.5 Harmonic Domain Evaluations Using Real Fourier Series

The product of two periodic, *real variables* x and y, expanded in trigonometric series form,

$$\begin{aligned} x(t) &= \sum_{i=0}^{\infty} X_i' \sin(i\omega t) + X_i'' \cos(i\omega t) \\ y(t) &= \sum_{h=0}^{\infty} Y_h' \sin(i\omega t) + Y_h'' \cos(i\omega t) \end{aligned} \tag{4.27}$$

gives rise to another periodic variable, say $z(t)$, that can also be expressed in the same domain,

$$\begin{aligned} \sum_{k=0}^{\infty} Z_k' \sin(k\omega t) + Z_k'' \cos(k\omega t) &= \left(\sum_{i=0}^{\infty} X_i' \sin(i\omega t) + X_i'' \cos(i\omega t)\right) \times \\ &\quad \left(\sum_{h=0}^{\infty} Y_h' \sin(i\omega t) + Y_h'' \cos(i\omega t)\right) \end{aligned} \tag{4.28}$$

A vector form of equation (4.28) can be obtained by using the harmonic coefficients only,

$$\left(\frac{Z'}{Z''}\right) = \left(\frac{X'}{X''}\right) \circledast \left(\frac{Y'}{Y''}\right) \tag{4.29}$$

where

$$\begin{aligned}
X' &= [X'_0, X'_1, X'_2, \ldots, X'_i]^t \\
X'' &= [X''_0, X''_1, X''_2, \ldots, X''_i]^t \\
Y' &= [Y'_0, Y'_1, Y'_2, \ldots, Y'_h]^t \\
Y'' &= [Y''_0, Y''_1, Y''_2, \ldots, Y''_h]^t \\
Z' &= [Z'_0, Z'_1, Z'_2, \ldots, Z'_k]^t \\
Z'' &= [Z'_0, Z''_1, Z''_2, \ldots, Z''_k]^t
\end{aligned}$$

The matrix representation of equation (4.29) provides an alternative for performing actual calculations,

$$\left(\frac{Z'}{Z''}\right) = \left(\begin{array}{c|c} X^{ss} & X^{sc} \\ \hline X^{cs} & X^{cc} \end{array}\right) \left(\frac{Y'}{Y''}\right) \tag{4.30}$$

The elements of matrices $[X^{ss}], [X^{sc}], [X^{cs}]$ and $[X^{cc}]$ are identified by taking one term of $y(t)$ at a time in equation (4.28) say, Y'_h:

$$\left(\sum_{i=0}^{\infty} X'_i \sin(i\omega t) + X''_i \cos(i\omega t)\right) Y'_h \sin(h\omega t) \tag{4.31}$$

and making use of the trigonometric identities

$$\begin{aligned}
\sin A \sin B &= \frac{1}{2}[\cos(A-B) - \cos(A+B)] \\
\sin A \cos B &= \frac{1}{2}[\sin(A+B) - \sin(A-B)] \\
\cos A \cos B &= \frac{1}{2}[\cos(A-B) + \cos(A+B)]
\end{aligned}$$

We have that,

$$\begin{aligned}
Z'_h &= \frac{1}{2}\left[\sum_{i=0}^{\infty} X'_i \cos((i-h)\omega t) - X'_i \cos((i+h)\omega t)\right] Y'_h \\
&+ \frac{1}{2}\left[\sum_{i=0}^{\infty} -X''_i \sin((i-h)\omega t) + X'_i \sin((i+h)\omega t)\right] Y'_h
\end{aligned} \tag{4.32}$$

Similarly for Y''_h:

$$\begin{aligned}
Z''_h &= \frac{1}{2}\left[\sum_{i=0}^{\infty} X'_i \sin((i-h)\omega t) - X'_i \sin((i+h)\omega t)\right] Y''_h \\
&+ \frac{1}{2}\left[\sum_{i=0}^{\infty} -X''_i \cos((i-h)\omega t) + X'_i \cos((i+h)\omega t)\right] Y''_h
\end{aligned} \tag{4.33}$$

After considering all terms of the input Y' and Y'', the matrices $[X^{ss}], [X^{sc}], [X^{cs}]$ and $[X^{cc}]$ are readily identified,

$$X_{sc} = \left(\begin{array}{c|c|c|c|c|c} 2X_0'' - X_2'' & X_1'' - X_3'' & X_2'' - X_4'' & X_3'' - X_5'' & \dots \\ \hline X_1'' - X_3'' & 2X_0'' - X_4'' & X_1'' - X_5'' & X_2'' - X_6'' & \dots \\ \hline X_2'' - X_4'' & X_1'' - X_5'' & 2X_0'' - X_6'' & X_1'' - X_7'' & \dots \\ \hline X_3'' - X_5'' & X_2'' - X_6'' & X_1'' - X_7'' & 2X_0'' - X_8'' & \dots \\ \hline \vdots & \vdots & \vdots & \vdots & \ddots \end{array}\right) \tag{4.34}$$

$$X^{sc} = \left(\begin{array}{c|c|c|c|c|c} 2X_1' & X_2' & -X_1' + X_3' & -X_2' + X_4' & -X_3' + X_5' & \dots \\ \hline 2X_2' & X_1' + X_3' & X_4' & X_1' + X_5' & X_2' + X_4' & \dots \\ \hline 2X_3' & X_2' + X_4' & X_1' + X_5' & X_6' & X_1' + X_7' & \dots \\ \hline 2X_4' & X_3' + X_5' & X_2' + X_6' & X_1' + X_7' & X_8' & \dots \\ \hline \vdots & \vdots & \vdots & \vdots & \ddots & \end{array}\right) \tag{4.35}$$

$$X^{cs} = \left(\begin{array}{c|c|c|c|c} X_1' & X_2' & X - 3' & X_4' & \dots \\ \hline X_2' & X_1' + X_3' & X_2' + X_4' & X_3' + X_5' & \dots \\ \hline -X_1' + X_3' & X_4 & X_1 + X_5 & X_2' + X_6' & \dots \\ \hline -X_2' + X_4' & -X_1' + X_5' & X_6' & X_1' + X_7' & \dots \\ \hline X_3' + X_5' & -X_2' + X_6' & -X_1 + X_7' & X_8 & \dots \\ \hline \vdots & \vdots & \vdots & \vdots & \ddots \end{array}\right) \tag{4.36}$$

$$X^{cc} = \left(\begin{array}{c|c|c|c|c|c} 2X_0'' & X_1'' & X_2'' & X_3'' & X_4'' & \dots \\ \hline 2X_1'' & 2X_0'' + X_2'' & X_1'' + X_3'' X_2'' + X_4'' & X_3'' + X_5'' & & \dots \\ \hline 2X_2'' & X_1'' + X_3'' & 2X_0 + X_4'' & X_1'' + X_5'' & X_2'' + X_6'' & \dots \\ \hline 2X_3'' & X_2'' + X_4'' & X_1'' + X_5'' & 2X_0'' + X_6'' & X_1'' + X_7'' & \dots \\ \hline 2X_4'' & X_3'' + X_5'' & X_2'' + X_6'' & X_1'' + X_7'' & 2X_0'' + X_8'' & \dots \\ \hline \vdots & \vdots & \vdots & \vdots & \vdots & \ddots \end{array}\right) \tag{4.37}$$

It is important to note that the matrix in equation (4.30) has the same dimensions as the matrix in equation (4.10) but whereas the latter is complex the former is real. In applications involving real signals, it is expected that equation (4.30) speeds up harmonic domain calculations while reducing storage requirements.

4.5.1 Dynamic elements

Dynamic elements are handled quite easily in this harmonic domain. Let us consider the basic relation,

$$z = \dot{x} \tag{4.38}$$

between the two periodic variables,

$$z(t) = \sum_{k=0}^{\infty} Z_k' \sin(k\omega t) + Z_k'' \cos(k\omega t) \tag{4.39}$$

and

$$x(t) = \sum_{k=0}^{\infty} X_k' \sin(k\omega t) + X_k'' \cos(k\omega t) \tag{4.40}$$

Then equation (4.38) may be written as,

$$\begin{aligned}\sum_{k=0}^{\infty} Z'_k \sin(k\omega t) + Z''_k \cos(k\omega t) &= \frac{d}{dt}\left(\sum_{k=0}^{\infty} X'_k \sin(k\omega t) + X''_k \cos(k\omega t)\right) \\ &= \sum_{k=0}^{\infty} k\omega X'_k \cos(k\omega t) - k\omega X''_k \sin(k\omega t) \qquad (4.41)\end{aligned}$$

Alternative, in terms of harmonic coefficients,

$$\begin{pmatrix} Z'_1 \\ Z'_2 \\ \vdots \\ Z'_k \\ Z''_0 \\ Z''_1 \\ Z''_2 \\ \vdots \\ Z''_k \end{pmatrix} = \begin{pmatrix} & & & & & -\omega & & & \\ & & & & & & -2\omega & & \\ & & & & & & & \ddots & \\ & & & & & & & & -k\omega \\ & & & & 0 & & & & \\ \omega & & & & & & & & \\ & 2\omega & & & & & & & \\ & & \ddots & & & & & & \\ & & & k\omega & & & & & \end{pmatrix} \begin{pmatrix} -\omega X'_1 \\ -2\omega X'_2 \\ \vdots \\ -k\omega X'_k \\ 0 \\ \omega X''_1 \\ 2\omega X''_2 \\ \vdots \\ k\omega X''_k \end{pmatrix} \qquad (4.42)$$

This shows that the evaluation of dynamic Real Fourier series is carried out by simple algebraic operations. Equation (4.42) can be written in compact form as,

$$\left(\frac{Z'}{Z''}\right) = \left(\begin{array}{c|c} 0 & D(-k\omega) \\ \hline D(k\omega) & 0 \end{array}\right)\left(\frac{X'}{X''}\right) \qquad (4.43)$$

from which the operational matrix of integration can be written as

$$\left(\frac{X'}{X''}\right) = \left(\begin{array}{c|c} 0 & D(\frac{1}{k\omega}) \\ \hline D(-\frac{1}{k\omega}) & 0 \end{array}\right)\left(\frac{Z'}{Z''}\right) \qquad (4.44)$$

4.5.2 Numeric example

The polynomial equation,

$$i = \psi(t) = 0.001\psi + 0.0743\psi^3 \qquad (4.45)$$

is subject to a base sinusoidal excitation,

$$\psi_b = \sin\omega t = \begin{pmatrix} 1 \\ 0 \\ 0 \\ 0 \\ 0 \end{pmatrix} \begin{matrix} 1 \\ 2 \\ 0 \\ 1 \\ 2 \end{matrix} \qquad (4.46)$$

The harmonic evaluation is carried out as follows,

$$\psi^2 = \psi \cdot \psi = \left(\frac{1}{0}\right) \begin{matrix} 1 \\ 2 \end{matrix} \circledast \left(\frac{1}{0}\right) \begin{matrix} 1 \\ 2 \end{matrix} \qquad (4.47)$$

or in matrix form, using $[X^{sc}]$,

$$\psi^2 = \frac{1}{2}\left(\begin{array}{c|c} 1 & 0 \\ \hline 0 & 1 \\ \hline -1 & 0 \end{array}\right) \begin{matrix} 0 \\ 1 \\ 2 \end{matrix} \times \frac{1}{2}\left(\frac{1}{0}\right) \begin{matrix} 1 \\ 2 \end{matrix} = \frac{1}{2}\begin{pmatrix} 1 \\ 0 \\ -1 \end{pmatrix} \begin{matrix} 0 \\ 1 \\ 2 \end{matrix} \qquad (4.48)$$

Also,

$$\psi^3 = \psi \cdot \psi^2 = \left(\frac{1}{0}\right)\begin{matrix}1\\2\end{matrix} \circledast \begin{pmatrix}1\\0\\-1\end{pmatrix}\begin{matrix}0\\1\\2\end{matrix} \tag{4.49}$$

or in matrix form,

$$\psi^3 = \frac{1}{2}\begin{pmatrix} 2 & 0 & -1 & 0 \\ 0 & 1 & 0 & -1 \\ 0 & 0 & 1 & 0 \end{pmatrix} \frac{1}{2}\begin{pmatrix}1\\0\\-1\\0\end{pmatrix}\begin{matrix}0\\1\\2\\3\end{matrix} = \frac{1}{4}\begin{pmatrix}3\\0\\-1\end{pmatrix}\begin{matrix}1\\2\\3\end{matrix} \tag{4.50}$$

The evaluation of the Fourier coefficients of the current is

$$\begin{pmatrix}I_1'\\I_2'\\I_3'\end{pmatrix} = 0.001 \times \begin{pmatrix}1\\0\\0\end{pmatrix}\begin{matrix}1\\2\\3\end{matrix} + \frac{0.0743}{4} \times \begin{pmatrix}3\\0\\-1\end{pmatrix}\begin{matrix}1\\2\\3\end{matrix} = \begin{pmatrix}0.0567\\0\\-0.0186\end{pmatrix}\begin{matrix}1\\2\\3\end{matrix} \tag{4.51}$$

or

$$i = 0.0567\sin(\omega t) - 0.0186\sin(3\omega t) \tag{4.52}$$

4.6 Harmonic Domain Evaluations Using Hartley Series Expansions

Hartley's series [96] is another transform which uses real coefficients only for modelling real waveforms. The advantage of working with real algebra as opposed to complex algebra has motivated the analysis presented in this section. For a detailed description of Hartley's transform see [96]. Important advantages of real transforms over the complex formulation are presented in [97]. Relevant aspects concerning the advantages of Hartley's transform over the complex formulation for the analysis of real functions are geometrically explained in [98].

The product of two periodic variables $x(t)$ and $y(t)$ can be expressed in terms of the real functions $\mathsf{cas}(\alpha)$ and $\mathsf{cas}(-\alpha)$,

$$\sum_{k=-\infty}^{\infty} Z_k \mathrm{cas}(k\nu t) = \left(\sum_{i=-\infty}^{\infty} X_i \mathrm{cas}(i\nu t)\right)\left(\sum_{h=-\infty}^{\infty} Y_h \mathrm{cas}(h\nu t)\right) \tag{4.53}$$

where

$$\begin{aligned} \mathrm{cas}(\nu t) &= \cos(\nu t) + \sin(\nu t) \\ \mathrm{cas}(\nu t) &= \cos(\nu t) - \sin(\nu t) \\ \nu &= 2\pi f \end{aligned} \tag{4.54}$$

Using the following Hartley's identity,

$$\mathrm{cas}(\alpha)\mathrm{cas}(\beta) = \frac{1}{2}\left[\mathrm{cas}(\alpha+\beta) + \mathrm{cas}(\alpha-\beta) + \mathrm{cas}(-\alpha+\beta) - \mathrm{cas}(-\alpha-\beta)\right]$$

leads to equation (4.55),

$$\sum_{k=-\infty}^{\infty} Z_k \mathrm{cas}(k\nu t) = \frac{1}{2}\sum_{i=-\infty}^{\infty}\sum_{h=-\infty}^{\infty} X_i Y_h \left[\mathrm{cas}(i+h) + \mathrm{cas}(i-h) + \mathrm{cas}(-i+h) - \mathrm{cas}(-i-h)\right] \tag{4.55}$$

A vector form of equation (4.55) can be obtained by using its harmonic coefficients only,

$$Z = \frac{1}{2}[X_I \circledast Y_I + X_I \circledast Y_{II} + X_{II} \circledast Y_I - X_{II} \circledast Y_{II}] \tag{4.56}$$

where

$$\begin{aligned} X_I &= [X_{-i}, \ldots, X_{-2}, X_{-1}, X_0, X_1, X_2, \ldots, X_i]^t \\ X_{II} &= [X_i, \ldots, X_2, X_1, X_0, X_{-1}, X_{-2}, \ldots, X_{-i}]^t \\ Y_I &= [Y_{-i}, \ldots, Y_{-2}, Y_{-1}, Y_0, Y_1, Y_2, \ldots, Y_h] \\ Y_{II} &= [Y_i, \ldots, Y_2, Y_1, Y_0, Y_{-1}, Y_{-2}, \ldots, Y_{-h}]^t \\ Z &= [Z_{-i}, \ldots, Z_{-2}, Z_{-1}, Z_0, Z_1, Z_2, \ldots, X_k]^t \end{aligned} \tag{4.57}$$

Equation (4.56) can be expressed in the following matrix form,

$$Z = \frac{1}{2}[X_I + X_{II}]Y \tag{4.58}$$

where the elements of matrices X_I and X_{II} are identified by taking one term of the variable $y(t)$ a the time in equation (4.55). For instance, Y_h will identify column h in both matrices,

$$\begin{pmatrix} Z_{-k} \\ \vdots \\ Z{-2} \\ Z_{-1} \\ Z_0 \\ Z_1 \\ Z_2 \\ \vdots \\ Z_k \end{pmatrix} = \frac{1}{2}\left(\begin{bmatrix} X_{-i+h} \\ \vdots \\ X_{-2+h} \\ X_{-1+h} \\ X_{0+h} \\ X_{1+h} \\ X_{2+h} \\ \vdots \\ X_{i+h} \end{bmatrix} + \begin{bmatrix} X_{-i-h} \\ \vdots \\ X_{-2-h} \\ X_{-1-h} \\ X_{0-h} \\ X_{1-h} \\ X_{2-h} \\ \vdots \\ X_{i-h} \end{bmatrix} + \begin{bmatrix} X_{i+h} \\ \vdots \\ X_{2+h} \\ X_{1+h} \\ X_{0+h} \\ X_{-1+h} \\ X_{-2+h} \\ \vdots \\ X_{-i+h} \end{bmatrix} - \begin{bmatrix} X_{i-h} \\ \vdots \\ X_{2-h} \\ X_{-1+h} \\ X_{0-h} \\ X_{-1-h} \\ X_{-2-h} \\ \vdots \\ X_{-i-h} \end{bmatrix} \right) Y_h \tag{4.59}$$

or

$$\begin{pmatrix} Z_{-k} \\ \vdots \\ Z{-2} \\ Z_{-1} \\ Z_0 \\ Z_1 \\ Z_2 \\ \vdots \\ Z_k \end{pmatrix} = \frac{1}{2}\left(\begin{bmatrix} X_{-i+h} + X_{-i-h} \\ \vdots \\ X_{-2+h} + X_{-2-h} \\ X_{-1+h} + X_{-1-h} \\ X_{0+h} + X_{0-h} \\ X_{1+h} + X_{1-h} \\ X_{2+h} + X_{2-h} \\ \vdots \\ X_{i+h} + X_{i-h} \end{bmatrix} + \begin{bmatrix} X_{i+h} - X_{i-h} \\ \vdots \\ X_{2+h} - X_{2-h} \\ X_{1+h} - X_{1-h} \\ X_{0+h} - X_{0-h} \\ X_{-1+h} - X_{-1-h} \\ X_{-2+h} - X_{-2-h} \\ \vdots \\ X_{-i+h} + X_{-i-h} \end{bmatrix} \right) Y_h \tag{4.60}$$

After considering all terms of Y, the matrices X_I and X_{II} become readily identified,

$$X_I = \left(\begin{array}{c|c|c|c|c|c|c}
\ddots & \ddots & \ddots & \ddots & & & \\ \hline
\ddots & 2X_0 & X_{-1}+X_1 & X_{-2}+X_2 & X_{-3}+X_3 & & \\ \hline
\ddots & X_1+X_{-1} & 2X_0 & X_{-1}+X_1 & X_{-2}+X_2 & X_{-3}+X_3 & \ddots \\ \hline
 & X_3+X_{-3} & X_2+X_{-2} & X_1+X_{-1} & 2X_0 & X_{-1}+X_1 & \ddots \\ \hline
 & & X_3+X_{-3} & X_2+X_{-2} & X_1+X_1+X_{-1} & 2X_0 & \ddots \\ \hline
 & & & \ddots & \ddots & \ddots & \ddots
\end{array}\right) \tag{4.61}$$

and

$$X_{II} = \left(\begin{array}{c|c|c|c|c|c|c}
 & & & \ddots & \ddots & \ddots & \ddots \\ \hline
 & & X_{-3}+X_3 & X_{-2}+X_2 & X_{-1}-X_1 & 0\ddots & \\ \hline
 & X_{-3}-X_3 & X_{-2}-X_2 & X_{-1}-X_1 & 0 & X_1-X_{-1} & \ddots \\ \hline
\ddots & X_{-2}-X_2 & X_{-1}-X_1 & 0 & X_1-X_{-1} & X_2-X_{-2} & \ddots \\ \hline
\ddots & X_{-1}-X_1 & 0 & X_1-X_{-1} & X_2-X_{-2} & X_3-X_{-3} & \\ \hline
\ddots & 0 & X_1-X_{-1} & X_2-X_{-2} & X_3-X_{-3} & & \\ \hline
\ddots & \ddots & \ddots & \ddots & & &
\end{array}\right) \tag{4.62}$$

4.6.1 Dynamic elements

The dynamic relation,

$$z = \dot{x} \tag{4.63}$$

can be written in Hartley domain as,

$$\sum_{k=-\infty}^{\infty} Z_k \mathrm{cas}(k\nu t) = \frac{d}{dt}\left(\sum_{k=-\infty}^{\infty} X_k \mathrm{cas}(k\nu t)\right) = \sum_{k=-\infty}^{\infty} k\nu X_k \mathrm{cas}(-k\nu t) \tag{4.64}$$

Alternatively, in terms of Hartley's harmonic coefficients,

$$\left(\begin{array}{c}
Z_{-k} \\ \hline \vdots \\ \hline Z_{-2} \\ \hline Z_{-1} \\ \hline Z_0 \\ \hline Z_1 \\ \hline Z_2 \\ \hline \vdots \\ \hline Z_k
\end{array}\right) = \left(\begin{array}{c|c|c|c|c|c|c|c|c|c}
 & & & & & & & & & k\nu \\ \hline
 & & & & & & & & \ddots & \\ \hline
 & & & & & & & 2\nu & & \\ \hline
 & & & & & & \nu & & & \\ \hline
 & & & & & 0 & & & & \\ \hline
 & & & & -\nu & & & & & \\ \hline
 & & & -2\nu & & & & & & \\ \hline
 & & \ddots & & & & & & & \\ \hline
-k\nu & & & & & & & & &
\end{array}\right) \left(\begin{array}{c}
X_{-k} \\ \hline \vdots \\ \hline X_{-2} \\ \hline X_{-1} \\ \hline X_0 \\ \hline X_1 \\ \hline X_2 \\ \hline \vdots \\ \hline X_k
\end{array}\right) = \left(\begin{array}{c}
k\nu X_k \\ \hline \vdots \\ \hline 2\nu X_2 \\ \hline \nu X_1 \\ \hline 0 \\ \hline -\nu X_{-1} \\ \hline -2\nu X_{-2} \\ \hline \vdots \\ \hline -k\nu X_{-k}
\end{array}\right) \tag{4.65}$$

The evaluation of dynamic terms in Hartley domain is carried out by means of simple algebraic operations. Equation (4.65) can be written in compact form as,

$$Z = D(k\nu)X \tag{4.66}$$

and the operational matrix of integration can be written as,

$$X = D(\frac{1}{k\nu})Z \tag{4.67}$$

4.6.2 Numeric example

The numeric example used in this chapter will now be solved using Hartley harmonic domain where the excitation is,

$$\psi_b = sin(\nu t) = \frac{1}{2}(\text{cas}(\nu t) - \text{cas}(-\nu t) = \frac{1}{2}\begin{pmatrix} 0 \\ -1 \\ 0 \\ 1 \\ 0 \end{pmatrix}\begin{matrix} -2 \\ -1 \\ 0 \\ 1 \\ 2 \end{matrix} \tag{4.68}$$

The harmonic evaluation is carried out as follows,

$$\psi^2 = \psi \cdot \psi = \frac{1}{2}\begin{pmatrix} 0 \\ -1 \\ 0 \\ 1 \\ 0 \end{pmatrix}\begin{matrix} -2 \\ -1 \\ 0 \\ 1 \\ 2 \end{matrix} \circledast \frac{1}{2}\begin{pmatrix} 0 \\ -1 \\ 0 \\ 1 \\ 0 \end{pmatrix}\begin{matrix} -2 \\ -1 \\ 0 \\ 1 \\ 2 \end{matrix} \tag{4.69}$$

or in matrix form, using X_{II},

$$\psi^2 = \frac{1}{2}\begin{pmatrix} & & & -2 & 0 \\ & & -2 & 0 & 2 \\ & -2 & 0 & 2 & \\ -2 & 0 & 2 & & \\ 0 & 2 & & & \end{pmatrix} \frac{1}{2}\begin{pmatrix} 0 \\ -1 \\ 0 \\ 1 \\ 0 \end{pmatrix}\begin{matrix} -2 \\ -1 \\ 0 \\ 1 \\ 2 \end{matrix} = \frac{1}{4}\begin{pmatrix} -1 \\ 0 \\ 2 \\ 0 \\ 1 \end{pmatrix}\begin{matrix} -2 \\ -1 \\ 0 \\ 1 \\ 2 \end{matrix} \tag{4.70}$$

Also,

$$\psi^3 = \psi^2 \cdot \psi = \frac{1}{4}\begin{pmatrix} 0 \\ -1 \\ 0 \\ 2 \\ 0 \\ 1 \\ 0 \end{pmatrix}\begin{matrix} -3 \\ -2 \\ -1 \\ 0 \\ 1 \\ 2 \\ 3 \end{matrix} \circledast \frac{1}{2}\begin{pmatrix} 0 \\ 0 \\ -1 \\ 0 \\ 1 \\ 0 \\ 0 \end{pmatrix}\begin{matrix} -3 \\ -2 \\ -1 \\ 0 \\ 1 \\ 2 \\ 3 \end{matrix} \tag{4.71}$$

or in matrix form, using X_I,

$$\psi^3 = \frac{1}{2}\begin{pmatrix} 2 & & -1 & & & & \\ & 2 & & -1 & & & \\ -1 & & 2 & & -1 & & \\ & -1 & & 2 & & -1 & \\ & & -1 & & 2 & & -1 \\ & & & -1 & & 2 & \\ & & & & -1 & & 2 \end{pmatrix} \frac{1}{2}\begin{pmatrix} 0 \\ 0 \\ -1 \\ 0 \\ 1 \\ 0 \\ 0 \end{pmatrix}\begin{matrix} -3 \\ -2 \\ -1 \\ 0 \\ 1 \\ 2 \\ 3 \end{matrix} = \frac{1}{4}\begin{pmatrix} 1 \\ 0 \\ -3 \\ 0 \\ 3 \\ 0 \\ 1 \end{pmatrix}\begin{matrix} -3 \\ -2 \\ -1 \\ 0 \\ 1 \\ 2 \\ 3 \end{matrix} \tag{4.72}$$

and finally the cubic polynomial in Hartley's domain is,

$$\begin{pmatrix} I_{-3} \\ I_{-2} \\ I_{-1} \\ I_0 \\ I_1 \\ I_2 \\ I_3 \end{pmatrix} = \frac{0.001}{2} \times \begin{pmatrix} 0 \\ 0 \\ -1 \\ 0 \\ 1 \\ 0 \\ 0 \end{pmatrix} \begin{matrix} -3 \\ -2 \\ -1 \\ 0 \\ 1 \\ 2 \\ 3 \end{matrix} + \frac{0.0743}{4} \times \begin{pmatrix} 1 \\ 0 \\ -3 \\ 0 \\ 3 \\ 0 \\ 1 \end{pmatrix} \begin{matrix} -3 \\ -2 \\ -1 \\ 0 \\ 1 \\ 2 \\ 3 \end{matrix} = \begin{pmatrix} 0.0186 \\ 0 \\ -0.0562 \\ 0 \\ 0.0562 \\ 0 \\ -0.0186 \end{pmatrix} \begin{matrix} -3 \\ -2 \\ -1 \\ 0 \\ 1 \\ 2 \\ 3 \end{matrix} \quad (4.73)$$

or,

$$i = 0.0562 \sin(\nu t) - 0.0186 \sin(3\nu t) \quad (4.74)$$

4.7 Harmonic Domain Newton-Raphson Techniques

For most practical purposes, a non-linear relationship,

$$y = f(x) \quad (4.75)$$

that can be expanded in Taylor series is amenable to an iterative solution via Newton-Raphson method,

$$f(x + \Delta x) = f(x_b) + \frac{\partial f(x)}{\partial x} \Delta x \quad (4.76)$$

or

$$\Delta y = \frac{\partial f(x)}{\partial x} \Delta y \quad (4.77)$$

where

$$\Delta y = f(x + \Delta x) - f(x_b) \quad (4.78)$$

Furthermore, if the variables x and y in equation (4.75) are periodic then for small increments about x_b and y_b, the following harmonic domain linearisation exists,

$$\Delta Y = J \Delta X \quad (4.79)$$

where J is a harmonic Jacobian matrix containing first order partial derivatives of the non-linear function $f(x)$ with respect to the harmonic coefficients of x. Also, by noticing that the linearisation has taken place about X_b, Y_b in the harmonic domain then,

$$\begin{aligned} \Delta Y &= Y - Y_b \\ \Delta X &= X - X_b \end{aligned} \quad (4.80)$$

Substituting relations (4.80) into equation (4.79) produces an alternative expression which provides further insight into harmonic domain techniques,

$$Y = JX + Y_N \quad (4.81)$$

where

$$Y_N = Y_b - JX_b \quad (4.82)$$

The subscript N indicates the possibility of interpreting this equation as a harmonic Norton equivalent. This will be the case when Y is a vector of harmonic current, X is a vector of harmonic voltages and J is a matrix of harmonic admittances. From equations (4.81) and (4.82) it is apparent that the harmonic domain solution of a single variable, non-linear function requires the evaluation of two vectors at each iterative step. The vector X_b corresponds to the evaluation of the original function $f(x)$ whilst Y_b corresponds to the evaluation of its derivative function $f'(x)$.

Equation (4.81) provides a suitable means to determine the steady state solution of non-linear circuits by iteration through a Newton-Raphson approach. Its nodal nature makes it attractive for incorporation into a general harmonic frame-of-reference where any number of both linear and linearised, non-linear components can be represented together to give a unified iterative solution that exhibits quadratic convergence. In this environment all the harmonics, cross-couplings between harmonics, nodes and phases present in the network share a global nodal admittance matrix which is also a Jacobian matrix. Any of the three harmonic transforms presented in this chapter can be used to determine the steady state solution of non-linear circuits via Newton-Raphson techniques.

4.7.1 Newton-Raphson in Real Fourier Harmonic Domain

In the Real Fourier harmonic domain the variables in equation (4.79) will be expressed as,

$$\Delta x = \sum_{h=0}^{\infty} \Delta X'_h \sin(h\omega t) + \Delta X''_h \cos(h\omega t) \tag{4.83}$$

$$\Delta y = \sum_{k=0}^{\infty} \Delta Y'_h \sin(k\omega t) + \Delta Y''_h \cos(k\omega t) \tag{4.84}$$

$$f'(x) = f'(x(t)) = \sum_{i=0}^{\infty} a'_i \sin(i\omega t) + a''_i \cos(i\omega t) \tag{4.85}$$

Substituting equations (4.83), (4.84) and (4.85) into equation (4.79) leads to the following matrix equation,

$$\begin{bmatrix} \Delta Y' \\ \Delta Y'' \end{bmatrix} = \begin{bmatrix} A' \\ A'' \end{bmatrix} \circledast \begin{bmatrix} \Delta X' \\ \Delta X'' \end{bmatrix} = \begin{bmatrix} A^{ss} & A^{sc} \\ A^{cs} & A^{cc} \end{bmatrix} \begin{bmatrix} \Delta X' \\ \Delta X'' \end{bmatrix} \tag{4.86}$$

where the vector and matrix arrangements are similar to those of equation (4.29) and (4.30).

A Norton representation of the kind given by equation (4.81) and (4.82) is easily obtained for this equation.

In the real Fourier harmonic domain a complex, linear admittance $G_k + B_k$ is represented as,

$$\begin{bmatrix} I'_k \\ I''_k \end{bmatrix} = \begin{bmatrix} G_k & B_k \\ -B_k & G_k \end{bmatrix} \begin{bmatrix} V'_k \\ V''_k \end{bmatrix} \tag{4.87}$$

4.7.2 Newton-Raphson in Complex Fourier Harmonic Domain

In the Complex Fourier domain the variables in equation (4.79) will be expressed as,

$$\Delta x = \sum_{h=-\infty}^{\infty} \Delta X_h e^{jh\omega t} \tag{4.88}$$

$$\Delta y = \sum_{k=-\infty}^{\infty} \Delta Y_k e^{jk\omega t} \tag{4.89}$$

$$f'(x) = f'(x(t)) = \sum_{i=-\infty}^{\infty} c_i e^{ji\omega t} \tag{4.90}$$

Substituting equations (4.88), (4.89) and (4.90) into equation (4.79) leads to the following matrix equation.

$$\Delta Y = [C]\Delta X \tag{4.91}$$

where the vector and matrix arrangements are similar to those of equation (4.9) and (4.10).

In the complex Fourier harmonic domain a complex, linear admittance $G_k + jB_k$ is represented as,

$$\begin{bmatrix} I_{-k} \\ I_k \end{bmatrix} = \begin{bmatrix} G_k - jB_k & 0 \\ 0 & G_k + jB_k \end{bmatrix} \begin{bmatrix} V_{-k} \\ V_k \end{bmatrix} \tag{4.92}$$

4.7.3 Newton-Raphson in Hartley Harmonic Domain

In the Hartley domain the variables in equation (4.79) will be expressed as,

$$\Delta x = \sum_{h=-\infty}^{\infty} \Delta X_h \mathrm{cas}(jh\nu t) \tag{4.93}$$

$$\Delta y = \sum_{k=-\infty}^{\infty} \Delta Y_k \mathrm{cas}(jk\nu t) \tag{4.94}$$

$$f'(x) = f'(x(t)) = \sum_{i=-\infty}^{\infty} c_i \mathrm{cas}(ji\nu t) \tag{4.95}$$

Substituting equations (4.93), (4.94) and (4.95) into equation (4.79) leads to the following matrix equation.

$$\Delta Y = [C_I + C_{II}]\Delta X \tag{4.96}$$

where the vector and matrix arrangements are similar to those of equation (4.56) and (4.58).

In the real Hartley harmonic domain a complex, linear admittance $G_k + jB_k$ is represented as,

$$\begin{bmatrix} I_{-k} \\ I_k \end{bmatrix} = \begin{bmatrix} G_k & -B_k \\ B_k & G_k \end{bmatrix} \begin{bmatrix} V_{-k} \\ V_k \end{bmatrix} \tag{4.97}$$

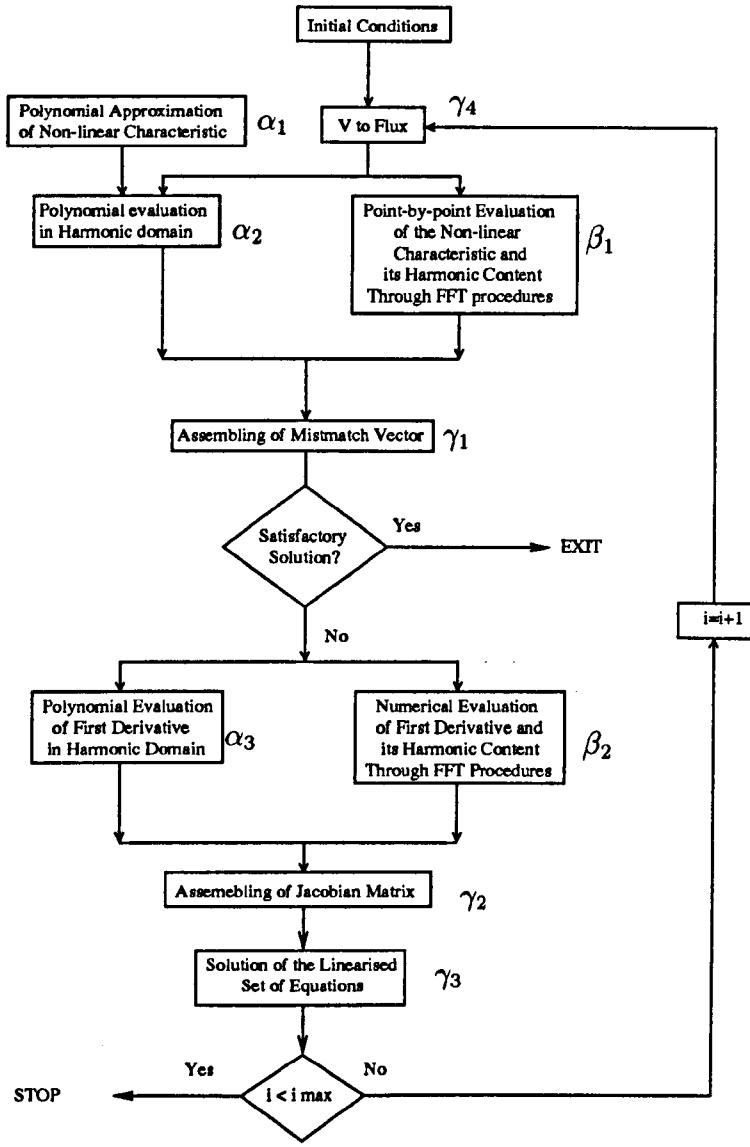

Fig. 4.1: General procedure for harmonic domain calculations

4.8 Harmonic Domain Computations

Figure 4.1 represents diagrammatically the computational procedure used in harmonic domain calculations. The blocks α and β are alternative routes for computations involving non-linearities whilst the γ blocks correspond to a harmonic domain Newton-Raphson procedure. Harmonic domain computations using alternative β are detailed in [17] whilst polynomial evaluations are described in [18]. In this chapter polynomial alternatives are preferred. Both alternatives can be carried out in any of the three frames of reference described in this chapter.

Some non-linear components, such as electric arcs, fluorescent lamps and magnetic non-linearities are amenable to a polynomial representation, and route α results in more efficient calculations. Also, some power electronic-base plant components such as TCRs are ameanable to frequency domain computations following route α but where the polynomial is a first degree polynomial i.e. switching function. An example of this modelling approach is the three phase

TCR model presented in chapter 7. Route β is used when the non-linearity are not accurately be represented by polynomials or switching functions. Here, a full cycle of the currents is evaluated in the time domain at each iterative step. Also, a full cycle of the derivative of the current with respect to flux with respect to time is required.

Block α_1 represents the fitting of a non-linear characteristic by a polynomial, a switching function or any representation amenable to direct frequency domain computations. This topic was addressed in Chapter 2. The process is carried out just once, outside the iterative loop. Polynomial evaluations required in blocks α_2 and α_3 are achieved efficiently by means of repeated convolutions. In blocks β_1 and β_2, a full cycle of the aveform at the fundamental frequency is obtained point-by-point and then a FFT is applied to find the harmonic content of the resultant waveforms. An advantage of route β is that there is no restriction in the representation of the non-linear characteristic.

Block γ_1 represents the calculation of the mismatch vector function whilst γ_2 represents the calculation of the Jacobian matrix. Sparsity techniques can be used to reduce storage and cpu time requirements. The updated harmonic state of the non-linear component is calculated in block γ_3. In block γ_4 the updated voltages are transformed into fluxes.

The general flow chart of Figure 4.1 shows the case when the Jacobian matrix is updated at each iterative step. This approach is a true Newton-Raphson method with quadratic convergence. Alternatively, faster Newton-type algorithms are derived from this basic diagram. A detailed analysis of the alternative numeric technique is presented in Chapter 7.

4.9 Case Studies

The harmonic domain methods presented in this chapter are used to analyse a practical transmission system for which data and results are available in open literature [16]. Detailed information of the geometry of the transmission line as well as data for transformers, shunt reactors and generators is given in Appendix B. The system is shown in Figure 4.2. The transformer is modelled as a three phase bank with the saturation characteristic taken to be curve 1 of Figure 2.2. The transmission line is modelled taking frequency dependence and long line effects into account. The transmission line geometric imbalances are responsible for the voltage imbalances shown in Figure 4.3.

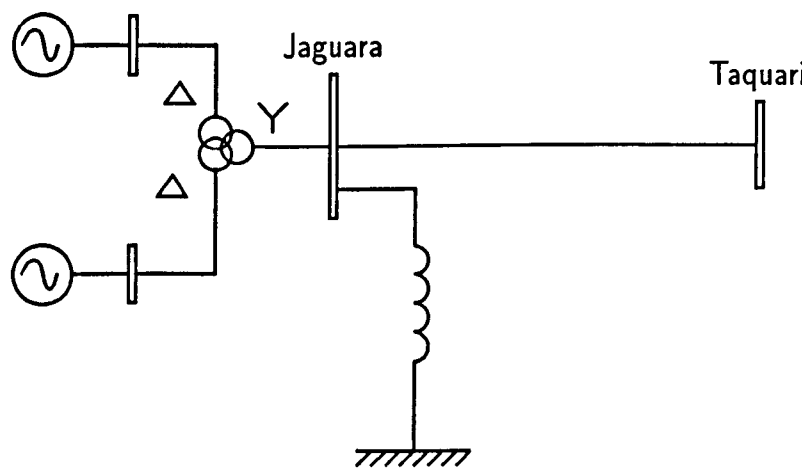

Fig. 4.2: Simplified Jaguara-Taquaril transmission system

When the transformer operates in the saturation region, it draws harmonic currents. The predominance of a particular harmonic order depends on the system configuration and the

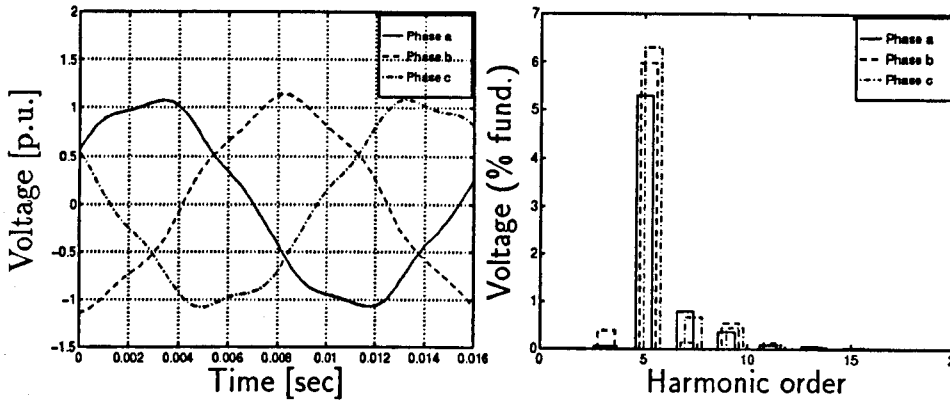

(a) (b)

Fig. 4.3: Voltages at Jaguara bus bar with voltage excitation of 1.1 [p.u.]

transformer connection. In this case, the excitation voltage in the generators is set to 1.1 [p.u.]. The voltage waveforms are shown in Figure 4.3(a). In this case, the predominant harmonic is the fifth harmonic. In most countries power grid regulations impose limits of 5%. In this case, corrective actions should be taken to reduce 5th harmonic voltage levels. All other harmonics are small enough to cause concern. Harmonic current injection due

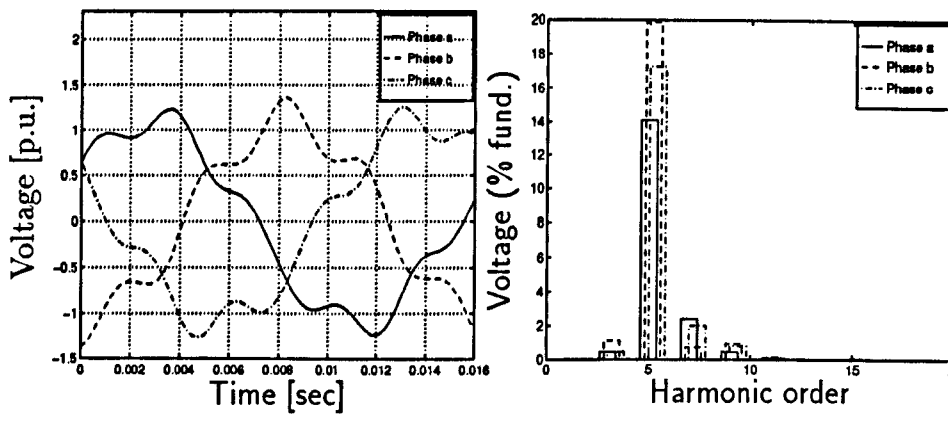

(a) (b)

Fig. 4.4: Voltages at Jaguara bus bar with an excitation voltage of 1.15 [p.u.]

to transformer saturation is a highly non-linear phenomenon. Small changes in the voltage excitation may result in the injection of large currents which, in their turn, may cause highly distorted voltages . To illustrate this point, a small change in voltage excitation is considered, from 1.1 to 1.15. The effect of this small change in voltage excitation causes highly distorted voltage waveforms. The voltages at the Jaguara bus bar are shown in Figure 4.4, the 5th harmonic goes far beyond any permissible limit. Full Newton-Raphson methods were used to calculate these results to a voltage tolerance of 10^{-6}.

4.10 Conclusions

Harmonic domain evaluations in real Fourier or Hartley domains are up to 4 times more efficient than their complex Fourier domain counterparts. An equal number of operations is needed in all three domains but real operations are required in both Real Fourier domain and Harley domain while complex operations are required in the Complex Fourier domain. The opportunity for savings in the real domains is quite significant as harmonic evaluations of each non-linear element involves convolutions and multiplications of vectors and matrices of relatively large dimensions.

New methods for solving power systems harmonic problems have been presented. They are based on the use of real transforms i.e. Real Fourier and Hartley, and provide more efficient alternatives then an existing method which uses the Complex Fourier transform. Any number of linear and non-linear plant components can be represented in these frames of reference and owing to their nodal nature, any number of buses, phase and harmonics can be represented with ease for a unified solution via Newton-Raphson techniques exhibiting quadratic convergence. The theory is tested in a practical transmission system.

Chapter 5

Three-Phase Thyristor Controlled Reactors

In this chapter new harmonic domain models for single and three-phase Thyristor Controlled Reactors (TCR) are presented. The modelling is carried out in the frequency domain using the complex Fourier domain. It makes use of harmonic switching vectors and discrete convolutions. In the presence of low harmonic distortion the switching vectors are calculated only once during the iterative process. This operation is performed entirely in the frequency domain. In cases of high harmonic content the switching times defining the switching functions may require further identifications during the iterative process. A portion of an actual power network is used to test the TCR model.

5.1 Introduction

Static VAR Compensators, SVCs, are an attractive means of alleviating a wide range of problems encountered in modern power systems [99]. They provide an adaptable form of compensation which responds almost instantly to most operating conditions of the power network.

Thyristor Controlled Reactors, TCRs, are static compensators capable of absorbing reactive power from a network as opposed to Thyristor Switched Capacitors, TSCs, which supply reactive power to a network [100]. This chapter is concerned with the harmonic modelling of TCRs and their interaction with the power network.

From the operational point of view TCRs act as controlled susceptances which achieve their fundamental frequency operating state at the expense of generating harmonic currents [99, 100]. These harmonics are merely a side effect and measures such as the use of different three phase arrangements or other control strategies must be used to prevent the harmonics from reaching the high voltage side of the network. Filtering equipment is often used, but many repetitive studies are necessary to establish the optimum design of such equipment which constitutes a significant fraction of the total capital cost of the compensating plant. Accordingly, there is a need for the development of versatile methods for the rapid and accurate calculation of TCR harmonics. Comprehensive analysis of TCRs operating under a wide range of conditions may be economically achieved by digital simulations based on steady-state techniques.

Power systems reactive compensation by means of solid state devices is a mature but relatively new technology. Over the last 20 years it has engaged a large number of researchers in both industry and academia. Reference [99] gives values of the maximum harmonic currents drawn by TCRs under balanced conditions. However, balanced conditions never occur in practice. Static compensators are prone to exhibit imbalances due to manufacturing tolerances in their parts and the high-voltage transmission network can be very unbalanced

at harmonic frequencies. In 1981 RM Mathur [101] modelled the TCR as an unbalanced harmonic current source affected by both firing and inductance asymmetries, but network interaction was ignored. In 1986 R Yacamini and JW Resende published a model which takes TCR imbalances fully into account [102]. In such a model each TCR branch is represented as a voltage-dependent set of harmonic current sources, which is injected back into the nodal impedance of the network to obtain an updated set of harmonic voltages with which the cycle can be repeated, reaching the harmonic solution by iteration. In this method the TCR harmonic current coefficients are determined by means of Fourier analysis. In 1988 W Xu, JR Marti and HW Dommel published a method based on alternate time domain and frequency domain representations of the TCR currents [103]. This involves deriving a full cycle of the current, at the fundamental frequency, across each TCR branch and then extracting their harmonic contents via FFT algorithms. These operations are carried out at each iteration. In this method each TCR branch is modelled as a voltage-dependent harmonic current source. In order to circumvent poor convergence performance associated with this representation, the same authors published in 1991 an alternative model whereby each individual TCR branch is modelled as a harmonically 'decoupled' Norton equivalent [104]. Harmonic current calculation in both methods is the same. The admittance element calculation is based on fundamental frequency information only, and scaled-down at each frequency of interest. The authors have reported marked improvements in convergence performance. In 1989 LJ Bohmann and RH Lasseter reported on a harmonic domain admittance model [105] which exhibits cross-couplings between frequencies. The model was intended for single phase TCRs and is based on the use of switching functions.

In 1991 E Acha put forward a three phase TCR model which uses the harmonic domain as the frame of reference [106], where all the harmonics and cross-couplings between harmonics are explicitly shown. Each single phase unit of the TCR is modelled as a voltage-dependent harmonic Norton equivalent. The admittance matrix of the Norton equivalent has a quasi-Toeplitz structure and plays the role of a Jacobian in the iterative solution. In this method a full cycle of the current at the fundamental frequency is determined and then a FFT is used to obtain the harmonic content of the current waveform. Also, a full cycle of the derivative of the current with respect to the flux is obtained and the harmonic coefficients obtained via a FFT are used to assemble the admittance matrix of the Norton equivalent. This procedure is carried out for each branch, then a three phase TCR model is assembled and combined with the nodal admittance matrix of the transmission network to obtain an updated set of harmonic voltages. These harmonic voltages can be used to calculate an updated harmonic Norton equivalent with which the cycle can be repeated. When a satisfactory degree of convergence has been achieved, the calculated harmonics will be in balance. This method requires two FFTs per iteration and there are plenty of opportunities for introducing unwanted errors in the solution process due to discretisation of the waveform, aliasing and round-off errors, hence degrading Newton method's quadratic convergence. A more efficient formulation which overcomes these limitations was published by E Acha and JJ Rico for the case of single phase TCRs [107]. This method is a harmonic domain Newton-Raphson technique, which uses frequency domain information only. It is based on the use of harmonic vectors and discrete convolutions. The process of transforming back and forth between time and frequency domains is avoided, as well as the use of FFTs. The Fourier coefficients of the switching vector are calculated directly in the frequency domain by means of simple, closed-form, equations. A discrete convolution of the switching vector and the input voltage, which is a frequency domain operation, provides the harmonic coefficients of the TCR current. The overall result is a 'true' Newton-Raphson algorithm exhibiting quadratic convergence even in cases of excessive harmonic distortion.

In the present chapter the author has generalised the single phase TCR model to the case

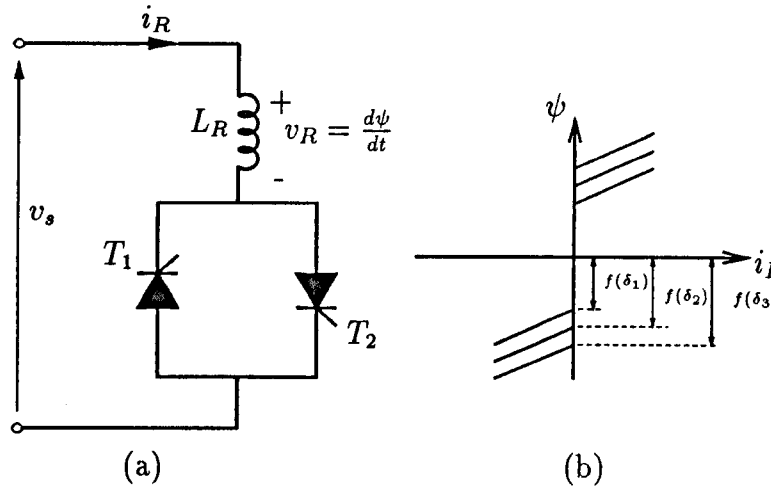

Fig. 5.1: (a)Schematic representation of a Single phase TCR (b)instantaneous $\psi - i_R$ characteristic

of multi-pulse TCRs. Six-pulse and twelve-pulse TCR solutions are derived in this chapter. These generalised models incorporate with ease any kind of imbalances present in the TCR or in the external network. The transmission system can be represented in full [108] or as a reduced equivalent network [109] incorporating detailed frequency-dependent, geometric and long-line effects [110].

5.2 Single Phase Modelling of Thyristor Controlled Reactors

In power systems compensation studies a single phase TCR is conveniently represented as a linear inductor in series with two reverse-parallel connected thyristors and a firing control system. Figure 5.1(a) shows a single phase TCR fed from a sinusoidal voltage source. This circuit is used as the starting point for deriving a TCR model in the harmonic domain frame of reference. The flux-current characteristics exhibited by a TCR, acting under a sinusoidal AC excitation flux, are a family of straight lines which are a function of the delay or firing angle δ, as shown in Figure 5.1(b).

The conduction angle σ depends on the firing angle δ according to the relationship,

$$\sigma = 2\,(\pi - \delta) \tag{5.1}$$

In principle at least, the firing angle δ can be controlled to take any value between 90° and 180°, corresponding to values of σ between 180° and 0°. The former case corresponds to the TCR in a fully conducting state while the latter corresponds to the TCR in a completely non-conducting state. Both operating conditions are free from harmonics, whereas any other condition in between will be accompanied by the generation of harmonics. If we were to define a switching function s in the time domain which takes a value of 1 if either thyristor is conducting and takes a value of 0 if neither thyristor is conducting, then we would have the situation shown in Figure 5.2. It must be noted that the conduction angles of thyristors T_1 and T_2 can be different. The excitation voltage and current are shown in Figure 5.2(a) whilst the switching function for a given conduction angle and its product with the voltage are shown in Figures 5.2(b) and 5.2(c), respectively.

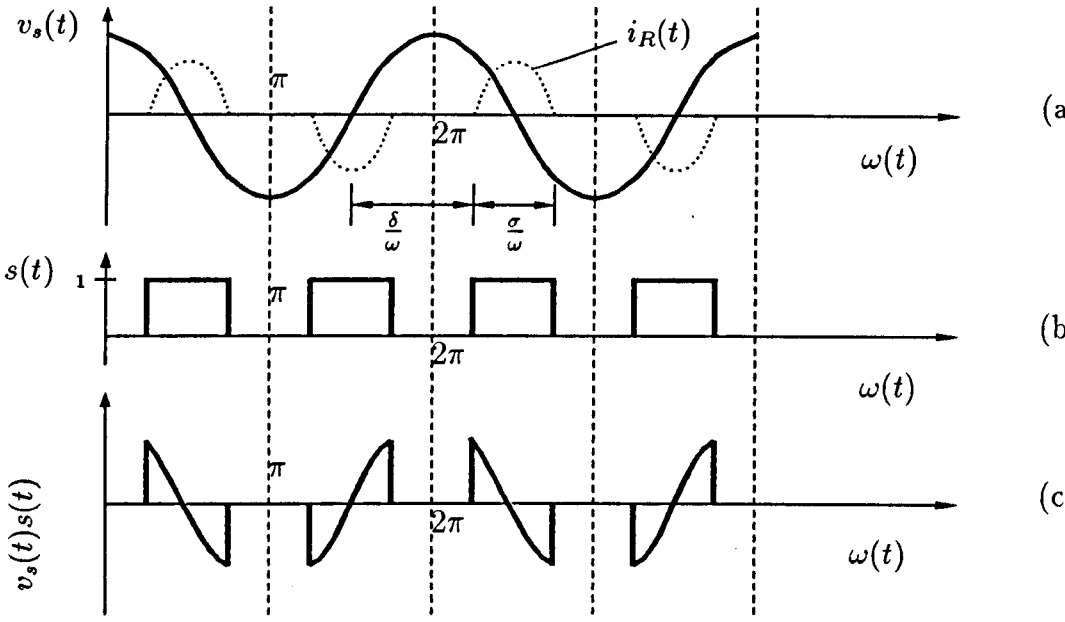

Fig. 5.2: (a)Excitation voltage and output current source, (b) switching function and (c) product of input and switching function

5.2.1 TCR Harmonic current vector

The circuit in Figure 5.1(a) may be used to write the dynamic equation of the current across the TCR,

$$\frac{di_R}{dt} = \frac{1}{L_R} s(t)v(t) \tag{5.2}$$

or

$$i_R = \frac{1}{L_R} \int_0^t s(\tau)v(\tau)d\tau \tag{5.3}$$

Applying Fourier Transform to both sides of equation (5.3) we have that,

$$I_R(jw) = \frac{1}{L_R} \mathcal{F}\left[\int_0^t s(\tau)v(\tau)d\tau\right] \tag{5.4}$$

Finally, taking the Integration and Frequency Convolution theorems into account and considering that $\mathcal{F}[s(t)] = S$ and $\mathcal{F}[v(t)] = V$, it is possible to write an expression for the current in the frequency domain as follows,

$$I_R = \frac{1}{jhwL_R} S \circledast V \tag{5.5}$$

Considering that $V = diag(jh\omega)\Psi$, where $diag()$ is a diagonal matrix with entries $j\omega h$, the current derivative with respect to the flux Ψ is expressed as follows,

$$f'(\Psi) = \frac{1}{L_R} S \tag{5.6}$$

which is the switching function scaled down by the inverse of the inductance of the linear reactor L_R. It must be noted that equations (5.5) and (5.6) are used to calculate a linearised equivalent about a base operating point V_b, I_b,

$$\Delta I_R = [F]\Delta\Psi \tag{5.7}$$

or,

$$\Delta I_R = [H]\Delta V \tag{5.8}$$

The matrix $[F]$ plays the role of a Jacobian matrix in the iterative solution. It has a Toeplitz structure [17] and it is assembled with the harmonic coefficients of equation (5.6).

The following relationship exists between $[H]$ and $[F]$,

$$[H] = [F]diag\left(\frac{1}{jwh}\right) \tag{5.9}$$

Equation (5.8) may be interpreted as a harmonic Norton equivalent,

$$I = [H]V_{+}I_N \tag{5.10}$$

where,

$$I_N = I_b - [H]V_b \tag{5.11}$$

The harmonic vector I_b is assembled with the Fourier coefficients of equation (5.5).

5.2.2 Harmonic switching functions

One way of obtaining the harmonic coefficients of the switching vector is by drawing a full cycle of the switching function at the fundamental frequency and then using a FFT [17]. However, a faster and more accurate way of achieving this result is by determining the harmonic coefficients of the switching function in terms of the conduction angles σ_1 and σ_2. The switching function $s(t)$ in equation (5.2), and shown in Figure 5.3, has values of one whenever the thyristor is on and zero whenever the thyristor is off. In the frequency domain a periodic train of pulses described by the switching function can be represented by the harmonic vector (5.12),

$$S = \begin{pmatrix} \frac{a_{-h}}{2} - j\frac{b_{-h}}{2} \\ \vdots \\ \frac{a_{-2}}{2} - j\frac{b_{-2}}{2} \\ \frac{a_{-1}}{2} - j\frac{b_{-1}}{2} \\ \frac{a_0}{2} \\ \frac{a_1}{2} + j\frac{b_1}{2} \\ \frac{a_2}{2} + j\frac{b_2}{2} \\ \vdots \\ \frac{a_h}{2} + j\frac{b_h}{2} \end{pmatrix} \tag{5.12}$$

In general, the complex coefficients are written as,

$$S_h = \frac{a_h}{2} + j\frac{b_h}{2} = \frac{1}{\pi}\int_{-\pi}^{\pi} s(t)e^{-jh\omega t}d\omega t \tag{5.13}$$

The coefficients a_h and b_h are obtained from the following relations,

$$\begin{aligned} \frac{1}{2}a_0 &= \frac{\sigma_1 + \sigma_2}{2\pi} \\ a_h &= \frac{2}{h\pi}\left[\sin\left(\frac{h\sigma_1}{2}\right) + \sin\left(\frac{h\sigma_2}{2}\right)\right]\cos\left(\frac{h\pi}{2}\right) \\ b_h &= \frac{2}{h\pi}\left[\sin\left(\frac{h\sigma_2}{2}\right) - \sin\left(\frac{h\sigma_1}{2}\right)\right]\sin\left(\frac{h\pi}{2}\right) \end{aligned} \tag{5.14}$$

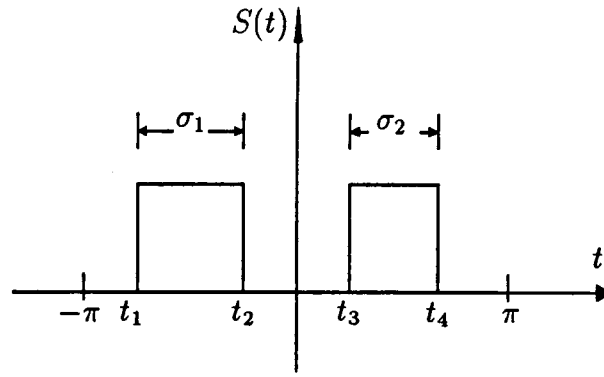

Fig. 5.3: Switching function

The Fourier coefficients a_h and b_h are calculated from equations (5.15), (5.16) and (5.17) which take into account that the switching function has a value of one in the following intervals $[\frac{-\pi}{2} - \frac{\sigma_1}{2}, \frac{-\pi}{2} + \frac{\sigma_1}{2}]$ and $[\frac{\pi}{2} - \frac{\sigma_2}{2}, \frac{\pi}{2} + \frac{\sigma_2}{2}]$.

$$a_0 = \frac{1}{\pi}\left[\int_{\frac{-\pi}{2}-\frac{\sigma_1}{2}}^{\frac{-\pi}{2}+\frac{\sigma_1}{2}} d\omega t + \int_{\frac{\pi}{2}-\frac{\sigma_2}{2}}^{\frac{\pi}{2}+\frac{\sigma_2}{2}} d\omega t\right] \tag{5.15}$$

$$a_h = \frac{1}{\pi}\left(\int_{\frac{-\pi}{2}-\frac{\sigma_1}{2}}^{\frac{-\pi}{2}+\frac{\sigma_1}{2}} \cos(h\omega t)d\omega t + \int_{\frac{\pi}{2}-\frac{\sigma_2}{2}}^{\frac{\pi}{2}+\frac{\sigma_2}{2}} \cos(h\omega t)d\omega t\right) \tag{5.16}$$

$$b_h = \frac{1}{\pi}\left(\int_{\frac{-\pi}{2}-\frac{\sigma_1}{2}}^{\frac{-\pi}{2}+\frac{\sigma_1}{2}} \sin(h\omega t)d\omega t + \int_{\frac{\pi}{2}-\frac{\sigma_2}{2}}^{\frac{\pi}{2}+\frac{\sigma_2}{2}} \sin(h\omega t)d\omega t\right) \tag{5.17}$$

Under normal operating conditions, the current across the TCR is comprised of the fundamental and odd harmonics which amplitude is a function of the conduction angles σ_1 and σ_2 [99]. The harmonic currents drawn by a single phase TCR connected to an infinite bus bar have been calculated with the model described above and the results are shown in Figure 5.4. It shows the percentage of all the relevant harmonics with respect to the maximum fundamental current at full conduction. These results are in full agreement with values available in open literature [99, 105], hence showing evidence of the accuracy of the single phase TCR model.

5.3 Firing Control Systems

Control firing systems of TCRs may, under certain circumstances, generate and magnify some of the harmonics present in power systems. In some cases, these effects are of little consequence but sometimes these disturbances may prevent stable operation of the system. Over the years new and more robust controllers have been developed. There are two main classes of TCRs controllers: closed loop and open-loop. Open loop controllers have poor performance and have been superseded by closed loop controllers. The TCR model developed in this chapter assumes the use of close-loop controllers. A widely used class of closed loop controller is the Phase-locked oscillator [102].

An important part of these controllers is that which determines the valve firing times. There are three firing control systems used in TCRs, namely individual phase control (IPC), pulse frequency control (PFC) and pulse phase control (PPC). All of them may be simulated

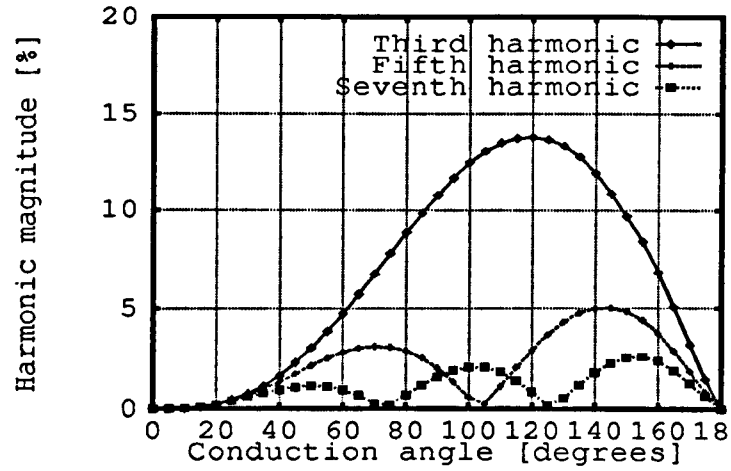

Fig. 5.4: Harmonic currents versus Conduction angle

in a computer program [111]. IPC controllers are no longer used in the new control schemes but their use in the early stages of TCR applications suggest the need to take them into account in modern analysis.

The purpose of a firing system is to determine the firing instants of the reference (phase a) under the presence of arbitrarily distorted a.c. bus voltages. Prior to the determination of such firing angles, in any scheme, the voltage zero crossings of the a.c. voltage must be calculated. This applies to all three iterative schemes.

5.3.1 Voltage zero crossing evaluation

The phase-to-neutral a.c. bus voltages can be generally expressed as,

$$v(\omega_0 t) = \sum_{h=0}^{nh} \left(V_h' \cos(\omega_0 t) + V_h'' \sin(\omega_0 t)\right) \tag{5.18}$$

where nh is the number of harmonics considered and ω_0 is the fundamental frequency of the system, V_h' and V_h'' are the Fourier coefficients corresponding to harmonic h. The voltage zero crossing angle $\omega_0 t$ can be calculated, for the reference phase, from following equation,

$$F(\omega_0 t) = 0 = \sum_{h=0}^{nh} \left(V_h' \cos(\omega_0 t) + V_h'' \sin(\omega_0 t)\right) \tag{5.19}$$

Equation (5.19) is non-linear and can be solved by Newton-Raphson method,

$$(\omega_0 t)^{n+1} = (\omega_0 t)^n + \Delta(\omega_0 t)^n \tag{5.20}$$

where

$$\Delta(\omega_0 t)^n = -\frac{F((\omega_0 t)^n)}{F'((\omega_0 t)^n)} \tag{5.21}$$

5.3.2 Firing angle evaluation

IPC, PFC and PPC firing schemes control the thyristor firing angles in such a way that the angle, measured from the voltage zero crossing to the instant of firing, is constant. However,

there is a fundamental difference between the various control schemes which relates to the starting point of the delay time, before a firing signal is triggered. In the IPC system a level detector senses the voltage zero crossing; at this point a ramp voltage is initiated and its value compared with a reference control voltage. The firing pulse is produced when both voltages are equal, this can be expressed as,

$$F(t) = K\omega_0 t = \sum_{h=0}^{nh} \left(V_h' \cos(\omega_0 t) + V_h'' \sin(\omega_0 t)\right) \tag{5.22}$$

or

$$F(t) = K\omega_0 t - \sum_{h=0}^{nh} \left(V_h \cos(\omega_0 t) + V_h \cos(\omega_0 t)\right) = 0 \tag{5.23}$$

The Newton-Raphson solution of equation (5.23) yields, for this nonlinear equation, the following iteration process,

$$t^{n+1} = t^n + \Delta t^n \tag{5.24}$$

where

$$\Delta t^n = -\frac{F(t^n)}{F'(t^n)} \tag{5.25}$$

Unlike IPC systems, PFC and PPC schemes initiate the ramp voltage at equidistant firing instants which are set to values proportional to the control voltage. PFC's frequency is controlled while the phase is controlled in PPCs. The triggering points do not, in general, correspond to the voltage zero crossings and the following relation holds,

$$\alpha = \psi + \delta \tag{5.26}$$

where ψ is the angle at the zero crossing time and δ is the angle elapsed from the zero crossing to instant of firing. Similarly to the IPC system, the angle δ is calculated with the following equation,

$$\delta = \omega_0 t \tag{5.27}$$

5.3.3 Turn-off time evaluation

A complete definition of the switching function requires knowledge of the firing times t_1 and t_3 and turn-off times t_2 and t_4 shown in Figure 5.3. The firing times are evaluated as explained above. Turns-off switching times are determined by the zero crossing of the thyristor's current. LJ Bohmann and RL Lasseter [105] have calculated these by solving the following non-linear equation,

$$i_R(t) = \int \frac{1}{L_R} v_R(\omega t) d\omega t \tag{5.28}$$

If the voltage across the TCR is assumed to be a complex harmonic series, the current is a similar summation of exponentials,

$$i_R(\omega t) = \sum_{h=-nh}^{nh} \frac{V_h}{jh\omega L_R} e^{jh\omega t} \tag{5.29}$$

In the zero crossing we have that,

$$0 = \sum_{h=-nh}^{nh} \frac{V_h}{jh\omega L_R} e^{jh\omega t} \tag{5.30}$$

A Newton-Raphson can be used to solve this non-linear equation. Proper initial conditions are required to ensure that the solution will converge to the desired solution point. Since the current also has a zero crossing at the firing instant. A good initial guess for turn off times can be obtained from a pure sinusoidal voltage.

5.4 Three Phase TCR Modelling

For most three phase applications, the branches of the TCR are delta-connected, in order to cancel out the third, ninth and fifteenth harmonic currents. Further harmonic cancellation is made possible by employing two three phase bridges with a shift of 30° between them.

In the case of a three phase delta-connected bridge, the harmonic Norton equivalent can be found by linear transformations. The harmonic Norton equivalent corresponding to the unconnected three phase TCR is,

$$\begin{pmatrix} I_1 \\ I_2 \\ I_3 \end{pmatrix} = \begin{pmatrix} G_{N,1} & & \\ & G_{N,2} & \\ & & G_{N,3} \end{pmatrix} \begin{pmatrix} V_1 \\ V_2 \\ V_3 \end{pmatrix} + \begin{pmatrix} I_{N,1} \\ I_{N,2} \\ I_{N,3} \end{pmatrix} \tag{5.31}$$

or, in compact form,

$$I_\varphi = [G_{\varphi\varphi}]V_\varphi + I_{\varphi N} \tag{5.32}$$

In a power invariant, delta-connected circuit the relationships between the unconnected and connected states are,

$$\begin{pmatrix} V_1 \\ V_2 \\ V_3 \end{pmatrix} = \frac{\angle 30^\circ}{\sqrt{3}} \begin{pmatrix} 1 & -1 & \\ & 1 & -1 \\ -1 & & 1 \end{pmatrix} \begin{pmatrix} V_a \\ V_b \\ V_c \end{pmatrix} \tag{5.33}$$

and,

$$\begin{pmatrix} I_a \\ I_b \\ I_c \end{pmatrix} = \frac{\angle 30^\circ}{\sqrt{3}} \begin{pmatrix} 1 & & -1 \\ -1 & 1 & \\ & -1 & 1 \end{pmatrix} \begin{pmatrix} I_1 \\ I_2 \\ I_3 \end{pmatrix} \tag{5.34}$$

or, in compact form,

$$V_\varphi = \frac{\angle 30^\circ}{\sqrt{3}}[C_{\varphi\alpha}]V_\alpha \tag{5.35}$$

$$I_\alpha = \frac{\angle 30^\circ}{\sqrt{3}}[C_{\alpha\varphi}]I_\varphi \tag{5.36}$$

Premultiplying equation (5.32) by $\frac{\angle 30^\circ}{\sqrt{3}}[C_{\alpha\varphi}]$, we have that

$$\begin{aligned} \frac{\angle 30^\circ}{\sqrt{3}}[C_{\alpha\varphi}]I_\varphi &= \frac{\angle 30^\circ}{\sqrt{3}}[C_{\alpha\varphi}][G_{\varphi\varphi}]V_\varphi \\ &+ \frac{\angle 30^\circ}{\sqrt{3}}[C_{\alpha\varphi}]I_{\varphi N} \end{aligned} \tag{5.37}$$

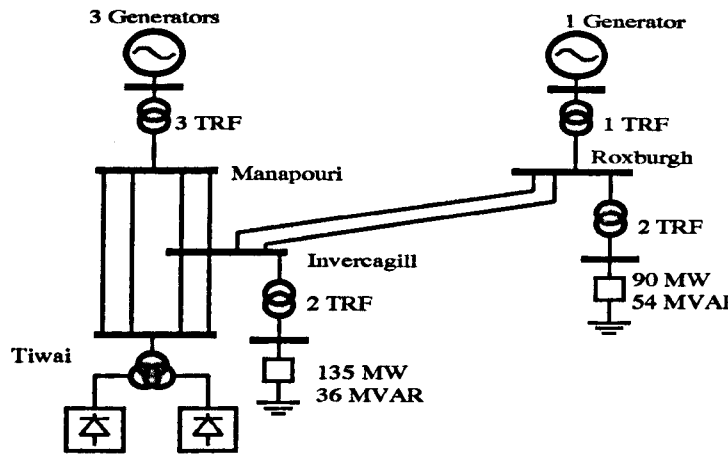

Fig. 5.5: South Island Test System

Substituting equations (5.35) and (5.36) into equation (5.37) gives the three phase Norton equivalent equation,

$$\begin{aligned} I_\alpha &= \frac{\angle 30^\circ}{\sqrt{3}}[C_{\alpha\varphi}][G_{\varphi\varphi}]\frac{\angle -30^\circ}{\sqrt{3}}[C_{\varphi\alpha}]V_\alpha \\ &+ \frac{\angle 30^\circ}{\sqrt{3}}[C_{\alpha\varphi}]I_{\varphi N} \end{aligned} \tag{5.38}$$

or,

$$\begin{aligned} I_\alpha &= \frac{1}{3}[C_{\alpha\varphi}][G_{\varphi\varphi}][C_{\varphi\alpha}]V_\alpha \\ &+ \frac{\angle 30^\circ}{\sqrt{3}}[C_{\alpha\varphi}]I_{\varphi N} \end{aligned} \tag{5.39}$$

In expanded matrix notation form, the three phase Norton equivalent of the delta-connected TCR is,

$$\begin{aligned} \begin{pmatrix} I_a \\ I_b \\ I_c \end{pmatrix} &= \frac{1}{3}\begin{pmatrix} G_{N,1}+G_{N,2} & -G_{N,2} & -G_{N,1} \\ -G_{N,2} & G_{N,2}+G_{N,3} & -G_{N,3} \\ -G_{N,1} & -G_{N,3} & G_{N,3}+G_{N,1} \end{pmatrix} \\ &\times \begin{pmatrix} V_a \\ V_b \\ V_c \end{pmatrix} + \frac{\angle 30^\circ}{\sqrt{3}}\begin{pmatrix} I_{\varphi N,1}-I_{\varphi N,2} \\ I_{\varphi N,2}-I_{\varphi N,3} \\ I_{\varphi N,3}-I_{\varphi N,1} \end{pmatrix} \end{aligned} \tag{5.40}$$

5.5 Case Studies

The three phase TCR model developed in the previous section has been tested on the reduced South Island system of the 220 kV New Zealand power network. It is a real power system for which complete data exists in open literature [112]. The relevant data is given in Appendix A. The system is shown in Figure 5.5. Actual measurements have indicated the presence of a parallel resonance near the 5th harmonic frequency, i.e. 250 Hz. Comprehensive simulation studies have been carried out for this reduced system in the past and its frequency response is well known [113]. This author has used his own multi-phase frequency scan program to

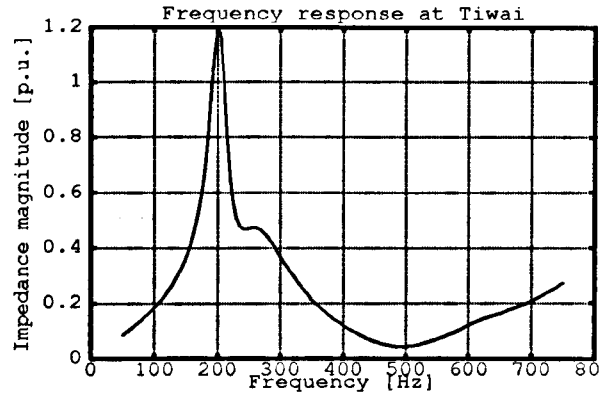

Fig. 5.6: Frequency scan

verify such simulation results independently and a good match has been found. Figure 5.6 shows the harmonic impedance of phase A in p.u., as seen from Tiwai. The presence of a parallel resonance laying between the 4th and the 5th harmonic frequency is clearly shown. To test our model, the large converter plant at Tiwai has been replaced by a delta-connected three phase TCR. Generators, transformers and loads have been assumed to behave linearly. The software has the option of representing the transmission system in full or as a reduced equivalent network. The latter option has been used for obtaining the results presented below because the interest is in analysing the interaction between the TCR and the network at the point of connection.

5.5.1 Six pulse, three phase TCR

As shown in Figure 5.4, a TCR will inject maximum 5th harmonic current when the conduction angle is 140°. In the case being analysed, this condition is compounded with the parallel resonance at the 5th harmonic frequency exhibited by the network to give rise to a badly distorted voltage waveform at Tiwai. Figure 5.7(a) shows the voltage waveforms whilst Figure 5.7(b) shows the harmonic content for the three phases. Large harmonic voltage imbalances are shown in this result where the percentage of the 5th harmonic reaches almost 12 per cent for phase C. The remaining harmonic voltages are well below recommended limits and are cause of no concern [114]. However, filtering equipment would have to be connected at Tiwai to provide a low impedance path for the 5th harmonic current. The TCR is delta-connected and under perfectly balanced conditions no third harmonic current should flow towards the high-voltage side of the network. However, small geometric imbalances in the transmission system will allow a small amount of 3rd harmonic current to escape the delta producing a small amount of 3rd harmonic voltage.

According to figure 5.4 the TCR also inject considerable 5th harmonic when the conduction angle is 70°, this condition has also been simulated and the results are shown in Figure 5.8. Figure 5.8(a) shows the voltage waveforms whilst Figure 5.8(b) shows the harmonic content for the three phases.

DC Component

The TCR model is capable of considering not just angle assymetries in the conduction angle but also conditions when a DC voltage component already exists at the TCR bus bar voltages. This may be due to the presence of a DC load in HVDC systems or problems with capacitors.

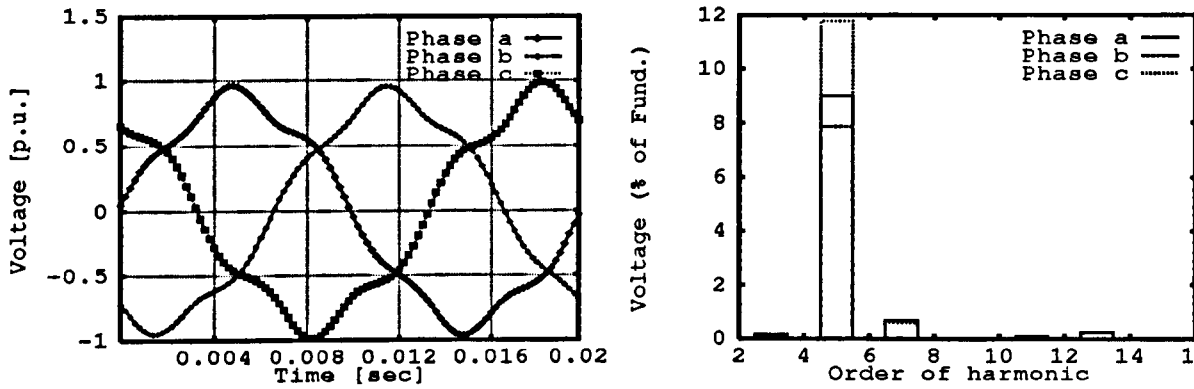

(a) (b)

Fig. 5.7: Voltages at Tiwai bus bar with $\sigma = 140^o$

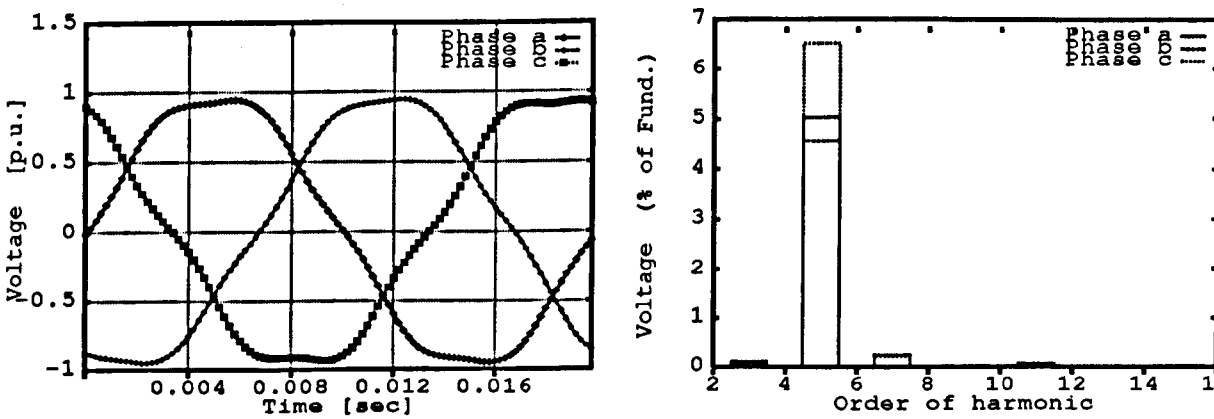

(a) (b)

Fig. 5.8: Voltages at Tiwai bus bar with $\sigma = 70^o$

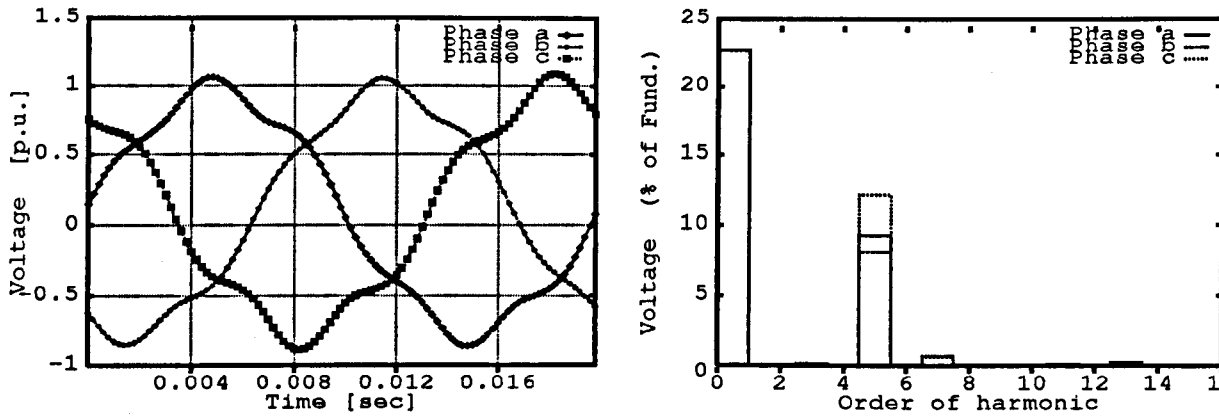

(a) (b)

Fig. 5.9: Voltages at Tiwai bus bar with $\sigma = 140^o$

To show the capability a DC voltage component of 0.2 p.u. was assumed at Tiwai. This was injected into the TCR producing the results shown in this Figure 5.9. Figure 5.9(a) shows the voltage waveforms whilst Figure 5.9(b) shows the harmonic content for the three phases.

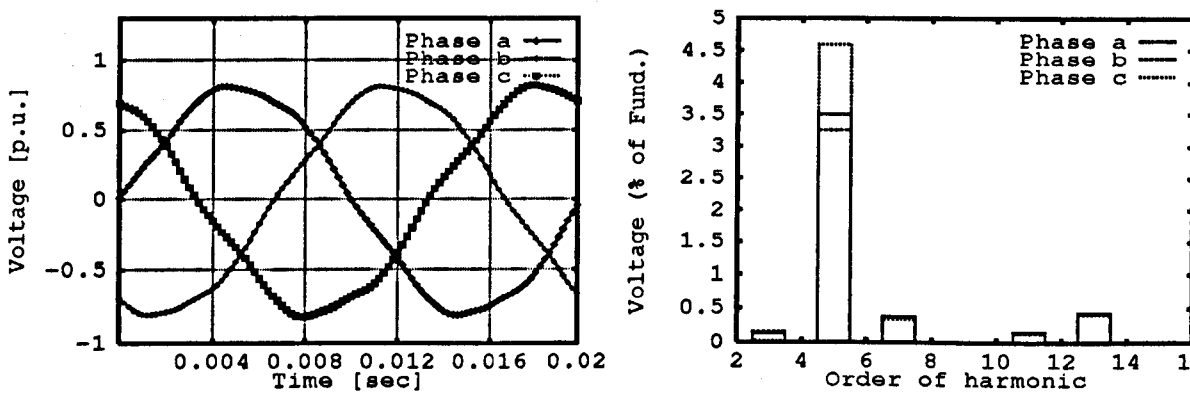

(a) (b)

Fig. 5.10: Voltages at Tiwai bus bar

5.5.2 Twelve pulse, three phase TCR

TCR harmonic currents can always be removed by means of filtering equipment. An alternative arrangement for eliminating 5th and 7th TCR harmonic currents is by splitting the six pulse TCR into two identical half-sized units and employing a three phase transformer with two secondary windings. The primary winding is grounded star-connected. One secondary winding is star-connected whilst the other secondary winding is delta-connected. One half-sized unit is connected to each secondary winding. This configuration produces a 30° phase shift between the fundamental frequency currents drawn by each TCR. Under balanced operating conditions, the 5th and 7th harmonic currents of both TCRs will be equal in magnitude and in phase opposition at the primary side of the transformer. Consequently, they

will cancel out with each other at the primary side of the transformer. However, if network or TCR asymmetries are present then a reduced amount of 5th and 7th harmonic currents will escape towards the network causing the voltage at the transformer connection point to be non-sinusoidal if conditions for harmonic voltage magnification exist. This situation is illustrated in Figure 5.10(a) where the TCR conduction conduction angle is 140°. The three phase waveform still shows a significant amount of 5th harmonic voltage due to transmission system imbalances compounded with the presence of a parallel resonance near the 5th harmonic. Figure 5.10(b) shows a value of 4.5 per cent for phase C. In this case, the use of a 12-pulse TCR has reduced 5th harmonic voltage distortion by almost a third compared to the 6-pulse TCR used above. Nevertheless, this value still is well above the threshold value permitted by existing legislation [114] and the use of filtering equipment will be needed to filter out any trace of 5th harmonic current at the high-voltage side of the transformer.

5.6 Conclusions

A new, three phase TCR harmonic model which is based on the use of harmonic switching vectors and discrete convolutions, has been presented. This harmonic model is completely general and can be interpreted as a harmonic Norton equivalent. It is suitable for direct incorporation into the multi phase harmonic domain frame of reference where it combines easily with the frequency dependent admittances of the transmission network and with other linearised components such as saturated transformers, rotating machinery, electric arcs and power converters. The use of harmonic switching vectors and discrete convolutions has been shown to be a simple and yet powerful combination in the solution of TCR harmonics. All operations are conducted in the frequency domain and the use of alternate time domain and frequency domain representations is avoided and so it is the use of FFTs. This approach leads to very efficient iterative solutions of power networks containing TCRs by means of a harmonic Newton-type technique exhibiting quadratic convergence.

Chapter 6

Duality-Based Three-Phase Multi-limb Transformers

The modelling approach presented in this chapter is based on the principle of Duality. New harmonic domain models of three phase, multi-limb transform are developed using this principle. The models accurately incorporates all relevant effects which become important when the transformer saturates. As opposed to existing harmonic domain models, the Duality-based methods proposed in this chapter incorporate construction details of the transformer. Commonly used core configurations are analysed. The complete linearised model is represented as a harmonic Norton Equivalent which combines easily with the external power network taking due account electrical of the transform's connection. A practical system is used to test the transformer model.

6.1 Introduction

Arguably, transformers are one of the most common and mechanically simple power plant components. However, no single model has proven appropriate for studying a wide range of frequencies and different operating conditions. Different component models are used for steady-state and for slow and fast transient studies. Transformer models for harmonic analysis as well as transient analysis require rigorous representations. Comprehensive transformer models have been developed for transient studies [115] but, so far, no transformer model incorporating such detail and level of sophistication has been developed for harmonic studies.

Over the years, an intensive search for determining models capable of modelling correctly the interaction of core fluxes, has been carried out. The principle of duality developed by Cherry [116] and generalised by Slemon [117] provides a means to tackle this problem. At first, this approach did not receive attention because computers were not powerful enough. An additional complication was the difficulty in measuring the required parameters. More recently the method has been successfully applied to the development of multi-limb, three phase transformers model [115, 118, 119, 120] in the transient analysis field. Promising results using this modelling approach has motivated research relating to parameter identification [121, 118]. Recent work in this field has been carried out by A. Narang and R. H. Brierley [119] and by B. A. Mork and D. L. Stuehm [120].

Accurate transformer models intended for steady state analysis at the fundamental frequency have been in existence for many years. Laughton [122], for instance, put forward a three-phase transformer model for three-phase banks. The lattice equivalent circuit used in this model can take into account asymmetries in the operating conditions. Chen and Dillon

[123] and V. Brandwajn, H.W. Dommel and I. I. Dommel [124] have put forward more general models. These models take account of network imbalances and can accommodate different types of electrical connections. Easy interfacing with the electrical network is achieved owing to their nodal nature. A recent publication reports on a more accurate model where the magnetic circuit of the transformer has been incorporated [125].

Accurate predictions of the electro-magnetic behaviour of the transformer under fast and slow transients call for more rigorous representations of the transformer's electric and magnetic circuits. A great deal of activity has been registered in this area. Recently, a comprehensive model has been put forward by F. De Leon and A. Semlyen in [121]. It represents accurately both leakage inductances and fluxes in the iron core. The trapezoidal rule of integration is used to solve the state equations describing the electric model, resulting in a Norton equivalent. This makes it easy to interface with the external electric network.

Likewise, predicting the periodic steady state behaviour of transformers also require rigorous electro-magnetic models in order to evaluate harmonic distortion due to saturated regions of the magnetic core. Although the periodic operation of transformers can be assessed by using time domain methods, steady-state methods are preferred [17]. A. Semlyen, E. Acha and J. Arrillaga have modelled single phase transformer in the harmonic domain. N. Rajakovic and A. Semlyen have applied harmonic domain modelling techniques to the problem laminated iron cores in [126] and in [127]. They also devised a simple way of including hysteresis effects. The extension of harmonic domain techniques to the solution of quasi-stationary phenomena has also been carried out by N. Rajakovick and A. Semlyen [128].

The concept of harmonic Norton equivalent in the harmonic domain was extended to the three phases by E. Acha, J. Arrillaga, A. Medina and A. Semlyen [129]. In this reference a model for three phase bank of transformer is presented which uses lattice equivalent circuits. These are easily combined with the rest of the network taking due account of the electrical connection. In general, however, power transformers used in high-voltage applications will have multi-limb core with different cross-sectional regions. In such cases, assuming that the core is magnetically equivalent to three single phase transformers may lead to inaccurate results. C. Hatziantoniu, G. D. Galanos and J. Milas-Argitis in an earlier publication [130] presented a three phase transformer model suitable for the study of slow transients and harmonic distortion. The model takes the structure of the iron core into account but all magnetic regions are considered to have the same level of saturation. Furthermore the tank is not considered. A better model which accounts for different cross-sectional branches, yet simplified in terms of the magnetic paths that can take place, was presented by N. Rajakovic and A. Semlyen [128]. A more detailed multi-limb transformer model has been put forward by A. Medina and J. Arrillaga in [131]. The model accounts for different cross-sectional regions of the iron core as well as magnetic flux paths in the air and tank. However, questions arise as to the assumption of distributing equally the magnetising admittance in all external points. This assumption is based on the absence of construction details. In some cases, attaching the iron branch to the winding nearest to the core produces acceptable results, especially for the case of three-legged stacked cores. Validity of the above assumption, however, will depended on the type of core being analysed.

In this chapter a harmonic domain model for multi-limb transformers which relaxes several of the constraints used in previous models is presented. The model represents correctly both leakage paths and the iron core. The transformer model is represented as a harmonic Norton equivalent which interfaces easily with the external network taking due account of the electric connection.

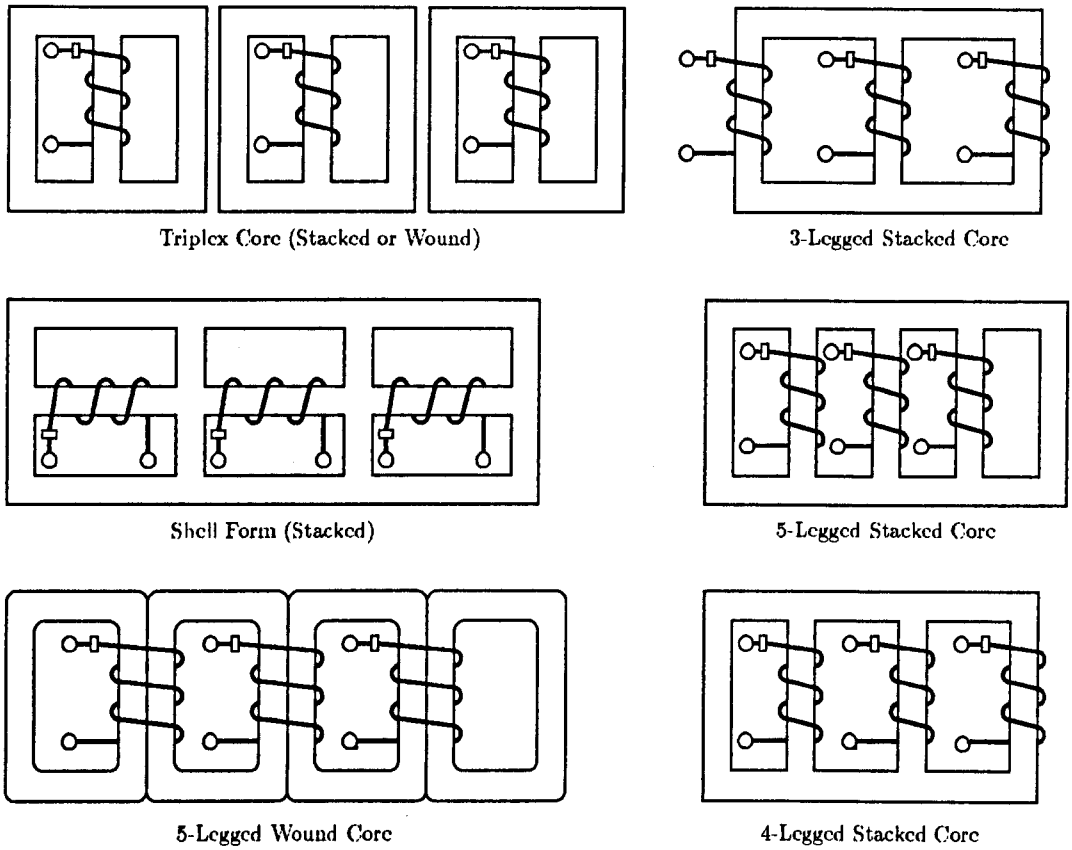

Fig. 6.1: Commonly used Iron Cores

6.2 Magnetic Behaviour of Three Phase Transformers

Under transient and unbalanced conditions, the structure of the iron core of three phase transformers plays an important role in the levels of harmonic distortion attained. In these cases modelling the transformer assuming similar magnetic behaviour to three phase banks may lead to inaccurate results. Figure 6.1 shows some of the most commonly used core configurations. Strictly speaking, only the triplex core displays similar magnetic characteristics to the three phase bank, provided that magnetic isolation between the phases is in place. Although, the three cores are enclosed in the same tank the only magnetic coupling between windings is through magnetic leakage.

Three-legged transformer cores require the least amount of core material to manufacture. The drawback is that their asymmetric structure introduces unbalanced magnetic paths, giving rise to zero sequence fluxes which cannot flow through the iron core but through the insulation oil and the transformer's tank. Eddy currents are exacerbated since tanks are not laminated. The heat generated by eddy currents in the tank can be quite large, resulting in considerable reduction in useful equipment life. Figure 6.2 shows the geometry of the three-legged transformer and its flux distribution. Dashed lines represent magnetic paths. The use of the Duality principle allows the transformer magnetic circuit to be reduced to an arrangement of nodes and flux tubes. All the necessary assumptions required to approximate the actual fields must be introduced at this stage e.g. number of nodes, magnetic branches,etc. The magnetic circuit in Figure 6.3 represents the three-legged transformer shown in Figure 6.2. Since the permeability of the magnetic system varies with the flux density, it is necessary to divide the magnetic material into sections having uniform fluxes.

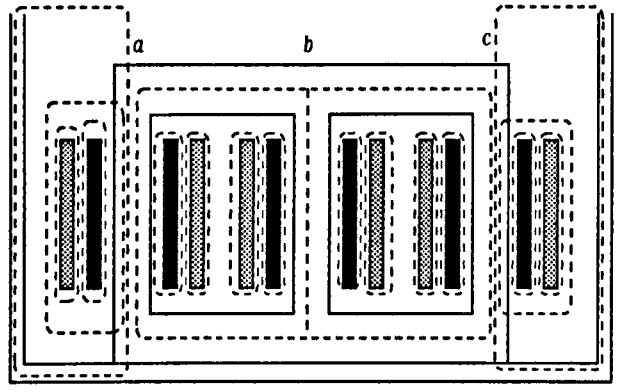

Fig. 6.2: Magnetic fields in a three-legged transformer

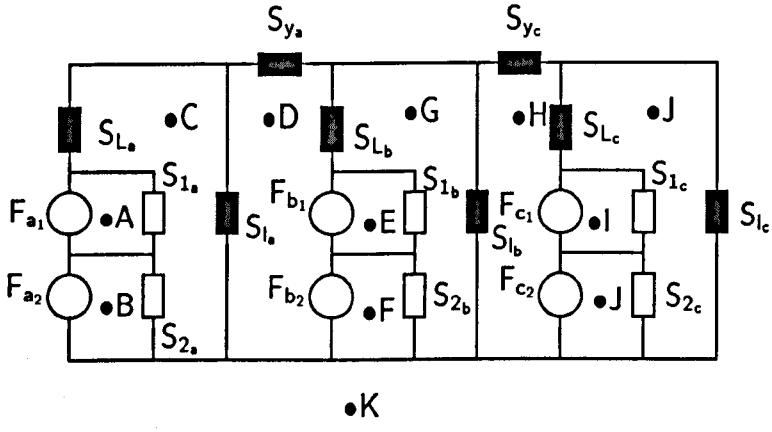

Fig. 6.3: Magnetic circuit in a three-legged transformer

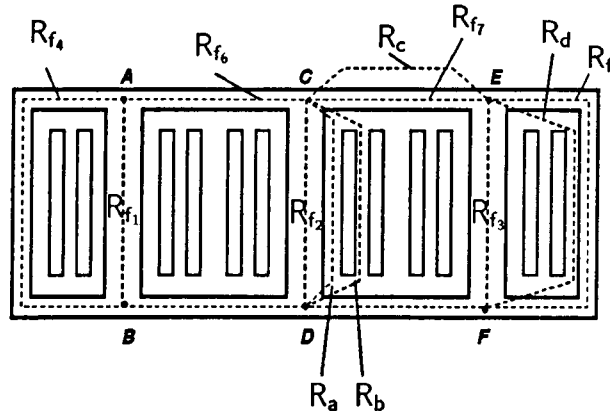

Fig. 6.4: Magnetic field distribution in a five-legged transformer

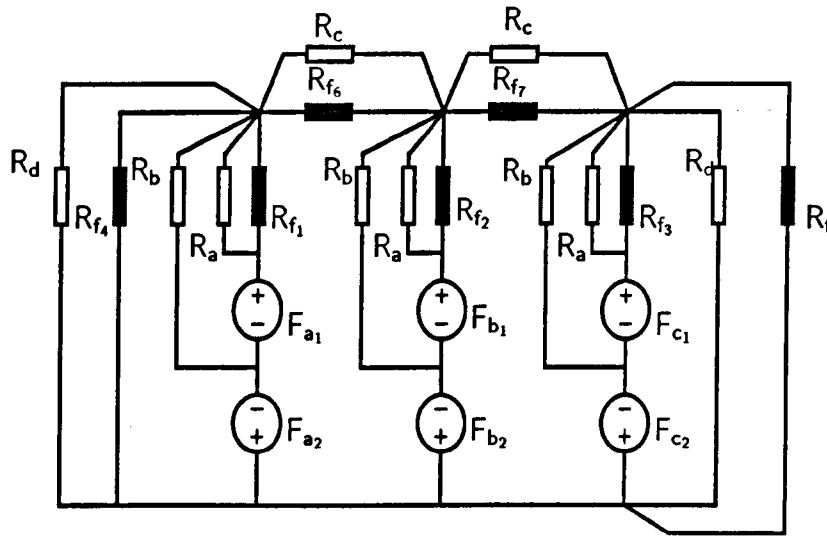

Fig. 6.5: Magnetic circuit associated to the 5-legged transformer

Five-Legged transformers are provided with magnetic paths for zero sequence fluxes. This makes them more expensive than 3-legged, 4-legged transformers or shell form transformers. It has a more symmetric core and sometimes is preferred for its visual appearance in urban sub-stations. The structure of this transformer and assumed magnetic paths are illustrated in Figure 6.4.

The first and perhaps critical step to be addressed when using the duality principle is to determine which flux paths need to be included in the model. This will depend, as seen in Figure 6.2 and Figure 6.4, on the physical structure of the transformer. For instance, the three-limb transformer model in Figure 6.3 must take the tank into account, as it serves as a return path for zero sequence fluxes. Five-limb transformer models do not require the tank to be included since flux paths for zero sequence fluxes are provided within the magnetic core. It is believed that analysis based on Finite Element can give a better an insight as to which flux paths must be considered in the analysis. However, this is consider a future enhancement of this research.

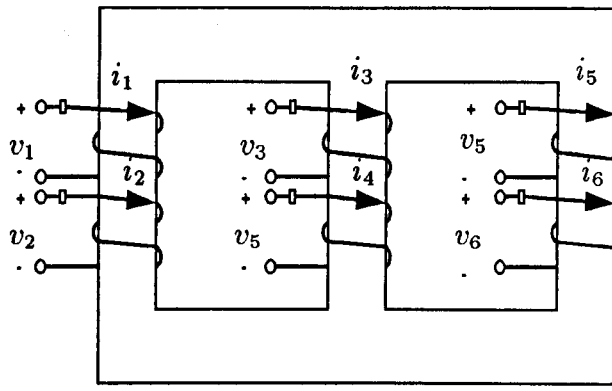

Fig. 6.6: 12-terminal Primitive Network of a three-legged Transformer

6.3 Harmonic Electro-Magnetic Models

Three phase transformers have primitive or unconnected networks consisting of six coupled coils if the transformer has two-winding or nine coupled coils for the case of three windings. Three phase transformers wounded on a common core will exhibit couplings between all windings. The values will depend on the type of iron core. Figure 6.6 illustrates the unconnected, 12-terminal, primitive network of a three-legged transformer.

The leakage admittance matrix for this network is as follows,

$$\begin{pmatrix} i_1 \\ i_2 \\ i_3 \\ i_4 \\ i_5 \\ i_6 \end{pmatrix} = \begin{pmatrix} y_l & -y_l & y_l' & y_l'' & y_l' & y_l'' \\ -y_l & y_l & y_l'' & y_l''' & y_l'' & y_l''' \\ y_l' & y_l'' & y_l & -y_l & y_l' & y_l'' \\ y_l'' & y_l''' & -y_l & y_l & y_l'' & y_l''' \\ y_l' & y_l'' & y_l' & y_l'' & y_l & -y_l \\ y_l'' & y_l''' & y_l'' & y_l''' & -y_l & y_l \end{pmatrix} \begin{pmatrix} v_1 \\ v_2 \\ v_3 \\ v_4 \\ v_5 \\ v_6 \end{pmatrix} \tag{6.1}$$

where

y_l : leakage admittance

y_l' : mutual leakage admittance between primary coils

y_l'' : mutual leakage admittance between primary and secondary coils

y_l''' : mutual leakage admittance between secondary coils

Equation 6.1 is now modified to include the multi-limb magnetic core,

$$\begin{pmatrix} i_1 \\ i_2 \\ i_3 \\ i_4 \\ i_5 \\ i_6 \end{pmatrix} = \begin{pmatrix} y_l + Y_{11} & -y_l + Y_{12} & y_l' + Y_{13} & y_l'' + Y_{14} & y_l' + Y_{15} & y_l'' + Y_{16} \\ -y_l + Y_{21} & y_l + Y_{22} & y_l'' + Y_{23} & y_l''' + Y_{24} & y_l'' + Y_{25} & y_l''' + Y_{26} \\ y_l' + Y_{31} & y_l''' + Y_{32} & y_l' + Y_{33} & -y_l' + Y_{34} & y_l'' + Y_{35} & y_l''' + Y_{36} \\ y_l''' + Y_{41} & y_l''' + Y_{42} & -y_l + Y_{43} & y_l + Y_{44} & y_l'' + Y_{45} & y_l''' + Y_{46} \\ y_l' + Y_{51} & y_l'' + Y_{52} & y_l' + Y_{53} & y_l'' + Y_{54} & y_l + Y_{55} & -y_l + Y_{56} \\ y_l'' + Y_{61} & y_l''' + Y_{62} & y_l'' + Y_{63} & y_l''' + Y_{64} & -y_l + Y_{65} & y_l + Y_{66} \end{pmatrix} \begin{pmatrix} v_1 \\ v_2 \\ v_3 \\ v_4 \\ v_5 \\ v_6 \end{pmatrix} \tag{6.2}$$

Equation (6.2) is general. It does not commit the transformer to any particular connection or to any particular iron core. Anyone of the standard electric connections can be represented.

6.3.1 Transformation from primitive to nodal parameters

The primitive parameters are converted into nodal parameters by using power-invariant transformations,

$$v_{prim} = [C]^t v_{node} \tag{6.3}$$

$$i_{node} = [C] i_{prim} \tag{6.4}$$

and

$$i_{prim} = [Y_{prim}] v_{prim} \tag{6.5}$$

Combining equation (6.3) and (6.5) and substituting the resulting equation into (6.4) yields,

$$I_{node} = [C][Y_{prim}][C]^t V_{node} \tag{6.6}$$

where

$$[Y_{node}] = [C][Y_{prim}][C]^t \tag{6.7}$$

Matrix $[Y_{node}]$ is the nodal admittance matrix of the mutually coupled transformer, including the three phase winding connection. Matrix $[C]$ is the incidence matrix relating connected and unconnected parameters. By way of example, matrix $[C]$ is written for the grounded star-delta connection,

$$\begin{pmatrix} v_1 \\ v_2 \\ v_3 \\ v_4 \\ v_5 \\ v_6 \end{pmatrix} = \begin{pmatrix} 1 & & & & & \\ & \sqrt{3} & & -\sqrt{3} & & \\ & & 1 & & & \\ & & & \sqrt{3} & & -\sqrt{3} \\ & & & & 1 & \\ & -\sqrt{3} & & & & \sqrt{3} \end{pmatrix} \begin{pmatrix} v_A \\ v_B \\ v_C \\ v_b \\ v_C \\ v_c \end{pmatrix} \tag{6.8}$$

Other commonly used connections are given in appendix A.

6.4 Harmonic Thevenin Equivalent

Applying duality to the magnetic circuit of Figure 6.3, the electric dual equivalent shown in Figure 6.7 is obtained. Unlike the models in references [116, 117], the circuit of Figure 6.7 displays three additional negative linear inductances. They model the thickness of windings [132, 118]. Using loop analysis, the following set of non-linear equations can be written for

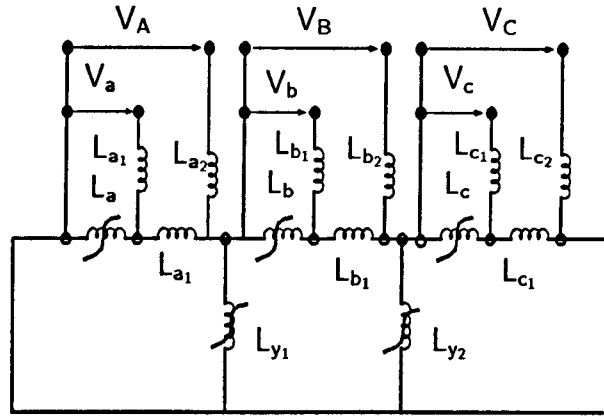

Fig. 6.7: Electric Dual of the three-legged transformer

the 3-phase, 2-winding transformer.

$$
\begin{pmatrix} V_A \\ V_B \\ V_C \\ V_a \\ V_b \\ V_c \\ 0 \\ 0 \\ 0 \end{pmatrix}
=
\begin{pmatrix}
X_{a_1}+X_a & & & X_a & & & -X_a & & \\
 & X_{b_1}+X_b & & & X_b & & & -X_b & \\
 & & X_{c_1}+X_c & & & X_c & & & -X_c \\
X_a & & & X_{a_2}+X_a & & & -X_a & & \\
 & X_b & & & X_{b_2}+X_b & & & -X_b & \\
 & & X_c & & & X_{c_2}+X_c & & & -X_c \\
-X_a & & & -X_a & & & X_{l_a}+X_a+X_{y_1} & -X_{y_1} & \\
 & -X_b & & & -X_b & & -X_{y_1} & X_{l_b}+X_b+X_{y_1}+X_{y_2} & -X_{y_2} \\
 & & -X_c & & & -X_c & & -X_{y_2} & X_{l_c}+X_c+X_{y_2}
\end{pmatrix}
\begin{pmatrix} I_A \\ I_B \\ I_C \\ I_a \\ I_b \\ I_c \\ I_{y_1} \\ I_{y_2} \\ I_{y_3} \end{pmatrix}
\tag{6.9}
$$

Equation (6.9) is non-linear since elements X_a, X_b, X_c, X_{y_1} and X_{y_2} vary with current in a non-linear fashion. The solution of this equation is achieved by repetitive linearisation through a Newton-Raphson method. The linearisation is about a base operating point $[V^0, I^0]$

in harmonic domain where,

$$V^0 = \begin{pmatrix} V_A^0 \\ \hline V_B^0 \\ \hline V_C^0 \\ \hline V_a^0 \\ \hline V_b^0 \\ \hline V_c^0 \\ \hline 0 \\ \hline 0 \\ \hline 0 \end{pmatrix} \qquad I^0 = \begin{pmatrix} I_A^0 \\ \hline I_a^0 \\ \hline I_B^0 \\ \hline I_b^0 \\ \hline I_C^0 \\ \hline I_c^0 \\ \hline I_{y_1} \\ \hline I_{y_2} \\ \hline I_{y_3} \end{pmatrix} \tag{6.10}$$

Perturbation of equation (6.9) around $[V_0, I_0]$ yields,

$$\begin{pmatrix} V_A \\ \hline V_B \\ \hline V_C \\ \hline V_a \\ \hline V_b \\ \hline V_c \\ \hline 0 \\ \hline 0 \\ \hline 0 \end{pmatrix} = \begin{pmatrix} V_A^0 \\ \hline V_B^0 \\ \hline V_C^0 \\ \hline V_a^0 \\ \hline V_b^0 \\ \hline V_c^0 \\ \hline 0 \\ \hline 0 \\ \hline 0 \end{pmatrix} + \left(\begin{array}{c|c|c|c|c|c||c|c|c}
\frac{\partial f_A}{\partial I_A} & \frac{\partial f_A}{\partial I_B} & \frac{\partial f_A}{\partial I_C} & \frac{\partial f_A}{\partial I_a} & \frac{\partial f_A}{\partial I_b} & \frac{\partial f_A}{\partial I_c} & \frac{\partial f_A}{\partial I_{y_1}} & \frac{\partial f_A}{\partial I_{y_2}} & \frac{\partial f_A}{\partial I_{y_3}} \\ \hline
\frac{\partial f_B}{\partial I_A} & \frac{\partial f_B}{\partial I_B} & \frac{\partial f_B}{\partial I_C} & \frac{\partial f_B}{\partial I_a} & \frac{\partial f_B}{\partial I_b} & \frac{\partial f_B}{\partial I_c} & \frac{\partial f_B}{\partial I_{y_1}} & \frac{\partial f_B}{\partial I_{y_2}} & \frac{\partial f_B}{\partial I_{y_3}} \\ \hline
\frac{\partial f_C}{\partial I_A} & \frac{\partial f_C}{\partial I_B} & \frac{\partial f_C}{\partial I_C} & \frac{\partial f_C}{\partial I_a} & \frac{\partial f_C}{\partial I_b} & \frac{\partial f_C}{\partial I_c} & \frac{\partial f_C}{\partial I_{y_1}} & \frac{\partial f_C}{\partial I_{y_2}} & \frac{\partial f_C}{\partial I_{y_3}} \\ \hline
\frac{\partial f_a}{\partial I_A} & \frac{\partial f_a}{\partial I_B} & \frac{\partial f_a}{\partial I_C} & \frac{\partial f_a}{\partial I_a} & \frac{\partial f_a}{\partial I_b} & \frac{\partial f_a}{\partial I_c} & \frac{\partial f_a}{\partial I_{y_1}} & \frac{\partial f_a}{\partial I_{y_2}} & \frac{\partial f_a}{\partial I_{y_3}} \\ \hline
\frac{\partial f_b}{\partial I_A} & \frac{\partial f_b}{\partial I_B} & \frac{\partial f_b}{\partial I_C} & \frac{\partial f_b}{\partial I_a} & \frac{\partial f_b}{\partial I_b} & \frac{\partial f_b}{\partial I_c} & \frac{\partial f_b}{\partial I_{y_1}} & \frac{\partial f_b}{\partial I_{y_2}} & \frac{\partial f_b}{\partial I_{y_3}} \\ \hline
\frac{\partial f_c}{\partial I_A} & \frac{\partial f_c}{\partial I_B} & \frac{\partial f_c}{\partial I_C} & \frac{\partial f_c}{\partial I_a} & \frac{\partial f_c}{\partial I_b} & \frac{\partial f_c}{\partial I_c} & \frac{\partial f_c}{\partial I_{y_1}} & \frac{\partial f_c}{\partial I_{y_2}} & \frac{\partial f_c}{\partial I_{y_3}} \\ \hline\hline
\frac{\partial f_{y_1}}{\partial I_A} & \frac{\partial f_{y_1}}{\partial I_B} & \frac{\partial f_{y_1}}{\partial I_C} & \frac{\partial f_{y_1}}{\partial I_a} & \frac{\partial f_{y_1}}{\partial I_b} & \frac{\partial f_{y_1}}{\partial I_c} & \frac{\partial f_{y_1}}{\partial I_{y_1}} & \frac{\partial f_{y_1}}{\partial I_{y_2}} & \frac{\partial f_{y_1}}{\partial I_{y_3}} \\ \hline
\frac{\partial f_{y_2}}{\partial I_A} & \frac{\partial f_{y_2}}{\partial I_B} & \frac{\partial f_{y_2}}{\partial I_C} & \frac{\partial f_{y_2}}{\partial I_a} & \frac{\partial f_{y_2}}{\partial I_b} & \frac{\partial f_{y_2}}{\partial I_c} & \frac{\partial f_{y_2}}{\partial I_{y_1}} & \frac{\partial f_{y_2}}{\partial I_{y_2}} & \frac{\partial f_{y_2}}{\partial I_{y_3}} \\ \hline
\frac{\partial f_{y_3}}{\partial I_A} & \frac{\partial f_{y_3}}{\partial I_B} & \frac{\partial f_{y_3}}{\partial I_C} & \frac{\partial f_{y_3}}{\partial I_a} & \frac{\partial f_{y_3}}{\partial I_b} & \frac{\partial f_{y_3}}{\partial I_c} & \frac{\partial f_{y_3}}{\partial I_{y_1}} & \frac{\partial f_{y_3}}{\partial I_{y_2}} & \frac{\partial f_{y_3}}{\partial I_{y_3}}
\end{array}\right) \begin{pmatrix} \Delta I_A \\ \hline \Delta I_B \\ \hline \Delta I_C \\ \hline \Delta I_a \\ \hline \Delta I_b \\ \hline \Delta I_c \\ \hline \Delta I_{y_1} \\ \hline \Delta I_{y_2}^0 \\ \hline \Delta I_{y_3}^0 \end{pmatrix} \tag{6.11}$$

This equation, in compact form, is,

$$V = V^0 + [Z]\Delta I \tag{6.12}$$

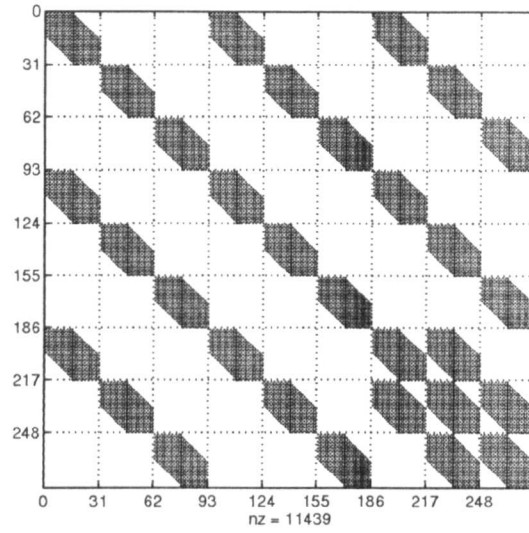

Fig. 6.8: Structure of linearised impedance matrix of the transformer

Each entry in matrix $[Z]$ consists of the product of a Toeplitz matrix and a $D(j\omega h)$ diagonal matrix,

$$\begin{pmatrix} \ddots & \ddots & \ddots & \ddots & & & \\ \ddots & c_0 & c_{-1} & c_{-2} & c_{-3} & & \\ \ddots & c_1 & c_0 & c_{-1} & c_{-2} & c_{-3} & \\ \ddots & c_2 & c_1 & c_0 & c_{-1} & c_{-2} & \ddots \\ & c_3 & c_2 & c_1 & c_0 & c_{-1} & \ddots \\ & & c_3 & c_2 & c_1 & c_0 & \ddots \\ & & & \ddots & \ddots & \ddots & \ddots \end{pmatrix} \begin{pmatrix} \ddots & & & & & & \\ & -j2\omega & & & & & \\ & & -j\omega & & & & \\ & & & * & & & \\ & & & & j\omega & & \\ & & & & & j2\omega & \\ & & & & & & \ddots \end{pmatrix}$$

The structure of the matrix $[Z]$ for the case when 15 harmonics are considered, is shown in Figure 6.8. The structure of the impedance matrix strongly suggests the use of sparsity techniques for an efficient solution.

In order to reduce model dimensions, the terms relating to the transformer nodes are eliminated mathematically by means of a Gaussian elimination. Equation 6.9 can be expressed in compact form as,

$$\left(\frac{V_w}{V_y}\right) = \left(\frac{Z_{ww}}{Z_{yw}} \middle| \frac{Z_{wy}}{Z_{yy}}\right) \left(\frac{I_w}{I_y}\right) + \left(\frac{V_{T_w}}{V_{T_y}}\right) \tag{6.13}$$

Reduction of equation (6.13) to the transformer terminals yields,

$$V_{w_e} = [Z_{ww_e}] I_{w_e} + V_{T_{w_e}} \tag{6.14}$$

where

$$\begin{aligned} [Z_{ww_e}] &= Z_{ww} - Z_{wy} Z_{yy}^{-1} Z_{yw} \\ V_{T_{w_e}} &= -Z_{wy} Z_{yy}^{-1} V_{T_y} + V_{T_{w_e}^o} \end{aligned}$$

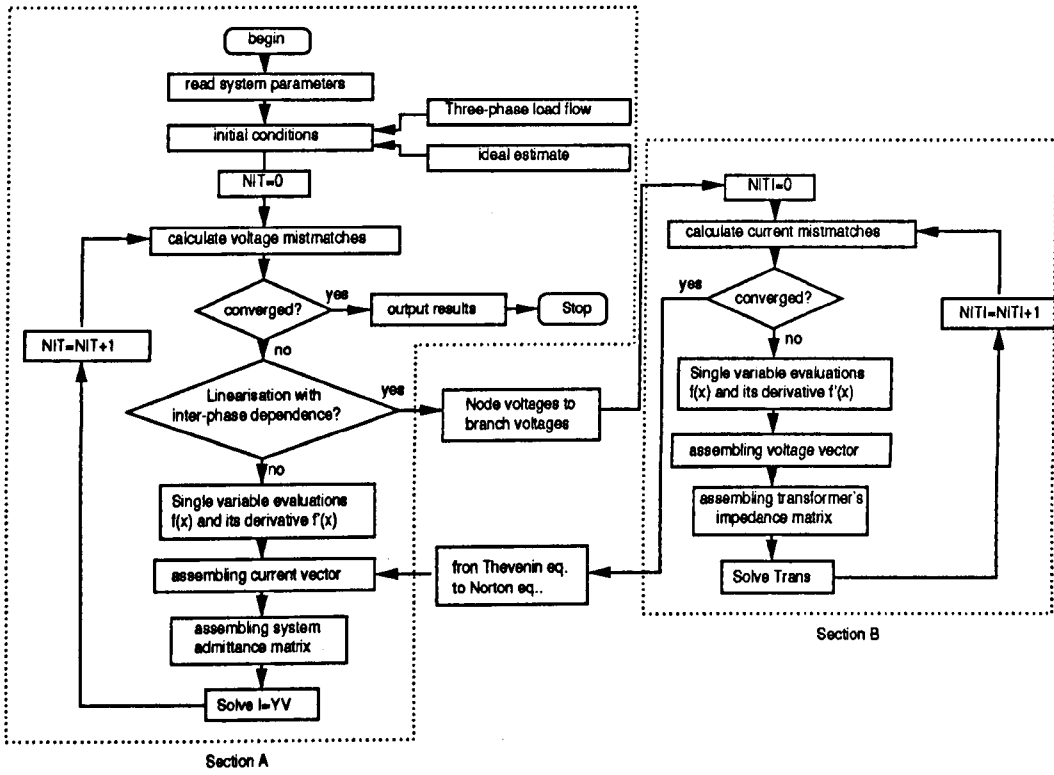

Fig. 6.9: Unified harmonic domain solution

6.5 Harmonic Norton Equivalent

Owing to the sparse structure of the admittance matrix, most studies in powers system analysis are carried out using nodal representations. Most industrial power systems applications, say EMTP or EMTDC use nodal analysis. The harmonic Norton equivalent for the transformer can be obtained by solving equation (6.14) for the currents at the transformer terminals,

$$I_w = I_w^0 + YV^0 \tag{6.15}$$

6.6 Harmonic Domain Solutions Via Newton-Rapshon Method

Multi-limb cores provide a magnetic link between all phases, at all ports of the transformer. A change in the value of harmonic k, in any phase, affects all harmonics in the rest of the circuit. Harmonic interaction is a non-linear problem which can be study by linearisating the problem about an operating point.

Linearisation of simple iron cores involves one phase only. For a given set of terminal conditions, the linearisation can be achieved with a single evaluation of the non-linear characteristic. This has been discussed earlier on in the thesis. In contrast, linearisation of multi-limb iron cores, presents a more difficult case. For a given set of terminal conditions, it is not possible to determine voltages and currents for all the non-linear branches in the iron core owing to the non-linear relationship between the branches. The linearisation process is itself a non-linear problem which can be solved by iteration.

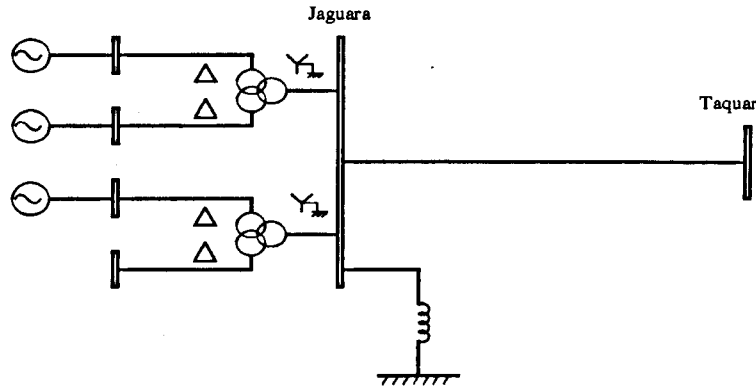

Fig. 6.10: jaguara Taquaril transmission system

Figure 6.9 shows the main algorithm, in diagram form, for the steady state solution of non-linear power systems with three-phase power transformers. Two main sections can be seen, namely sections A and B. One iteration process is used to solve the harmonic behavior of the network where the interaction between different non-linear devices is accounted for. The network is represented in the nodal frame of reference, where the sparse nature of the system admittance matrix can be efficiently exploited. Several non-linear devices such as TCRs or single banks of transformers may be linearised in harmonic domain with no need for the extra iterative process of section B. However, if the device has *inter-phase dependence*, such as multi-limb power transformers then section B of the algorithm is executed until a linearised element is obtained.

For power transformers, the non-linear equations relating currents and voltages are given in the loop frame of reference and a power invariant transformation is required to interface the transformer model with the rest of the network. After the sub-iteration process in B has converged, and a reduced equivalent transformer model has been obtained, the algorithm returns to section A.

It is important to notice that the sub-iteration process of section B can be stopped just after one iteration. This reduces the global number of sub-iterations but this is achieved at the expense of increasing the number of iterations in the main loop, section A. The advantage of the internal iterative process can be better appreciated when one considers that, in general, the main loop consists of a much larger set of equations. An increment in the number of iterations in the main loop gives rise, therefore, to a very large increment in the total number of operations. It has been observed that near the solution, the linearisation of the transformer does not change significantly, so only one sub-iteration is required. Taking the above observations into account, several alternatives can be considered, in order to optimise the efficiency of the solution process.

6.7 Case Study

The prowess of the harmonic domain model described in this chapter is demonstrated by example. The transmission network shown in Figure 11.9 is used for this purpose. This network has been used in previous works and data and results are available in open literature [16]. General information for the test system is given in Appendix B. Detailed information of magnetisation curves of multi-limb cores is seldom available. Manufacturers do not provide the information required to analyse the transformer in rigorous studies such harmonic analysis or transient analysis. The magnetisation information used in this chapter has been taken from

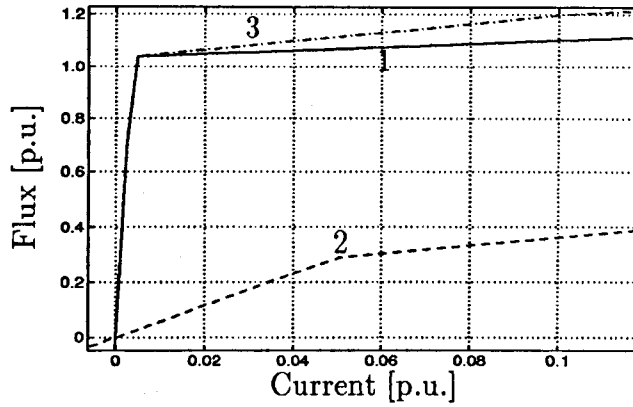

Fig. 6.11: Magnetisation curves of a power transformer

one of the few sources available in open literature [20]. Further information is presented in chapter 2.

6.7.1 Voltage supply

Figure 6.12(a) shows a full period of the voltage waveforms at the Jaguara busbar for the case when the excitation at the supply point is 1.1 p.u. whereas Figure 6.12(b) presents the harmonic content as a percentage of the fundamental component in phase a. It is quite likely that, for this case, power grid regulations are satisfied since 3% harmonic voltage distortion is considered to be within acceptable limits. However, as the supply voltage increases, an amplification of the harmonic distortion is expected. Figure 6.13(a) shows o full period of the voltage waveforms at the Jaguara busbar whereas Figure 6.13(b) presents the respective harmonic content, as a percentage of the fundamental component in phase a. It is clear that in this case the harmonic content is beyond permissible limits and corrective actions must be carried out. All other harmonics are within permissible limits. In both cases the transformer shows its ability to inject 5th harmonic current as the supply voltage increases. Harmonic voltage amplification depends on the operating conditions of the network and transformer configuration.

As far as the model performance is concerned, it was observed that quadratic convergence was obtained even for the case of 1.2 p.u. of voltage supply.

6.7.2 Multiple saturation levels

In the absence of detailed information in saturation levels of the transformer, the same magnetising characteristic for different core branches is normally used [130]. Figure 6.14(a) shows a full period of the voltage wave form at the Jaguara busbar when all branches of the core are assumed to have the same characteristic, i.e curve 1 Figure 2.2. The level of harmonics are lower in all phase than for the case shown in Figure 6.13.

6.8 Conclusions

A new harmonic domain model for modelling multi-limb transformers has been presented. The model has been developed using the Principle of Duality. It takes into account important electromagnetic effects present when the transformer is operating under saturation conditions. Duality takes accurately into account the electromagnetic effects introduced by iron cores with

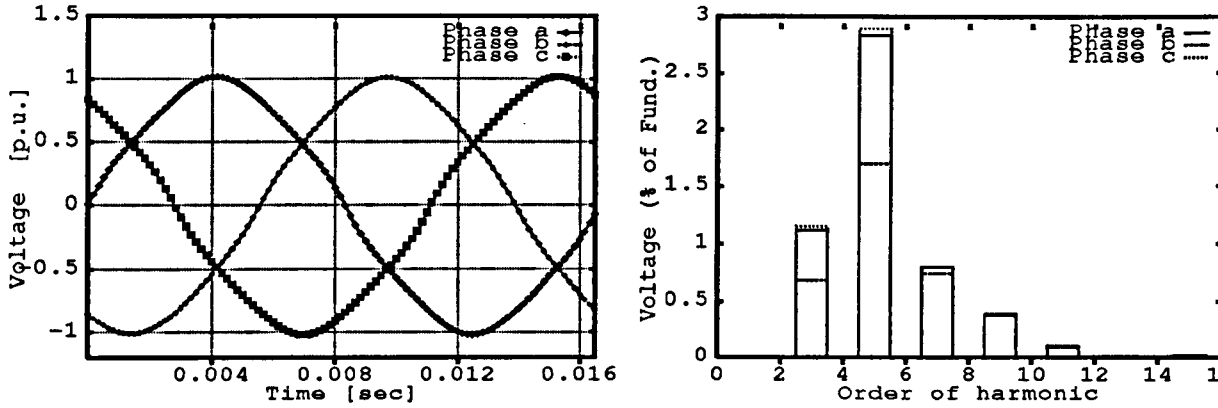

(a) (b)

Fig. 6.12: Voltages at Jaguara busbar with 1.1 p.u. of voltage supply

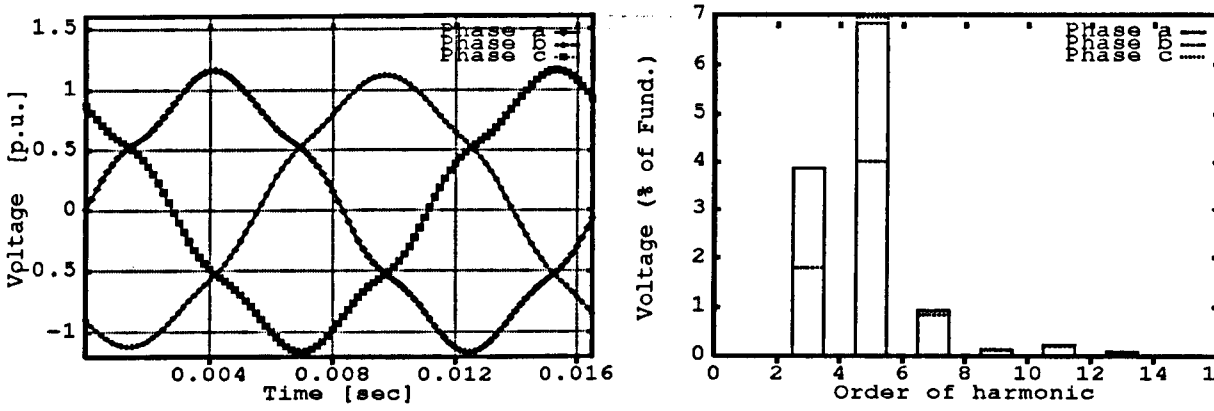

(a) (b)

Fig. 6.13: Voltages at Jaguara busbar with 1.2 p.u. of voltage supply

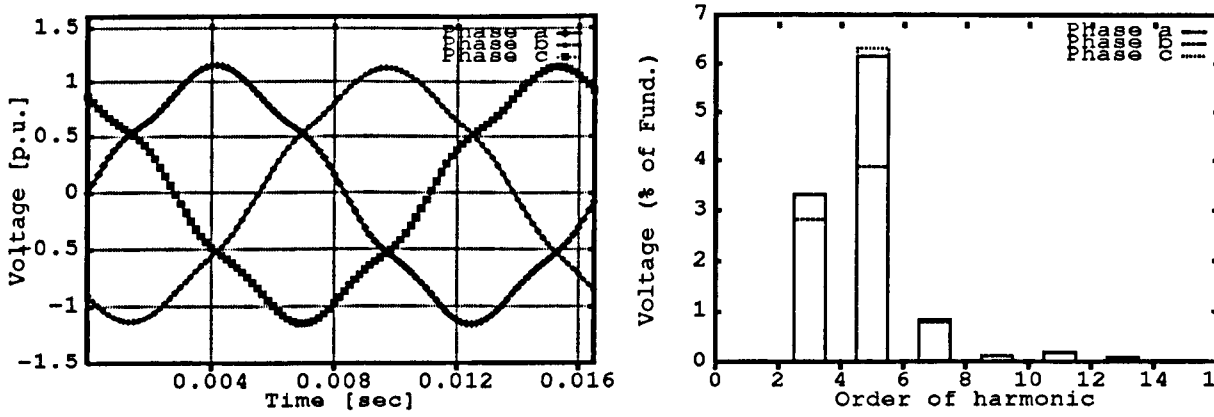

(a) (b)

Fig. 6.14: Voltages at Jaguara busbar with 1.2 p.u. of voltage supply

multi-limb, multi transversal iron cores, and the effect of the transformer tank and magnetic air paths.

The iterative process uses a first order Newton-Raphson that shows quadratic convergence. However, as opposed to single phase iron cores, where the linearisation can be achieved with a single evaluation of the non-linear characteristic, in multi-limb transformers this linearisations process requires an iterative solution. The latter iterative process is also carried out using a first order Newton-Raphson algorithm. Accordingly, the overall solution can be seen as a Newton-Raphson method with a nested iterative solutions. The modelling approach has been tested using a practical transmission system.

Chapter 7

Analysis of Convergence and Relaxation Methods

This chapter compares the convergence characteristics of several harmonic domain iterative techniques. The basic formulation is a frequency domain Newton-Raphson technique which observes quadratic convergence. Starting from sinusoidal conditions, convergence is obtained within 4 to 5 iterations to a specified voltage tolerance of 1e-6. The technique's convergence characteristic is not compromised by the level of harmonic distortion being considered. The Newton-Raphson equations may be solved 'in-block' leading to very robust harmonic solutions. However, 'in-block' solutions are not the only alternative. The harmonic Newton-Raphson technique is also amenable to diakoptical solutions. They exhibit linear convergence characteristics, as opposed to quadratic, but their overall efficiency compares favourably with cases in which 'in-block' solutions are carried out. Test cases corresponding to a practical transmission system are presented to show the prowess of the basic Newton-Raphson and the diakoptical Newton-Raphson techniques.

7.1 Introduction

Harmonic solutions based on the integration of the differential equations which described the non-linear network were used in the early 60's. The basic principle involved is to integrate these equations over many cycles until the transient response vanishes, leaving only the periodic steady state response. In most cases this approach requires a great deal of computational effort and was soon abandoned. Instead, Shooting methods [1] and harmonic balance techniques [15] were developed. Early harmonic balance techniques relied on gradient-based optimisation techniques in order to assure convergence. In power systems applications Gaussian relaxation [16] and Newton techniques [17] were developed.

Gaussian relaxation methods allow for fast solutions when solving mild non-linearities but are a poor choice for solving networks with significant harmonic distortion. Newton-type methods exhibit stronger convergence characteristics than Gauss-Seidel methods, but hybrid methodologies which use time and frequency information do not yield quadratic convergence [129]. This is due, in part, to the use of FFT algorithms, as a means of transforming information from the time domain into the frequency domain, at each iterative step. Harmonic Newton-Raphson algorithms are not necessarily easy to implement. They require the utmost careful programming since even minor oversights in the coding will prevent it from converging quadratically [17]. 'In-block' Newton-Raphson solutions are not the only alternative available

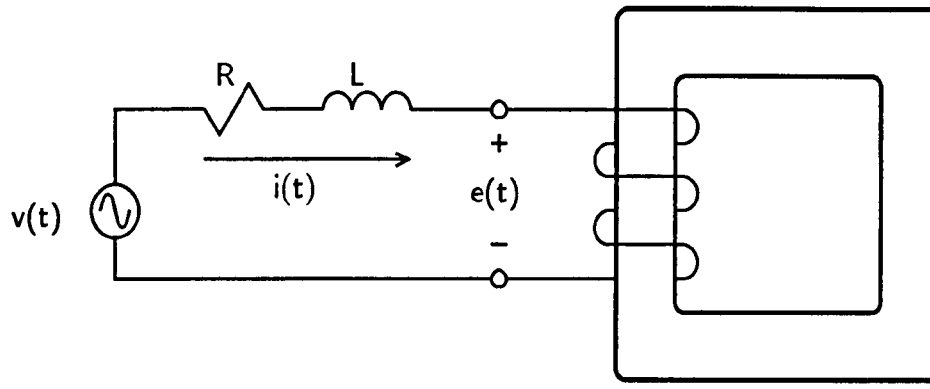

Fig. 7.1: Non-linear inductor excited from a periodic voltage source

with this algorithm and results are presented for a variant of the algorithm which combines the strengths of the Newton-Raphson formulation with diagonal relaxation.

7.2 The Non-linear Inductor in Harmonic Domain

Harmonic domain Newton-Raphson techniques for the solution of the PSS of power systems have been described in Chapter 4. In this section a non-linear inductor is used to demonstrate the convergence properties of the harmonic Newton-Raphson techniques. Hence, the dynamic equations of the non-linear inductor shown in Figure 7.1 will be linearised in the harmonic domain.

The dynamic equation describing the non-linear inductor is:

$$Ri(t) + L\frac{di(t)}{dt} + N\frac{d\varphi(t)}{dt} = v(t) \tag{7.1}$$

Accordingly, the non-linear state equations of the inductor may be written as:

$$\dot{\Phi} = -(R + j\omega L)f(\Phi) + v \tag{7.2}$$

$$i = f(\Phi) \tag{7.3}$$

where equation (7.3) is the magnetising characteristic of the non-linear inductor, N is the number of turns and $\Phi = N\varphi$ is the total flux linkage.

For harmonic domain calculation purposes the state equations (7.2) and (7.3) must be transformed into algebraic equations. The linearised form of these equations is:

$$D(j\omega h)\Delta\Phi = -D(R + j\omega hL)(F_\phi) + \Delta V \tag{7.4}$$

$$\Delta I = (F_\varphi)\Delta\phi \tag{7.5}$$

where (F_ϕ) is a Toeplitz matrix corresponding to partial derivatives of equation (7.3) with respect to the elements of the harmonic domain vector Φ, $D(j\omega h)$ is a diagonal matrix with entries $j\omega h$ and $D(R + j\omega hL)$ is a diagonal matrix with entries $R + j\omega hL$. ΔV, $\Delta\Phi$ and ΔI are vectors of harmonic voltages, fluxes and currents increments, respectively.

Equations (7.4) and (7.5) can be combined together to give rise to the following input-output relationship:

$$\Delta I = (H_V)\Delta V \tag{7.6}$$

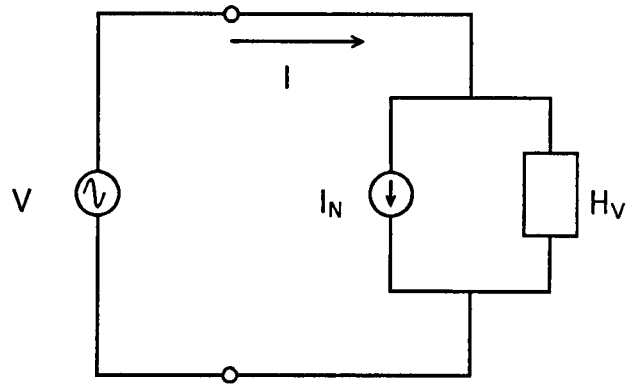

Fig. 7.2: Harmonic Norton equivalent of the non-linear inductor and periodic voltage source.

where $H_V = (F_\Phi)\,[D(j\omega h) + D(R + j\omega hL)(F_\Phi)]^{-1}$ is a matrix of harmonic admittances which, for the case of an ideal non-linear inductor, reduces to $(F_\Phi)D(j\omega h)^{-1}$.

The harmonic Norton equivalent representation of the non-linear inductor shown in Figure 7.2 is realised by incorporating the base point of linearisation, (V_o, I_o), in equation (7.6):

$$I_V = (H_V)V + I_N \tag{7.7}$$

where $I_N = I_o - (H_V)V_o$ is the current source of the harmonic Norton equivalent.

Equation (7.7) posses many distintic properties. For one, it provides a means for the harmonic solution of the non-linear inductor by iteration. Full evaluation of equation (7.7) at each iterative step produces a solution via Newton-Raphson method, where the nodal admittance matrix (H_V) plays the role of Jacobian. When close to the solution, the algorithm's rate of convergence is quadratic, i.e. the number of significant figures doubles at each iteration. Furthermore, the equation's structure allows for an efficient interfacing with frequency-dependent transmission line admittances and also with other harmonic Norton equivalents. The interfacing takes place in a harmonic domain frame of reference where all the harmonics, cross-couplings between harmonics, phases and bus bars of the network are explicitly represented. The overall nodal admittance matrix of the network also plays the role of a global Jacobian matrix.

For harmonic calculation purposes the non-linear inductor of Figure 7.1 can be better modelled as the Norton equivalent of an ideal, non-linear inductor in series with a linear admittance, as shown in Figure 7.3. This representation allows easy access to the internal (ficticious) inductor's node, a point where the core flux is proportional to the circuit voltage, i.e. $D(j\omega h)\Phi = V$. The following nodal matrix equation,

$$\left(\frac{I_1}{-I'_N}\right) = \left(\begin{array}{c|c} D(R+j\omega hL)^{-1} & -D(R+j\omega hL)^{-1} \\ \hline -D(R+j\omega hL)^{-1} & -D(R+j\omega hL)^{-1} + H'_V \end{array}\right)\left(\frac{V}{V'}\right) \tag{7.8}$$

represents the circuit of Figure 7.3, where the solution of the harmonic vectors V' and I_1 is reached by iteration.

7.2.1 Test cases

Power transformers are basic and essential components of any transmission system. Intensive research to determine adequate models capable of accurately reproducing their behaviour

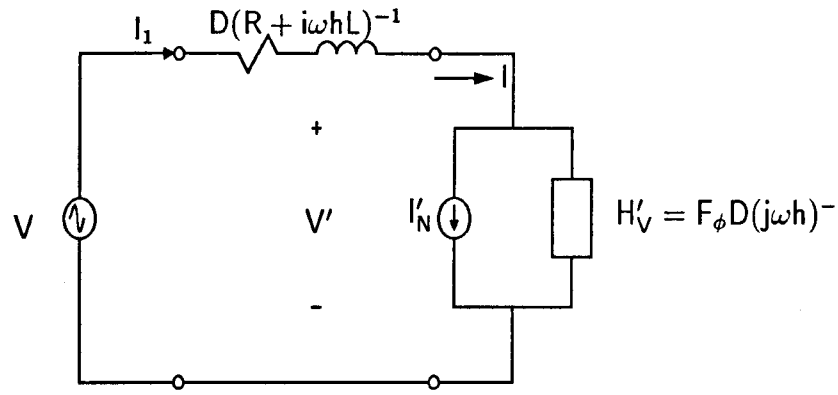

Fig. 7.3: Harmonic Norton equivalent of the ideal, non-linear inductor in series with leakage admittance.

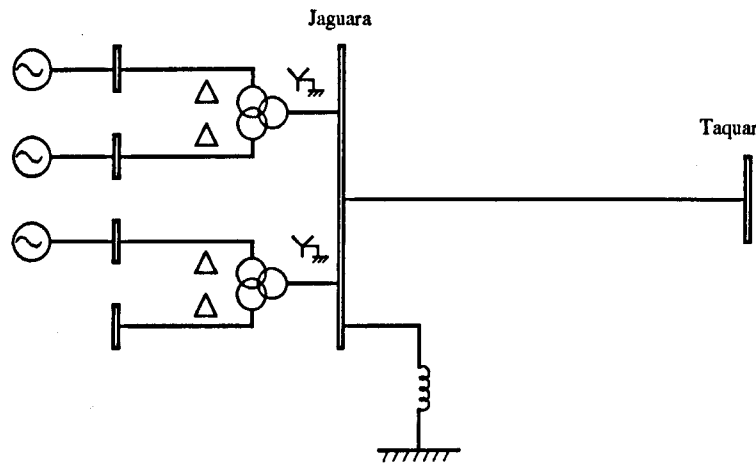

Fig. 7.4: Jaguara-Taquaril transmission system

under transient and steady state operation has been carried out over the years. It was seen in the previous chapter that to fully described the power transformer the electric and magnetic circuits should be properly taken into account. In particular, the magnetic circuit representation can be quite involved as it depends on the magnetic and physical core characteristics. Arguable, the simplest transformer model is that of a three phase bank of transformers. In such a case the transformer is modelled as a combinations of three single phase transformers. Each single phase transformer is modelled by a Norton equivalent such as in Figure 7.3. Below a test case which considers a transmission system having a three phase single bank, three windings is used to validate the steady state response of the full Newton-Raphson and derived algorithms. The transmission system is also useful for comparing the efficiency and reliability of the various methods towards the convergence. Figure 7.4 shows the 220 kV Jaguara-Taquaril transmission system. The convergence criterion adopted in all results shown below is a voltage difference smaller than 10^{-6} between successive iterations. This applies for all coefficients of the series.

Owing to unloaded conditions in the transmission circuit, the magnetising branch of the transformer is pushed into saturation and becomes a source of distortion.

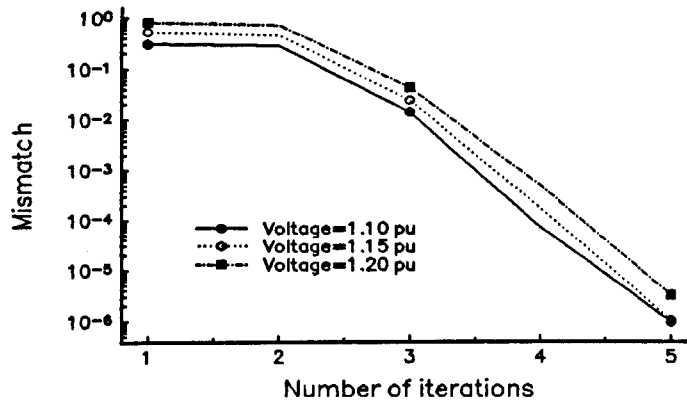

Fig. 7.5: Convergence of full Newton-Raphson

7.2.2 Full Newton-Raphson Method

Provided the harmonic Norton equivalent of the magnetising branch of the transformer is recalculated at each iterative step the solution will be obtained in true quadratic convergence fashion. Furthermore, the excitation voltage and number of harmonics considered in the analysis is not expected to affect the quadratic convergence characteristics of the method. This is shown in Figure 7.5 where maximum voltage mismatches at each iteration are plotted for three different voltage excitation conditions.

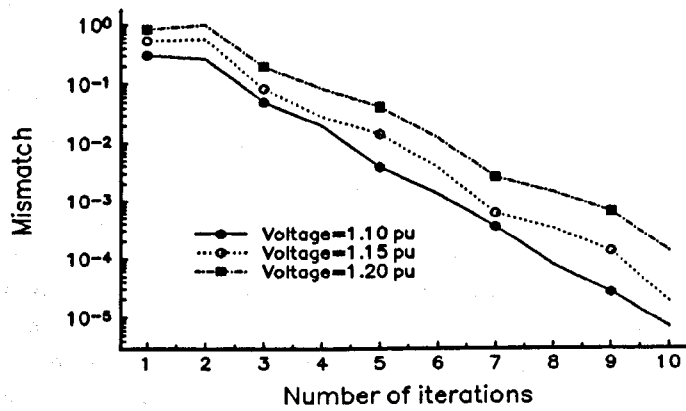

Fig. 7.6: Convergence of single-valued Newton-Raphson

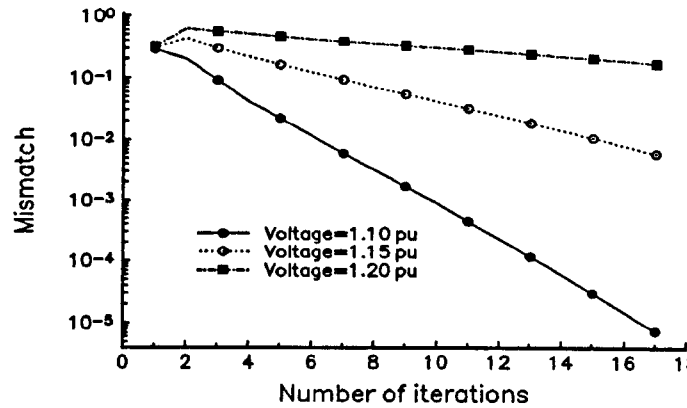

Fig. 7.7: Convergence characteristics of Gauss-Seidel methods

7.3 Single-valued Newton-Raphson method

If the harmonic Norton equivalent of the magnetising branch of the transformer is re-calculated at each iteration and combined with the admittances of the linear part of the transmission system then the global nodal admittance of the system requires re-factorisation. This process yields considerable overheads to the algorithm even when sparsity-oriented solutions are used.

The numeric overheads can be reduced greatly if the harmonic Norton equivalent is partially calculated only, i.e. the vector current source is calculated at each iterative step while the admittance matrix is evaluated only once and then kept constant for the remaining of the iterative process. This simplification in the algorithm reduces numeric overheads but at the expenses of weakening convergence characteristic, which are linear as opposed to quadratic. This is shown 7.6.

7.3.1 Gauss-Seidel scheme

If the admittance matrix of the harmonic equivalent is neglected altogether during the iterative solution then the magnetising branch of the transformer will be modelled as a set of harmonic current sources. One harmonic current will be injected at the time into the nodal impedance matrix representing the linear part of the transmission circuit. This is a Gauss-Seidel method. it requires a low number of operations at each iteration but this is at the expense of degrading robustness even further. For circuits with high harmonic distortion this methods will converge slowly and it may even fail to converge. However, because of its decoupled structure the formulation is amenable to parallel solutions. Figure 7.7 shows the convergence characteristics of the Gauss-Seidel method. The solutions with excitation voltages of 1.10, 1.15 and 1.20 converge in 17, 25 and 128 iterations, respectively.

7.3.2 Diagonal relaxation

An interesting variant of the Newton-Raphson method which is also amenable to parallel solutions is described below. It retains most of the Newton-Raphson strong convergence characteristics. Here, the admittance matrix of the linearised element H'_V is separated into

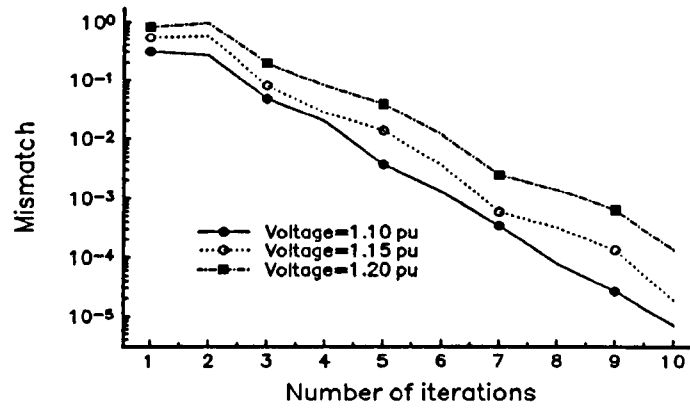

Fig. 7.8: Convergence characteristics of the NR with diagonal relaxation

diagonal and off-diagonal components, say matrices B and C, respectively,

$$H'_V = B + C \tag{7.9}$$

The diagonal elements C are grouped together with the linear admittance matrix of the transmission network while the off-diagonal elements B are grouped together with the current. This action decouples, coefficient-wise, the network system equations. Furthermore, if the diagonal elements C are evaluated in the iteration 1 only and then kept constant, the nodal admittance matrixes of the network will be factorised just once. For instance, equation 7.8 would be modified as follows,

$$\begin{aligned}\left(\frac{I_1}{-I'_N}\right)^{(k)} &= \left(\begin{array}{c|c} D(R+j\omega hL)^{-1} & -D(R+j\omega hL)^{-1} \\ \hline -D(R+j\omega hL)^{-1} & -D(R+j\omega hL)^{-1}+C \end{array}\right)^{(1)} \left(\frac{V}{V'}\right)^{k+1} \\ &+ \left(\frac{0}{BV'}\right)^{(k)} \end{aligned} \tag{7.10}$$

With the decomposition of equation (7.9) and using voltage values from iteration (k), the off-diagonal elements B are converted into harmonic currents, which are combined with the Norton current sources $I_N^{(k)}$, and injected back into the constant, decoupled nodal network admittances. These harmonic currents are calculated using the most up to date harmonic voltage information available in order to tighten convergence even further. Figure 7.8 shows the linear convergence characteristics of this method.

In oder to emphasis the reliability towards the solution of the methods above, Figure 7.9 shows the various methods together for the case of 1.20 p.u. voltage excitation.

7.4 Conclusions

The efficiency of harmonic domain algorithms applied to practical power networks is addressed in this chapter. It is shown that this efficiency is related to the number of nodes, the number of non-linear elements and the number of harmonics considered. The computational burden will increase exponentially with all the above factors. As a first step to achieve efficient

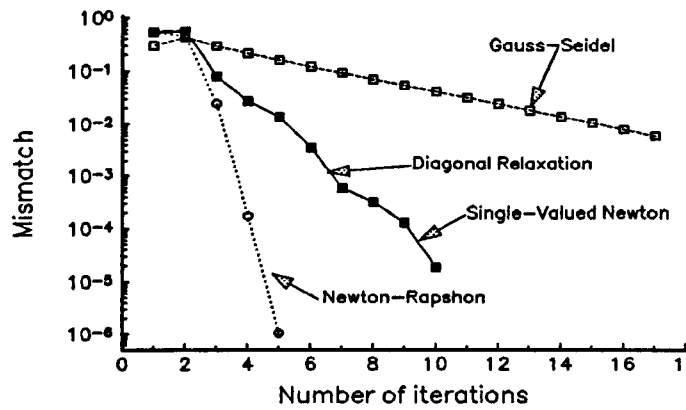

Fig. 7.9: Convergence characteristics of the various methods

harmonic solutions, traditional sparse matrix techniques can be applied, however, additional improvements can be made by further exploiting the Jacobian's structure. In this chapter advantage is taken from the fact that the Jacobian is used to generate updated values of the state variables but is not used for confirming convergence. This means that the error in the Jacobian only affect the rate and region of convergence and not the the accuracy of the final solution. Here, several alternatives to approximate the Jacobian are used in order to reduce the number of operations required to achieve harmonic domain evaluations at each iteration. However, this is at the expense of degrading the asymptotic rate of convergence. It was shown, for instance that Gauss-Seidel algorithms do not use Jacobian (Norton elements). Thus , each iterative step requires fewer operations but poor characteristics of convergence are obtained for network with high harmonic content. The Jacobian is most effectively deployed when a full Newton-Raphson technique is used. In this case the accuracy with which the Jacobian is calculated at each iterative step increases the rate and the region of convergence but a larger number of operations is required at each iterative step. To take advantage of the best properties of Gauss-Seidel and Newton-Raphson techniques several alternatives are given. In particular, a Newton-Raphson which uses diagonal relaxation has proved efficient and has shown good characteristics of convergence.

Part III

Sequency Domain Modelling

Chapter 8

Sequency Domain Modelling of Linear Time-Invariant Electric Power Networks

The steady-state solution technique presented in this chapter is based on Walsh functions. It is no longer a frequency domain technique but, rather, a sequency domain technique. Important properties of the Walsh functions are given. Together with the Walsh domain representation of linear, time-varying and non-linear elements, the models presented in this chapter yield a new framework for the study of non-linear distortion in power systems. Linear, time varying networks and non-linear networks will be addressed in the next two chapters.

8.1 Introduction

Traditionally, Fourier-type frequency analysis has been used in power systems analysis owing to the near sinusoidal waveforms present in power networks. However, Fourier-type analyses are not the only alternative. The set of periodic inputs and outputs can also be expressed as series of Walsh functions which, when truncated to a finite number of coefficients, are stair-step approximations of the waveforms. Walsh series have most of the properties of Fourier series. An interesting characteristic of Walsh series is that when a zero memory, non-linear operation is applied to a Walsh series, the output series can be derived by simple algebraic operation. This fact is exploited in this and subsequent chapters. The output coefficients will differ from the input coefficients in magnitude but no new terms will be created.

Walsh series quickly became popular in signal processing and communication systems analysis [133, 134] owing to their simplicity. Walsh transforms can be calculated by addition operations as opposed to the multiplication operations required by Fourier series. It was MS Corrington who in the early sixties first brought up the advantages of using Walsh series for the analysis of electric circuits [135] but it was not until 1973 that the idea was widely adopted [43]. Similar ideas are proposed in [134] but minimum analysis is provided. Since then, a number of publications has been dedicated to exploit these ideas with good results. For instance, CF Chen and CH Hsiao [51] and VR Karan, PA Frick and RR Mohler [55] show that the estimation of system parameters is reduced to algebraic operations. They also show that differential and integral equation can be solved by means of Walsh functions. Walsh functions have also been applied to the problem of order identification [63]. A comprehensive review of Walsh functions for the problem of system identification is given in [61]. Recently, Stoten [71] has used high-speed digital implementations of identification algorithms based on Walsh functions.

An interesting characteristic of Walsh functions is that they can be used to predict the

existence of limit cycles and in both linear and non-linear systems. The analysis of LTIS using Walsh function was first carried out in reference [51].

It is apparent from open literature that Walsh functions have been widely applied in the areas of signal processing and in control but very few applications have taken place in the area of waveform distortion in Power Systems. In fact, it seems that the only application of Walsh functions in this area is the work of DJ Kish and GT Heydt [69]. Walsh functions have been applied in the area of power systems protection, for calculating symmetrical components [136].

This chapter is organized as follows. Firstly, the theory of Walsh functions is given. The advantages and disadvantages of Walsh series with respect to Fourier series, for the approximation of single variable functions, are stated. Their derivations from Rademacher functions is fully discussed. Secondly, the structure of the operational matrix of integration and the operational matrix of direct product are discussed. A simple circuit is used to illustrate the application of the theory.

8.2 Theory of Walsh Functions

The representation of functions by the superposition of simple functions is a useful attribute which can have many applications. Orthogonal sets of functions can be used to synthesise any time function to a required degree of accuracy. In many cases, it may be easier to analyse systems through this representation than through its original form. The application of digital techniques in systems design and analysis has motivated the use of orthogonal functions other than sine and cosine functions. The alternative sets may not have all the properties of sine-cosine functions but have other advantages which allow a more effective use in some applications. The Walsh and Haar sets of functions are examples of such orthogonal sets. Both sets are characterised by taking only two values, namely +1 and -1, thus matching the behavior of digital logic.

Historically, the Haar series was first described by the Hungarian mathematician, Alfred Haar in 1910 [137]. He proposed a set of orthogonal functions, taking essentially only two values. This was a property not possessed by any orthogonal set known until then. The Walsh functions were defined in 1923 by the American mathematician JL Walsh [138]. They also take only two values +1 and -1. This set was found to have more similar properties to the trigonometric basis than the Haar basis. Just before Walsh's work was published, Rademacher had presented another set of two-level orthogonal functions [139], which were found to form an incomplete subset of Walsh functions. In fact, Walsh functions can be expressed as products of Rademacher functions.

8.2.1 Rademacher Functions

The Rademacher functions are an orthonormal set of functions. They represent a series of rectangular pulses or square-waves having unity ratios. All Rademacher functions have two arguments n and t. They can be derived from sinusoidal functions as,

$$r_n(t) = Sign[\sin(2^n \pi t)] \tag{8.1}$$

where n is the order of the function, t is the independent variable and

$$Sign(x) = \begin{cases} 1 & x \geq 0 \\ -1 & x < 0 \end{cases}$$

The first 8 Rademacher functions are shown in Figure 8.1. It can be observed that all the functions have odd symmetry about $t = 0$ and $t = \frac{1}{2}$. This means that the set is

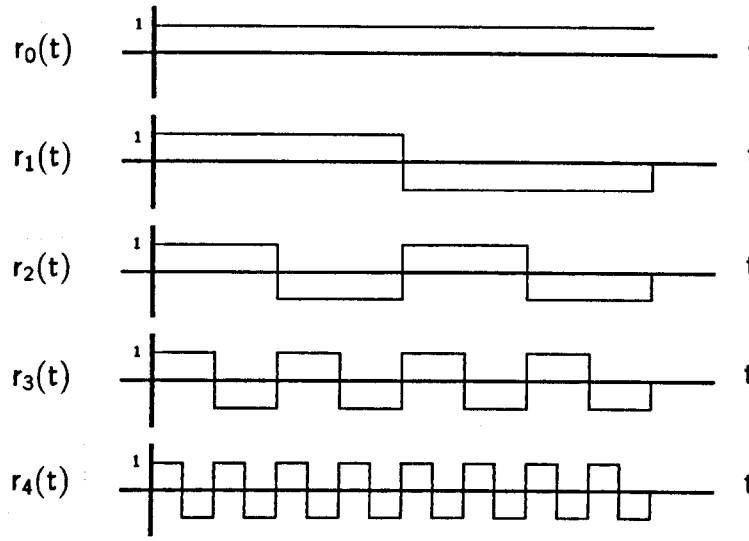

Fig. 8.1: Rademacher functions

incomplete since the sum of any number of functions will have odd symmetry about this point. Accordingly, it is not possible to expand functions which have even symmetry.

8.2.2 Walsh Functions

Walsh functions are also rectangular functions, however, they form a complete set of functions. Like Rademacher functions, they hold only one of two values, either -1 or 1. This renders them ideal candidates for high-speed digital implementation. Figure 8.2 shows the first 8 Walsh functions.

Open literature abounds with definitions and alternatives for forming the complete set of Walsh functions. In this work, only two alternatives are considered, Rademacher functions and Hadamard functions.

From Rademacher Functions

Rademacher functions can be combined to form a complete orthonormal set of Walsh functions. Let $b_n, \ldots, b_2, b_1$ be a n-digit binary number where the b_i are either 0 or 1. The Walsh function will be defined as the product of n Rademacher functions [133, 134],

$$\phi_{b_n \ldots b_2 b_1}(t) = [r_n(t)]^{b_n} \ldots [r_2(t)]^2 [r_1(t)] \tag{8.2}$$

Where,

$$\begin{aligned}
\phi_0(t) &= r_0(t) \\
\phi_1(t) &= r_1(t) \\
\phi_2(t) &= \phi_{10}(t) = r_2(t) \\
\phi_3(t) &= \phi_{11}(t) = r_2(t) r_1(t) \\
\phi_4(t) &= \phi_{100}(t) = r_3(t) \\
\phi_5(t) &= \phi_{101}(t) = r_3(t) r_1(t) \\
&\vdots \\
\phi_n(t) &= \phi_{b_n \ldots b_2 b_1}
\end{aligned} \tag{8.3}$$

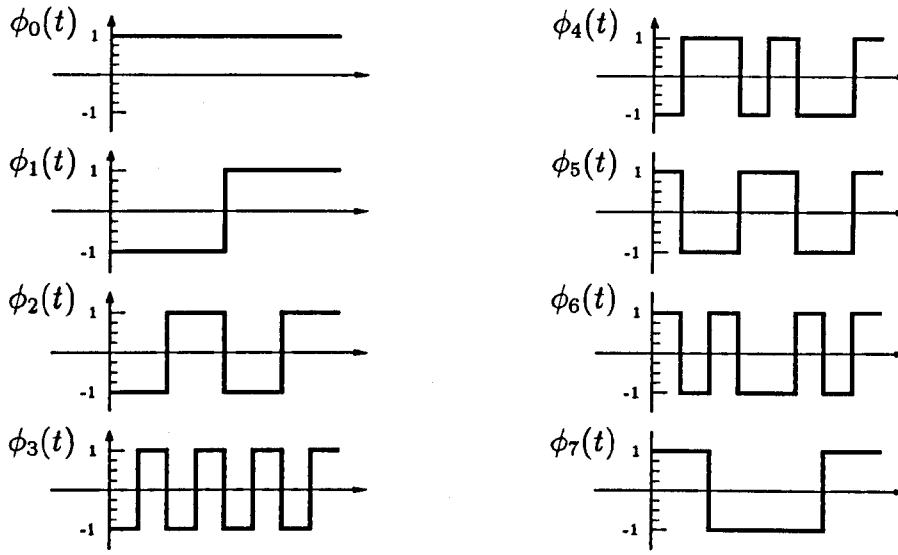

Fig. 8.2: A set of 2^3 Walsh functions

For many applications, it is convenient to relate the order n of the Walsh function to the number of zero crossings. Open literature provides a wide range of function definitions holding this characteristic. For instance, Harmuth [133] gives a recursive relationship having the virtue of ordering the Walsh functions in such a way that increasing n corresponds to increasing the zero crossings (zc). In such a case it is useful to define *waveform sequency* θ as,

$$\theta = \frac{\mathrm{zc}}{2T} \tag{8.4}$$

where T is the time base. Accordingly, it follows that sequency, measured in zero crossings per second (ZC/s), is a more general form of frequency definition. It can be seen as a measured frequency but without the restriction of having zero crossings equally spaced. With this in mind, it is possible to obtain Walsh functions, which preserve their natural order, by means of Rademacher functions [140]. In this case, the ordered Walsh functions, can be obtained according to the relationship,

$$\phi_n(t) = \Pi_{i=1}^{n} g_i r_i(t) \tag{8.5}$$

where

$$n = b_m b_{m-1} \ldots b_2 b_1$$

and

$$g_i = b_i \oplus b_{i+1}$$

Here, $\otimes$ is the EXCLUSIVE OR operation.

As an example, the generation of $\phi_{13}(t)$ is carried out as follows:

$$13_{10} = 1101_2 = 1011_g$$

i.e.

$$\phi_{13}(t) = r_4(t) r_2(t) r_1(t)$$

From Hadamard Matrices

Uniform sampling of Walsh functions results in the formation of a matrix called Walsh-Hadamard matrix [141]. The rows of these matrices represent the Walsh functions uniquely. For example, periodic sampling of the first 16 Walsh functions with increasing zero crossings, yields the following matrix,

$$H_w(4) = \begin{array}{c} \\ \left(\begin{array}{c|c|c|c|c|c|c|c|c|c|c|c|c|c|c|c}
+ & + & + & + & + & + & + & + & + & + & + & + & + & + & + & + \\ \hline
+ & + & + & + & + & + & + & + & - & - & - & - & - & - & - & - \\ \hline
+ & + & + & + & - & - & - & - & - & - & - & - & + & + & + & + \\ \hline
+ & + & + & + & - & - & - & - & + & + & + & + & - & - & - & - \\ \hline
+ & + & - & - & - & - & + & + & + & + & - & - & - & - & + & + \\ \hline
+ & + & - & - & - & - & + & + & - & - & + & + & + & + & - & - \\ \hline
+ & + & - & - & + & + & - & - & - & - & + & + & - & - & + & + \\ \hline
+ & + & - & - & + & + & - & - & + & + & - & - & + & + & - & - \\ \hline
+ & - & - & + & + & - & - & + & + & - & - & + & + & - & - & + \\ \hline
+ & - & - & + & + & - & - & + & - & + & + & - & - & + & + & - \\ \hline
+ & - & - & + & - & + & + & - & - & + & + & - & + & - & - & + \\ \hline
+ & - & - & + & - & + & + & - & + & - & - & + & - & + & + & - \\ \hline
+ & - & + & - & - & + & - & + & + & - & + & - & - & + & - & + \\ \hline
+ & - & + & - & - & + & - & + & - & + & - & + & + & - & + & - \\ \hline
+ & - & + & - & + & - & + & - & - & + & - & + & - & + & - & + \\ \hline
+ & - & + & - & + & - & + & - & + & - & + & - & + & - & + & -
\end{array}\right) \end{array} \begin{array}{c} \text{Sequence} \\ \overbrace{} \\ 0 \\ 1 \\ 1 \\ 2 \\ 2 \\ 3 \\ 3 \\ 4 \\ 4 \\ 5 \\ 5 \\ 6 \\ 6 \\ 7 \\ 7 \\ 8 \end{array} \tag{8.6}$$

where $H_w(4)$ is the $2^4 \times 2^4$ Walsh-Hadamard matrix in Walsh or sequency order. The rows of this matrix represent the Walsh functions whose sequencies are listed. The lower order Walsh-Hadamard matrices, $H_w(0)$ to $H_w(3)$, are given below,

$$H_w(0) = 1, \quad H_w(1) = \begin{array}{c} \left(\begin{array}{c|c} + & + \\ \hline + & - \end{array}\right) \end{array} \begin{array}{c} \text{Sequence} \\ \overbrace{} \\ 0 \\ 1 \end{array} \quad H_w(2) = \begin{array}{c} \left(\begin{array}{c|c|c|c} + & + & + & + \\ \hline + & + & - & - \\ \hline + & - & - & + \\ \hline + & - & + & - \end{array}\right) \end{array} \begin{array}{c} \text{Sequence} \\ \overbrace{} \\ 0 \\ 1 \\ 1 \\ 2 \end{array} \tag{8.7}$$

and

$$H_w(3) = \begin{array}{c} \left(\begin{array}{c|c|c|c|c|c|c|c} + & + & + & + & + & + & + & + \\ \hline + & + & + & + & - & - & - & - \\ \hline + & + & - & - & - & - & + & + \\ \hline + & + & - & - & + & + & - & - \\ \hline + & - & - & + & + & - & - & + \\ \hline + & - & - & + & - & + & + & - \\ \hline + & - & + & - & - & + & - & + \\ \hline + & - & + & - & + & - & + & - \end{array}\right) \end{array} \begin{array}{c} \text{sequence} \\ \overbrace{} \\ 0 \\ 1 \\ 1 \\ 2 \\ 2 \\ 3 \\ 3 \\ 4 \end{array} \tag{8.8}$$

Walsh-Hadamard matrices can be obtained by reordering the rows of their respective Hadamard matrices. The lowest Hadamard matrix is of order 2,

$$H(1) = \left(\begin{array}{c|c} + & + \\ \hline + & - \end{array}\right) \tag{8.9}$$

Higher matrices, restricted to having powers of two, can be obtained from the recursive relationship,

$$H_N = H_{N/2} \odot H_2 \tag{8.10}$$

where $\odot$ denotes the Kronecker product and N is a power of two. The Kronecker product means replacing each element in matrix $H_{N/2}$ by matrix H_2.

Thus,

$$H_4 = H_2 \odot H_2 = \left(\begin{array}{c|c|c|c} + & + & + & + \\ \hline + & - & + & - \\ \hline + & + & - & - \\ \hline + & - & - & + \end{array}\right) \tag{8.11}$$

and

$$H_8 = \left(\begin{array}{c|c|c|c|c|c|c|c} + & + & + & + & + & + & + & + \\ \hline + & - & + & - & + & - & + & - \\ \hline + & + & - & - & + & + & - & - \\ \hline + & - & - & + & + & - & - & + \\ \hline + & + & + & + & - & - & - & - \\ \hline + & - & + & - & - & + & - & + \\ \hline + & + & - & - & - & - & + & + \\ \hline + & - & - & + & - & + & + & - \end{array}\right) \begin{array}{c} \overbrace{}^{\text{Walsh order}} \\ \phi_0(t) \\ \phi_7(t) \\ \phi_3(t) \\ \phi_4(t) \\ \phi_1(t) \\ \phi_6(t) \\ \phi_2(t) \\ \phi_5(t) \end{array} \tag{8.12}$$

Matrices in equations (8.8) and (8.12) highlight the relationship between Hadamard matrices and Walsh-Hadamard. The ordering of the two matrices is related to each other by the Gray Code [134, 133, 141]:

$$\phi_n(t) = \phi_{GCBC(n)}(t) \tag{8.13}$$

where $GCBC$ is the Gray Code to the Binary Conversion of n and then bit reversing. For this case,

Kronecker Order	Gray code	Bit reversing	Sequency order
0	000	000	0
7	100	001	1
3	010	010	2
4	110	011	3
1	001	100	4
6	101	101	5
2	011	110	6
5	111	111	7

Tab. 8.1: Ordering of relationship between Walsh-Hadamard and Hadamard matrices

8.3 Fundamental Properties of Walsh Functions

Some important properties of the Walsh functions are discussed below.

8.3.1 Multiplications

The product of two Walsh functions, $\phi_m(t)$ and $\phi_n(t)$, is achieved by mod-2 additions of binary digits. The Walsh functions form a closed set under the multiplication, i.e. the product of two Walsh functions is also a Walsh function. For example, the multiplication $\phi_5(t)$ and $\phi_3(t)$ is,

$$\phi_5(t)\phi_3(t) = \phi_{101}(t)\phi_{011}(t) = \phi_{110}(t) = \phi_6(t)$$

8.3.2 Trigonometric functions

The trigonometric functions of Walsh functions are also Walsh functions since Walsh functions are piecewise constant functions having either values 1 or -1.

In particular the following identities,

$$\begin{aligned} \sin(k\phi_m(t)) &= \sin(k)\phi_m(t) \\ \cos(k\phi_m(t)) &= \cos(k)\phi_0(t) \end{aligned} \tag{8.14}$$

are very useful.

8.3.3 Orthonormality

It is shown in [138] that Walsh functions form an orthonormal system in $0 \leq t < 1$. Thus,

$$\int_0^1 \phi_m(t)\phi_n(t)dt = \begin{cases} 1 & m \neq n \\ 0 & m = n \end{cases} \tag{8.15}$$

8.4 Walsh Series

Like Fourier series, Walsh series can be used to expand a function $f(t)$ that is absolutely integrable in the interval [0,1). This can be expressed as,

$$f(t) = c_0\phi_0(t) + c_1\phi_1(t) + \ldots + c_n\phi_n(t) + \ldots \tag{8.16}$$

where c_n are the coefficients of the Walsh series of $f(t)$ which, owing to orthogonal properties, can be determined using the following relation,

$$c_n = \int_0^1 f(t)\phi_n(t)dt \tag{8.17}$$

8.4.1 Walsh series of a ramp function

An important Walsh expansion is that of a ramp function, $f(t) = t$ in $0 \leq t < 1$,

$$f(t) = t = \sum_{n=0}^{\infty} D_n\phi_n(t) \tag{8.18}$$

where, due to orthogonal properties, the coefficients d_n can be calculated from,

$$D_n = \int_0^1 t\phi_n(t)dt \tag{8.19}$$

Taking the first four terms only, the following relations are obtained,

$$D_0 = \int_0^1 t\phi_0(t)dt = \frac{1}{2} \tag{8.20}$$

$$D_1 = \int_0^1 t\phi_2(t)dt = \int_0^{\frac{1}{2}} tdt - \int_{\frac{1}{2}}^1 tdt = -\frac{1}{4} \tag{8.21}$$

$$D_2 = \int_0^1 t\phi_2(t)dt = \int_0^{\frac{1}{4}} tdt - \int_{\frac{1}{4}}^{\frac{1}{2}} tdt + \int_{\frac{1}{2}}^{\frac{3}{4}} tdt - \int_{\frac{3}{4}}^1 tdt = -\frac{1}{8} \tag{8.22}$$

$$D_3 = \int_0^1 t\phi_3(t)dt = \int_0^{\frac{1}{4}} tdt - \int_{\frac{1}{4}}^{\frac{3}{4}} tdt + \int_{\frac{3}{4}}^1 tdt = 0 \tag{8.23}$$

Expressing equation (8.18) in matrix form,

$$f(t) \cong \begin{pmatrix} \frac{1}{2} & -\frac{1}{4} & -\frac{1}{8} & 0 \end{pmatrix} \begin{pmatrix} \phi_0(t) \\ \phi_1(t) \\ \phi_2(t) \\ \phi_3(t) \end{pmatrix} \tag{8.24}$$

8.4.2 Discrete formulation

Quite often, functions are not in analytic form but, rather, in tabulated-data or graphical forms. In such cases, the Walsh series is expressed as follows,

$$f(k) = \sum_{n=0}^{m-1} c_n\phi_n(k), \quad k = 0, 1, 2, \ldots, m-1 \tag{8.25}$$

and the coefficients c_n are calculated as follows,

$$c_n = \frac{1}{m}\sum_{k=0}^{m-1} f(k)\phi_n(k), \quad n = 0, 1, 2, \ldots, m-1 \tag{8.26}$$

To illustrate these relations let us consider the first four terms in Equation (8.25), can be expanded and put in matrix,

$$\begin{pmatrix} c_0 \\ \hline c_1 \\ \hline c_2 \\ \hline c_3 \end{pmatrix} = \frac{1}{4}\begin{pmatrix} \phi_0(0) & \phi_0(1) & \phi_0(2) & \phi_0(3) \\ \hline \phi_1(0) & \phi_1(1) & \phi_1(2) & \phi_1(3) \\ \hline \phi_2(0) & \phi_2(1) & \phi_2(2) & \phi_2(3) \\ \hline \phi_3(0) & \phi_3(1) & \phi_3(2) & \phi_3(3) \end{pmatrix} \begin{pmatrix} f(0) \\ \hline f(1) \\ \hline f(2) \\ \hline f(3) \end{pmatrix} \tag{8.27}$$

or,in compact form,

$$\mathbf{c} = \frac{1}{m}Wf \tag{8.28}$$

Where W is the Walsh matrix.

8.4.3 Convergence

The convergence characteristics of Walsh series are discussed in [138]. If $f(t)$ is a continuous function in the interval $0 \leq t < 1$, the series (8.16) converges uniformly to $f(t)$. If the series is truncated, so that the series contains $N = 2^p$ terms, then the weighted sum of the first N terms will equal the average value of $f(t)$ in each subinterval of length 2^{-p}.

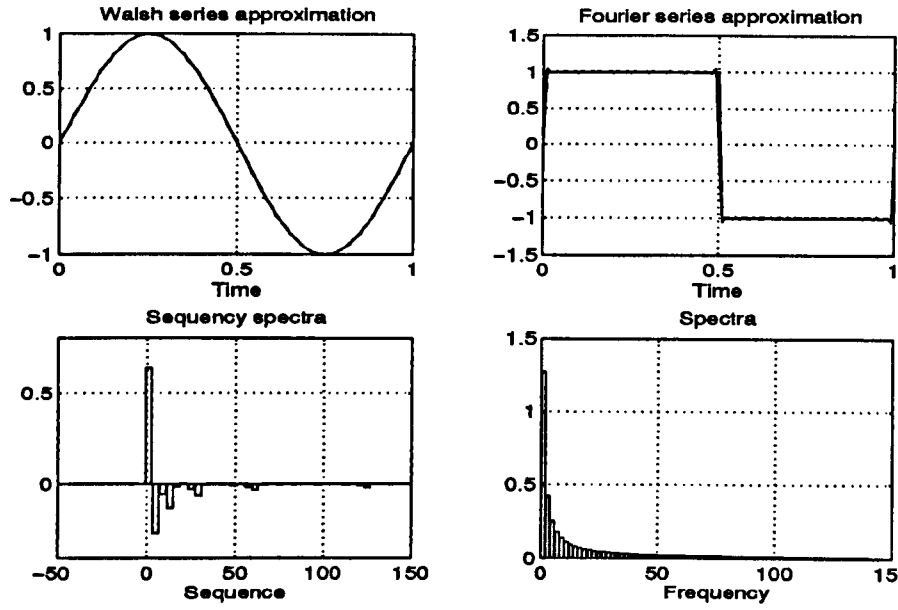

Fig. 8.3: Comparison of Walsh and Fourier spectra

8.4.4 Walsh Series Versus Fourier Series

Walsh series are adequate for the study of signals with sharp edges or discontinuities. In this context, an equivalent Fourier analysis requires many more terms to achieve a similar degree of accuracy than a corresponding Walsh series. This situation is depicted in Figure 8.3. In this case the Fourier series requires a large number of high frequency components to reproduce the sharp edges of the Walsh function $\phi_1(t)$. Figure 8.3 also describes the opposite situation where a smooth sinusoidal function is approximated by a Walsh series. In this case, high sequency terms are required to smooth out the stair-step functions in order to closely reproduce the sine function. The number of high sequency terms is substantially smaller than the number of high frequency terms required by Fourier to approximate the sharp edges of the rectangular waveform. Accordingly, it may be said that a Walsh series is useful for dealing with a wide range of smooth and non-smooth signals. In situations where the signals have sharp edges it will proof more useful than Fourier series. In addition, Walsh functions are easier to generate and to handle in digital applications.

8.4.5 Numeric examples

Ramp function

The ramp function is analysed below,

k	0	1	2	3
$f(k)$	$\frac{1}{8}$	$\frac{3}{8}$	$\frac{5}{8}$	$\frac{7}{8}$

Substituting the tabulated data of the ramp function in equation (8.27) and noting that the 4×4 matrix W corresponds to the Walsh-Hadamard matrix of order 2, with natural order

[141], we have that,

$$\begin{pmatrix} c_0 \\ c_1 \\ c_2 \\ c_3 \end{pmatrix} = \frac{1}{4} \begin{pmatrix} 1 & 1 & 1 & 1 \\ 1 & 1 & -1 & -1 \\ 1 & -1 & 1 & -1 \\ 1 & -1 & -1 & 1 \end{pmatrix} \begin{pmatrix} \frac{1}{8} \\ \frac{3}{8} \\ \frac{5}{8} \\ \frac{7}{8} \end{pmatrix} = \begin{pmatrix} \frac{1}{2} \\ -\frac{1}{4} \\ -\frac{1}{8} \\ 0 \end{pmatrix} \tag{8.29}$$

Triangular function

Let us consider now the triangular function shown in Figure 8.4,

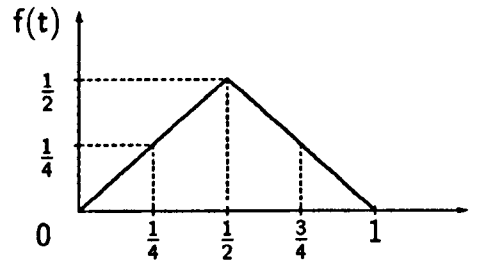

Fig. 8.4: Triangular function

The function can also be given in numeric form as,

k	$f(k)$	$\bar{f}(k)$
0	0	$\frac{1}{2}\left(0+\frac{1}{4}\right)=\frac{1}{8}$
1	$\frac{1}{4}$	$\frac{1}{2}\left(\frac{1}{4}+\frac{1}{2}\right)=\frac{3}{8}$
2	$\frac{1}{2}$	$\frac{1}{2}\left(\frac{1}{2}+\frac{1}{4}\right)=\frac{3}{8}$
3	$\frac{1}{4}$	$\frac{1}{2}\left(\frac{1}{4}+0\right)=\frac{1}{8}$

Substituting these values in equation (8.26), we have that,

$$\begin{pmatrix} c_0 \\ c_1 \\ c_2 \\ c_3 \end{pmatrix} = \frac{1}{4} \begin{pmatrix} 1 & 1 & 1 & 1 \\ 1 & 1 & -1 & -1 \\ 1 & -1 & 1 & -1 \\ 1 & -1 & -1 & 1 \end{pmatrix} \begin{pmatrix} \frac{1}{8} \\ \frac{3}{8} \\ \frac{3}{8} \\ \frac{1}{8} \end{pmatrix} = \begin{pmatrix} \frac{1}{8} \\ 0 \\ 0 \\ -\frac{1}{8} \end{pmatrix} \tag{8.30}$$

Double triangular

Triangular functions, like the one shown in Figure 8.5, are of particular interest in systems analysis. Their Walsh coefficients can be evaluated by following the approach presented above.

The data for these calculations, in tabulated form, is given below,

k	$f(k)$	$\bar{f}(k)$
0	0	$\frac{1}{2}\left(0+\frac{1}{4}\right)=\frac{1}{8}$
1	$\frac{1}{4}$	$\frac{1}{2}\left(\frac{1}{4}+0\right)=\frac{1}{8}$
2	0	$\frac{1}{2}\left(0+\frac{1}{4}\right)=\frac{1}{8}$
3	$\frac{1}{4}$	$\frac{1}{2}\left(\frac{1}{4}+0\right)=\frac{1}{8}$

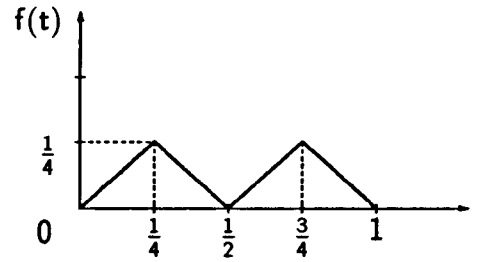

Fig. 8.5: Double triangular function

The Walsh coefficients are calculated as,

$$\begin{pmatrix} c_0 \\ c_1 \\ c_2 \\ c_3 \end{pmatrix} = \frac{1}{4} \begin{pmatrix} 1 & 1 & 1 & 1 \\ 1 & 1 & -1 & -1 \\ 1 & -1 & 1 & -1 \\ 1 & -1 & -1 & 1 \end{pmatrix} \begin{pmatrix} \frac{1}{8} \\ \frac{1}{8} \\ \frac{1}{8} \\ \frac{1}{8} \end{pmatrix} = \begin{pmatrix} \frac{1}{8} \\ 0 \\ 0 \\ 0 \end{pmatrix} \tag{8.31}$$

Alternating triangular

The alternating triangular function shown in Figure 8.6 is a double triangular function with the second triangle inverted. The sampled values of the alternating triangular function and its average value in each interval are tabulated below,

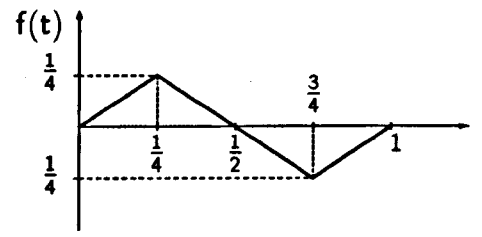

Fig. 8.6: Alternating triangular function

k	$f(k)$	$\bar{f}(k)$
0	0	$\frac{1}{2}\left(0+\frac{1}{4}\right)=\frac{1}{8}$
1	$\frac{1}{4}$	$\frac{1}{2}\left(\frac{1}{4}+0\right)=\frac{1}{8}$
2	0	$\frac{1}{2}\left(0-\frac{1}{4}\right)=-\frac{1}{8}$
3	$-\frac{1}{4}$	$\frac{1}{2}\left(-\frac{1}{4}+0\right)=-\frac{1}{8}$

The Walsh coefficients can calculated as,

$$\begin{pmatrix} c_0 \\ c_1 \\ c_2 \\ c_3 \end{pmatrix} = \frac{1}{4} \begin{pmatrix} 1 & 1 & 1 & 1 \\ 1 & 1 & -1 & -1 \\ 1 & -1 & 1 & -1 \\ 1 & -1 & -1 & 1 \end{pmatrix} \begin{pmatrix} \frac{1}{8} \\ \frac{1}{8} \\ -\frac{1}{8} \\ -\frac{1}{8} \end{pmatrix} = \begin{pmatrix} 0 \\ \frac{1}{8} \\ 0 \\ 0 \end{pmatrix} \tag{8.32}$$

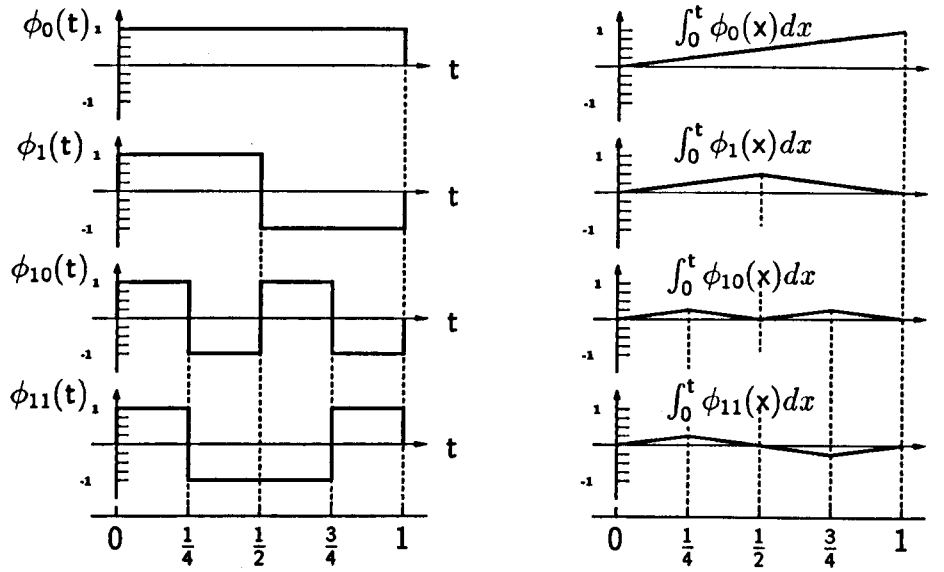

Fig. 8.7: Integral of Walsh functions

8.4.6 Integrals of Walsh functions

The integrals of rectangular Walsh functions are sets of triangular waveforms. The first four Walsh functions and their integrals are shown Figure 8.7. These integral can be expanded into Walsh series. In fact, the expansion correspond to the triangular waveforms analysed in the previous sections. For most analysis it is useful to write the relationship between Walsh functions and their integral in matrix form,

$$\begin{pmatrix} \int \phi_0(t) \\ \hline \int \phi_1(t) \\ \hline \int \phi_2(t) \\ \hline \int \phi_3(t) \end{pmatrix} = \left(\begin{array}{cc|cc} \frac{1}{2} & -\frac{1}{4} & -\frac{1}{8} & \\ \hline \frac{1}{4} & 0 & 0 & -\frac{1}{8} \\ \hline \frac{1}{8} & 0 & 0 & 0 \\ 0 & \frac{1}{8} & 0 & 0 \end{array}\right) \begin{pmatrix} \phi_0(t) \\ \phi_1(t) \\ \phi_2(t) \\ \phi_3(t) \end{pmatrix} \tag{8.33}$$

or, in compact form,

$$\int \Phi_{(4)} dt = P_{(4\times4)} \phi_{(4)}(t) \tag{8.34}$$

where P is called the operational matrix [51].

The accuracy of the operational matrix depends on the dimensions of P and ϕ. These matrices are, for convenience, chosen to be square. Larger matrices than equation (8.34) can be obtained following similar reasoning. For instance, for the case of eight subdivisions,

$$\begin{pmatrix} \int \phi_0(t)dt \\ \int \phi_1(t)dt \\ \int \phi_2(t)dt \\ \int \phi_3(t)dt \\ \int \phi_4(t)dt \\ \int \phi_5(t)dt \\ \int \phi_6(t)dt \\ \int \phi_7(t)dt \end{pmatrix} = \left(\begin{array}{cc|cc|cccc} \frac{1}{2} & -\frac{1}{4} & -\frac{1}{8} & 0 & -\frac{1}{16} & 0 & 0 & 0 \\ \hline \frac{1}{4} & 0 & 0 & -\frac{1}{8} & 0 & -\frac{1}{16} & 0 & 0 \\ \hline \frac{1}{8} & 0 & 0 & 0 & 0 & 0 & \frac{1}{16} & 0 \\ 0 & \frac{1}{8} & 0 & 0 & 0 & 0 & 0 & \frac{1}{16} \\ \hline \frac{1}{16} & 0 & 0 & 0 & 0 & 0 & 0 & 0 \\ 0 & \frac{1}{16} & 0 & 0 & 0 & 0 & 0 & 0 \\ 0 & 0 & \frac{1}{16} & 0 & 0 & 0 & 0 & 0 \\ 0 & 0 & 0 & \frac{1}{16} & 0 & 0 & 0 & 0 \end{array}\right) \begin{pmatrix} \phi_0(t)dt \\ \phi_1(t)dt \\ \phi_2(t)dt \\ \phi_3(t)dt \\ \phi_4(t)dt \\ \phi_5(t)dt \\ \phi_6(t)dt \\ \phi_7(t)dt \end{pmatrix} \tag{8.35}$$

or, in compact form,

$$\int \phi_{(8)} dt = P_{(8\times8)} \Phi_{(}8) \tag{8.36}$$

It must be noted that the upper left corner of $P_{(8\times8)}$ is equal tp $P_{(4\times4)}$. The upper right corner matrix and the lower left corner are diagonal matrices. The lower right corner matrix is the null matrix. In general, if m terms are chosen, where $m = 2^n$ and n is a positive integer of power 2, the general operational matrix can be written as follows:

$$P_{(m\times m)}=\left[\begin{array}{c:c:c:c}
\frac{1}{2} & -\frac{1}{m/2}I_{m/8} & -\frac{1}{m}I_{m/4} & -\frac{1}{2m}I_{m/2} \\
\hdashline
\frac{1}{m/2}I_{m/8} & 0_{(m/8)} & & \\
\hdashline
\multicolumn{2}{c:}{\frac{1}{m}I_{m/4}} & 0_{(m/4)} & \\
\hdashline
\multicolumn{3}{c:}{\frac{1}{2m}I_{m/2}} & 0_{(m/2)}
\end{array}\right]$$

8.4.7 Integral representation of differential functions

The differentiation of a Walsh function is a series of Dirac delta-functions, one for each discontinuity. Accordingly, Walsh series are not useful for solving differential equations, since the resulting functions are usually divergent. However, differential equations can still be solved provided they are written in their integral representation first [43]. This is done by defining the highest order derivative,

$$\frac{d^n y}{dx^n} = u(x) \tag{8.37}$$

Then, the lower order derivatives can be expressed as,

$$\frac{d^{n-1} y}{dx^{n-1}} = \int_0^x u(t)dt \tag{8.38}$$

However, this approach is tedious and unnecessary because any nth order differential equation can be converted into a set of n state equations and the need for representing higher order derivatives is avoided. Therefore, the state space approach put forward by CF Chen and CH Hsiao is used instead. It is an elegant alternative that results in a unique Kronecker product formula for the solution of the linear system of equations,

$$\dot{X} = AX + BU, \qquad X(0) = X_o \tag{8.39}$$

Where X is a state vector of n components and U is an input vector of l components. A and B are $n \times n$ and $n \times l$ matrices, respectively. Chen and Hsiao solved this problem by using Walsh functions. The rate vector $\dot{X}$ instead of the state vector X is approximated by Walsh series as follows,

$$\begin{aligned}
\dot{x}_1 &= c_{10}\phi_0(t) + c_{11}\phi_1(t) + c_{12}\phi_2(t) + \ldots \\
\dot{x}_2 &= c_{20}\phi_0(t) + c_{21}\phi_1(t) + c_{22}\phi_2(t) + \ldots \\
&\vdots \\
\dot{x}_3 &= c_{30}\phi_0(t) + c_{31}\phi_1(t) + c_{32}\phi_2(t) + \ldots
\end{aligned}$$

where the c_{ij} are the constants to be determined. Once the $\dot{X}$ is determined, X can be obtained by normal integration procedures. If m terms are used to approximate the solution then one can write,

$$\dot{X} = \begin{bmatrix} c_{10} & c_{11} & \cdots & c_{1(m-1)} \\ c_{20} & c_{21} & \cdots & c_{2(m-1)} \\ \vdots & \vdots & \vdots & \vdots \\ \vdots & \vdots & \vdots & \vdots \\ c_{n0} & c_{n1} & \cdots & c_{n(m-1)} \end{bmatrix} \begin{bmatrix} \phi_0(t) \\ \phi_1(t) \\ \phi_2(t) \\ \vdots \\ \phi_{(m-1)}(t) \end{bmatrix} = \begin{bmatrix} \mathbf{c}_1' \\ \mathbf{c}_2' \\ \vdots \\ \vdots \\ \mathbf{c}_n' \end{bmatrix} \phi(t) \tag{8.40}$$

By defining,

$$C_{(m\times m)} = \begin{bmatrix} c_{10} & c_{11} & \cdots & c_{1(m-1)} \\ c_{20} & c_{21} & \cdots & c_{2(m-1)} \\ \vdots & \vdots & \vdots & \vdots \\ \vdots & \vdots & \vdots & \vdots \\ c_{n0} & c_{n1} & \cdots & c_{n(m-1)} \end{bmatrix} = [\ \mathbf{c}_0 \quad \mathbf{c}_1 \quad \mathbf{c}_2 \quad \ldots \quad \mathbf{c}_{(m-1)}] \tag{8.41}$$

and

$$\phi'_{(m)}(t) = \ \phi_0 \quad \phi_1 \quad \phi_2 \quad \ldots \quad \phi_{(m-1)} \tag{8.42}$$

The state variables may be obtained by integration,

$$X(t) = C\int_0^t \phi(\tau)d\tau + X_0 \tag{8.43}$$

However, as discussed above, the integral can be evaluated via the operational matrix,

$$X(t) = CP\phi(t) + X_0 \tag{8.44}$$

With the input also expressed by Walsh series,

$$U(t) = \begin{bmatrix} u_1(t) \\ u_2(t) \\ \vdots \\ \vdots \\ u_l(t) \end{bmatrix} = \begin{bmatrix} h_{10} & h_{11} & h_{12} & \cdots & h_{1(m-1)} \\ h_{20} & h_{21} & h_{22} & \cdots & h_{2(m-1)} \\ \vdots & \vdots & \vdots & \vdots & \\ \vdots & \vdots & \vdots & \vdots & \\ h_{l0} & h_{l1} & h_{l2} & \cdots & h_{l(m-1)} \end{bmatrix} \begin{bmatrix} \phi_0(t) \\ \phi_1(t) \\ \vdots \\ \vdots \\ \phi_{(m-1)} \end{bmatrix} = H\phi(t) \tag{8.45}$$

the state space equation (8.39) can be rewritten as,

$$C\phi = ACP\phi + AX_0\phi + BH\phi \tag{8.46}$$

where AX_0 represents initial condition (constant) and can be written in terms of the constant Walsh function $\phi_0(t)$,

$$AX_0 = [\ AX_0 \quad 0 \quad \ldots \quad 0\ ]\phi(t) = G\phi(t) \tag{8.47}$$

Defining a new matrix K as,

$$K = G + BH \tag{8.48}$$

the matrix equation to be solved becomes,

$$C = ACP + K \tag{8.49}$$

In oder to solve equation (8.49) matrix C can be rearranged to form a vector of nm elements. This is done by taking the first column of C to be the first n entries of such a vector, then the second column, etc. so as to obtain the following expression,

$$\begin{bmatrix} \mathbf{c}_0 \\ \mathbf{c}_1 \\ \vdots \\ \mathbf{c}_{(m-1)} \end{bmatrix} = [A \odot P^t] \begin{bmatrix} \mathbf{c}_0 \\ \mathbf{c}_1 \\ \vdots \\ \mathbf{c}_{(m-1)} \end{bmatrix} + \begin{bmatrix} \mathbf{k}_0 \\ \mathbf{k}_1 \\ \vdots \\ \mathbf{k}_{(m-1)} \end{bmatrix} = [A \odot P^t]\mathbf{c} + \mathbf{k} \tag{8.50}$$

where $A \odot P^t$ is the Kronecker product defined as

$$A \odot P^t = \begin{bmatrix} p_{11}A & p_{21}A & \dots & p_{m1}A \\ p_{12}A & p_{22}A & \dots & p_{m2}A \\ \vdots & \vdots & \vdots & \vdots \\ \vdots & \vdots & \vdots & \vdots \\ p_{1m}A & p_{2m}A & \dots & p_{mm}A \end{bmatrix} \tag{8.51}$$

The solution is,

$$\mathbf{c} = [A - I \odot P^t]^{-1}\mathbf{k} \tag{8.52}$$

8.5 Case Studies

The Walsh theory presented in this chapter is now applied to the solution of the circuit shown in Figure 8.8. The results agree with those obtained by using time domain simulations.

The circuit in Figure 8.8 has the three kinds of elements considered in this work, namely resistors, inductors and capacitors. The governing differential equations are given in matrix forms as follows,

$$\begin{bmatrix} \dot{x}_1 \\ \dot{x}_2 \\ \dot{x}_3 \\ \dot{x}_4 \\ \dot{x}_5 \\ \dot{x}_6 \end{bmatrix} = \begin{bmatrix} -\frac{1}{R_1C_1} & 0 & 0 & -\frac{1}{C_1} & 0 & -\frac{1}{C_1} \\ 0 & \frac{1}{R_2C_2} & 0 & 0 & -\frac{1}{C_2} & \frac{1}{C_2} \\ 0 & 0 & 0 & 0 & 0 & \frac{1}{3} \\ \frac{1}{L_1} & 0 & 0 & 0 & 0 & 0 \\ 0 & \frac{1}{L_2} & 0 & 0 & 0 & 0 \\ \frac{1}{L_1} & -\frac{1}{L_3} & 0 & 0 & -\frac{R_3}{L_3} & \end{bmatrix} \begin{bmatrix} x_1 \\ x_2 \\ x_3 \\ x_4 \\ x_5 \\ x_6 \end{bmatrix} + \begin{bmatrix} 1 \\ 0 \\ 0 \\ 0 \\ 0 \\ 0 \end{bmatrix} u \tag{8.53}$$

or, in compact form,

$$\dot{\mathbf{x}} = \mathbf{A}\mathbf{x} + \mathbf{B}u \tag{8.54}$$

The circuit is initially relaxed, i.e. initial zero conditions. The parameters are such that matrices $\mathbf{A}$ and $\mathbf{B}$ become,

$$\mathbf{A} = \begin{bmatrix} -1 & 0 & 0 & -1 & 0 & -1 \\ 0 & -1 & 0 & 0 & -1 & 1 \\ 0 & 0 & 0 & 0 & 0 & 1 \\ 1 & 0 & 0 & 0 & 0 & 0 \\ 0 & 1 & 0 & 0 & 0 & 0 \\ 1 & -1 & -1 & 0 & 0 & -1 \end{bmatrix}, \qquad \mathbf{B} = \begin{bmatrix} 1 \\ 0 \\ 0 \\ 0 \\ 0 \\ 0 \end{bmatrix}$$

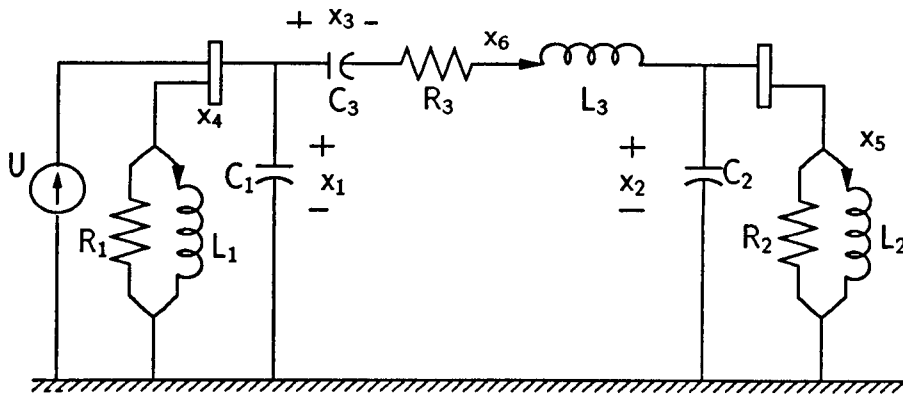

Fig. 8.8: Six order circuit

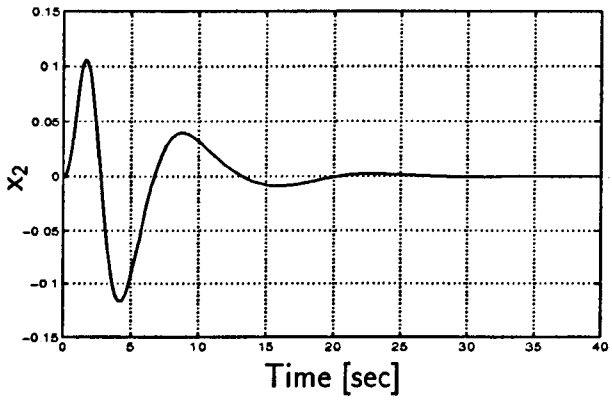

(a) State variable x_2 Vs Time

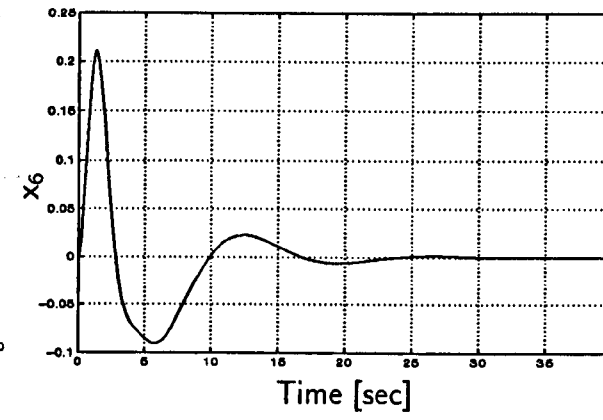

(b) State variable x_6 Vs Time

Fig. 8.9: Runge-Kutta's solution

8.5.1 Response to step functions with Walsh approach

The circuit was solved first using Runge-Kutta's method. Only the dynamics of state variables $\mathbf{x_2}$ and $\mathbf{x_6}$ are shown in Figure 8.9. The stability of the circuit has been tested using Phase Plane analysis. Figure 8.10 shows the phase plane of the two state variables. Two perspectives are presented to show the evolution of the state variables and their derivatives until they reach the equilibrium point. The two curves on top, in each Figure 8.10, present the two dimensional view of the phase planes. The applied function is a step function of unit amplitude.

If the number of Walsh coefficients is restricted to $m = 8$, the solution can be written as,

$$\begin{bmatrix} \mathbf{c}_0 \\ \mathbf{c}_1 \\ \mathbf{c}_2 \\ \mathbf{c}_3 \\ \mathbf{c}_4 \\ \mathbf{c}_5 \\ \mathbf{c}_6 \\ \mathbf{c}_7 \end{bmatrix} = \begin{bmatrix} \frac{1}{2}\mathbf{A} & \frac{1}{4}\mathbf{A} & \frac{1}{8}\mathbf{A} & 0 & \frac{1}{16}\mathbf{A} & 0 & 0 & 0 \\ \frac{1}{4}\mathbf{A} & 0 & 0 & \frac{1}{8}\mathbf{A} & 0 & \frac{1}{16}\mathbf{A} & 0 & 0 \\ -\frac{1}{8}\mathbf{A} & 0 & 0 & 0 & 0 & 0 & \frac{1}{16}\mathbf{A} & 0 \\ 0 & -\frac{1}{8}\mathbf{A} & 0 & 0 & 0 & 0 & 0 & \frac{1}{16}\mathbf{A} \\ -\frac{1}{16}\mathbf{A} & 0 & 0 & 0 & 0 & 0 & 0 & 0 \\ 0 & -\frac{1}{16}\mathbf{A} & 0 & 0 & 0 & 0 & 0 & 0 \\ 0 & 0 & -\frac{1}{16}\mathbf{A} & 0 & 0 & 0 & 0 & 0 \\ 0 & 0 & 0 & -\frac{1}{16}\mathbf{A} & 0 & 0 & 0 & 0 \end{bmatrix} \tag{8.55}$$

The Runge-Kutta's method and the Walsh solution are compared in Figure 8.11. In this case

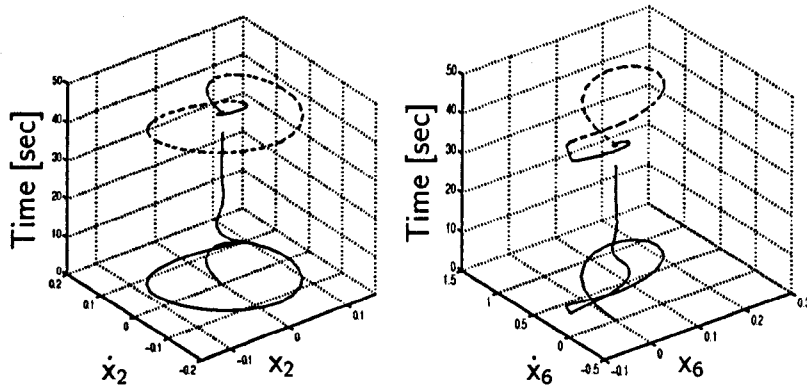

(a) State variable x_2 (b) State variable x_6

Fig. 8.10: Phase plane analysis

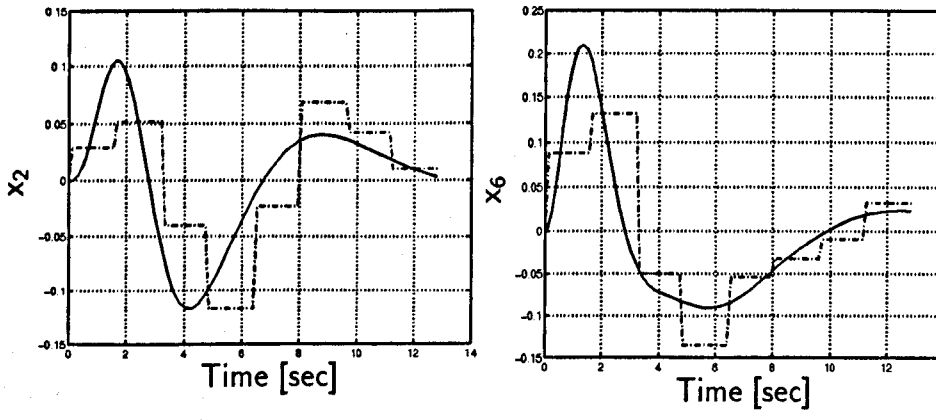

(a) State variable x_2 Vs Time (b) State variable x_6 Vs Time

Fig. 8.11: Solution with 8 Walsh coefficients

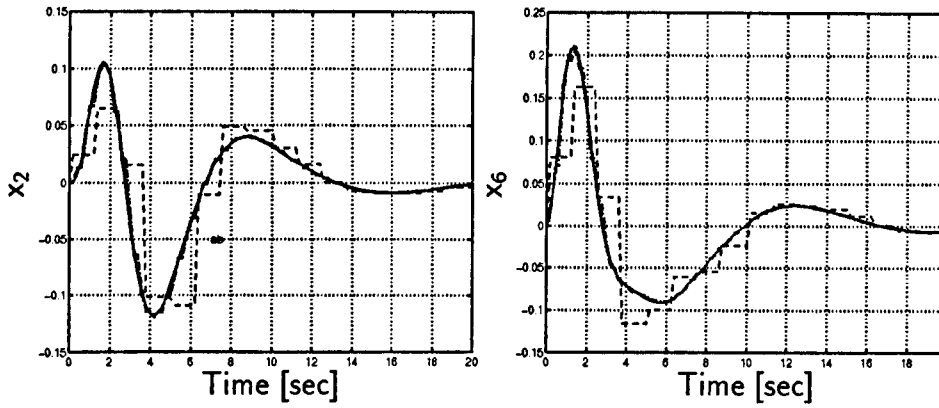

(a) State variable x_2 Vs Time (b) State variable x_6 Vs Time

Fig. 8.12: Comparison of time domain solution and the Walsh solution

the accuracy is poor due to the small number of Walsh coefficients being used. However, for the same case and with the same number of time intervals the Runge-Kutta method fails to find the solution.

The accuracy of the solution is substantially improved if m increases. Different values of m where considered i.e. $m = 16$, $m = 32$ and $m = 128$. The solution with $m = 128$ was quite accurate but with $m = 64$ the result is considered satisfactory. Figure 8.12 shows the various approximations to the time domain solution (solid line). The solution with $m = 32$ is still poor, but approximations obtained with $m = 64$ and $m = 128$ are so accurate that is very difficult to differentiate them, in Figure 8.12, from the exact solution.

8.5.2 Response to periodic inputs

The periodic response of the circuit shown in Figure 8.8 is carried out below. The circuit parameters are changed so as to yield the matrix **A** below,

$$\mathbf{A} = \begin{bmatrix} -1 & 0 & 0 & -1 & 0 & -1 \\ 0 & -1 & 0 & 0 & -1 & 1 \\ 0 & 0 & 0 & 0 & 0 & 1 \\ 3 & 0 & 0 & 0 & 0 & 0 \\ 0 & 3 & 0 & 0 & 0 & 0 \\ 3 & -3 & -1 & 0 & 0 & -1 \end{bmatrix}$$

These values produce periodic responses with magnitudes values of around one. The input used in this case is the square waveform current shown in Figure 8.13. It is represented by one Walsh coefficient. Results for the state variables x_2 and x_6 are shown in Figure 8.14. The limit cycles were determined in the phase plane. Figure 8.14 shows the dynamics of the two state variables, calculated with Runge-Kutta and Walsh methods. The Walsh solution was obtained with $m = 128$. The large number of Walsh coefficients used is due to the large period of time over which the response is analysed. Figure 8.15 shows the evolution of the state variables until the limit cycle is reached. It is interesting to see the high accuracy achieved by the Walsh domain solution . Also, it is important to mention that the set of equations to be solved is highly sparse and efficient solutions can be obtained taking advantage of this fact.

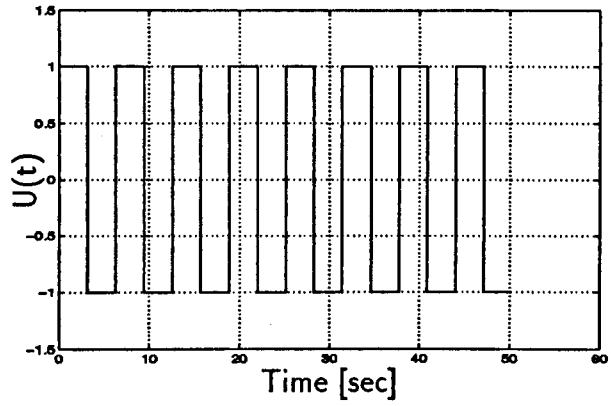

Fig. 8.13: Input waveform

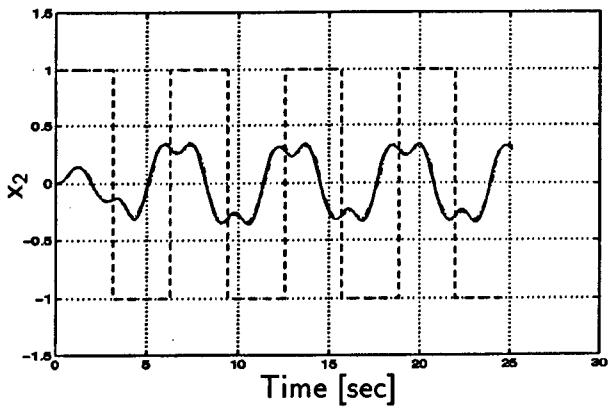

(a) State variable x_2 and input Vs Time

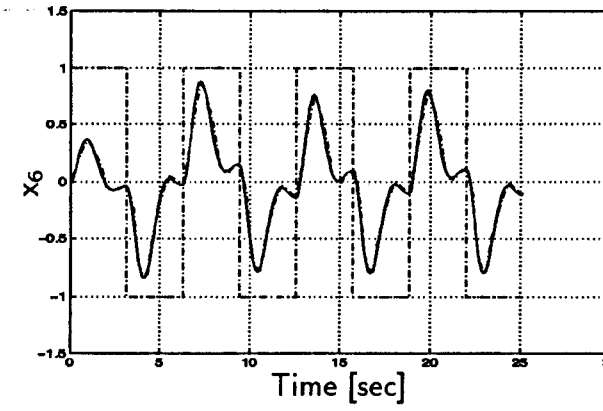

(b) State variable x_6 and input Vs Time

Fig. 8.14: Comparison of Walsh and Time domain solutions

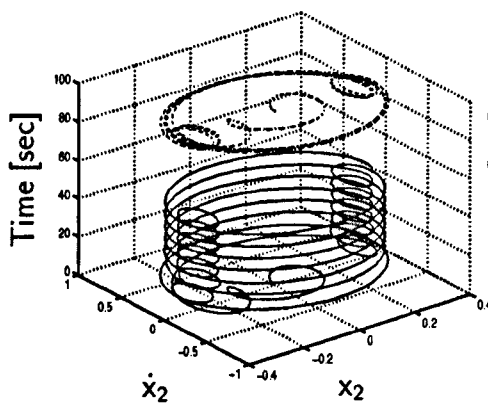

(a) State variable x_2

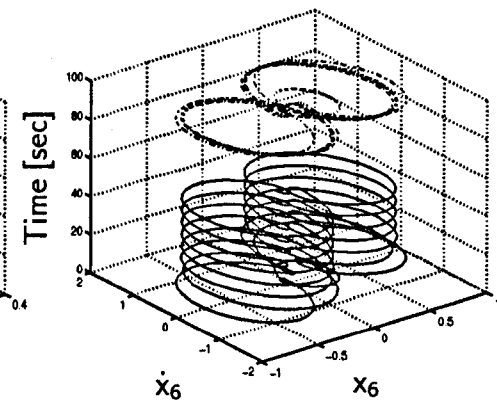

(b) State variable x_6

Fig. 8.15: Limit Cycles

8.6 Conclusions

The basic theory of Walsh functions has been described. The ground has been prepared for the theory to be presented in the three coming chapters where novel ways of analysing non-linear circuits in the Walsh domain are presented. It has been shown that although Walsh functions are piecewise constant, they can be used to model smooth signals. They are easy to generate and to deal with in numerical operations. The best of these functions is obtained when analysing signals with sharp edges or discontinuities. In such cases, Fourier series may require an extremely large number of coefficients.

Also, the structure of the operational matrix of integration in the Walsh domain has been presented. A simple example was used to show the prowess of the Walsh approach. The results presented were validated using traditional, time domain solutions via Runge-Kutta method.

The Walsh domain is an alternative technique for the analysis of electric circuits subjected to periodic functions with sinusoidal and non-sinusoidal inputs.

Chapter 9

Analysis of Linear Time Varying Power Plant Components Via Walsh Functions

This chapter presents a methodology for analysing LTVS using Walsh orthogonal functions. Closed form solutions for this class of systems are carried out in the Walsh domain. The product operational matrix is crucial to achieving this task. It is shown that, if a large number of coefficients in the Walsh series is considered, the dynamics of limit cycles can be accurately represented and determined in one iteration. Alternatively, if a smaller number of coefficients is used, the same level of accuracy can be achieved by resorting to an iterative process. A detailed numeric example is presented to show the application of the theory.

9.1 Introduction

Approximations of signals with orthogonal functions have been widely used in the signal processing camp. They have also played an important role in the solution of problems in system analysis, parameter identification and optimal control. The main attractions of these techniques is that they reduce the differential equations describing the problem to algebraic equations. For LTIS and LTVS, the basic idea is to define an operational matrix of integration which relates, in the same basis, the orthogonal basis and their integrals. Also, as part of the solution, a product operational matrix which relates the coefficients of the two operands and the result is defined. These matrices have been defined for several basis functions and successfully applied to the solution of several problems. The solution methods can be classified into three groups, i.e. those which use orthogonal functions, those which use orthogonal polynomials and those which use non-orthogonal expansions.

The use of the operational matrix was introduced by CF Chen and CH Hsiao in [51], using Walsh functions as the basis. After that, the use of orthogonal expansions has been applied extensively in system analysis. Previously, the study of linear systems was confined to traditional transforms such as Laplace, Fourier and Z transforms.

Arguably, Walsh functions were first used by MS Corrington [43], with the purpose of solving linear and non-linear differential equations. Since then, there has been a number of publications were such functions have been used to solve a variety of problems. The concept of operational matrix was first presented in this domain and later it was extended to other orthogonal basis.

Operational matrices have also been defined for simple piecewise basis functions, namely block-pulse orthonormal basis. This basis, as well as the Haar basis, are considered to be

within the Wavelets family. The simple form of this block-pulse basis renders them good candidates for digital implementation. They are amenable to the solution of non-linear problems and can be applied to the analysis of waveform distortion of power systems.

In recent years, Wavelet analysis has been applied to many fields of science and engineering. The integration operational matrix has been defined recently [79].

Several researchers have used orthogonal polynomials to transform the differential equations representing the system into a set of algebraic equations. However, this approach is inflexible as the function has to be approximated with polynomials. Polynomials are sufficiently accurate for small intervals but, for large intervals, severe oscillations may appear.

Non-orthogonal series have also been applied to the analyses of linear, time-varying systems and bilinear systems. When compared to orthogonal polynomials, Taylor series show the advantage of simplicity in integration and product operational matrices. However, they also have the problem of being inaccurate for large intervals.

In this chapter, the product operational matrix in the Walsh domain is reviewed. This operational matrix and the operational matrix of integration play an important role in the analysis of LTVS and NLS.

9.2 Product Operational Matrix

The product of a vector and its transposed is called the product operational matrix $\Phi_{(m\times m)}$,

$$\phi_{(m)}(t)\phi^t_{(m)}(t) = \Phi_{(m\times m)} \tag{9.1}$$

For the case when $m = 2$ the matrix is,

$$\Phi_{(2\times 2)} = \begin{bmatrix} \phi_0 & \phi_1 \\ \phi_1 & \phi_0 \end{bmatrix} \tag{9.2}$$

For the case when $m = 4$ the matrix is,

$$\Phi_{(4\times 4)} = \left[\begin{array}{cc|cc} \phi_0 & \phi_1 & \phi_2 & \phi_3 \\ \phi_1 & \phi_0 & \phi_3 & \phi_2 \\ \hline \phi_2 & \phi_3 & \phi_0 & \phi_1 \\ \phi_3 & \phi_2 & \phi_1 & \phi_0 \end{array}\right] \tag{9.3}$$

and for the case when $m = 8$,

$$\left[\begin{array}{cccc|cccc} \phi_0 & \phi_1 & \phi_2 & \phi_3 & \phi_4 & \phi_5 & \phi_6 & \phi_7 \\ \phi_1 & \phi_0 & \phi_3 & \phi_2 & \phi_5 & \phi_4 & \phi_7 & \phi_6 \\ \phi_2 & \phi_3 & \phi_0 & \phi_1 & \phi_6 & \phi_7 & \phi_4 & \phi_5 \\ \phi_3 & \phi_2 & \phi_1 & \phi_0 & \phi_7 & \phi_6 & \phi_5 & \phi_4 \\ \hline \phi_4 & \phi_5 & \phi_6 & \phi_7 & \phi_0 & \phi_1 & \phi_2 & \phi_3 \\ \phi_5 & \phi_4 & \phi_7 & \phi_6 & \phi_1 & \phi_0 & \phi_3 & \phi_2 \\ \phi_6 & \phi_7 & \phi_4 & \phi_5 & \phi_2 & \phi_3 & \phi_0 & \phi_1 \\ \phi_7 & \phi_6 & \phi_5 & \phi_4 & \phi_3 & \phi_2 & \phi_1 & \phi_0 \end{array}\right] \tag{9.4}$$

If one defines

$$\Phi_{+\frac{m}{2}(\frac{m}{2}\times\frac{m}{2})} = \phi_{(\frac{m}{2}\times\frac{m}{2})} \tag{9.5}$$

where the subscript of every time-dependent element of $(\frac{m}{2} \times \frac{m}{2})$ is increased by $\frac{m}{2}$, the general form of the product matrix $(m \times m)$ is,

$$\Phi_{(m\times m)} = \begin{bmatrix} \Phi_{(\frac{m}{2}\times\frac{m}{2})} & \Phi_{+\frac{m}{2}(\frac{m}{2}\times\frac{m}{2})} \\ \Phi_{+\frac{m}{2}(\frac{m}{2}\times\frac{m}{2})} & \Phi_{(\frac{m}{2}\times\frac{m}{2})} \end{bmatrix} \tag{9.6}$$

The approximation of a function $f(t)$ in matrix form can be written as,

$$f(t) = \mathbf{c}^t \phi_m(t) \tag{9.7}$$

Similarly to the product matrix, the matrix of coefficients can be defined in general form as,

$$\mathbf{C}_{(m\times m)} = \begin{bmatrix} \mathbf{C}_{(\frac{m}{2}\times\frac{m}{2})} & \mathbf{C}_{+\frac{m}{2}(\frac{m}{2}\times\frac{m}{2})} \\ \mathbf{C}_{+\frac{m}{2}(\frac{m}{2}\times\frac{m}{2})} & \mathbf{C}_{(\frac{m}{2}\times\frac{m}{2})} \end{bmatrix} \tag{9.8}$$

The following relation is an important property which facilitates the solution of linear, time-varying and bilinear systems,

$$\Phi_{(m\times m)}\mathbf{c}_m = \mathbf{C}_{m\times m}\phi_m \tag{9.9}$$

By way of example, lets take the case when $m = 4$,

$$\left[\begin{array}{cc|cc} \phi_0 & \phi_1 & \phi_2 & \phi_3 \\ \phi_1 & \phi_0 & \phi_3 & \phi_2 \\ \hline \phi_2 & \phi_3 & \phi_0 & \phi_1 \\ \phi_3 & \phi_2 & \phi_1 & \phi_0 \end{array}\right] \begin{bmatrix} c_0 \\ c_1 \\ c_2 \\ c_3 \end{bmatrix} = \left[\begin{array}{cc|cc} c_0 & c_1 & c_2 & c_3 \\ c_1 & c_0 & c_3 & c_2 \\ \hline c_2 & c_3 & c_0 & c_1 \\ c_3 & c_2 & c_1 & c_0 \end{array}\right] \begin{bmatrix} \phi_0 \\ \phi_1 \\ \phi_2 \\ \phi_3 \end{bmatrix} \tag{9.10}$$

9.3 Solution of Time-varying Systems

Let us consider a linear, time-varying system,

$$\dot{\mathbf{x}}(t) = \mathbf{A}(t)\mathbf{x}(t) + \mathbf{B}(t)\mathbf{u}(t), \qquad \mathbf{x} = \mathbf{x}_0 \tag{9.11}$$

where $\mathbf{x}(t)$ is an $n-$vector, $\mathbf{u}$ is a $q-$vector, $\mathbf{A}(t)$ is an $n \times n$ matrix and $\mathbf{B}(t)$ is an $n \times q$ matrix. Let us define $\mathbf{b}_j$ to be the jth column of $\mathbf{B}(t)$ so that equation (9.11) becomes,

$$\dot{\mathbf{x}}(t) = \mathbf{A}(t)\mathbf{x} + \sum_{j=1}^{q} \mathbf{b}_j(t)u_j(t) \tag{9.12}$$

Let a_{ij} and b_{ij} be elements of $\mathbf{A}$ and $\mathbf{B}$, respectively. $b_{ij}(t)$ is the ith element of the vector $\mathbf{b}_j$. Let us assume now that every element of $\mathbf{A}$ and $\mathbf{B}$ is absolutely integrable in the time interval [0,1) and each element can be approximated by a Walsh series, i.e.

$$a_{ij}(t) = c_{ij0}\phi_0(t) + c_{ij1}\phi_1(t) + \ldots + c_{ij(m-1)}(t)\phi_{(m-1)}(t) \tag{9.13}$$

or, in matrix form,

$$a_{ij}(t) = \mathbf{c}_{ij}^t \Phi_{(m)}(t) \tag{9.14}$$

where

$$\mathbf{c}_{ij}^t = [c_{ij0}, c_{ij1}, \ldots, c_{ij(m-1)}] \tag{9.15}$$

and

$$\begin{aligned} b_{ij}(t) &= w_{ij0}\phi_0(t) + w_{ij1}\phi_1(t) + \ldots + w_{ij(m-1)}\phi_{(m-1)}(t) && (9.16) \\ &= \mathbf{w}_{ij}^t \Phi_m(t) && (9.17) \end{aligned}$$

where

$$\mathbf{w}_{ij}^t = [w_{ij0}, w_{ij1}, \ldots, w_{ij(m-1)}] \tag{9.18}$$

Therefore,

$$\mathbf{A}(t) = \begin{bmatrix} \mathbf{c}_{11}^t\Phi_{(m)} & \mathbf{c}_{12}^t\Phi_{(m)} & \cdots & \mathbf{c}_{1n}^t\Phi_{(m)}(t) \\ \mathbf{c}_{21}^t\Phi_{(m)} & \mathbf{c}_{22}^t\Phi_{(m)} & \cdots & \mathbf{c}_{2n}^t\Phi_{(m)}(t) \\ \vdots & \vdots & \vdots & \vdots \\ \mathbf{c}_{n1}^t\Phi_{(m)} & \mathbf{c}_{n2}^t\Phi_{(m)} & \cdots & \mathbf{c}_{nn}^t\Phi_{(m)}(t) \end{bmatrix} \tag{9.19}$$

or

$$\mathbf{A}(t) = \begin{bmatrix} \mathbf{c}_{11}^t & \mathbf{c}_{12}^t & \cdots & \mathbf{c}_{1n}^t \\ \mathbf{c}_{21}^t & \mathbf{c}_{22}^t & \cdots & \mathbf{c}_{2n}^t \\ \vdots & \vdots & \vdots & \vdots \\ \mathbf{c}_{n1}^t & \mathbf{c}_{n2}^t & \cdots & \mathbf{c}_{nn}^t \end{bmatrix} \begin{bmatrix} \Phi_{(m)}(t) & 0 & \cdots & 0 \\ 0 & \Phi_{(m)}(t) & \cdots & 0 \\ \vdots & \vdots & & \vdots \\ 0 & 0 & \cdots & \Phi_{(m)}(t) \end{bmatrix} \tag{9.20}$$

In compact form,

$$\mathbf{A}(t) = \mathbf{c}\Phi^*(t) \tag{9.21}$$

Similarly,

$$\mathbf{b}_j(t) = \begin{bmatrix} \mathbf{w}_{1j}^t\Phi_{(m)}(t) \\ \mathbf{w}_{2j}^t\Phi_{(m)}(t) \\ \vdots \\ \mathbf{w}_{nj}^t\Phi_{(m)}(t) \end{bmatrix} = \begin{bmatrix} \mathbf{w}_{1j}^t \\ \mathbf{w}_{2j}^t \\ \vdots \\ \mathbf{w}_{nj}^t \end{bmatrix} \Phi_{(m)}(t) \triangleq \beta_j\Phi_{(m)}(t) \tag{9.22}$$

If the input variables $u_j(t), j = 1, 2, \ldots, q$ are absolutely integrable in the time interval [0,1), then they can be expanded into Walsh series,

$$u_j(t) = g_{j0}\phi_0(t) + g_{j1}\phi_1(t) + \ldots + g_{j(m-1)}\phi_{(m-1)}(t) \tag{9.23}$$

$$= \mathbf{g}_j^t\Phi_{(m)}(t) \tag{9.24}$$

where

$$\mathbf{g}_{ij}^t = [g_{j0}, g_{j1}, \ldots, g_{j(m-1)}] \tag{9.25}$$

The Walsh series approximation of the state variable $\mathbf{x}(t)$ is,

$$\mathbf{x}(t) = \begin{bmatrix} h_{10}\phi_0(t) + h_{11}\phi_1(t) + \ldots + h_{1,m-1}\phi_{m-1}(t) \\ h_{20}\phi_0(t) + h_{21}\phi_1(t) + \ldots + h_{2,m-1}\phi_{m-1}(t) \\ \vdots \\ h_{n0}\phi_0(t) + h_{n1}\phi_1(t) + \ldots + h_{n,m-1}\phi_{m-1}(t) \end{bmatrix} \tag{9.26}$$

$$= \begin{bmatrix} h_{10} & h_{11} & \cdots & h_{1,m-1} \\ h_{20} & h_{21} & \cdots & h_{2,m-1} \\ \vdots & \vdots & & \vdots \\ h_{n0} & h_{n1} & \cdots & h_{n,m-1} \end{bmatrix} \begin{bmatrix} \phi_0(t) \\ \phi_1(t) \\ \vdots \\ \phi_{m-1}(t) \end{bmatrix} \tag{9.27}$$

$$= \begin{bmatrix} \mathbf{h}_0^t(t) \\ \mathbf{h}_1(t) \\ \vdots \\ \mathbf{h}_{m-1}(t) \end{bmatrix} \Phi_{(m)}(t) \triangleq \mathbf{H}\Phi_{(m)}(t) \tag{9.28}$$

where

$$\mathbf{h}_i = [h_{i0}, h_{i1}, \ldots, h_{i,m-1}] \tag{9.29}$$

Then the product $A(t)x(t)$ is carried out,

$$A(t)x(t) = \begin{bmatrix} \mathbf{c}_{11}^T\Phi(t)\mathbf{h}_1^T\Phi(t) + \mathbf{c}_{12}^T\Phi(t)\mathbf{h}_2^T\Phi(t) + \ldots + \mathbf{c}_{1r}^T\Phi(t)\mathbf{h}_r^T\Phi(t) \\ \mathbf{c}_{21}^T\Phi(t)\mathbf{h}_1^T\Phi(t) + \mathbf{c}_{22}^T\Phi(t)\mathbf{h}_2^T\Phi(t) + \ldots + \mathbf{c}_{1r}^T\Phi(t)\mathbf{h}_r^T\Phi(t) \\ \vdots \\ \mathbf{c}_{r1}^T\Phi(t)\mathbf{h}_1^T\Phi(t) + \mathbf{c}_{r2}^T\Phi(t)\mathbf{h}_2^T\Phi(t) + \ldots + \mathbf{c}_{rr}^T\Phi(t)\mathbf{h}_r^T\Phi(t) \end{bmatrix} \tag{9.30}$$

$$= \begin{bmatrix} \mathbf{h}_1^T\mathbf{c}_{11}\Phi(t) + \mathbf{h}_2^T\mathbf{c}_{12}\Phi(t) + \ldots + \mathbf{h}_r^T\mathbf{c}_{1r}\Phi(t) \\ \mathbf{h}_1^T\mathbf{c}_{21}\Phi(t) + \mathbf{h}_2^T\mathbf{c}_{22}\Phi(t) + \ldots + \mathbf{h}_r^T\mathbf{c}_{2r}\Phi(t) \\ \vdots \\ \mathbf{h}_1^T\mathbf{c}_{r1}\Phi(t) + \mathbf{h}_2^T\mathbf{c}_{r2}\Phi(t) + \ldots + \mathbf{h}_r^T\mathbf{c}_{rr}\Phi(t) \end{bmatrix} \tag{9.31}$$

$$= \begin{bmatrix} G_1 \\ G_2 \\ \vdots \\ G_r \end{bmatrix} \Phi(t) \tag{9.32}$$

where

$$\mathbf{c}_{ij}^T\mathbf{T}(t)\mathbf{h}_j^T\mathbf{T}(t) = \mathbf{h}_j^T\mathbf{T}(t)\mathbf{T}^T(t)\mathbf{c}_{ij} = \mathbf{h}_j^T\mathbf{c}_{ij}\mathbf{T}(t) \tag{9.33}$$

In general,

$$\mathbf{c}_i = \sum_{j=1}^{r} \mathbf{h}_j^T\mathbf{c}_{ij} \tag{9.34}$$

where $\mathbf{c}_{ij}$ is a product operational matrix.

Now we reconstruct $A(t)x(t)$ as follows:

$$\begin{aligned} [\ \mathbf{c}_1 \quad \mathbf{c}_2 \quad \ldots \quad \mathbf{c}_n\ ]\Phi^*(t) &= [\ \mathbf{h}_1^T \quad \mathbf{h}_2^T \quad \ldots \quad \mathbf{h}_n^T\ ] \begin{bmatrix} \mathbf{c}_{11} & \mathbf{c}_{12} & \ldots & \mathbf{c}_{1r} \\ \mathbf{c}_{21} & \mathbf{c}_{22} & \ldots & \mathbf{c}_{1r} \\ \vdots & \vdots & & \vdots \\ \mathbf{c}_{r1} & \mathbf{c}_{r2} & \ldots & \mathbf{c}_{rr} \end{bmatrix} \Phi^*(t) \\ &= \mathbf{h}^*\mathbf{c}^*\Phi^*(t) \end{aligned} \tag{9.35}$$

In the same way, we arrange the product $B(t)u(t)$ as,

$$\begin{aligned} [\ \mathbf{B}_1 \quad \mathbf{B}_2 \quad \ldots \quad \mathbf{B}_n\ ]\Phi^*(t) &= [\ \mathbf{U}_1^T \quad \mathbf{U}_2^T \quad \ldots \quad \mathbf{U}_n^T\ ] \begin{bmatrix} \mathbf{B}_{11} & \mathbf{B}_{12} & \ldots & \mathbf{B}_{1q} \\ \mathbf{B}_{21} & \mathbf{B}_{22} & \ldots & \mathbf{B}_{1q} \\ \vdots & \vdots & & \vdots \\ \mathbf{B}_{r1} & \mathbf{B}_{r2} & \ldots & \mathbf{B}_{rq} \end{bmatrix} \Phi^*(t) \\ &= \mathbf{U}^*\mathbf{B}^*\Phi^*(t) \end{aligned} \tag{9.36}$$

$$B(t) = \begin{bmatrix} \mathbf{B}_{11}^T\Phi(t) & \mathbf{B}_{12}\Phi(t) & \ldots & \mathbf{B}_{1q}^T\Phi(t) \\ \mathbf{B}_{21}^T\Phi(t) & \mathbf{B}_{22}\Phi(t) & \ldots & \mathbf{B}_{2q}^T\Phi(t) \\ \vdots & \vdots & & \vdots \\ \mathbf{B}_{1r}^T\Phi(t) & \mathbf{B}_{r2}\Phi(t) & \ldots & \mathbf{B}_{rq}^T\Phi(t) \end{bmatrix}_{(r\times r)} \tag{9.37}$$

or

$$B(t) = \begin{bmatrix} \mathbf{B}_{11}^T & \mathbf{B}_{12} & \dots & \mathbf{B}_{1q}^T \\ \mathbf{B}_{21}^T & \mathbf{B}_{22} & \dots & \mathbf{B}_{2q}^T \\ \vdots & \vdots & & \vdots \\ \mathbf{B}_{1r}^T & \mathbf{B}_{r2} & \dots & \mathbf{B}_{rq}^T \end{bmatrix} \begin{bmatrix} \Phi(t) & 0 & \dots & 0 \\ 0 & \Phi(t) & \dots & 0 \\ \vdots & \vdots & & \vdots \\ 0 & 0 & \dots & \Phi(t) \end{bmatrix} = \widehat{\mathbf{B}}\Phi^*(t) \tag{9.38}$$

If the input $u(t)$ is written as,

$$u(t) = \begin{bmatrix} u_1(t) \\ u_2(t) \\ \vdots \\ u_r(t) \end{bmatrix} = \begin{bmatrix} \mathbf{U}_1^T\Phi(t) \\ \mathbf{U}_2^T\Phi(t) \\ \vdots \\ \mathbf{U}_r^T\Phi(t) \end{bmatrix} = \begin{bmatrix} \mathbf{U}_1^T \\ \mathbf{U}_2^T \\ \vdots \\ \mathbf{U}_r^T \end{bmatrix} \Phi(t) = \widehat{\mathbf{U}}\Phi(t) \tag{9.39}$$

then,

$$B(t)u(t) = \begin{bmatrix} \mathbf{B}_1^T \\ \mathbf{B}_2^T \\ \vdots \\ \mathbf{B}_r^T \end{bmatrix} \tag{9.40}$$

$\mathbf{B}_{ij}$ is the coefficient matrix of B_{ij},

$$\begin{aligned} B_{ij} &= [\ B_{ij0} \quad B_{ij1} \quad B'_{j1} \quad \dots \quad B_{ijn} \quad B'_{jn}\ ] \\ U_{ij} &= [\ U_{ij0} \quad U_{ij1} \quad U'_{j1} \quad \dots \quad U_{ijn} \quad U'_{jn}\ ] \end{aligned}$$

Substituting $A(t)x(t)$ and $B(t)u(t)$ into the differential equation (9.11),

$$\dot{\mathbf{h}}^*\Phi^*(t) = \mathbf{h}^*\mathbf{c}^*\Phi^*(t) + \mathbf{U}^*\mathbf{B}^*\Phi^*(t) \tag{9.41}$$

Integration of (9.41) yields,

$$\mathbf{h}^*\Phi^*(t) - \mathbf{h}^*\Phi^*(0) = \int_0^t \mathbf{h}^*\mathbf{c}^*\Phi^*(\tau)d\tau + \int_0^t \mathbf{U}^*\mathbf{B}^*\Phi^*(\tau)d\tau \tag{9.42}$$

then,

$$\mathbf{h}^* - \mathbf{h}_0^* = \mathbf{h}^*\mathbf{c}^*P* + \mathbf{U}^*\mathbf{B}^*\mathbf{P}^* \tag{9.43}$$

where

$$\begin{aligned} \mathbf{h}_0^* &= [\ x_1(0) \quad 0 \quad \dots \quad 0 \ \vdots \ x_2(0) \quad 0 \quad \dots \quad 0 \ \vdots \ \dots \ \vdots \ x_r(0) \quad 0 \quad \dots \quad 0\ ] \\ \mathbf{h}^* &= [\ c_{10} \quad c_{11} \quad c'_{11} \dots \quad c_{1n} \quad X'_{1n} \ \vdots \ \dots \ \vdots \ c_{10} \quad c_{11} \quad c'_{11} \dots \quad c_{1n} \quad c'_{1n}\ ] \\ \mathbf{h}_i &= [\ c_{i0} \quad c_{i1} \quad c'_{i1} \quad \dots \quad c_{in} \quad c'_{in}\ ] \\ x &= [\ x_1 \quad x_2 \quad \dots \quad x_r\ ]^T \\ \mathbf{U}^* &= [\ U_{10} \quad U_{11} \quad U'_{11} \dots \quad U_{1n} \quad U'_{1n} \ \vdots \ \dots \ \vdots \ U_{10} \quad U_{11} \quad U'_{11} \dots \quad U_{1n} \quad U'_{1n}\ ] \\ u &= [\ u_1 \quad u_2 \quad \dots \quad u_q\ ]^T \\ \mathbf{P}^* &= \begin{bmatrix} \mathbf{P} & \mathbf{0} & \dots & \mathbf{0} \\ \mathbf{0} & \mathbf{P} & \dots & \mathbf{0} \\ \vdots & \vdots & & \vdots \\ \mathbf{0} & \mathbf{0} & \dots & \mathbf{P} \end{bmatrix}_{(r(2n+1)\times r(2n+1))} \end{aligned} \tag{9.44}$$

The above equations form a set of $(2n+1) \times r$ algebraic equations that can be computed as follows:

$$\mathbf{h}^*(I - \mathbf{c}^*\mathbf{P}^*) = \mathbf{U}^*\mathbf{B}^*\mathbf{P}^* + \mathbf{h}_0^* \tag{9.45}$$

or

$$\mathbf{h}^* = (\mathbf{U}^*\mathbf{B}^*\mathbf{P}^* + \mathbf{h}_0^*)(I - \mathbf{c}^*\mathbf{P}^*)^{-1} \tag{9.46}$$

9.3.1 Numeric Example

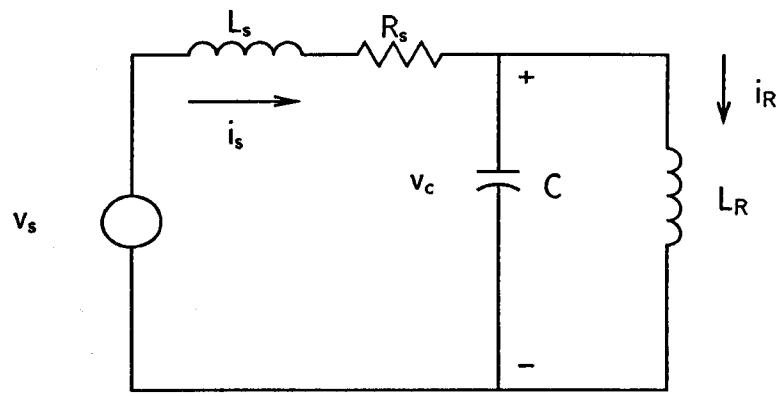

Fig. 9.1: Periodic circuit

To show the use of Walsh basis for solving time varying problems, the circuit of Figure 9.1 is solved. The voltage source is sinusoidal and the linear, periodic inductor holds the relationship,

$$i_R(t) = \frac{1}{L_R}\int_0^t \sin(\tau)v_c(\tau) \tag{9.47}$$

The existence of the limit cycle, i.e. the periodic steady state, is determined via numeric integration. The dynamic equations are,

$$\begin{bmatrix} \dot{i}_R \\ \dot{v}_c \\ \dot{i}_s \end{bmatrix} = \begin{bmatrix} 0 & \frac{1}{L_R}\sin(t) & 0 \\ -\frac{1}{C} & 0 & \frac{1}{C} \\ 0 & -\frac{1}{L_s} & -\frac{R_s}{L_s} \end{bmatrix} \begin{bmatrix} i_R \\ v_c \\ i_s \end{bmatrix} + \begin{bmatrix} 0 \\ 0 \\ \frac{v_s}{L_s} \end{bmatrix} \tag{9.48}$$

or, in compact form,

$$\dot{\mathbf{x}} = \mathbf{A}(t)\mathbf{x} + \mathbf{B}u(t) \tag{9.49}$$

The parameters of the circuit have been selected so that matrices $\mathbf{A}$ and $\mathbf{B}$ are,

$$\mathbf{A} = \begin{bmatrix} 0 & \sin(t) & 0 \\ -1 & 0 & 1 \\ 0 & -1 & -1 \end{bmatrix}, \qquad \mathbf{B} = \begin{bmatrix} 0 \\ 0 \\ 1 \end{bmatrix}$$

The voltage source is $u(t) = \sin(t)$. The current through the time-varying inductor is shown in Figure 9.2(a) and the limit cycle is shown in Figure 9.2(b). The solution was first carried out in the time domain using a Runge-Kutta integration method of integration. The

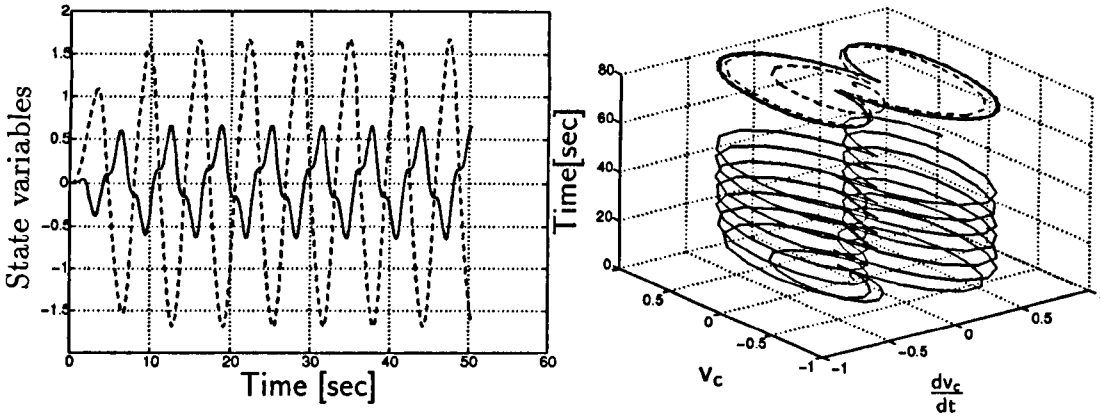

(a) Current through time-varying inductor

(b) Limit cycle

Fig. 9.2: Response of a time-varying circuit

numeric example was also solved by using the Walsh approach for linear, time-varying systems presented in this chapter. Figure 9.3 (a)-(i) show simulation results. The Walsh series can be used to approximate limit cycles to various degrees of accuracy. The accuracy is directly related to the number of coefficients considered in the series. In Figure 9.3(a) to (c), for instance, the response of the system has been approximated using the first 32 coefficients of the Walsh series. It can be appreciated from Figure 9.3(c) that, for this case, the approximation of the limit cycle is rather poor, although the approximation of the first periods of the transient response resembles the behaviour of the system in such periods. Figures 9.3(d) to (f) illustrate the approximation obtained when the first 64 coefficients of the Walsh series are considered. It can be seen that the first cycles of the transient period, Figure 9.3(e), has improved significantly. However, the approximation of the limit cycle, Figure 9.3(f), has to be further improved. Good agreement between time domain solutions and Walsh solutions was found when the first 128 terms of the Walsh series were considered. This is shown in Figure 9.3(g) and (h). The approximation of the limit cycle, Figure 9.3(i), is quite good and may be accurate enough for some applications. However, rigorous waveform distortion analysis requires even better solutions.

In theory, the limit cycle could only be represented exactly by an infinite number coefficeints in the Walsh series. In digital implementations, however, the Walsh series must be truncated to a finite number of coefficients. In cases of closed form solutions, the accuracy with which the limit cycle is to be calculated dictates the number of Walsh coefficients used in the series. A very good approximation of the limit cycle, for the case in hand, was obtained by using the first 512 coefficients the of the Walsh series. This is shown in Figure 9.4. As an alternative, to the use of such a large number of coefficients to achieve this level of accuracy, an iterative process can be used.

It was seen in Figure 9.3(h) that Walsh series with 128 terms could represent quite well the first 4 cycles of the system's transient response. This result can be used as the starting point of a new solution process, containing the same number of Walsh coefficients. In its turn, the result of the second solution process can be used to recalculate the series and so on. This results in a much improved accuracy whilst keeping the number of Walsh coefficients to a reasonable level. This can be achieved very efficiently owing to the fact that the updated initial conditions are reflected just in vector $\mathbf{h}_0^*$ and the solution can be carried out with little extra computational effort since the operation $(I - \mathbf{c}^*\mathbf{P}^*)^{-1}$, in equation 9.46, needs to be performed only once. To show the accuracy of this approach two results are represented

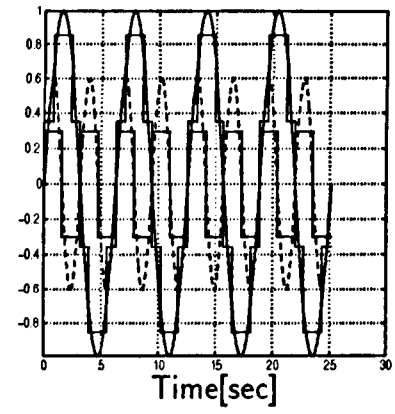

(a) Input and periodic inductance Vs Time

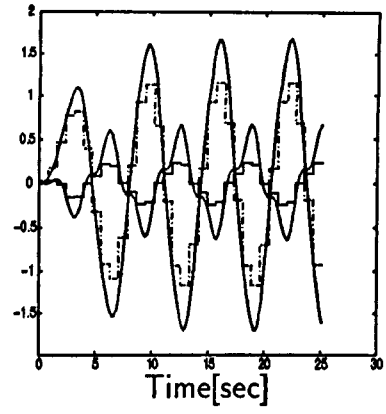

(b) $i(t)$ and $v_c(t)$ Vs Time

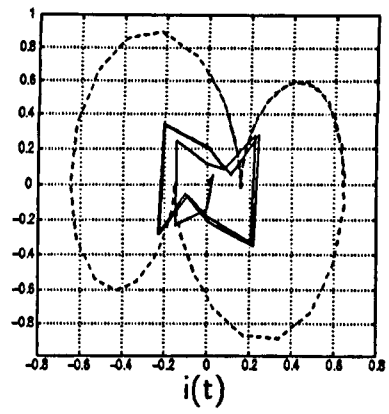

(c) Phase plane, $i(t)$, $\frac{di(i)}{dt}$

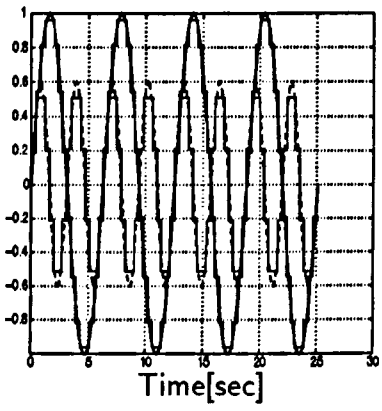

(d) Input and periodic inductance Vs Time

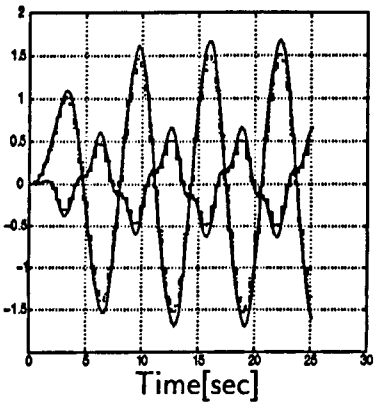

(e) i and v_c Vs Time

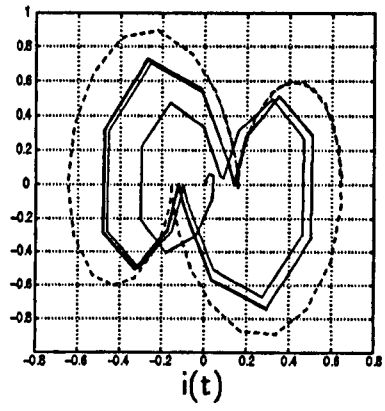

(f) Phase plane, $i(t)$, $\frac{di(i)}{dt}$

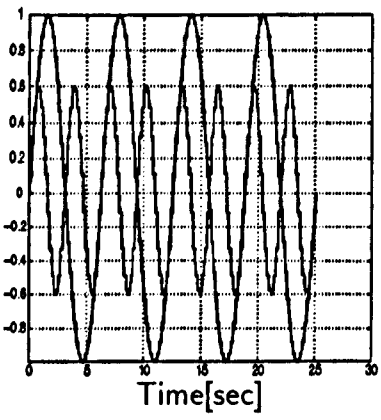

(g) Input and periodic inductance Vs Time

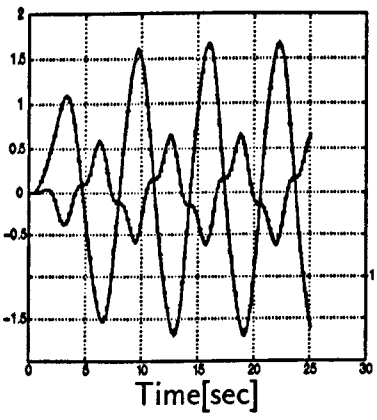

(h) i and v_c Vs Time

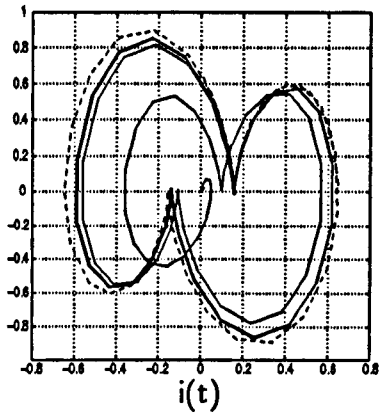

(i) Phase plane, $i(t)$, $\frac{di(i)}{dt}$

Fig. 9.3: Response of a time-varying circuit in the Walsh domain, (a)-(b) solution with 32 Walsh coefficients, (d)-(f) solution with 64 Walsh coefficients, (h)-(i) solution with 128 Walsh coefficients

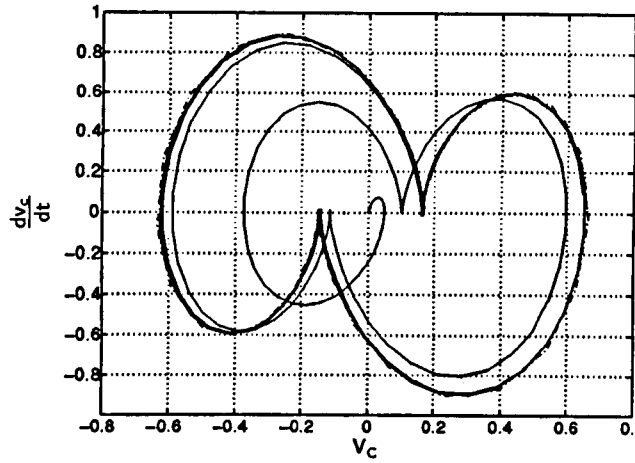

Fig. 9.4: Solution with 512 Walsh coefficients

below. One corresponds to the case when initial conditions were updated every 4 cycles of the excitation source. This results is shown in Figures 9.5(a). Very good results were obtained when initial conditions were updated every two cycles. This result is shown in Figure 9.5(b).

The above analyses were carried out considering that the circuit was initially relaxed. In these cases, a large number of coefficients is required to reproduce both the transient and steady state responses. However, if the interest is to calculate the PSS response of the circuit and good initial estimate of the PSS solution can be obtained then the number of Walsh coefficients required to approximate the limit cycle can be reduced substantially. Results shown in Figure 9.6 were obtained with the values of the sate variables at the fourth cycle as the driving force. A number of 256 Walsh coefficients were used. Only the limit cycle is presented.

Matrix structure of the set of linear equations

In steady state analysis of power systems, a large part of the network can be considered linear and the only interaction between the various sequences or frequencies is through linear, time-varying elements. These interactions are best taken into account when a multi-frequency or multi-sequence framework is used. In practical studies, the mix of time-invariant and non-linear elements generate sets of large, sparse equations. For example, the structure of the transposed transfer matrix i.e. equation (9.48), when 32 coefficients of the Walsh serires are considered, is illustrated in Figure 9.7. In this application, the computational burden depends on the sequency spectrum. Accordingly, this approach is best suited to cases were the state variables are themselves switched. In such a case, fewer Walsh coefficients are required to represent the waveforms. Depending on the waveforms being approximated and on the orthogonal basis, the matrix in Figure 9.7 will be more or less sparse. Few terms are required in the Walsh series when the state variables show sharp edges. Waveform currents in power electronic-based devices are examples of these kind of waveforms. In general, a large number of Fourier coefficients are required to reproduce waveforms with sharp edges and the matrix in Figure 9.7 is expected to become less sparse.

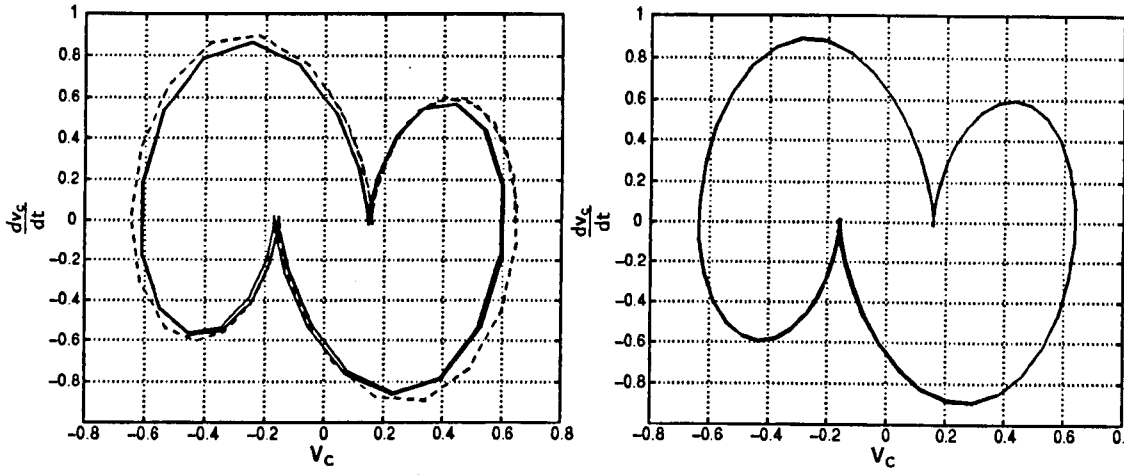

(a) Initial conditions re-calculated every 4 cycles

(b) Initial conditions re-calculated every 2 cycles

Fig. 9.5: Approximation of limit cycle

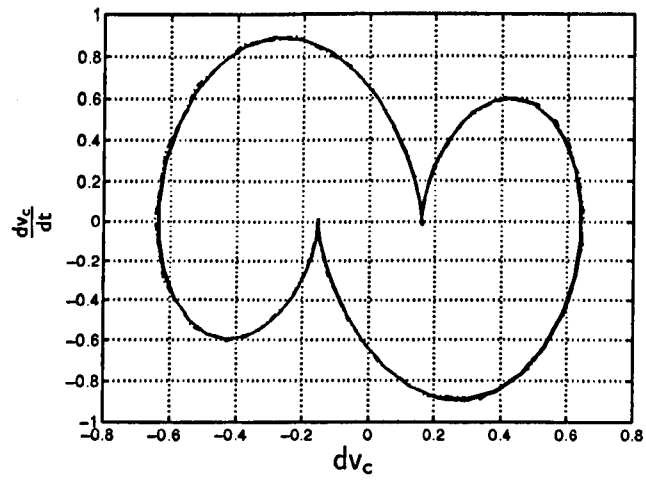

Fig. 9.6: Solution with 256 Walsh coefficients and a good guess of the initial condition

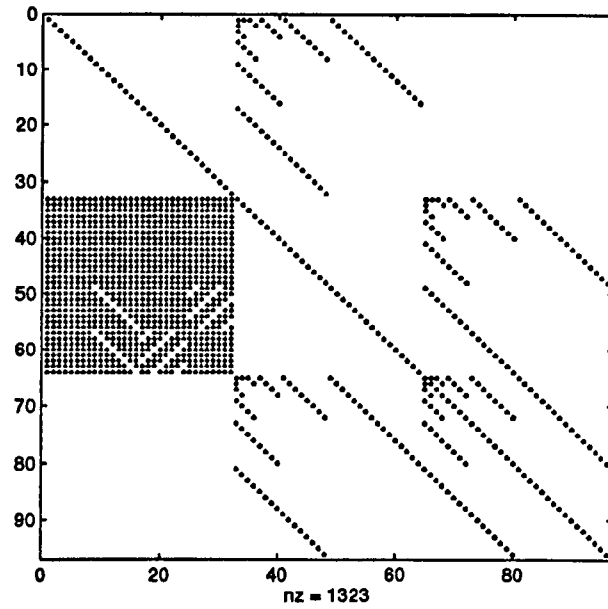

Fig. 9.7: Structure of transfer matrix where 32 Walsh coefficients are considered

9.4 Conclusions

In this chapter, the Walsh series have been used to study linear, time varying circuits. Solutions of time varying circuits are achieved in just one iteration. This has been achieved by using a large number of coefficients in the Walsh series to approximate the limit cycle. It has been shown that solution's accuracy is adversely affected if a much reduced number of coefficients is used in the series. However, solution accuracy can be restored by resorting to an iterative process where updated initial conditions are used at each iteration. This is achieved with little computational effort.

This approach can be applied to approximate smooth responses of LTVS. However, it is better suited to the analysis of waveforms relating to switched signals such as those observed in electronic loads. In this case, the solutions with the Walsh approach would require far less coefficients when compared to solutions based on complex Fourier series, leading to significant reductions in computatinal burden.

Chapter 10

Steady State Analysis of Non-linear Systems

This chapter describes an approach to solve the steady state response of non-linear electric circuits. The solution takes place in the Walsh domain but the theory is more general and can be extended to any other domain, e.g. Fourier, Hartley, etc. The product operational matrix presented in the previous chapter is used here to solve non-linear circuits having polynomial representation and Hammerstein structure.
The chapter also investigates the use of non-linear approximations using bi-linearisations, as opposed to linearisations, to represent non-linear systems about an operating point. Bi-linearisation is amenable to iterative solutions with stronger convergence characteristics than the quadratically convergent first order, Newton-Raphson. Bi-linearisations are shown to possess super-quadratic convergence characteristics. Illustrative numerical examples are used to show the advantages of the methodology proposed.

10.1 Introduction

Linear systems theory is a mature subject with a variety of powerful methods and a long history of successful industrial applications. Thus, it is sensible for one to wonder why a non-linear systems theory is required for the analysis of physical systems. Several reasons can be cited. Firstly, physical systems are indeed non-linear and electric circuits are the rule rather than the exception. Secondly, linear models rely on the key assumption of small range operations for the linear models to be valid. When large variations are registered about the operating points these representations perform poorly and the use of successive, linear approximations are required for accurate solutions. The latter approach, in its turn, may or may not converge to the PSS solution, depending on the amplitude of the variations and the class of non-linearities involved. Thirdly, many systems may not be linearisable about all operating points, owing to their discontinuous nature.

The method presented in this chapter accounts for non-linearities in two ways, namely Bilinear Systems Theory (BLS) and polynomial representations. It is shown that BLS theory provides a better way to solve non-linear systems.

10.1.1 Bilinear Systems

BLS are perhaps the simplest class of NLS. These are systems that are linear in control and linear in state but not jointly linear in state and control. For instance, they may involve products of state and control. Hence, superposition does not apply. They are slight gener-

alizations of linear systems and are sometimes referred to as linear systems with parametric control.

It will be shown in this chapter that solutions of BLS can be analytically handled. Hence, they are better representations of physical systems than linearisations. A wide range of physical systems are amenable to BLS representation. Engineering applications include variable-impedance networks and variable-field-controlled motors. BLS also arise as a natural representations for an ample range of applications such as mechanical links, Surface vehicle, heat transfer, airplanes, nuclear fission, socioeconomics, chemistry, demography agriculture, etc [40]. BLS may be used to accurately approximate other non-linear systems yielding better results that linearised models where the non-linearity is neglected altogether. BLS can arise from Taylor series expansions. In such cases, non-linear systems which are not directly recognised as bilinear in form, may be transformed to BLS by an appropriate redefinition of state variables. This approach is used in this chapter to approximate non-linear circuits by BLS. BLS can be considered generalisations of linear systems, hence some important analysis in linear systems such stability, controllability, observability, etc., can be extended to BLS.

In this chapter, it is shown how non-linear circuits can be reduced to systems with bilinear structure. In this situation, the steady state solution of non-linear circuits can be found with iterative methods possessing super-quadratic convergence. As far as the the author is aware, bilinear methods have not been used elsewhere in power systems applications.

The analysis carried out in this chapter uses nonlinearities with polynomial representation. However, any non-linear, system representation can be approximated by a BLS.

10.1.2 Polynomial systems

The polynomial systems addressed in this chapter comprise systems which are non-linear in control but linear in state. For a specified set of control variables the global system is linear and its solution can be very carried out efficiently by using properties related to the product of two signals in the Walsh domain.

10.2 Analysis of Bilinear Systems in Walsh Domain

Time varying bilinear systems have the following state form representation:

$$\dot{\mathbf{x}}(t) = \mathbf{A}(t)\mathbf{x}(t) + \mathbf{B}(t)\mathbf{u}(t) + \sum_{k=1}^{m} \mathbf{N}_k(t)u_k(t)\mathbf{x}(t) \tag{10.1}$$

where the state $\mathbf{x} \in \mathbb{R}^n$, the control $\mathbf{u} \in \mathbb{R}^m$ and $\mathbf{N}_k \in \mathbb{R}^{n\times n}$ where $k = \{1, \ldots, m\}$. The corresponding BLS state diagram is shown in Figure 10.1. The output may be generated by $\mathbf{y} = \mathbf{C}\mathbf{x}(t)$. Time invariant bi-linear systems are a particular case of equation (10.1).

A powerful property of bi-linear systems is that their analysis is essentially the same as that of time-varying linear systems. Therefore, the analysis presented in previous chapters can be applied here.

Equation (10.1) can be written as,

$$\dot{\mathbf{x}}(t) = \mathbf{L}(t)\mathbf{x}(t) + \mathbf{B}(t)\mathbf{u}(t) \tag{10.2}$$

where

$$\mathbf{L}(t) = \mathbf{A}(t) + \sum_{k=1}^{m} \mathbf{N}_k(t)u_k$$

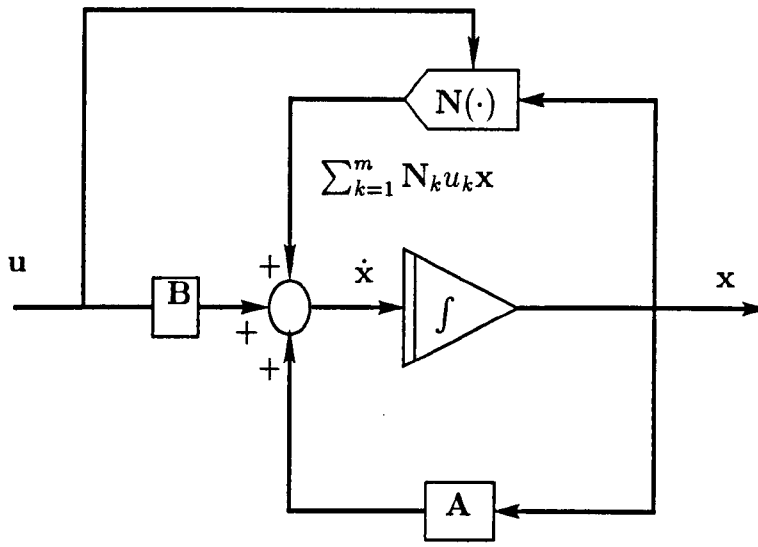

Fig. 10.1: Bilinear system state diagram

Matrix $\mathbf{A}(t)$ can be expanded in the Walsh domain where it has the following structure,

$$\mathbf{A}(t) = \begin{bmatrix} \mathbf{c}_{11}^t \phi_{(m)}(t) & \mathbf{c}_{12}^t \phi_{(m)}(t) & \dots & \mathbf{c}_{1n}^t \Phi_{(m)}(t) \\ \mathbf{c}_{21}^t \phi_{(m)}(t) & \mathbf{c}_{22}^t \phi_{(m)}(t) & \dots & \mathbf{c}_{2n}^t \Phi_{(m)}(t) \\ \vdots & \vdots & \vdots & \vdots \\ \mathbf{c}_{n1}^t \phi_{(m)}(t) & \mathbf{c}_{n2}^t \phi_{(m)}(t) & \dots & \mathbf{c}_{nn}^t \phi_{(m)}(t) \end{bmatrix} \tag{10.3}$$

or

$$\mathbf{A}(t) = \begin{bmatrix} \mathbf{c}_{11}^t & \mathbf{c}_{12}^t & \dots & \mathbf{c}_{1n}^t \\ \mathbf{c}_{21}^t & \mathbf{c}_{22}^t & \dots & \mathbf{c}_{2n}^t \\ \vdots & \vdots & \vdots & \vdots \\ \mathbf{c}_{n1}^t & \mathbf{c}_{n2}^t & \dots & \mathbf{c}_{nn}^t \end{bmatrix} \begin{bmatrix} \phi_{(m)}(t) & 0 & \dots & 0 \\ 0 & \phi_{(m)}(t) & \dots & 0 \\ \vdots & \vdots & & \vdots \\ 0 & 0 & \dots & \phi_{(m)}(t) \end{bmatrix} \tag{10.4}$$

In compact form,

$$\mathbf{A}(t) = \mathbf{c}\Phi(t) \tag{10.5}$$

Similarly,

$$\mathbf{b}_j(t) = \begin{bmatrix} \mathbf{w}_{1j}^t \phi_{(m)}(t) \\ \mathbf{w}_{2j}^t \phi_{(m)}(t) \\ \vdots \\ \mathbf{w}_{nj}^t \phi_{(m)}(t) \end{bmatrix} = \begin{bmatrix} \mathbf{w}_{1j}^t \\ \mathbf{w}_{2j}^t \\ \vdots \\ \mathbf{w}_{nj}^t \end{bmatrix} \phi_{(m)}(t) \triangleq \beta_j \phi_{(m)}(t) \tag{10.6}$$

The Walsh series approximation of the state variable $\mathbf{x}(t)$ is,

$$\mathbf{x}(t) = \begin{bmatrix} h_{10}\phi_0(t) + h_{11}\phi_1(t) + \ldots + h_{1,m-1}\phi_{m-1}(t) \\ h_{20}\phi_0(t) + h_{21}\phi_1(t) + \ldots + h_{2,m-1}\phi_{m-1}(t) \\ \vdots \\ h_{n0}\phi_0(t) + h_{n1}\phi_1(t) + \ldots + h_{n,m-1}\phi_{m-1}(t) \end{bmatrix} \tag{10.7}$$

$$= \begin{bmatrix} h_{10} & h_{11} & \ldots & h_{1,m-1} \\ h_{20} & h_{21} & \ldots & h_{2,m-1} \\ \vdots & \vdots & & \vdots \\ h_{n0} & h_{n1} & \ldots & h_{n,m-1} \end{bmatrix} \begin{bmatrix} \phi_0(t) \\ \phi_1(t) \\ \vdots \\ \phi_{m-1}(t) \end{bmatrix} \tag{10.8}$$

$$= \begin{bmatrix} \mathbf{h}_0^t(t) \\ \mathbf{h}_1(t) \\ \vdots \\ \mathbf{h}_{m-1}(t) \end{bmatrix} \phi_{(m)}(t) \triangleq \mathbf{H}\phi_{(m)}(t) \tag{10.9}$$

where

$$\mathbf{h}_i = [h_{i0}, h_{i1}, \ldots, h_{i(m-1)}] \tag{10.10}$$

If the control variable is written as,

$$u(t) = \begin{bmatrix} u_1(t) \\ u_2(t) \\ \vdots \\ u_r(t) \end{bmatrix} = \begin{bmatrix} \mathbf{U}_1^t\phi_{(m)}(t) \\ \mathbf{U}_2^t\phi_{(m)}(t) \\ \vdots \\ \mathbf{U}_r^t\phi_{(m)}(t) \end{bmatrix} = \begin{bmatrix} \mathbf{U}_1^t \\ \mathbf{U}_2^t \\ \vdots \\ \mathbf{U}_r^t \end{bmatrix} \phi_{(m)}(t) = \mathbf{U}\phi_{(m)}(t) \tag{10.11}$$

Then integration of (10.1) to yield,

$$\mathbf{h}^*\Phi(t) - \mathbf{h}^*\Phi(0) = \int_0^t \mathbf{h}^*\mathbf{c}^*\Phi(\tau)d\tau + \int_0^t \mathbf{U}^*\mathbf{B}^*\Phi(\tau)d\tau \tag{10.12}$$

or,

$$\mathbf{h}^* - \mathbf{h}_0^* = \mathbf{h}^*\mathbf{c}^*P* + \mathbf{U}^*\mathbf{B}^*\mathbf{P}^* \tag{10.13}$$

where

$$\begin{aligned}
\mathbf{h}_0^* &= [\, x_1(0) \;\; 0 \;\; \ldots \;\; 0 \;\vdots\; x_2(0) \;\; 0 \;\; \ldots \;\; 0 \;\vdots\; \ldots \;\vdots\; x_r(0) \;\; 0 \;\; \ldots \;\; 0 \,] \\
\mathbf{h}^* &= [\, c_{10} \;\; c_{11} \;\; c'_{11} \ldots \;\; c_{1n} \;\; X'_{1n} \;\vdots\; \ldots \;\vdots\; c_{10} \;\; c_{11} \;\; c'_{11} \ldots \;\; c_{1n} \;\; c'_{1n} \,] \\
\mathbf{h}_i &= [\, c_{i0} \;\; c_{i1} \;\; c'_{i1} \;\; \ldots \;\; c_{in} \;\; c'_{in} \,] \\
x &= [\, x_1 \;\; x_2 \;\; \ldots \;\; x_r \,]^T \\
\mathbf{U}^* &= [\, U_{10} \;\; U_{11} \;\; U'_{11} \ldots \;\; U_{1n} \;\; U'_{1n} \;\vdots\; \ldots \;\vdots\; U_{10} \;\; U_{11} \;\; U'_{11} \ldots \;\; U_{1n} \;\; U'_{1n} \,] \\
u &= [\, u_1 \;\; u_2 \;\; \ldots \;\; u_q \,]^T \\
\mathbf{P}^* &= \begin{bmatrix} \mathbf{P} & \mathbf{0} & \ldots & \mathbf{0} \\ \mathbf{0} & \mathbf{P} & \ldots & \mathbf{0} \\ \vdots & \vdots & & \vdots \\ \mathbf{0} & \mathbf{0} & \ldots & \mathbf{P} \end{bmatrix}_{(r(2n+1)\times r(2n+1))}
\end{aligned} \tag{10.14}$$

The above equations form a set of $(2n+1) \times r$ algebraic equations that can be solved as follows:

$$\mathbf{h}^*(I - \mathbf{c}^*\mathbf{P}^*) = \mathbf{U}^*\mathbf{B}^*\mathbf{P}^* + \mathbf{h}_0^* \tag{10.15}$$

or

$$\mathbf{h}^* = (\mathbf{U}^*\mathbf{B}^*\mathbf{P}^* + \mathbf{h}_0^*)(I - \mathbf{c}^*\mathbf{P}^*)^{-1} \tag{10.16}$$

10.3 Numeric Example

The analysis of the response of bi-linear systems to a periodic input is presented in this section. This is illustrated with an example available in open literature [48]. The solution was carried out in the time domain and the systems representation is,

$$\dot{\mathbf{x}} = \mathbf{A}(t)\mathbf{x}(t) + \mathbf{B}(t)\mathbf{u} + \sum_{j=1}^{q} \mathbf{N}_j(t)\mathbf{x}(t)u_j(t)$$

with $q = 2$ and

$$\begin{aligned}
\mathbf{A}(t) &= \begin{bmatrix} -4 & 1.5 * \sin(t) + 1.8 * \sin(3 * t) \\ -20 & 3t \end{bmatrix}, \quad \mathbf{B}(t) = \begin{bmatrix} t & 1 \\ 1 & t \end{bmatrix} \\
\mathbf{N}_1(t) &= \begin{bmatrix} 2 & 3t \\ -5 & t \end{bmatrix}, \quad \mathbf{N}_2(t) = \begin{bmatrix} 3 & -1 \\ 20 & -5t \end{bmatrix} \\
\mathbf{u}(t) &= \begin{bmatrix} 0 \\ 1 \end{bmatrix}, \quad \mathbf{x}_0 = \begin{bmatrix} 0 \\ 1 \end{bmatrix}
\end{aligned}$$

Thus we have that for the given input

$$\mathbf{L}(t) = \mathbf{A}(t) + \sum_{k=1}^{m} \mathbf{N}_k(t)u_k = \begin{bmatrix} -1 & 1.5\sin(2t) + 1.8\sin(3t) - 1 \\ 0 & -2t \end{bmatrix}$$

The bi-linear systems is essentially a linear system. In this case, the linear system is also periodic and can be rewritten as,

$$\begin{bmatrix} \dot{x}_1 \\ \dot{x}_2 \end{bmatrix} = \begin{bmatrix} -1 & 1.5\sin(2t) + 1.8\sin(3t) - 1 \\ 0 & -2t \end{bmatrix} \begin{bmatrix} x_1 \\ x_2 \end{bmatrix} + \begin{bmatrix} t & 1 \\ 1 & t \end{bmatrix} \begin{bmatrix} 0 \\ 1 \end{bmatrix} \tag{10.17}$$

It can be seen that matrix $\mathbf{A}$ is responsible for the periodic solutions. This is shown in Figure 10.2. Figure 10.2(a) shows the state variables while Figure 10.2(b) shows the limit cycle corresponding to $x_1(t)$. It can be seen that the limit cycle is reached in few cycles. The set of equations presented in (10.17) is linear and periodic. This allows its solution via any set of orthogonal functions. In this example, it is shown that eventhough bi-linear systems are non-linear, they can be analysed as linear systems.

10.4 Bi-linearisations of non-linear systems

In many cases, systems which are not recognised as bi-linear in form can be transformed into bi-linear systems by an appropriate redefinition of state variables. An important aspect of bilinear systems is that they can be used to approximate other more complex non-linear systems about an operating point. It must be noticed that bi-linearisations, in this case,

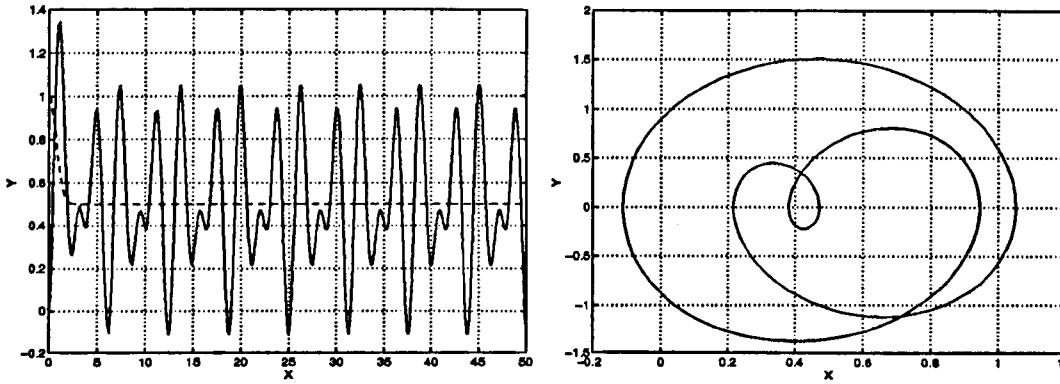

(a) States (b) Phase plane of $x_1(t)$

Fig. 10.2: Time response of a simple bilinear system

will not only provide more accurate representation of the non-linear system in hand but they will also provide a better way to emulate qualitative properties of the non-linear system. In this section, it is shown that it is possible to obtain bilinear approximations of non-linear systems from the Taylor series representation. Consider a non-linear system represented by the following state equation,

$$\dot{x} = \mathbf{A}f(x) + \mathbf{B}u \tag{10.18}$$

where $f(x)$ is a single valued, non-linear function of the state variable x. If we consider that the system is operating about the point x_b, equation (10.18) can be rewritten taking into account the first three terms of the Taylor series as,

$$\dot{x} = \mathbf{A}\left(f(x_b) + J\Delta x + H\Delta x^2 + O\Delta x^3\right) + \mathbf{B}u \tag{10.19}$$

where J, H and O are the matrices of first, second and third order derivatives, respectively. Δx is the increment in the state variable. We also know that,

$$\Delta x = x - x_b \tag{10.20}$$
$$\Delta x^2 = (x - x_b)^2 = x^2 - 2xx_b + x_b^2 \tag{10.21}$$
$$\Delta x^3 = (x - x_b)^3 = x^3 - 3x^2x_b + 3xx_b^2 - x_b^3 \tag{10.22}$$

Substituting equations (10.20) to (10.22) into equation (10.19), we have taht

$$\dot{x} = \mathbf{A}f(x_b) + \mathbf{A}J(x - x_b) + \mathbf{A}H(x^2 - 2xx_b + x_b^2) \tag{10.23}$$
$$+ \mathbf{A}O(x^3 - 3x^2x_b + 3xx_b^2 - x_b^3) + \mathbf{B}u \tag{10.24}$$

If we define x_b to be a control variable and knowing that about the operating point,

$$x^2 \approx xx_b \tag{10.25}$$
$$x^3 \approx xx_b^2 \tag{10.26}$$

then

$$\dot{x} = \mathbf{A}(f(x_b) - Jx_b + k_1Hx_b^2 - k_2Ox_b^3) + \mathbf{A}(Jx_b - k_1Hx_b^2 + k_2Ox_b^2)x + \mathbf{B}u \tag{10.27}$$

where k_1 and k_2 are constants that can be identified by means of linear search to produce better approximations.

It is possible to recognise the bilinear structure of equation (10.27). In the third factor the state variable x and the new control variable x_b are multiplied and the superposition theorem no longer applies. In this case the representation is non-linear in control, linear in state and non-linear together. It can be said that whereas the classic Newton-Raphson approach takes account of the non-linearity via injection sources, the Newton-Raphson approach using bi-linearisation takes account of the non-linearity by using bi-linearised elements. These elements are linear, time varying elements. It is important to note that similarly to the way first order Newton-Raphson techniques improve the convergence over Gauss-Seidel approaches, the Newton-Raphson approach proposed in this section improves the convergence over first order Newton-Raphson methods. The approximation proposed in this section is truly a non-linear approximation. This approximation is more accurate than calssical methods and provides a way to emulate better the non-linear behaviour of the non-linear system. It can be said that whilst Gauss-Seidel methods have monotonic convergent characteristics and first order Newton-Raphson methods have quadratic convergent characteristics, bi-linear methods have super-quadratic convergent characteristics.

The derivations presented in this chapter are not restricted to any particular orthogonal basis and are not restricted to steady state analysis of electric circuits.

10.5 The n-Product Operational Matrix

The product operational matrix presented in the previous chapter is generalised in this section to the case of n products. Polynomial type, non-linear terms such x^n with x as scalar can be handled using two lemmas presented in [55].

Lemma 1:

$$\Phi_{(m)}(t)\Phi^t_{(m)}(t)\mathbf{c} = \mathbf{C}_{(m\times m)}\Phi_{(m)}(t)$$

and

Lemma 2:

$$\phi_{(m)}(t)\phi^t_{(m)}(t)\mathbf{c}\mathbf{b}^t\phi_{(m)}(t) = \Lambda_{\mathbf{c}}\Lambda_{\mathbf{b}}\phi_{(m)}(t)$$

The product of a vector and its transpose is called the product operational matrix $\Phi_{(m\times m)}$,

$$\phi_{(m)}(t)\phi^t(t) = \Phi_{(m\times m)} \tag{10.28}$$

If one defines

$$\Phi_{+n(\frac{m}{2}\times\frac{m}{2})} = \phi_{(\frac{m}{2}\times\frac{m}{2})} \tag{10.29}$$

where the subscript of every element of $(\frac{\mathbf{m}}{\mathbf{2}} \times \frac{\mathbf{m}}{\mathbf{2}})$ is increased by n then the general form of the product matrix $(\mathbf{m} \times \mathbf{m})$ is,

$$\Phi_{(m\times m)} = \begin{bmatrix} \Phi_{(\frac{m}{2}\times\frac{m}{2})} & \Phi_{+\frac{m}{2}(\frac{m}{2}\times\frac{m}{2})} \\ \Phi_{+\frac{m}{2}(\frac{m}{2}\times\frac{m}{2})} & \Phi_{(\frac{m}{2}\times\frac{m}{2})} \end{bmatrix} \tag{10.30}$$

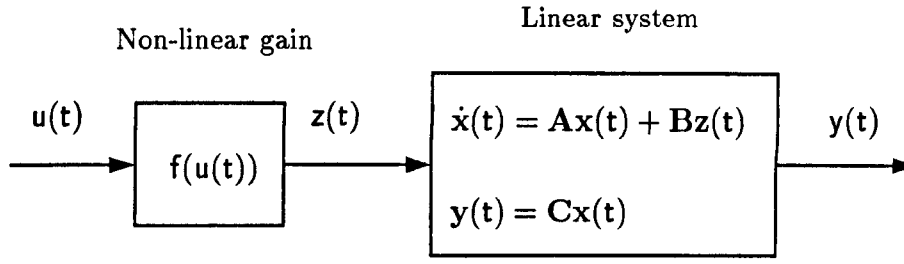

Fig. 10.3: Hammerstein model

The approximation of a function $f(t)$, in matrix form, can be written as,

$$f(t) = \mathbf{c}^t \phi_m(t) \tag{10.31}$$

Similarly to the product matrix, the matrix of coefficients can be defined in general form as,

$$\mathbf{C}_{(m\times m)} = \begin{bmatrix} \mathbf{C}_{(\frac{m}{2}\times\frac{m}{2})} & \mathbf{C}_{+\frac{m}{2}(\frac{m}{2}\times\frac{m}{2})} \\ \mathbf{C}_{+\frac{m}{2}(\frac{m}{2}\times\frac{m}{2})} & \mathbf{C}_{(\frac{m}{2}\times\frac{m}{2})} \end{bmatrix} \tag{10.32}$$

An important property that will facilitate the solution of linear, time-varying and bilinear systems is the identity of the following relation

$$\Phi_{(m\times m)}\mathbf{c}_m = \mathbf{C}_{m\times m}\phi_m \tag{10.33}$$

Taking $m = 4$ as example yields

$$\left[\begin{array}{cc|cc} \phi_0 & \phi_1 & \phi_2 & \phi_3 \\ \phi_1 & \phi_0 & \phi_3 & \phi_2 \\ \hline \phi_2 & \phi_3 & \phi_0 & \phi_1 \\ \phi_3 & \phi_2 & \phi_1 & \phi_0 \end{array}\right] \begin{bmatrix} c_0 \\ c_1 \\ c_2 \\ c_3 \end{bmatrix} = \left[\begin{array}{cc|cc} c_0 & c_1 & c_2 & c_3 \\ c_1 & c_0 & c_3 & c_2 \\ \hline c_2 & c_3 & c_0 & c_1 \\ c_3 & c_2 & c_1 & c_0 \end{array}\right] \begin{bmatrix} \phi_0 \\ \phi_1 \\ \phi_2 \\ \phi_3 \end{bmatrix} \tag{10.34}$$

Accordingly, the following two lemmas can be established

Proof of these lemmas is found in [55].

10.6 Analysis of Hammerstein Model

Consider a Hammerstein model of a non-linear system,

$$\dot{\mathbf{x}} = \mathbf{A}\mathbf{x} + \mathbf{B}f(u(t)) \tag{10.35}$$

where $\mathbf{x}(t)$ is a $n-$vector, $\mathbf{A}$ is a $n \times n$ matrix and $\mathbf{B}$ is a $n \times q$ matrix. $u(t)$ is the control input and

$$f(u(t)) = a_0 + a_1 u(t) + a_2 u^2(t) + \ldots + a_p u^p(t)$$

is the memoryless, non-linear gain for which the coefficients a_i and the order p are selected. The structure of a Hammerstein model is shown in Figure 10.3.

10.6.1 Solution and Analysis

Let the Walsh expansion $\mathbf{x}(t)$ and of $u(t)$ be represented as,

$$\begin{aligned}
\mathbf{x} &= \begin{bmatrix} x_1 = h_{10}\phi_0(t) + h_{11}\phi_1(t) + \ldots + h_{1(m-1)}\phi_{(m-1)}(t) \\ x_2 = h_{20}\phi_0(t) + h_{21}\phi_1(t) + \ldots + h_{2(m-1)}\phi_{(m-1)}(t) \\ \vdots \\ x_n = h_{n0}\phi_0(t) + h_{n1}\phi_1(t) + \ldots + h_{n(m-1)}\phi_{(m-1)}(t) \end{bmatrix} \\
&= \begin{bmatrix} h_{10} & b_{11} & \ldots & h_{1,m-1} \\ h_{20} & h_{21} & \ldots & h_{2,m-1} \\ \vdots & \vdots & & \vdots \\ h_{n0} & h_{n1} & \ldots & h_{n,m-1} \end{bmatrix} \begin{bmatrix} \phi_0(t) \\ \phi_1(t) \\ \vdots \\ \phi_{m-1}(t) \end{bmatrix} \qquad (10.36) \\
&= [\ \mathbf{h}_0 \quad \mathbf{h}_1 \quad \ldots \quad \mathbf{h}_{m-1}\ ]\phi_{(m)}(t) = \mathbf{H}\phi_{(m)}(t) \qquad (10.37)
\end{aligned}$$

$$u(t) = \begin{bmatrix} u_1(t) \\ u_2(t) \\ \vdots \\ u_r(t) \end{bmatrix} = \begin{bmatrix} \mathbf{u}_1^T\phi(t) \\ \mathbf{u}_2^T\phi(t) \\ \vdots \\ \mathbf{u}_r^T\phi(t) \end{bmatrix} = \begin{bmatrix} \mathbf{u}_1^T \\ \mathbf{u}_2^T \\ \vdots \\ \mathbf{u}_r^T \end{bmatrix} \phi(t) = \mathbf{U}\phi(t) \qquad (10.38)$$

With reference to Figure 10.3 and integration of equation 10.35 yields,

$$\mathbf{c}^* - \mathbf{c}_0^* = \mathbf{c}^*\mathbf{A}^*\mathbf{P}^* + \mathbf{Z}^*\mathbf{B}^*\mathbf{P}^* \qquad (10.39)$$

or

$$\mathbf{c}^* = (\mathbf{c}_0^* + \mathbf{Z}^*\mathbf{B}^*\mathbf{P}^*)(\mathbf{I} - \mathbf{A}^*\mathbf{P}^*)^{-1} \qquad (10.40)$$

where

$$\begin{aligned}
\mathbf{c}_0^* &= [\ x_1(0) \quad 0 \quad \ldots \quad 0 \ \vdots \ x_2(0) \quad 0 \quad \ldots \quad 0 \ \vdots \ \ldots \ \vdots \ x_r(0) \quad 0 \quad \ldots \quad 0\ ] \\
\mathbf{c}^* &= [\ c_{10} \quad c_{11} \quad c'_{11} \ldots \quad c_{1n} \quad X'_{1n} \ \vdots \ \ldots \ \vdots \ c_{10} \quad c_{11} \quad c'_{11} \ldots \quad c_{1n} \quad c'_{1n}\ ] \\
\mathbf{c}_i &= [\ c_{i0} \quad c_{i1} \quad c'_{i1} \quad \ldots \quad c_{in} \quad c'_{in}\ ] \\
x &= [\ x_1 \quad x_2 \quad \ldots \quad x_r\ ]^T \\
\mathbf{U}^* &= [\ U_{10} \quad U_{11} \quad U'_{11} \ldots \quad U_{1n} \quad U'_{1n} \ \vdots \ \ldots \ \vdots \ U_{10} \quad U_{11} \quad U'_{11} \ldots \quad U_{1n} \quad U'_{1n}\ ] \\
u &= [\ u_1 \quad u_2 \quad \ldots \quad u_q\ ]^T \\
\mathbf{P}^* &= \begin{bmatrix} \mathbf{P} & \mathbf{0} & \ldots & \mathbf{0} \\ \mathbf{0} & \mathbf{P} & \ldots & \mathbf{0} \\ \vdots & \vdots & & \vdots \\ \mathbf{0} & \mathbf{0} & \ldots & \mathbf{P} \end{bmatrix} \qquad (10.41)
\end{aligned}$$

The non-linear terms are contained in matrix $\mathbf{Z}$ which has the following form,

$$\mathbf{Z}^* = [\ z_1 \quad z_2 \quad \ldots \quad z_q\ ]$$

and

$$z_i = a_0 + a_1 u_i(t) + a_2 u_i^2(t) + \ldots + a_p u_i^p(t)$$

Using Lemmas 1 and 2 repeatedly, z_i can be written as follows,

$$z_i = [\ a_0 \quad 0 \quad \ldots \quad 0\ ] + a_1 \mathbf{u}_i^t \phi_{(m)} + a_2 \mathbf{u}_i^t \Lambda_u \phi_{(m)} + \ldots + a_p \mathbf{u}_i^t \Lambda_u^{n-1} \phi_{(m)}$$

Here, matrices $\mathbf{A}^*$ and $\mathbf{B}^*$ have the same meaning as in the time varying case described in previous chapter. The only difference is that matrices $\mathbf{A}^*$ and $\mathbf{B}^*$ are time-invariant and diagonal.

10.6.2 Numeric example: Polynomial systems

To illustrate the use of the n-product operational matrix the response of a static, non-linear element to a periodic input is given. The non-linearity has the polynomial representation,

$$y = ax + bx^{27} + cx^{29} \tag{10.42}$$

and the periodic input has the form,

$$x(t) = 1.3\sin(t) + 0.15\sin(3t) - 0.1\cos(8t) \tag{10.43}$$

If $x(t)$ is approximated in Walsh domain as,

$$x(t) = X_{(m)}^t \gamma_{(m)}(t) \tag{10.44}$$

$$y(t) = Y_{(m)}^t \gamma_{(m)}(t) \tag{10.45}$$

and by using Lemmas

Lemma 3: 1 and

Lemma 4: 2 the output can be expressed as,

$$Y = aX + b\Lambda_X^{26} + c\Lambda_X^{28} \tag{10.46}$$

The input is shown in Figure 10.4(a) and the output is shown in Figure 10.4(b). Their respective spectra are shown in Figures 10.4(c) and (d). No new terms in the output were generated as result of the non-linear operation on the input but sequence coefficients were re-scaled to reflect the effect of the non-linear operation.

10.7 Numeric example: Bi-linear systems

In order to show, of the of successive approximations via BLS, the network shown in Figure 10.5 has been used. The network represents a single phase system with two loads and one transmission line. The inductor and both capacitors are non-linear and have the following characteristics,

$$\begin{aligned} f_1(q_1) &= 0.5q_1 + 0.1q_1^{27} \\ f_2(\varphi_2) &= 0.5\varphi_2 + 0.3\varphi_2^{15} \\ f_3(q_3) &= 0.5q_3 + 0.1q_3^{27} \end{aligned} \tag{10.47}$$

In general, the non-linear relations can be written as,

$$\begin{aligned} v_1 &= f_1(q_1) \\ v_3 &= f_3(q_3) \\ i_2 &= f_2(\varphi_2) \end{aligned} \tag{10.48}$$

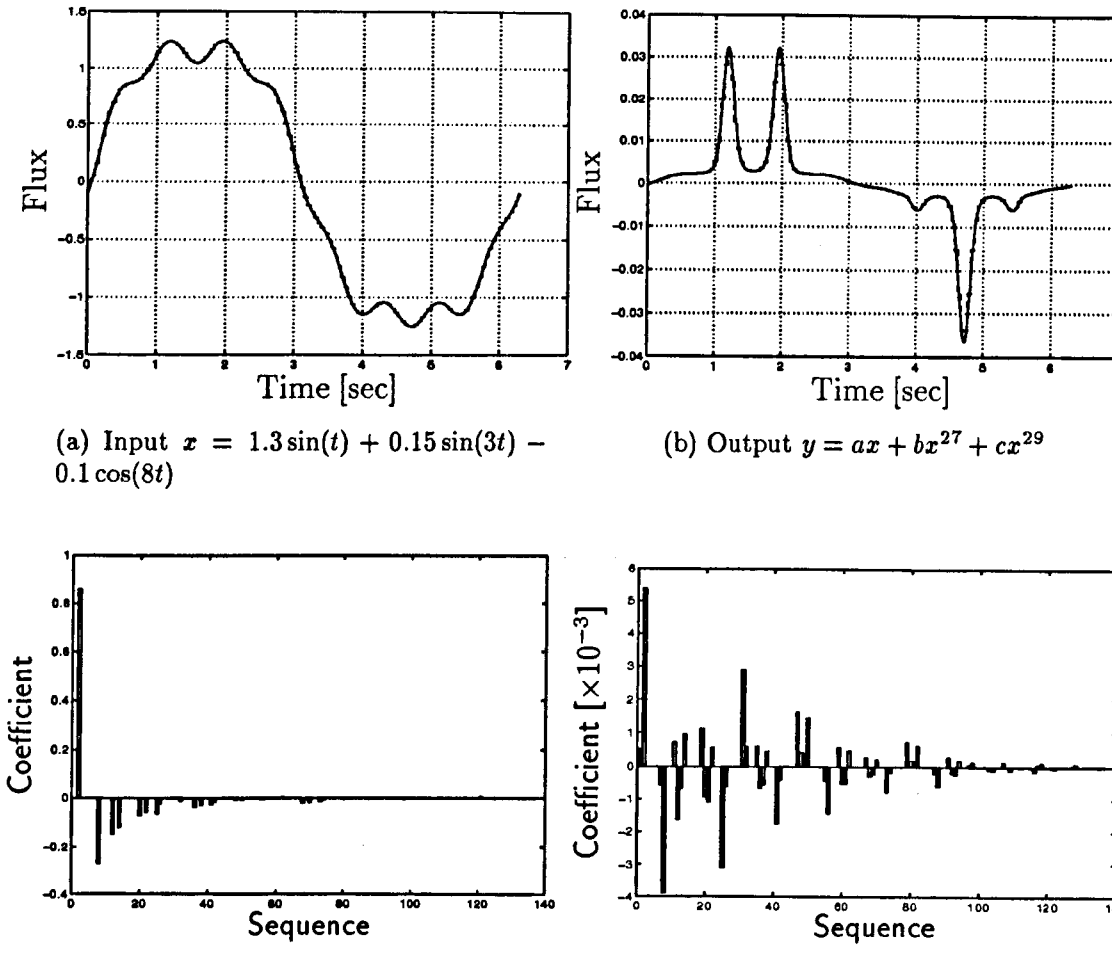

(a) Input $x = 1.3\sin(t) + 0.15\sin(3t) - 0.1\cos(8t)$

(b) Output $y = ax + bx^{27} + cx^{29}$

(c) Input sequence spectra

(d) Output sequence spectra

Fig. 10.4: Products of Walsh series

where q is the charge in the capacitors and φ is the flux in the inductor.

Applying Kirchoffs laws the following three equations can be written,

$$\begin{aligned} n_1 &: u = i_4 + i_1 + i_2 \\ n_2 &: i_2 = i_3 + i_5 \\ l_1 &: v_1 = v_2 + v_3 \end{aligned} \tag{10.49}$$

Writing equation (10.49) in terms of state variables q_1, φ_2 and q_3 and their derivatives we have that,

$$\begin{aligned} i_1 &= \frac{dq_1}{dt} & v_1 &= f_1(q_1) & i_4 &= f_1(q_1) \\ i_2 &= f_2(\varphi_2) & v_3 &= f_3(q_3) & i_5 &= f_3(q_3) \\ i_3 &= \frac{dq_3}{dt} & v_L &= \frac{d\varphi_2}{dt} \end{aligned} \tag{10.50}$$

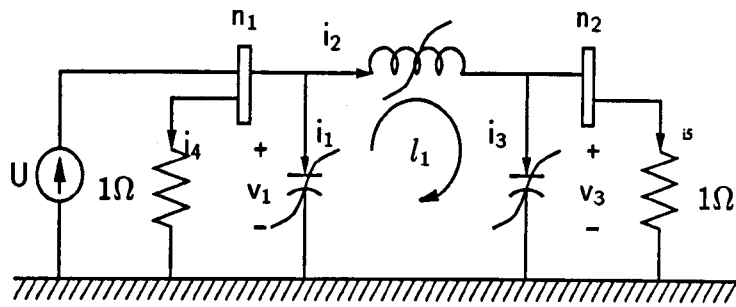

(a) Non-linear circuit

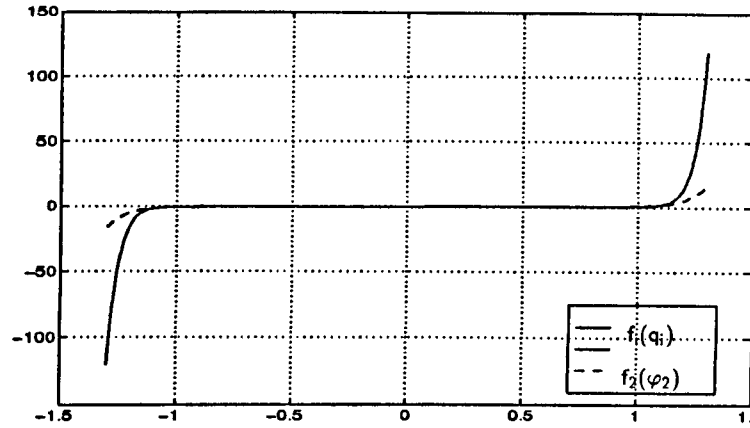

(b) Non-linear characteristics

Fig. 10.5: Non-linear characteristics, – $f_1(q_i)$ –$f_3(q_3)$ and _$f_2(\varphi_2)$

The dynamic equations of the circuit shown in Figure 10.5(a) are:

$$\begin{aligned} u &= f_1(q_1) + \frac{dq_1}{dt} + f_2(\varphi_2) \\ f_2(\varphi_2) &= \frac{dq_3}{dt} + f_3(q_3) \\ f_1(q_1) &= \frac{d\varphi_2}{dt} + f_3(q_3) \end{aligned} \tag{10.51}$$

In matrix form,

$$\begin{bmatrix} \frac{dq_1}{dt} \\ \frac{d\varphi_2}{dt} \\ \frac{dq_3}{dt} \end{bmatrix} = \begin{bmatrix} -1 & -1 & \\ 1 & & -1 \\ & 1 & -1 \end{bmatrix} \begin{bmatrix} f_1(q_1) \\ f_2(\varphi_2) \\ f_3(q_3) \end{bmatrix} + \begin{bmatrix} 1 \\ \\ \end{bmatrix} u \tag{10.52}$$

Substituting the polynomial representation (10.47), into matrix equation (10.52),

$$\begin{bmatrix} \frac{dq_1}{dt} \\ \frac{d\varphi_2}{dt} \\ \frac{dq_3}{dt} \end{bmatrix} = \begin{bmatrix} -1 & -1 & \\ 1 & & -1 \\ & 1 & -1 \end{bmatrix} \begin{bmatrix} q_1 \\ \varphi_2 \\ q_3 \end{bmatrix} + \begin{bmatrix} -1 & -1 & \\ 1 & & -1 \\ & 1 & -1 \end{bmatrix} \begin{bmatrix} 0.1q_1^{27} \\ 0.3\varphi_2^{15} \\ 0.1q_3^{27} \end{bmatrix} + \begin{bmatrix} 1 \\ \\ \end{bmatrix} u \tag{10.53}$$

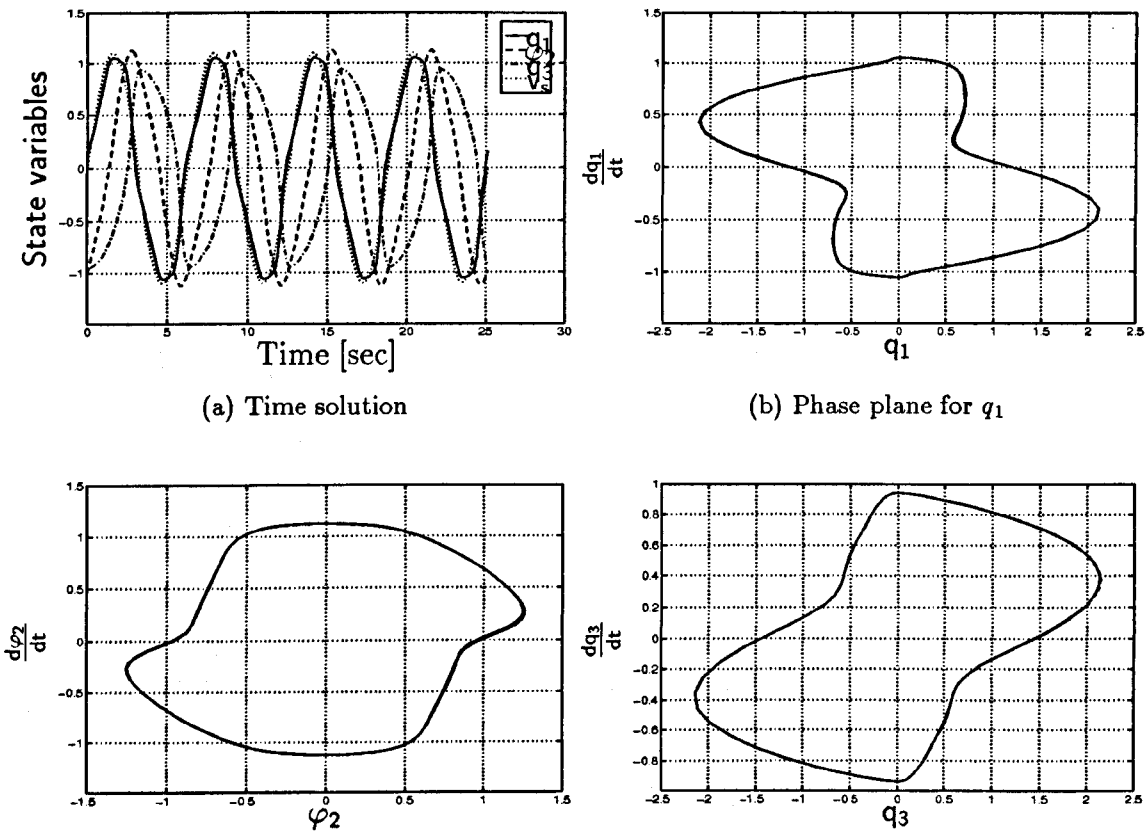

(a) Time solution

(b) Phase plane for q_1

(c) Phase Plane for φ_2

(d) Phase plane for q_3

Fig. 10.6: Steady state solution for an input of $1.1\sin(t)$

10.7.1 Time domain solutions

As a first step, the existence of a unique solution for the circuit in hand was investigated using time domain solutions. Two conditions were tested, the case when $U = 1.1\sin(t)$ and the case when $U = 1.2\sin(t)$. The limit cycles and the state variables have been calculated using a Runge-Kutta algorithm. These are shown in Figure 10.6 for the case when the input is $1.1\sin(t)$.

Figure 10.6(a) shows the state variables in the time domain and Figures 10.6(b)-(d) present the limit cycles. The solution for the case when the input is $1.2\sin(t)$ is shown in Figure 10.7. The state variables in the time domain are shown in Figure 10.7(a) while the limit cycles are shown in Figure 10.7(b) to (d). Both input conditions have unique steady-state solutions. If a steady state response exists then time domain simulations always reach it. However, in the case of circuits with large time constants, long simulation runs are required to arrive at the steady-state. Accordingly, steady state techniques provide a more natural alternative for the solution of steady state problems.

10.7.2 First order Newton-Raphson solution

The solution of the non-linear circuit was obtained with a Newton-Raphson iterative method in Walsh Domain. The process took 7 iterations. It must be pointed out that waveforms are

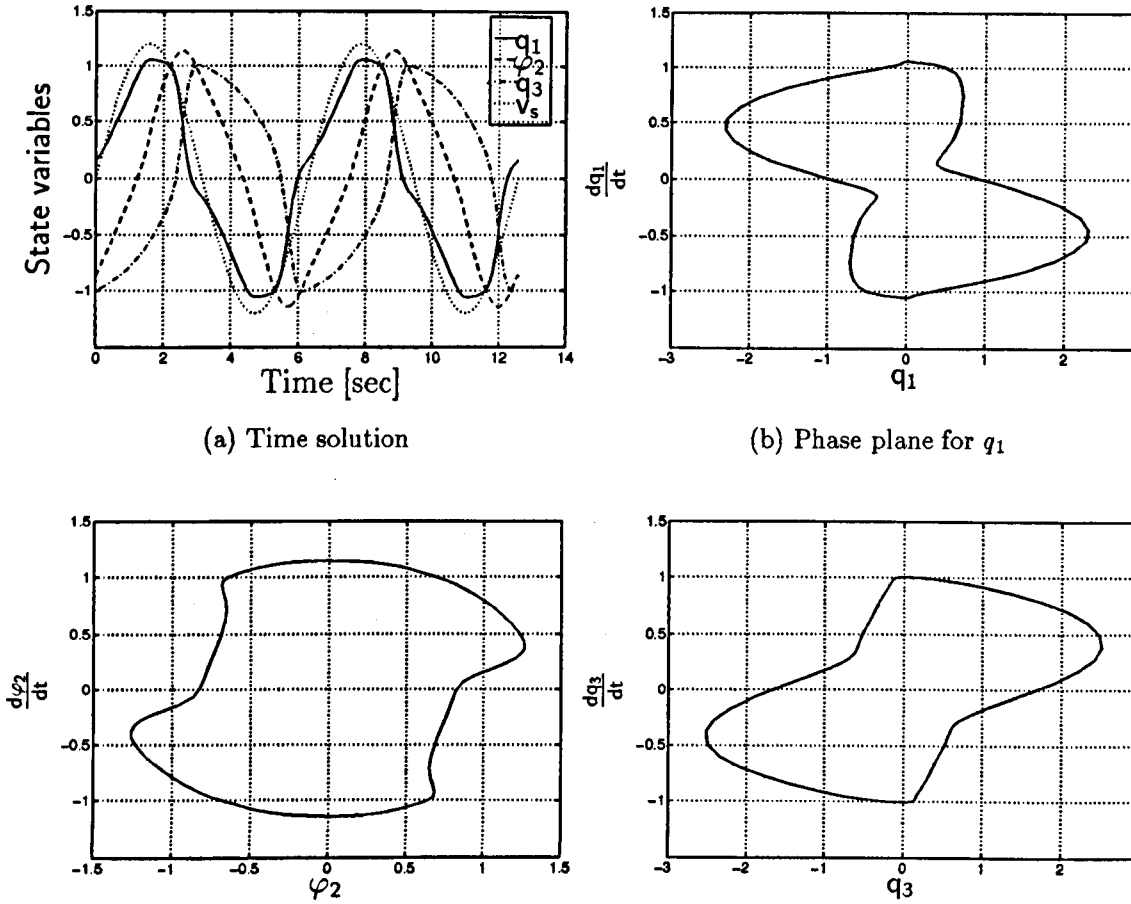

(a) Time solution

(b) Phase plane for q_1

(c) Phase Plane for φ_2

(d) Phase plane for q_3

Fig. 10.7: Steady state solution for an input of $1.2\sin(t)$

highly distorted and this represent a difficult problem for the Newton-Raphson method. Nevertheless, the method shows strong convergence even in these circumstances. The methods shows near quadratic convergence. Figures 10.8(a) to (g) show the progress of the iterative process towards the solution.

It has been observed that although first order Newton-Raphson methods provide strong convergence characteristics in most cases, they often produces overshootings in the first iteration. This can be observed in Figure 10.8(a). These over-shootings cause an increment in the number of iterations and, may cause the iterative method to diverge. It can be seen in Figure 10.8 that changes between successive iterations are significant, specially in those zones where the over-shooting took place.

10.7.3 Newton-Raphson retaining non-linearity

The steady state solution of the circuit in Figure 10.5 is now calculated using bi-linear approximations. The results are very good indeed. The progress of the process towards the convergence is illustrated in Figure 10.9. In this case, only the first and third order terms of the Taylor series were considered. Numerical problems were observed in cases where only the first two derivative terms were used, presumably of the even symmetry nature of the

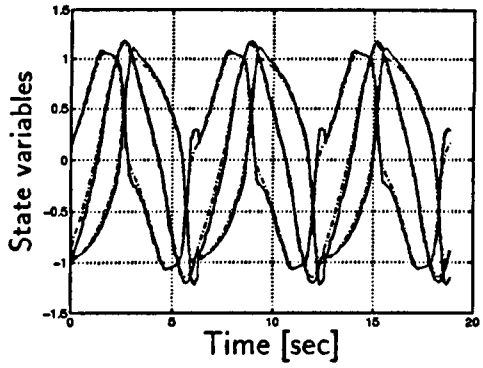

(a) First iteration

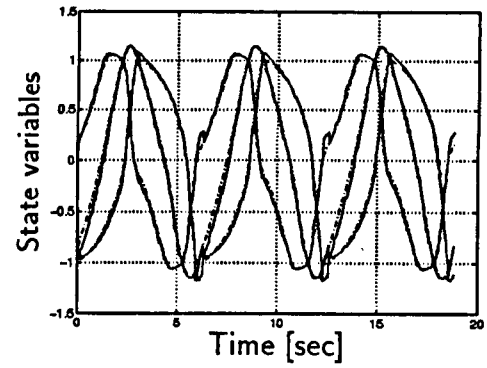

(b) Second iteration

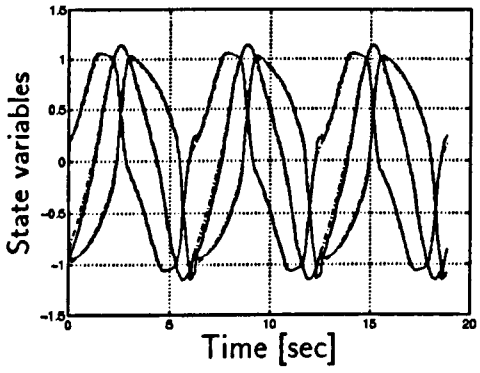

(c) Third iteration

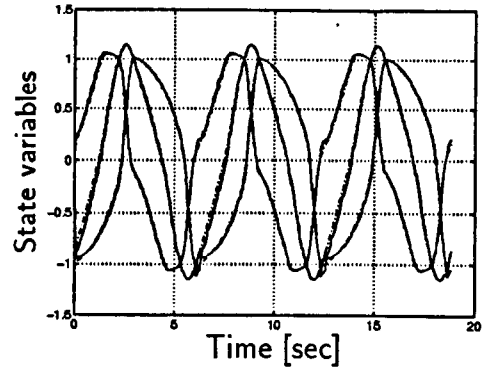

(d) Forth iteration

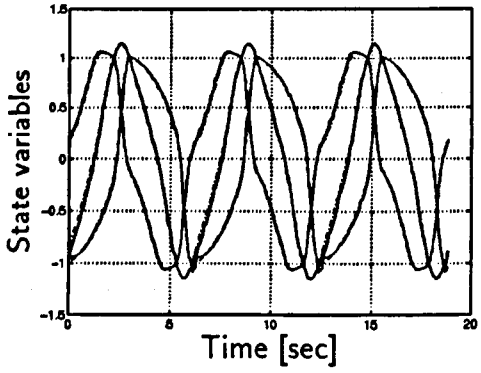

(e) Fifth iteration

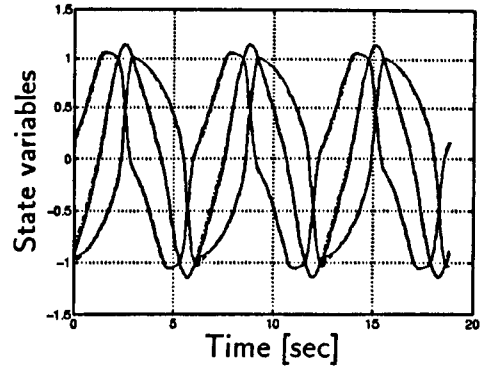

(f) Sixth iteration

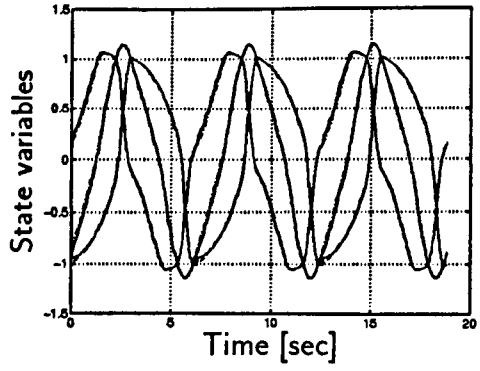

(g) Seventh iteration

Fig. 10.8: Newton-Raphson Iterative process,— Walsh solution, - - Time Domain solution

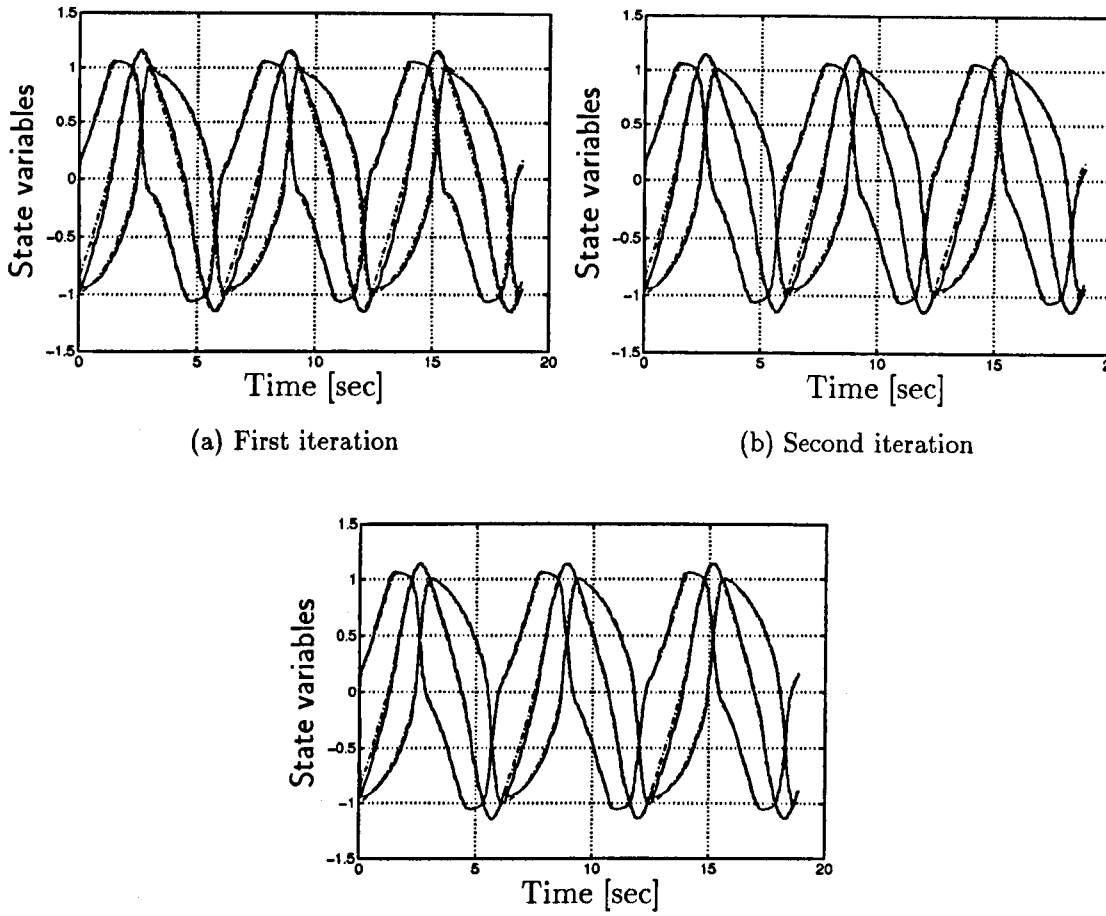

(a) First iteration

(b) Second iteration

(c) Third iteration

Fig. 10.9: Iterative process using a third order Newton-Raphson retaining non-linearity via bilinear terms

approximation whilst the non-linear characteristic shows odd symmetry. A similar problem is found when fitting transformer characteristics with polynomial equations containing even terms.

The number iterations has been reduced substantially at the expense of having to calculate third derivatives terms of the non-linear relations. The computational expense of calculating these derivative terms are, however, minor when compared to the computational effort required for the factorisation of the matrix system. It is this process which always takes most of the execution time. It must be mentioned that even higher order derivatives can be taken into account and that this is expected to improve the solution process. However, in the cases tested the improvements were observed to be minimal. For instance, a case where the first and the fifth derivatives were taken into account was solved in three iterations. This can be explained if one considers that whereas x^3 can arguably be approximated by xx_b^2, the approximation of x^5 by xx_b^4 is rather poor.

It can be observed in Figure 10.9(a) that from the beginning, bi-linearisations produce a good approximation of the non-linear system and avoids overshootings. Similar results were found in all analysed cases. The agreement between Walsh domain solutions and time domain, solutions agree rather well.

10.7.4 Effect of bi-linearisations in the convergence region

The above results suggest that the region of convergence increases when considering higher order, bi-linear terms in the Taylor series. To investigate this, the current source magnitude was further increased.It was found that for an input of $1.3\sin(t)$ both Newton approaches failed to converge but whereas the first order Newton-Raphson diverged in the second iteration, the Newton-Raphson approach using bi-linearity diverged after the seventh iteration. In this case, however, the limit cycle was reach via numerical integration. The three approaches converged for an input of $1.25\sin(t)$. Other tests where carried out but a case where bi-linearisation reached convergence while linearisations failed to converge were not found.

10.8 Conclusions

When one is confronted with a non-linear engineering problem, the natural reacton is to linearise the set of equations describing the problem; since this is way of avoiding the non-linear aspects of the problem. NLS theory is regarded by most engineers as a difficult and confusing endeavor. The scepticism of engineers for using non-linear approaches to tackle real problems is to an extent justifiable. When compared to the variety of techniques available in linear system theory, the tools for analysis and design of non-linear systems are rather limited. Bilinear structures, however, comprise a step forward in the search for solutions where systems can be better represented, taking account of their natural non-linear behaviour. An important feature of the use of bilinear systems is that they do possess non-linear qualities with the advantage that they can still be solved with the same tools as those used to solve LTIS and LTVS.

It was shown in this chapter that the use of bi-linearisations provide iterative methods for the steady state solution of non-linear circuits, with stronger convergence than first order Newton-Raphson techniques. The new alternative shows super-quadratic, convergence characteristics. It is also shown that while the bi-linear method converges substantially faster than linear methods, it also diverges slower than first order Newton-Raphson for cases when no solution is found. Although, it was expected that bi-linearisations would increased the region of convergence of the iterative methods owing to the stronger, convergence characteristics shown, this was not proven with the cases analysed.

It was presented in this chapter a way to obtain bi-linear approximations of more general non-linear systems form the linear and non-linear terms of Taylor series.

Chapter 11

Applications of Walsh Functions to Power Systems Distortion

In this chapter applications of Walsh functions to powers system waveform distortion are presented. Three applications are considered. In the first application the model of a single phase TCR which uses switching functions, is provided. A TCR admittance representation is used as opposed to a Norton equivalent representation. The second application addresses the modelling of three phase bank of transformers. Finally, a model for frequency dependent transmission lines in the sequency domain is provided,. This is significant as it makes possible to carry out analysis in the sequency domain via unified Newton-Raphson techniques.

11.1 Introduction

As switching circuits in power systems proliferate, there is an increasing need to model accurately the waveform distortion problems that they introduce. In the past, these circuits have been modelled using time domain and frequency domain techniques [17]. However, a large number of coefficients is required to accurately model the sharp edges of the signals present in this kind of circuits. Walsh functions, however, are themselves switching functions and a finite number of them will represent exactly the switching functions observed in many power electronic-based devices. With this in mind, a single phase TCR, which admittance matrix is a switching function, is analysed in the sequency domain.

In harmonic domain, the combined use of NA and the technique of linearisation described in [17] allows a global harmonic representation for the entire network in the form of equation,

$$\Delta I = [Y_J]\Delta V \tag{11.1}$$

where $[Y_J]$ is a harmonic admittance matrix for the entire network, ΔV is a vector of incremental voltages and ΔI is a vector of incremental currents. The nodal matrix accommodates all the nodes, phases and the most significant harmonics of the full spectrum. This matrix also combines the linear and linearised, non-linear components and therefore the solution is reached by iteration. This implies a re-linearisation of the non-linear components at each iterative step which may also be interpreted as a linearisation of the entire system and, thus, finding the harmonic solution through a Newton type procedure, where the admittance matrix $[Y_J]$ plays the role of a Jacobian. This Jacobian matrix is only used to generate updated voltages, ΔV. It is not used to confirm convergence, so errors in the Jacobian only affect the rate of convergence, not the accuracy of the solution. When a non-linear component is

excited by a sinusoidal input, the output will always consist of a sinusoid with a frequency equal to the frequency of the input and all harmonics. Accordingly, owing to the practical need to consider a limited number of harmonics the Jacobian will always be approximated with an error which depends on the pruning of the Jacobian, and affecting the rate and the region of convergence of the Newton-Raphson process.

A very interesting characteristic of Walsh functions is that when a non-linear component is excited by a Walsh series, it will have an output which consists of another Walsh series having the same coefficients as the input but different magnitudes. Therefore, in the Walsh domain the Jacobian at each iterative step is never pruned and, thus, the rate of convergence is not degraded due to truncations errors. In this chapter a three phase bank of transformers is modelled in the Walsh domain.

Transmission lines are frequency dependent elements that must be accurately modelled in rigorous distortion analysis. Traditionally, the models for transmission lines have been developed in the time domain or in the frequency domain. As a last application in this chapter, a model for frequency dependent transmission lines in the sequency domain is provided. With this model, it is now possible to obtain a unified Newton-Raphson method in the sequency domain which accommodates all power plant components and which is free of convergence problems due to truncation errors.

11.2 Single Phase TCRs

In modern power systems there are many devices which exhibit non-linear characteristics. Here, an important device that is used for purposes of voltage control, namely TCR, is analysed. Several methods have been put forward in open literature to study the waveform distortion introduced by TCRs [105, 41]. They can be classified into three categories. Time domain solutions solve the dynamic equations through numerical integration. Another approach uses harmonic domain techniques [142]. In the third approach, the state equations are formulated and then solved using linear system theory [105].

An alternative approach is proposed below. It also uses the TCR state equations but rather than solving them directly, they are transformed into algebraic equations by using orthogonal functions. The algebraic equations are then solved analytically. This approach is used in this section to provide a model for single phase TCRs. The model is presented in general form thus allowing for any orthogonal set to be used but the solution is obtained using sequency domain techniques.

11.2.1 The TCR and Power Systems Equations

In this section expressions for the current through the TCR and voltage across the TCR are give. Consider first the single phase TCR shown in Figure 11.1(b). The thyristors T_1 and T_2 are gated once each half cycle allowing control of the current in the reactor and thus allowing control of the reactive current drawn by the circuit. The current in the reactor can be found by integrating the voltage across the reactor, $v_R(t)$, which can be represented by the terminal voltage, v_T, multiplied by the switching function $s(t)$. The switching function is shown in Figure 11.1(b). It has a value of 1 whenever a thyristor is on and a value of zero whenever the thyristors are off.

The current in the reactor can be expressed as the integral,

$$i_R(t) = \frac{1}{L_r}\int_0^t s(t-\tau)v_r(\tau)d\tau + i_R(0) \tag{11.2}$$

where $i_R(0)$ represents the initial condition of the reactor.

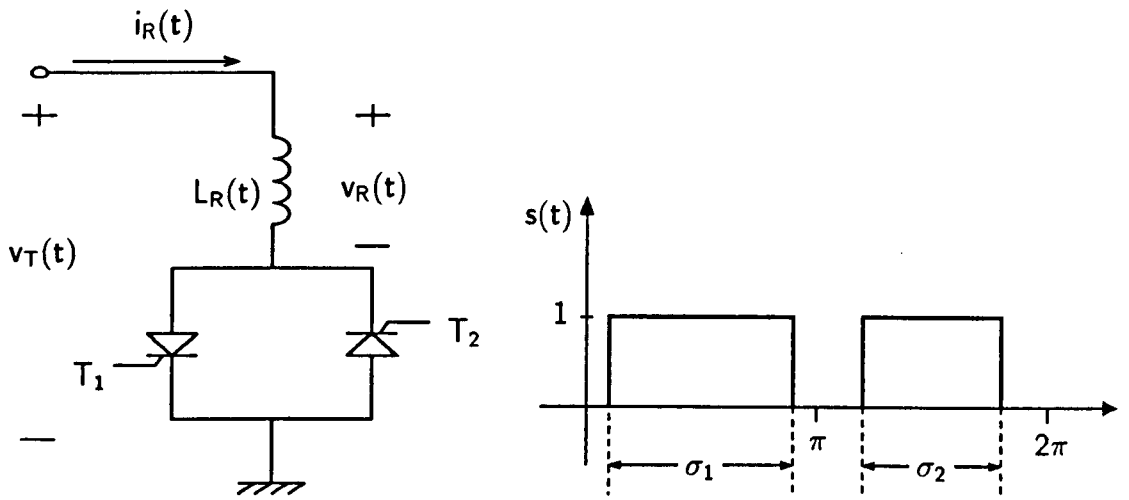

(a) Single phase Thyristor Controlled Reactor

(b) Switching function

Fig. 11.1: Piecewise-linear approximation

On the other hand, the power system is represented by a Thevenin equivalent as seem from the bus bar connecting the TCR to the external system. The system to be analysed in this case is shown in Figure 11.2. In the sequency domain the equivalent system impedance is represented by a diagonal matrix. In this circuit $f = 50Hz$, $L_s = 0.000318$, $L_R = 0.0016$ and $v_s = \sqrt{2}\sin(\omega t)$. The state equation of the system can be written as,

$$\frac{di_R}{dt} = \frac{s(t)v_s(t)}{(L_s + L_R)} \tag{11.3}$$

which in canonical form is,

$$\dot{\mathbf{x}} = \mathbf{A}(t)\mathbf{x} + \mathbf{B}(t)\mathbf{u}(t) \tag{11.4}$$

with $x(t) = i_R(t)$, $\mathbf{A}(t) = 0$, $\mathbf{B}(t) = \frac{s(t)}{L_s+L_R}$ and $\mathbf{u}(t) = v_s(t)$.

Time domain solution

Equation 11.4 can be solved in the time domain by means of numerical integration to calculate the current flowing through the rector. This current is shown in Figure 11.3(a). The integration process was carried out using a fourth order Runge-Kutta with variable step size. The voltage across the TCR is shown in Figure 11.3(a). It must be mentioned that the discontinuous nature of the switching function and the current in the TCR present a difficult case for most numerical integration methods. In this case a very small step size had to be used in order to achieve this result. Accordingly, long solutions times were experienced.

Also, in the time domain but using linear system theory, equation 11.4 can be solved using Floquet theory [39]. The strength of this approach is its great theoretical depth. It allows qualitative assessment of stability. Floquet theory can also be used to analyse periodic systems where the transfer function $s(t)$ is not necessarily a switching function but rather a smooth function.

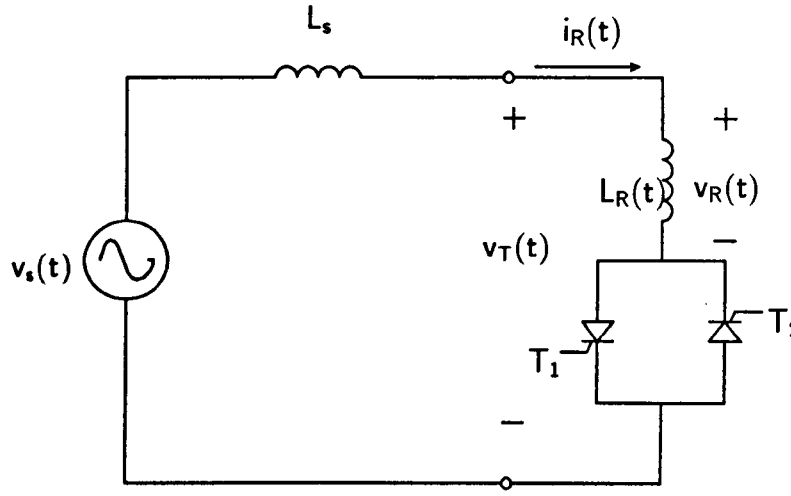

Fig. 11.2: The reduced equivalent system

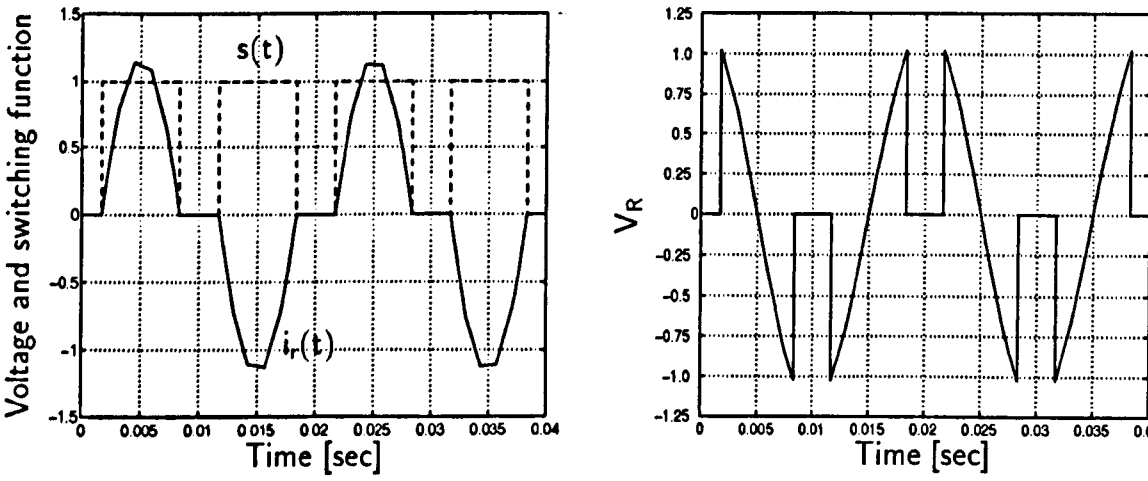

(a) Current flowing through TCR

(b) Voltage across TCR's inductor

Fig. 11.3: Time domain solution for $\sigma_1 = \sigma_2 = 30^o$

Walsh domain solution

Alternatively to time domain solutions, equation (11.4) can be solved in frequency domain [142] or in sequency domain. Walsh functions are used to transform the state equation (11.4) into the sequency domain.

Equation (11.4) is written in integral form as,

$$i_R(t) = \frac{1}{L_s + L_R} \int_0^t s(t-\tau) v_s(\tau) d\tau + i_R(0) \tag{11.5}$$

Then approximation of $s(t)$, $v_s(t)$ and $i_s(t)$,

$$\begin{aligned} s(t) &\approx S^t\phi_{(m)}(t) && (11.6)\\ v_s(t) &\approx V_s^t\phi_{(m)}(t) && (11.7)\\ i_R(t) &\approx I_R^t\phi_{(m)}(t) && (11.8)\\ i_R(0) &= I_{R_0}^t\phi_{(m)}(t) && (11.9) \end{aligned}$$

where

$$\begin{aligned} S^t &= [\ S_0 \quad S_1 \quad \dots \quad S_{(m-1)}\ ]\\ I_R^t &= [\ I_{R_0} \quad I_{R_1} \quad \dots \quad I_{R_{(m-1)}}\ ]\\ V_s^t &= [\ V_{s_0} \quad V_{s_1} \quad \dots \quad V_{s_{(m-1)}}\ ]\\ I_{R_0}^t &= [\ i_R(0) \quad 0 \quad \dots \quad 0\ ] \end{aligned}$$

allows to rewrite equation (11.5) as,

$$I_R^t\phi_{(m)}(t) = \frac{1}{(L_s+L_R)}\int_0^t V_s^t\phi_{(m)}(\tau)S^t\phi_{(m)}(\tau)d\tau + I_{R_0}^t\phi_{(m)}(t) \tag{11.10}$$

or

$$I_R^t\phi_{(m)}(t) = \frac{1}{(L_s+L_R)}\int_0^t V_s^t\phi_{(m)}(\tau)\phi_{(m)}^t(\tau)S^t d\tau + I_{R_0}^t\phi_{(m)}(t) \tag{11.11}$$

Using properties of the product of Walsh functions we have that,

$$I_R^t\phi_{(m)}(t) = \frac{1}{(L_s+L_R)}\int_0^t V_s^t\mathrm{S}\phi_{(m)}(\tau)d\tau + I_{R_0}^t\phi_{(m)}(t) \tag{11.12}$$

where S is the matrix of coefficients corresponding to the switching function, $s(t)$. Using the operational matrix of integration the current in the TCR's reactor can be calculated as,

$$I_R^t\phi_{(m)}(t) = \frac{1}{(L_s+L_R)}V_s^t\mathrm{S}P\phi_{(m)} + I_{R_0}^t\phi_{(m)}(t) \tag{11.13}$$

Solving for the coefficients of the current yields,

$$I_R^t = \frac{1}{(L_s+L_R)}V_s^t\mathrm{S}P + I_{R_0}^t \tag{11.14}$$

From equation (11.14), it is possible to give an admittance matrix representation of the TCR. In this case, the admittance can be written as,

$$\mathrm{Y} = \frac{1}{(L_s+L_R)}\mathrm{S} \tag{11.15}$$

where S is the matrix of coefficients corresponding to vector S. It has the following structure when only four Walsh coefficients are considered,

$$\mathrm{S} = \left[\begin{array}{cc|cc} S_0 & S_1 & S_2 & S_3\\ S_1 & S_0 & S_3 & S_2\\ \hline S_2 & S_3 & S_0 & S_1\\ S_3 & S_2 & S_1 & S_0 \end{array}\right] \tag{11.16}$$

Similarly, one can write the admittance matrix representation of the TCR as,

$$Y_{TCR} = \frac{1}{L_R}\mathrm{S} \tag{11.17}$$

Having found Y_{TCR}, it is possible to write an expression to determine the voltage at TCR terminals,

$$V_T^t = V_s^t - I_R^t Z_s \tag{11.18}$$

where Z_s is related to the matrix of coefficients corresponding to L_s. Substituting of the I_R yields,

$$V_T^t = V_s^t - V_T^t Y_{TCR} Z_s \tag{11.19}$$

and solving for V_T,

$$V_T^t = V_s^t (1 + Y_{TCR} Z_s)^{-1} \tag{11.20}$$

It is important to say that assumptions made in the switching function affects greatly the complexity of the problem. In this case the switching function was assumed constant for a given conduction angle. Therefore, from equation (11.20) it can be seen that the solution of equation (11.20) is non-iterative. However, more realistic studies will involve system impedances with resistive part different from zero as well as capacitive effects. In this case, the switching function shifted to an unknown position and an iterative process will required.

The circuit of Figure 11.2 is now solved using equation (11.14). This result is shown in Figure 11.4. The current flowing through the circuit is shown in Figure 11.4(b) whilst the voltages is shown in Figure 11.4(b). Figure 11.4(c) shows that the TCR switching functions can be approximated with a finite number of Walsh coefficients. The voltage at the TCR

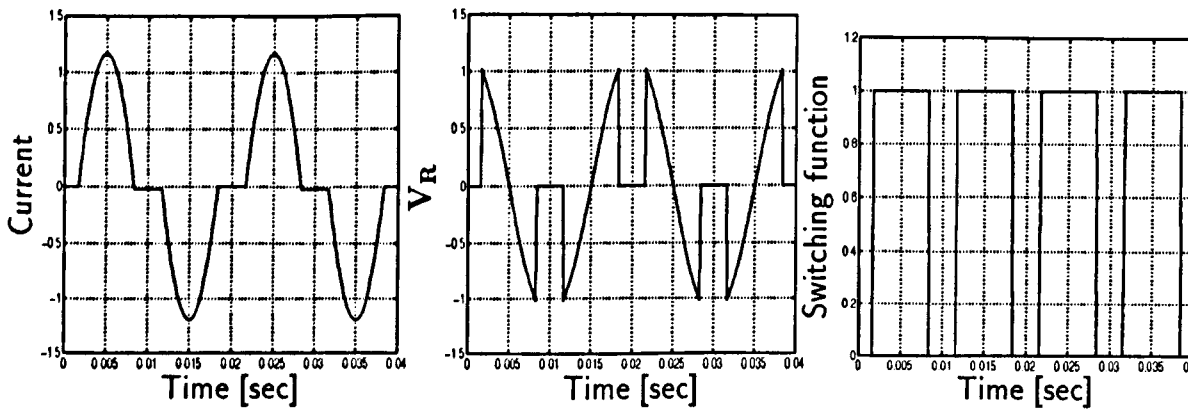

(a) Current flowing through TCR

(b) Voltage across TCR's inductor

(c) Approximation of switching function

Fig. 11.4: Walsh domain solution $\sigma_1 = \sigma_2 = 30^o$

terminals is shown in Figure 11.5(a). The harmonic content of this voltage is shown in Figure 11.5(b)

The model presented in this section accounts for imbalances in the firing control, i.e. different conduction angles. In Figure 11.6, results are obtained for conduction angles of $\sigma_1 =$

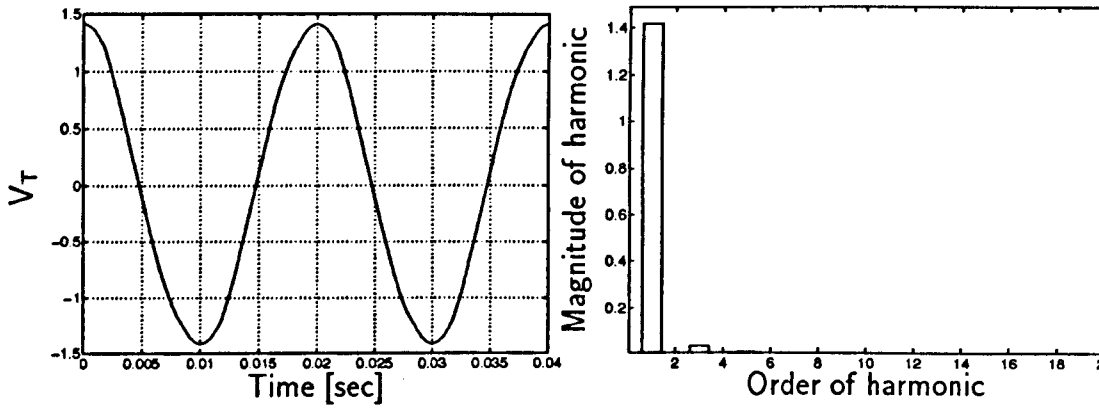

(a) Voltage at terminals of TCR

(b) Harmonic content of voltage at terminals of TCR

Fig. 11.5: TCR, Terminal voltage waveform

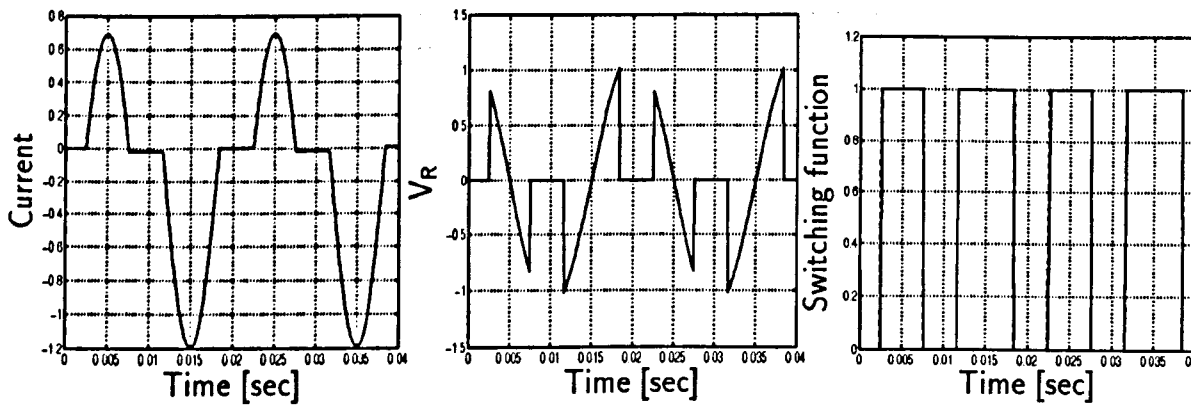

(a) Current flowing through TCR

(b) Voltage across TCR's inductor

(c) Approximation of switching function

Fig. 11.6: Walsh domain solution for $\sigma_1 = 30^o$ and $\sigma_2 = 45^o$

30^0 and $\sigma_2 = 45^o$. Figure 11.6(a) shows the current flowing through the TCR whilst Figures 11.6(b) shows the voltage across the TCR inductor and the switching function, respectively.

The waveform distortion injected by the TCR into the system depends on system impedance and on conduction angles. In Figure 11.7(a) the sequency currents injected to the system are plotted for various conduction angles.

In Figure 11.7(b) only the most significant sequences are plotted. It can be seen that the single phase TCR will inject mainly currents of sequence 2, 14, 22, 26, 38 and 42. All other sequence magnitudes are very small and do not contribute significantly to waveform distortion. Significant differences can be seen between the behaviour of the sequence currents and harmonic currents. It can be observed in Figure 11.7(b) that several sequence currents increase monotonically as the conduction angle increases.

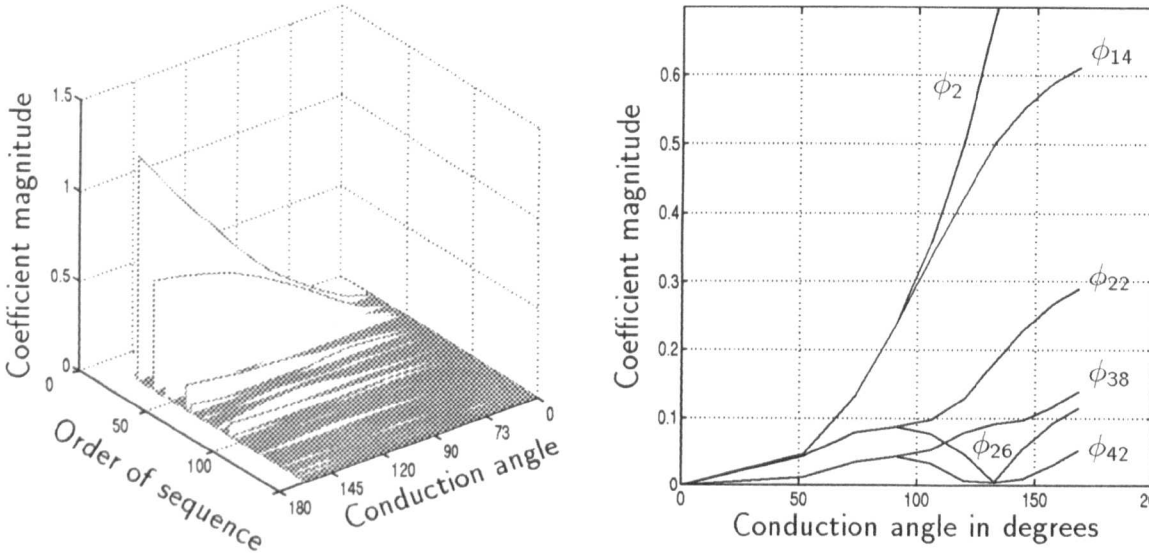

(a) Order of sequence Vs Conduction angle

(b) Main sequence coefficients Vs Conduction angle

Fig. 11.7: Sequence currents Vs conduction angles

11.3 Modelling of Single Core Three Phase Transformers

In this section, three phase bank of transformers are modelled in the sequency domain. Some important properties relating non-linear input-output characteristics in terms of Walsh series are discussed to show how Newton Raphson iterative methods may circumvent convergence problems when pruned Jacobians are used.

The harmonic admittance matrix of equation (11.1) combines linear and linearised, non-linear plant components. The distorted solution is reached by means of an iterative process. The non-linear components are re-linearised at each iterative step. In this section the linearisation process is carried out in the sequency domain as opposed to the frequency domain [17].

11.3.1 Newton-Raphson in the Sequency Domain

In the sequency domain, variables relating to the Newton-Raphson formulation will be expressed as,

$$x(t) = \sum_{h=0}^{\infty} X_h \phi_h(t) \tag{11.21}$$

$$y(t) = \sum_{k=0}^{\infty} Y_k \phi_k(t) \tag{11.22}$$

$$f'(x) = f'(x(t) = \sum_{i=0}^{\infty} c_i \phi_i(t) \tag{11.23}$$

Substituting relations (11.21) to (11.23) into equation (4.77) leads to the following matrix equation,

$$\Delta Y = [C]\Delta X \tag{11.24}$$

where the matrix arrangement is similar to that of equation (11.46).

In the sequency domain, a linear admittance is represented as,

$$I = \frac{1}{L}[P]^t V \tag{11.25}$$

where $[P]$ is the operational matrix of integration. In harmonic domain applications or in sequence domain applications the problem may be purely static, as in equation (11.24), or it may contain dynamic terms, as in equation (11.25). The task, however, is always to evaluate a non-linear function of one or several variables. This evaluation can be carried out in the sequency domain. In this domain non-linear evaluations are carried out very efficiently as only summations are required. An additional attraction of using sequence domain Newton-Raphsons is that no truncation errors are introduced in the Jacobian. In the section below the evaluation of single valued non-linear functions is carried out in the sequency domain.

11.3.2 Effect of Non-Linear Operations on Walsh Series

Perhaps the most elegant and powerful property of Walsh functions, when applied to non-linear systems, is the one described by Corrington in [43],

Property 1: If a zero memory non-linear transformation is applied to a Walsh series, the output series can be derived by simple algebraic processes. The magnitude of the coefficients of the input series will change but no new terms will be created.

Consider a single valued, non-linear relation exhibiting odd symmetry, $(N_o(x(t))$, and subjected to an input of the form,

$$x(t) = a\phi_2(t) + b\phi_1(t) \tag{11.26}$$

The input and the non-linear transformation are shown in Figure 11.8, where it can be seen that the output may be written as,

$$x(t) = \alpha\phi_2(t) + \beta\phi_1(t) \tag{11.27}$$

where

$$2\alpha = N_o(a+b) - N_o(b-a) \tag{11.28}$$
$$2\beta = N_o(b-a) + N_o(a+b) \tag{11.29}$$

This property is analogous to the behavior of a linear system subjected to a sinusoidal input with frequencies ω. In such a case the emerging signal contains the same frequency but different amplitude.

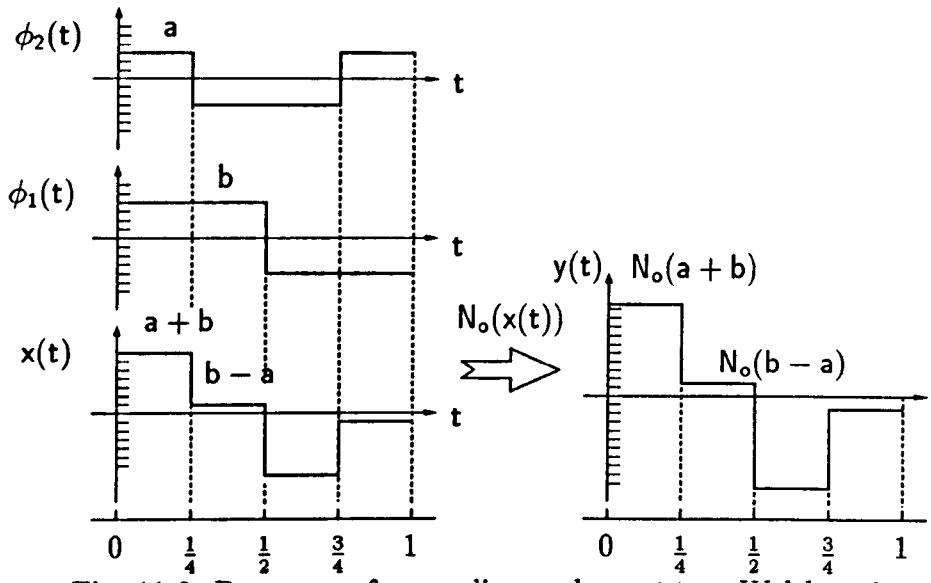

Fig. 11.8: Response of a non-linear element to a Walsh series

11.3.3 Response of a non-linear element to a Walsh series

Based on Property 1, the coefficients of the input Walsh series to a memoryless, non-linear element are related to the coefficients of the output Walsh series by algebraic means. Let us consider a stair step input represented by Walsh series,

$$x(t) = c_0\phi_0(t) + c_1\phi_1(t) + \ldots + c_n\phi_n(t) + \ldots \tag{11.30}$$

and the non-linear relation,

$$y(t) = N(x(t)) \tag{11.31}$$

Where $N(\cdot)$ can have any analytical representation.

If only the coefficients of equation (11.30) are used, this equation can be written in vector form,

$$x(t) = \mathbf{c}_x^t \phi \tag{11.32}$$

where

$$\mathbf{c} = [c_0, c_1, \ldots, c_{N-1}]^t \tag{11.33}$$

$$\phi = [\phi_0(t), \phi_1(t), \ldots, \phi_{N-1}(t)] \tag{11.34}$$

$\mathbf{c}$ is called the Walsh coefficient vector and ϕ is called the Walsh vector.

The magnitude of each one of the N segments can be found with the discrete formula,

$$x(k) = W\mathbf{c}_x \tag{11.35}$$

where W is the Walsh matrix.

If a non-linear transformation $N(x(t))$ is applied to $x(t)$ the coefficients of the input can be found as follows,

$$y(k) = N(x(k)) = W\mathbf{c}_y \tag{11.36}$$

Substituting equation (11.35) into equation (11.36),

$$N(W\mathbf{c}_x) = W\mathbf{c}_y \tag{11.37}$$

Then,

$$\mathbf{c}_y = W^{-1}N(W\mathbf{c}_x) \tag{11.38}$$

Since W is an orthogonal matrix,

$$W^t = W^{-1} \tag{11.39}$$

the coefficients of the output can be calculated as,

$$\mathbf{c}_y = \frac{1}{m}W^tN(W\mathbf{c}_x) \tag{11.40}$$

Equation (11.40) relates the coefficients of the input and the output but, unlike the Fourier transform, there will be no truncations error. It is important to mention that since W is a matrix with all entries set to 1 or -1, no products are required in the evaluation of equation (11.40)

11.3.4 Product of Walsh Series

The product of two real variables x and y expressed in Walsh Domain as,

$$x(t) = \sum_{i=0}^{N_i} X_i\phi_i(t) \tag{11.41}$$

$$y(t) = \sum_{j=0}^{N_j} Y_j\phi_j(t) \tag{11.42}$$

gives rise to another periodic variable, say z,

$$\sum_{k=0}^{N_k} Z_k\phi_k(t) = \left(\sum_{i=0}^{N_i} X_i\phi_i(t)\right)\left(\sum_{j=0}^{N_j} Y_j\phi_j(t)\right) \tag{11.43}$$

A vector form equation can be obtained by using the Walsh coefficients only,

$$Z = X \oplus Y \tag{11.44}$$

where

$$\begin{aligned} X &= [\, X_0 \;\; X_1 \;\; \ldots \;\; X_i \;\; \ldots \;\; X_{N_{i-1}} \,] \\ Y &= [\, Y_0 \;\; Y_1 \;\; \ldots \;\; Y_j \;\; \ldots \;\; Y_{N_{j-1}} \,] \\ Z &= [\, Z_0 \;\; Z_1 \;\; \ldots \;\; Z_k \;\; \ldots \;\; Z_{N_{k-1}} \,] \end{aligned}$$

The matrix form representation of equation (11.44) is an alternative for performing actual calculations,

$$Z = \mathbf{X}Y \tag{11.45}$$

where the elements of matrix $\mathbf{X}$ can be easily identified by performing hand calculations and taking account that the product of two Walsh functions gives rise to another Walsh function. Then, it can be shown that,

$$\mathbf{X} = \left[\begin{array}{c|c|c|c|c|c} X_0 & X_1 & \dots & X_i & \dots & X_{N-1} \\ \hline X_1 & X_0 & \dots & X_{i+1} & \dots & X_{N-2} \\ \hline \vdots & \vdots & \vdots & \vdots & \vdots & \vdots \\ \hline X_i & X_{i+1} & \dots & X_0 & \dots & X_{N-i} \\ \hline \vdots & \vdots & \vdots & \vdots & \vdots & \vdots \\ \hline X_{N-1} & X_{N-2} & \dots & X_{N-i} & \dots & X_0 \end{array}\right] \tag{11.46}$$

11.3.5 Effect of Trigonometric Transformations

Consider again the waveform $x(t)$ in Walsh domain,

$$x(t) = c_0\phi_0(t) + c_1\phi_1(t) + c_2\phi_2(t) + \dots \tag{11.47}$$

which is required to evaluate the following trigonometric relations,

$$y(t) = \sin(kx(t)) \tag{11.48}$$

$$z(t) = \cos(kx(t)) \tag{11.49}$$

$$\tag{11.50}$$

The procedure to determine the relationship between the Walsh coefficients of the variable $x(t)$ and the above trigonometric function is similar to the one followed to find the integration and operational matrices. For $m = 4$, we have that,

$$x(t) = c_0\phi_0(t) + c_1\phi_1(t) + c_2\phi_2(t) + c_3\phi_3(t) \tag{11.51}$$

and for the trigonometric operation,

$$\sin(kx(t)) = \sin\left[kc_0\phi_0(t) + kc_1\phi_1(t) + kc_2\phi_2(t) + kc_3\phi_3(t))\right] \tag{11.52}$$

Applying, recursively, the trigonometric identities,

$$\sin(A+B) = \sin A\cos B + \cos A\sin B$$
$$\cos(A+B) = \cos A\cos B - \sin A\sin B$$

yields,

$$\begin{aligned} & \sin(kx(t)) = \\ - & \sin(kc_0\phi_0(t))\sin(kc_1\phi_1(t))\sin(kc_2\phi_2(t))\cos(kc_3\phi_3(t)) \\ - & \sin(kc_0\phi_0(t))\sin(kc_1\phi_1(t))\cos(kc_2\phi_2(t))\sin(kc_3\phi_3(t)) \\ - & \sin(kc_0\phi_0(t))\cos(kc_1\phi_1(t))\sin(kc_2\phi_2(t))\sin(kc_3\phi_3(t)) \\ - & \cos(kc_0\phi_0(t))\sin(kc_1\phi_1(t))\sin(kc_2\phi_2(t))\sin(kc_3\phi_3(t)) \\ + & \sin(kc_0\phi_0(t))\cos(kc_1\phi_1(t))\cos(kc_2\phi_2(t))\cos(kc_3\phi_3(t)) \\ + & \cos(kc_0\phi_0(t))\sin(kc_1\phi_1(t))\cos(kc_2\phi_2(t))\cos(kc_3\phi_3(t)) \\ + & \cos(kc_0\phi_0(t))\cos(kc_1\phi_1(t))\sin(kc_2\phi_2(t))\cos(kc_3\phi_3(t)) \\ + & \cos(kc_0\phi_0(t))\cos(kc_1\phi_1(t))\cos(kc_2\phi_2(t))\sin(kc_3\phi_3(t)) \end{aligned} \tag{11.53}$$

From the properties of Walsh function, described in Chapter 4, we can rewrite equation (11.53) as,

$$\begin{aligned}
& \sin(kx(t)) = \\
- \; & \sin(kc_0)\sin(kc_1)\sin(kc_2)\cos(kc_3)\,\phi_{1\oplus 2}(t) \\
- \; & \sin(kc_0)\sin(kc_1)\cos(kc_2)\sin(kc_3)\,\phi_{1\oplus 3}(t) \\
- \; & \sin(kc_0)\cos(kc_1)\sin(kc_2)\sin(kc_3)\,\phi_{2\oplus 3}(t) \\
- \; & \cos(kc_0)\sin(kc_1)\sin(kc_2)\sin(kc_3)\,\phi_{1\oplus 2\oplus 3}(t) \\
+ \; & \sin(kc_0)\cos(kc_1)\cos(kc_2)\cos(kc_3)\,\phi_0(t) \\
+ \; & \cos(kc_0)\sin(kc_1)\cos(kc_2)\cos(kc_3)\,\phi_1(t) \\
+ \; & \cos(kc_0)\cos(kc_1)\sin(kc_2)\cos(kc_3)\,\phi_2(t) \\
+ \; & \cos(kc_0)\cos(kc_1)\cos(kc_2)\sin(kc_3)\,\phi_3(t)
\end{aligned} \tag{11.54}$$

Performing Module-2 additions,

$$\begin{bmatrix} \phi_{1\oplus 2} \\ \phi_{1\oplus 3} \\ \phi_{2\oplus 3} \\ \phi_{1\oplus 2\oplus 3} \end{bmatrix} = \begin{bmatrix} \phi_3 \\ \phi_2 \\ \phi_1 \\ \phi_0 \end{bmatrix}$$

equation (11.54) simplifies to,

$$\begin{aligned}
& \sin(kx(t)) = \\
- \; & \sin(kc_0)\sin(kc_1)\sin(kc_2)\cos(kc_3)\,\phi_3(t) \\
- \; & \sin(kc_0)\sin(kc_1)\cos(kc_2)\sin(kc_3)\,\phi_2(t) \\
- \; & \sin(kc_0)\cos(kc_1)\sin(kc_2)\sin(kc_3)\,\phi_1(t) \\
- \; & \cos(kc_0)\sin(kc_1)\sin(kc_2)\sin(kc_3)\,\phi_0(t) \\
+ \; & \sin(kc_0)\cos(kc_1)\cos(kc_2)\cos(kc_3)\,\phi_0(t) \\
+ \; & \cos(kc_0)\sin(kc_1)\cos(kc_2)\cos(kc_3)\,\phi_1(t) \\
+ \; & \cos(kc_0)\cos(kc_1)\sin(kc_2)\cos(kc_3)\,\phi_2(t) \\
+ \; & \cos(kc_0)\cos(kc_1)\cos(kc_2)\sin(kc_3)\,\phi_3(t)
\end{aligned} \tag{11.55}$$

Finally, using the relations,

$$\begin{aligned}
\sin A \sin B &= \frac{1}{2}(A-B) - \frac{1}{2}(A+B) \\
\cos A \cos B &= \frac{1}{2}(A-B) + \frac{1}{2}(A+B) \\
\sin A \cos B &= \frac{1}{2}(A+B) + \frac{1}{2}(A-B)
\end{aligned} \tag{11.56}$$

and assuming that Y_0, Y_1, Y_2 and Y_3 are the Walsh functions at the input,

$$Y_0 = \begin{array}{l} +0.25\sin(c_0+c_1-c_2-c_3) \\ +0.25\sin(c_0-c_1+c_2-c_3) \\ +0.25\sin(c_0-c_1-c_2+c_3) \\ +0.25\sin(c_0+c_1+c_2+c_3) \end{array} \tag{11.57}$$

$$Y_1 = \begin{array}{l} +0.25\sin(c_0 + c_1 - c_2 - c_3) \\ -0.25\sin(c_0 - c_1 + c_2 - c_3) \\ -0.25\sin(c_0 - c_1 - c_2 + c_3) \\ +0.25\sin(c_0 + c_1 + c_2 + c_3) \end{array} \tag{11.58}$$

$$Y_2 = \begin{array}{l} -0.25\sin(c_0 + c_1 - c_2 - c_3) \\ +0.25\sin(c_0 - c_1 + c_2 - c_3) \\ -0.25\sin(c_0 - c_1 - c_2 + c_3) \\ +0.25\sin(c_0 + c_1 + c_2 + c_3) \end{array} \tag{11.59}$$

$$Y_3 = \begin{array}{l} -0.25\sin(c_0 + c_1 - c_2 - c_3) \\ -0.25\sin(c_0 - c_1 + c_2 - c_3) \\ +0.25\sin(c_0 - c_1 - c_2 + c_3) \\ +0.25\sin(c_0 + c_1 + c_2 + c_3) \end{array} \tag{11.60}$$

It can be seen that these relations can be expressed in matrix form as,

$$\begin{bmatrix} Y_0 \\ Y_1 \\ Y_2 \\ Y_3 \end{bmatrix} = \begin{bmatrix} 1 & 1 & 1 & 1 \\ 1 & -1 & -1 & 1 \\ -1 & 1 & -1 & 1 \\ -1 & -1 & 1 & 1 \end{bmatrix} \sin\left(\begin{bmatrix} 1 & 1 & -1 & -1 \\ 1 & -1 & 1 & -1 \\ 1 & -1 & -1 & 1 \\ 1 & 1 & 1 & 1 \end{bmatrix} \begin{bmatrix} c_0 \\ c_1 \\ c_2 \\ c_3 \end{bmatrix} \right) \frac{1}{m} \tag{11.61}$$

If we recall that,

$$\mathbf{W} = \begin{bmatrix} 1 & 1 & -1 & -1 \\ 1 & -1 & 1 & -1 \\ 1 & -1 & -1 & 1 \\ 1 & 1 & 1 & 1 \end{bmatrix} \tag{11.62}$$

is the Walsh matrix then equation (11.61) can be rewritten in compact form as,

$$Y = W^t \sin(W\mathbf{c}) \tag{11.63}$$

which has exactly the same form as equation (11.40). It is important to note that the analytical expression agrees exactly with the discrete transforms and anti-transforms from Walsh to time domain and vice versa. Also, it can be seen that the sine function can be substituted by any non-linear function. The entries of the Walsh matrix W are either 1 or -1 and evaluations of equation (11.61) are reduced to summations.

11.3.6 Transformer Equivalent Circuit

A transformer consists of a magnetic part (magnetising branch) and an electric part (leakage reactance). The former is represented as a sequence Norton equivalent but it can also be represented as an admittance matrix, similarly to the application above. The latter may be seen as a lattice-diagram, one for each sequence. Here, both representations are combined resulting in a model for the single phase transformer, in the sequency domain. Two-winding, single phase transformer models are then used to assemble three phase bank of transformers. This is achieved by suitable combinations of three sequence lattice equivalent circuits.

11.3.7 Test Case

A small but real transmission system has been used for the purpose of validating the theory. Complete data exist for the test system, which has already served for the purpose of validation [131]. The criterion of convergence in all iterative solutions was a voltage difference smaller than 10^{-6} between two successive iterations. This criterion applies to the fundamental and harmonic frequencies. All solutions have been achieved in less than five iterations. The

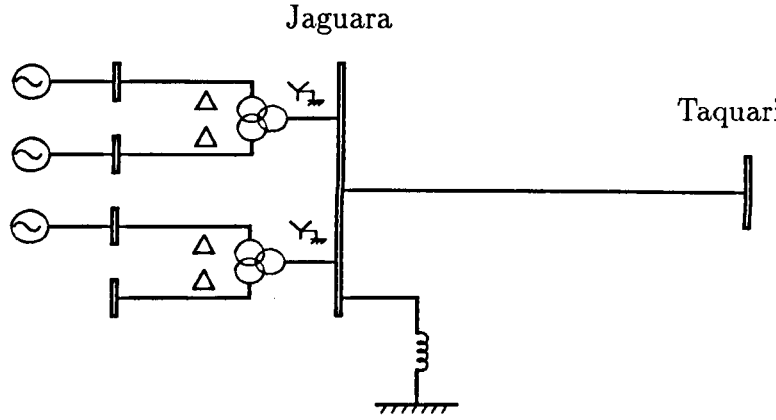

Fig. 11.9: Jaguara-Taquaril transmission system

relevant data for this system is given in Appendix B. Figure 11.10 shows the voltage waveform at Jaguara bus bar for the case when the voltage in the generator is 1.2 p.u. Good agreement between the solution given by the sequency and alternative formulations [17] was achieved. Figure 11.10 shows both solutions where no differences can be detected. The Walsh approach is used to calculate the coefficients of the output in a more efficient and 'clean' manner.

11.4 Transmission Line Representation in Walsh Series

For most practical purposes, transmission lines behave linearly because they normally operate below the corona threshold. However, transmission line impedances will vary with frequency in a non-linear fashion and as the electrical distance increases with frequency even relatively short transmission lines will exhibit long-line effects at frequencies higher than the fundamental. Hence, realistic models of multi-conductor transmission lines for the analysis of

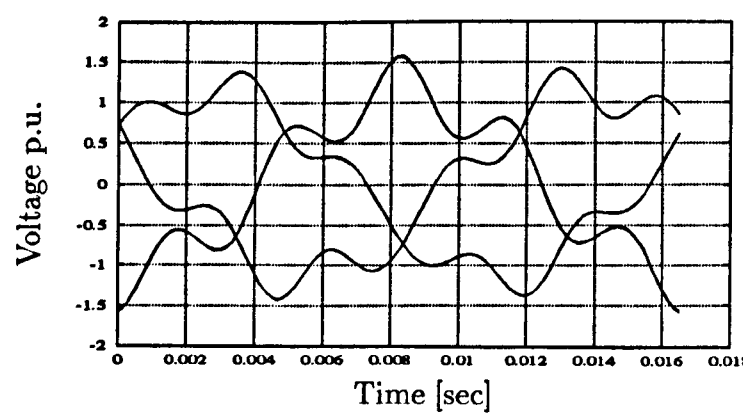

Fig. 11.10: Voltages at Jaguara bus bars

harmonic propagation studies should incorporate several effects which are normally of little or no consequence at fundamental frequency studies. These effects are frequency dependence, long-line effects, line transpositions and geometric imbalances. They can be represented and efficiently manipulated by using ABCD equivalents [143],

$$\begin{bmatrix} V_s \\ I_s \end{bmatrix} = \begin{bmatrix} A & B \\ C & D \end{bmatrix} \begin{bmatrix} V_r \\ -I_r \end{bmatrix} \tag{11.64}$$

where the subscripts s and r stand for the sending and receiving ends of the transmission lines, respectively.

By interchanging block rows and columns and partially inverting equation (11.64), an impedance form representation is arrived at,

$$\begin{bmatrix} V_s \\ V_r \end{bmatrix} = \begin{bmatrix} Z & Z' \\ Z' & Z \end{bmatrix} \begin{bmatrix} I_s \\ I_r \end{bmatrix} \tag{11.65}$$

or, in expanded form,

$$\begin{bmatrix} V_a \\ V_b \\ V_c \\ V_A \\ V_B \\ V_C \end{bmatrix} = \left[\begin{array}{c|c|c|c|c|c} Z_{aa} & Z_{ab} & Z_{ac} & Z_{aA} & Z_{aB} & Z_{aC} \\ \hline Z_{ba} & Z_{bb} & Z_{bc} & Z_{bA} & Z_{bB} & Z_{bC} \\ \hline Z_{ca} & Z_{cb} & Z_{cc} & Z_{cA} & Z_{cB} & Z_{cC} \\ \hline Z_{Aa} & Z_{Ab} & Z_{Ac} & Z_{AA} & Z_{AB} & Z_{AC} \\ \hline Z_{Ba} & Z_{Bb} & Z_{Bc} & Z_{BA} & Z_{BB} & Z_{BC} \\ \hline Z_{Ca} & Z_{Cb} & Z_{Cc} & Z_{CA} & Z_{CB} & Z_{CC} \end{array}\right] \cdot \begin{bmatrix} I_a \\ I_b \\ I_c \\ I_A \\ I_B \\ I_C \end{bmatrix} \tag{11.66}$$

In the real Fourier domain and considering h harmonics, each elements of matrix equation (11.66) has the following generic form,

$$V_\alpha = Z_{\alpha\gamma} I_\gamma \tag{11.67}$$

where

$$V_\alpha = \begin{bmatrix} V'_{\alpha_0} \\ \hline V'_{\alpha_1} \\ \hline \vdots \\ \hline V'_{\alpha_h} \\ \hline\hline V''_{\alpha_1} \\ \hline V''_{\alpha_2} \\ \hline \vdots \\ \hline V''_{\alpha_h} \end{bmatrix} \qquad I_\alpha = \begin{bmatrix} I'_{\alpha_0} \\ \hline I'_{\alpha_1} \\ \hline \vdots \\ \hline I'_{\alpha_h} \\ \hline\hline I''_{\alpha_1} \\ \hline I''_{\alpha_2} \\ \hline \vdots \\ \hline I''_{\alpha_h} \end{bmatrix}$$

$$Z_{\alpha\gamma} = \left[\begin{array}{c|c|c|c||c|c|c|c} R_{\alpha\gamma_0} & & & & & & & \\ \hline & R_{\alpha\gamma_1} & & & & -X_{\alpha\gamma_1} & & \\ \hline & & \ddots & & & & \ddots & \\ \hline & & & R_{\alpha\gamma_h} & & & & X_{\alpha\gamma_h} \\ \hline\hline & & & & R_{\alpha\gamma_0} & & & \\ \hline & X_{\alpha\gamma_1} & & & & R_{\alpha\gamma_1} & & \\ \hline & & \ddots & & & & \ddots & \\ & & & X_{\alpha\gamma_h} & & & & R_{\alpha\gamma_h} \end{array}\right] \tag{11.68}$$

where $\alpha = \{a, b, c, A, B, C\}$, $\gamma = \{a, b, c, A, B, C\}$ and $h = 1, 2, 3, \ldots$. At this point, an operational matrix is introduced which gives the real Fourier expansion of a Walsh series. The trigonometric series and the Walsh series are related as follows,

$$F = A\phi \tag{11.69}$$

Where A is the operational matrix and F and ϕ are the vectors of coefficients corresponding to Fourier series and Walsh series, respectively. Matrix A has the following structure,

$$
\begin{bmatrix} F_0'' \\ F_1'' \cos(t) \\ F_2'' \cos(2t) \\ F_3'' \cos(3t) \\ F_4'' \cos(4t) \\ \vdots \\ F_1' \sin(t) \\ F_2' \sin(2t) \\ F_3' \sin(3t) \\ F_4' \cos(4t) \\ \vdots \end{bmatrix}
=
\begin{bmatrix}
1 & & & & & & & & & & & \\
 & 0.629 & & & & & & -0.261 & & & & \\
 & & 0.604 & & & & & & & & & \\
 & 0.187 & & & & & & 0.452 & & & & \\
 & & & & 0.5 & & & & & & & \\
\vdots & \vdots & \vdots & \vdots & \vdots & \vdots & \vdots & \vdots & \vdots & \vdots & \vdots & \vdots \\
 & & & 0.629 & & 0.261 & & & & 0.125 & & \\
 & & & & & & 0.604 & & & & 0.250 & \\
 & & & -0.187 & & 0.452 & & & & 0.125 & & \\
 & & & & & & & & & & &
\end{bmatrix}
\begin{bmatrix} \phi_0 \\ \phi_1 \\ \phi_2 \\ \phi_3 \\ \phi_4 \\ \phi_5 \\ \phi_6 \\ \phi_7 \\ \phi_8 \\ \phi_9 \\ \vdots \end{bmatrix}
$$

Using these relationships, the transmission line equation in the sequency domain can be written as,

$$V_W = \mathbf{A}^t Z \mathbf{A} I_W \tag{11.70}$$

where,

$$
\mathbf{A} = \begin{bmatrix}
A & & & & & \\
 & A & & & & \\
 & & A & & & \\
 & & & A & & \\
 & & & & A & \\
 & & & & & A
\end{bmatrix}
$$

Since A is an orthogonal matrix,

$$A^t = A^{-1}$$

In the sequency domain each element of the Walsh impedance matrix, $A^t Z_{\alpha\gamma} A$, has the following structure, for the when $m = 64$,

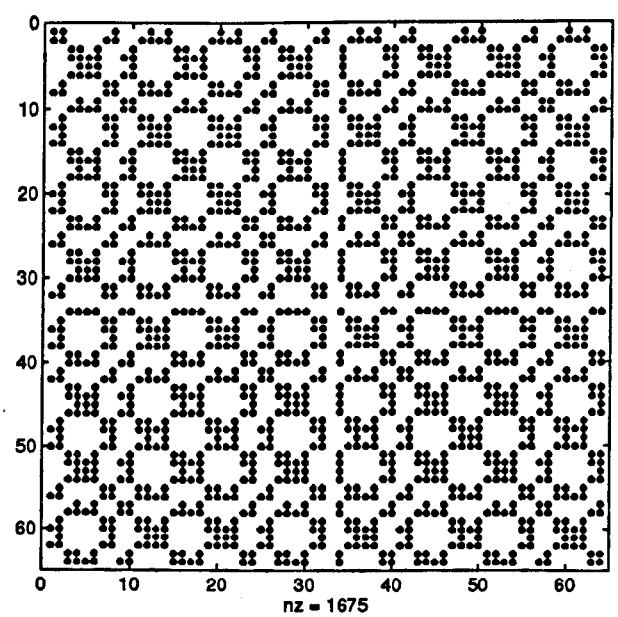

11.5 Conclusions

Three applications which take advantage of Walsh function properties have been presented in this chapter. A model for a single phase TCR in the sequency domain has been put forward. An admittance representation of the TCR is given as opposed to the Norton equivalent representation used previously in the thesis. If the switching function is considered 'blind' to changes in the voltage across the TCR then the switching function is periodic and the entire system can be represented by a linear, periodic system which in its turn is solved in closed form, i.e. no iterative process is required.

Three phase bank of transformers have been modelled in the sequency domain where the input output relations of the magnetic branch are evaluated very efficiently. A sequence Newton-Raphson was used to evaluate waveform distortion in a transmission system where a three phase bank of transformers is pushed into saturation.

Multi-phase, frequency dependent transmission line have also been modelled in the sequency domain. This allow a unified solution of the waveform distortion problem in power systems via sequency domain Newton type methods.

Chapter 12

Conclusions and Suggestions for Future Research Work

12.1 General Conclusions

Accurate models of plant components making up the electric power network are a necessity for the operation and control of modern power systems. Rigorous digital models for predicting waveform distortion give information from which better corrective action can be taken. Also, the specifications of future power networks can be better established to keep the level of waveform distortion within the recommended limits. Waveform distortion studies may be carried out in the computer using several methods. These methods can range from simple numerical integration of the dynamic equations to very sophisticated methods which use the most up-to-date developments in the area of non-linear analysis.

A fundamental aim of this research has been to provide accurate and comprehensive models of power plant components such as multi-limb transformers and power electronic-based devices. As a first step towards a more rigorous modelling approach, the analytical representation of the non-linear characteristics of commonly used power plant components has been carefully addressed. It has been found that splines representations can achieve very accurate approximations. Linear piecewise are the simplest form of splines, they can be used to approximate smooth non-linearities. They are also the most suitable representations for approximating non-linearities relating to power electronic-based devices. Polynomials are most suitable for frequency domain evaluations, however, practical non-linear characteristics are often difficult to represent by these analytical functions. Other representations such hyperbolic functions may be very efficient when repetitive evaluations are required but they are limited to certain classes of non-linearities. They do not offer the possibility of performing harmonic domain evaluations in the frequency domain.

Traditionally, harmonic domain methods have been formulated in the Complex Fourier domain in spite of the fact that all waveforms in electric networks are real. The complex formulation is adequate for solving all harmonic problems such as harmonic interaction of non-linear components but it can be substituted by more efficient formulations which use real algebra. This reduces storage requirements as well as the number of required operations. Two real harmonic domain formulations are presented in this thesis: the Real Fourier Harmonic Domain and the Hartley Domain.

First order Newton-Raphson techniques provide solutions which show strong characteristics of convergence. However, the computational effort required to perform harmonic domain evaluations at each iterative step increases with the number of harmonics considered and with the size of the network. One approach is to evaluate the non-linearity in the time do-

main and then using FFT algorithms to extract the harmonic content. However, the FFT is not necessarily accurate and it may compromise the accuracy and rate of convergence of the solution. To provide faster and more reliable harmonic domain solutions the use of discrete convolutions and Newton-Raphson techniques which use diagonal relaxation have been proposed in this work.

New harmonic domain models for single phase and three phase TCRs have been given. The modelling approach uses discrete convolutions and switching vectors as a way of providing 'clean' and more efficient calculations. The method shows quadratic rate of convergence.

A New model for multi-limb, three phase transformer is presented. It follows a more rigorous modelling approach than existing models. It is based on the Duality principle where proper representation of leakage admittances can be take into account. Also, a more rigorous evaluation of the flux circulating through the different magnetic branches of the core can be obtained by using this principle.

A unified frame of reference in the Walsh domain is developed in this thesis. A comprehensive description of important properties of the Walsh functions is given, highlighting those ones which make the Walsh domain an attractive alternative for the study of switching circuits and non-linear systems. The application of Walsh series to the solution of linear, time invariant systems, linear, time varying systems and non-linear systems is addressed separately. It is shown that linear, time varying systems can be solved analytically, using Walsh series or any other orthogonal series. These analytical solutions provide insight into the waveform distortion introduced by linear, time varying systems. The same theory is also used in the linearisation of non-linear systems.

A simple class of non-linear systems is analysed in this work. Bi-linear systems are perhaps the simplest class of non-linear systems. They are linear in state and linear in control but non-linear together. They are considered generalisations of linear systems which present some of the qualities observed in non-linear systems. Superposition does not apply to bi-linear systems. However, an important feature of this class of system is that even though they are non-linear they can still be analysed with the tools used in linear system theory. With this in mind, bi-linear systems are proposed as a better approximation of non-linear systems than the approximations based on linearisations. It is shown that the use of bi-linearisations provides solutions with stronger characteristics of convergence than those shown by algorithms using first order Newton-Raphsons.

To show the prowess of the Walsh approach, three power systems applications are presented. Firstly, a Walsh domain model of a single phase TCR is given. An admittance matrix representation is given for this device as opposed to a Norton equivalent. Another application relates to a three phase bank of transformers. It is shown in this application that memoryless, non-linear operations can be efficiently performed since analytical relations between the Walsh coefficients of the input and the Walsh coefficients of the output can be easily established. Finally, a model for frequency dependent transmission lines in the Walsh domain is presented.

12.2 Future Research Work

In many ways, this research work can be seen as a step towards a more general and rigorous modelling approach for predicting waveform distortion in power systems. It is expected that the generalised method for evaluating the periodic steady state response of power plant

components will facilitate development of other unified frames of reference which have not been considered in this thesis. With the hope of facilitating further investigation and research contributions in this area of a power systems, the author wishes to put forward the following ideas:

- Applying sparse matrix techniques to solve waveform distortion problems via Newton-Raphson methods increases greatly the efficiency of the solution. However, more actions can be taken to improve solution times. Reduction of the density of the Jacobian matrix will make this matrix sparser, reducing substantially the number of operations required to reach the solution. In order to achieve sparser Jacobian matrices, adaptive pruning of the Jacobian has been used in the past. The idea is to set to zero those Fourier coefficients with values close to zero. The pruning of the Jacobian, in this case, affects the rate and region of convergence but, at the same time, reduces substantially the total number of operations. The above idea should be further investigated in future work to evaluate the effects of the pruned Jacobians on the rate and region of convergence and to provide guidelines as to which values of the Jacobian can be set to zero to reduce the number of operations without affecting significantly the convergence characteristics.

- The author suggests that there is an alternative solution to this problem which may reduce the density of the Jacobian without affecting the rate and region of convergence. This is based on the use of Wavelets theory. Wavelets have proved a valuable tool for signal and image coding because most of the information about global characteristics of signals and systems are retained in a small number of coefficients. The operational matrix of integration in the Wavelet domain has already been provided in open literature. Further research must address the issue of developing other operational matrices such as the product operational matrix.

- The bi-linear solutions used in this thesis to solve waveform distortion problems in power systems provide a step towards a non-linear and more natural form of solution. The benefit of this approach is to achieve solutions with stronger characteristics of convergence. The author suggests that the periodic, steady state solution of power systems may be addressed by using a truly non-linear approach based on the use of Volterra series, which is a non-iterative method. So far, Volterra series have been applied to systems with polynomial representation. Volterra series have received attention over the the years and some headway has been made in their application to engineering systems. These achievements, for instance, have made it possible to apply of Volterra series to non-linear systems such as ACDC converters.

- A sequency domain, single phase TCR has been provided in this thesis. Its extension to the three phase case should be undertaken. Also, the Walsh approach must be applied to other switching devices such as ACDC power converters.

- The Newton-Raphson methods using diagonal relaxation provide very fast waveform distortion solutions. However, even faster solutions could be achieved by using parallelised solutions. Owing to the large dimensions of waveform distortion problems, this issue should be addressed in the near future

- The Sparse Tableau Method has been found to be a powerful technique to generate the dynamic equations of a given network. It also provides a means for implementing a generalised hybrid method where different non-linear elements can be modelled in different domains. It is recommended that a computer program which fully exploits the Sparse Tableau Method characteristics be written.

Bibliography

[1] T. J. Aprille and T. N. Trick. A computer algorithm to determine the steady-state response of nonlinear oscillators. *IEEE Transactions on Circuit Theory*, CT-19(4):354–360, July 1972.

[2] T.J. Aprille and T.N. Trick. A computer algorithm to determine the steady-state analysis for large signal electronic circuits. *IEEE Transactions on Circuit Theory*, CT-19(4):354–360, July 1972.

[3] F.B. Grosz and T. N. Trick. Some modifications to newton's method for the determination of the steady state response of nonlinear oscillatory circuits. *IEEE Transactions on Computer Aided Design*, CAD-1(3):116–119, July 1982.

[4] M. Kakizaki and T. Sugawara. A modified newton method for the steady-state analysis. *IEEE Transactions on Computer Aided Design*, CAD-4(4):662–667, October 1985.

[5] S. Skelboe. Computation of the periodic steady-state response of non-linear networks by extrapolation methods. *IEEE Transactions on Circuits and Systems*, CAS-27(1):161–175, March 1980.

[6] M.S. Nakhla and F. H. Branin. Determining the periodic response of non-linear systems by a gradient method. *International Journal of Circuit Theory Applications*, 5(3):255–273, January 1977.

[7] J. R. Parkhurst and L.O. Ogborn. Deteremining the steady-state output of non-linear oscillatory circuits using multiple shooting. *IEEE Transactions on Computer Aided Design Of Itcgrated Circuits and Systems*, 14(7):882–889, July 1995.

[8] M. Schentzen. *The Volterra and Wiener Theories of Nonlinear Systems.* John Wiley, New York, 1980.

[9] W. J Rugh. *Nonlinear System Theory: The Volterra/Wiener Approach.* USA, Johns Hopkins, Baltimore, 1981.

[10] J. J. Bussgang, L. Ehrham, and J. W. Graham. Analysis of non-linear systems with multiple inputs. *Proceedings of the IEEE*, 62(8):1088–1119, August 1974.

[11] L. O. Chua and C. Y. Ng. Frequency-domain analysis of non-linear systems: General theory. *IEE Journal of Electronic Circuits and Systems*, 3(6):165–185, July 1979.

[12] L. O. Chua and C. Y. Ng. Frequency-domain analysis systems: Formulation of transfer functions. *IEE Journal of Eletronic Circuits and Systems*, 3(6):257–269, November 1979.

[13] M. Lamnahbi M. Fliess and F. Lamnahbi-Lagarrigue. An algebraic approach to non-linear functional expansions. *IEEE Transactions on Circuits and Systems*, CAS-30(8):554–570, August 1983.

[14] M. Lamnabhi. Functional analysis of non-linear circuits: a generating power series approach. *IEE Proceedings of the IEE*, 133(5):375–384, October 1986.

[15] M.S. Nakhla and J. Vlach. A piecewise harmonic balance technique for the determination of periodic response of nonlinear systems. *IEEE Transactions on Circuits and Systems*, CAS-23(2):85–91, February 1976.

[16] A. Yan H. W. Dommel and S. Wei. Harmonics from transformer saturation. *IEEE Transactions on Power Delivery*, PWRD-1, No. 2(2):209–214, April 1986.

[17] A. Semlyen, E. Acha, and J. Arrillaga. Newton-type algorithms for the harmonic phasor analysis of non-linear power circuits in periodical steady state with special reference to magnetic non-linearities. *IEEE Transactions on Power Delivery*, 3(3):1090–1098, July 1988.

[18] A. Semlyen and N. Rajakovic. Harmonic domain modeling of laminated iron core. *IEEE Transactions on Power Delivery*, 4, No. 1(1):382–390, January 1989.

[19] A. Semlyen and A. Medina. Computation of the periodic steady state with non-linear components using a hybrid time and frequency domain methodology. *IEEE Transaction on Power Delivery*, 10(3):1498–1504, August 1995.

[20] E. P. Dick and W. Watson. Transformer models for transient studies based on field measurements. *IEEE Transactions on Power and Apparatus and Systems*, PAS-100(1):409–419, January 1981.

[21] F.C. Trutt, E.A. Erdelyi, and R.E. Hopkins. Representation of the magnetization characteristics of dc machines for computer use. *IEEE Transactions on Power Apparatus and Systems*, PAS-87(3):665–669, March 1968.

[22] S.N. Talukdar, J.K. Dickson, R.C. Dugan, M.J. Sprinzen, and C.J. Lenda. On modelling transformer and reactor saturation characteristics for digital and analog studies. *IEEE Transcations on Power Apparatus and Systems*, PAS-94(2):612–621, March 1975.

[23] A. Medina. *Power Systems Modelling in the harmonic Domain.* PhD thesis, The University of Canterbury, Christchurch, New Zealand, 1992.

[24] C. Kahlert and Leon O. Chua. A generalised canonical piecewise-linear representation. *IEEE Transactions on Circuits and Systems*, 37(3):373–383, March 1990.

[25] L.O. Chua and S.M. Kang. Section-wise piecewise-linear functions: Canonical representation, properties and applications. *Proceedings of IEEE*, 65(1):915–929, June 1977.

[26] L. O. Chua and R.L.P. Ying. Canonical piecewise-linear analysis. *IEEE Transactions on Circuits and Systems*, CAS-30(3):125–140, March 1983.

[27] P. Lancaster and K. Salkauskas. *Curve and Surface Fitting.* Academic Press, Great Britain, third edition, 1990.

[28] S. Prusty and M.V.S. Rao. New method for prediction of true saturation characteristics of transformers and non-linear reactors. *IEE Proceedings*, 127, Pt C(2):106, March 1980.

[29] M. Jerumich. A note on limiter output. *Proceedings of IEEE*, 56:1128–1129, 1968.

[30] R.G. Sea and A. G. Vacroux. Steady state analysis of non-linear systems and multiple input describing functions (m.i.d.f.). *Automatica*, 5(1):763–772, 1969.

[31] A. Gelb and W. E. vander Velde. *Multiple-Input Describing Functions and Non-linear System Design.* McGraw-Hill, 1968.

[32] D. P. Atherton. *Nonlinear Control Egineering.* Van Nostrand Reinhold, 1982.

[33] G.F.T. Widger. Representation of magnetisations curves over extensive range by rational-fraction approximations. *Proceedings of the IEE*, 116(1):156–160, January 1969.

[34] A. Semlyen and A. Castro. A digital trasformer models for switching transient calculations in three-phase systems. In *PICA 9th Conference*, pages 12–126, New Orleans, LA, July 1975.

[35] L.O. Chua and K. A. Stromsmoe. Lumped-circuit models for non-linear inductors exhibiting hysteresis loops. *IEEE Transactions on circuit Theory*, CT-17(4):564–574, November 1970.

[36] J.G. Santesmases, J. Ayala, and A.H. Cachero. Analitical approximation of dynamic hysteresis loops and its application to a series ferroresonant circuit. *Proceedings of the IEE*, 117(1):234–240, January 1970.

[37] S. H. Charap. Magnetic hysteresis model. *IEEE Transaction on Magnetics*, MAG-10(4):1091–1096, December 1974.

[38] C.E. Lin, J.B. Wei, C.L. Huang, and C.J. Huang. A new method for representation of hysteresis loops. *IEEE Transactions on Power Delivery*, 4(1):413–419, January 1989.

[39] H. D'Angelo. *Linear Time-Varying Systems: Analysis and Syntheis.* Allyn and Bacon, Boston, 1970.

[40] R.R. Mohler. *Nonlinear Systems*, volume 2. Prentice hall, Englewood Cliffs, New Jersey, 1991.

[41] L.J. Bhomann and R.H. Lasseter. Stability and harmonics in thyristor cotrolled reactors. *IEEE Transactions on Power Delivery*, 5(2):1175–1181, April 1990.

[42] J. Guckenheimer and P. Holmes. *Nonlinear Oscillations, Dynamical Systems and Bifurcations of Vector Fields.* Springer-Verlag, 1983.

[43] M. S. Corrington. Solution of differential and integral equations with Walsh functions. *IEEE Transcations on Circuit Theory*, CT-20, No. 5(5):470–477, September 1973.

[44] S.G. Kuo C. Y. Yang and C.K. Chen. Fourier exponential series matrix of integration. *International Journal of Systems Science*, 18(12):2395–2400, 1987.

[45] M. Razzaghi and M. Razzaghi. Fourier series direct method for variational problems. *International Journal of Control*, 48(3):887–895, 1988.

[46] P.N. Paraskevopoulos, P.D. Sparis, and S.G. Mouroutsos. The fourier series operational matrix of integration. *International Journal of Systems Science*, 16(2):171–176, 1985.

[47] P.N. Paraskevopoulos. The operational matrices of integration and differentiation for the fourier sine-cosine and exponential series. *IEEE Transaction on Automatic Control*, AC-32(7):648–651, July 1987.

[48] M. Razzaghi and A. Arabashahi. Analysis of linear time varying systems and bilinear systems via fourier series. *International Journal of Control*, 50(3):889–898, 1989.

[49] C.Y Yang and C.K. Chen. Analsis and optimal control of time-varying systems via fourier series. *International Journal of Systems Science*, 25(11):1663–1678, 1994.

[50] C. Y. Yang. Using a functional integration matrix to solve time-varying bilinear systems. *International Journal of Systems Science*, 26(6):1321–1331, 1995.

[51] C. F. Chen and H. Hsiao. Time domain synthesis via walsh functions. *Proceedings of the IEE*, 122(5):565–570, May 1975.

[52] CF Chen and CH Hsiao. A state-space approach to walsh series solution of linear systems. *International Journal of Systems Science*, 6(9):833–858, 1975.

[53] C.F. Chen and C.H. Hsiao. Design of piecewise constant gains for optimal control via walsh functions. *IEEE Transactions on Automatic Control*, AC-20(5):595–603, October 1975.

[54] C.F. Chen and Y.T. Tsay. Walsh operational matrices for fractional calculus and their applications to distributed systems. *Journal of The Franklin Institute*, 303(3):267–284, March 1977.

[55] VR. Karanan, P.A. Frick, and R.R. Mohler. Bilinear system identification by walsh functions. *IEEE Transactions on Automatic Control,*, AC-23(4):709–713, August 1978.

[56] W.L. Chen and Y.P. Shih. Parameter estimation of bilinear systems via Walsh functions. *Journal of the Franklin Institute*, 305(5):249–257, May 1978.

[57] R. Cameron, B. Kauvaritakis, and S. Mossaheb. A new approach to the prediction of limit cycles. *International Journal of Control*, 32(6):963–981, 1980.

[58] T. Beer. Walsh transforms. *American Journal Physics*, 49(5):466–472, May 1981.

[59] G.P. Rao, K.R. Palanisamy, and K.R. Srinisavan. Extension of computation beyond the limit of initial normal interval in walsh series analysis of dynamical systems. *IEEE Transactions on Automatic Control*, AC-25(1):317–321, 1980.

[60] G. P. Rao and L. Sivamukar. Piecewise linear systems identification via Walsh functions. *International Journal of Systems Science*, 13(5):525–530, 1982.

[61] G.P. Rao and K.R. Palanisamy. Improved algorithms for parameter identification in continuous systems via Walsh functions. *Proceedings of the IEE*, 130, Pt. D.(1):9–16, January 1983.

[62] K.R. Palanisamy and D.K. Bhattacharya. Analysis of non-linear systems via single term Walsh series approach. *International Journal of Systems Science*, 12(1):643, 1981.

[63] G.P. Rao and L. Sivakumar. Order and parameter identification in continuous linear systems via Walsh functions. *Proceedings of the IEEE*, 70(7):764–766, July 1982.

[64] R.G. Cameron and M. Tabatabia. Predicting the excistance of limit cycles using walsh functions: Some further results. *International Journal of Systems Science*, 14(9):1043–1064, 1983.

[65] H. F. Ahner. Walsh functions and the solution of non-linear differential equations. *American Journal of Physiss*, 56(7):628–633, July 1988.

[66] K.R. Palanisamy. Analysis and optimal control of linear systems via single Walsh series approach. *International Journal of Systems Science*, 12(1):443, 1981.

[67] W.L. Chen and C. L. Lee. Walsh series expansions of composite functions and its applications to linear systems. *International Of Journal Systems Science*, 13(2):219–226, 1982.

[68] I. R. Horng and S.J. Ho. Discrete walsh operational matrices for analysis and optimal control of linear digital systems. *International Journal Control*, 42(1):1443–1449, 1985.

[69] D. J. Kish and G. T. Heydt. A generalization of the concept of impedance and a novel Walsh domain immittance. *IEEE Transactions on Power Delivery*, 9(2):970–976, April 1994.

[70] F.L. Lewis and D.W. Fountain. Walsh function analysis of linear and bilinear discrete time systems. *International Journal of Control*, 53(4):847–853, 1991.

[71] D.P. Stoten and J. Harkness. Walsh functions for the off-line identification of non-linear plants and their control. *International Journal of Control*, 60(6):1121–1136, 1994.

[72] K. R. Palanasamy and V.P. Arunachalam. Solution of variational problems using block pulse functions. *International Journal of Systems and Science*, 16(2):257–267, 1985.

[73] P. Sannuti. Analysis and synthesis of dynamic systems via block-pulse functions. *Proceedings of the IEE*, 124(6):569–571, June 1977.

[74] K.R. Palanisamy and D.K. Bhattacharya. System identification via block-pulse functions. *International Journal of Systems Science*, 12(5):643–647, 1981.

[75] L.S. Shieh, C.K. Yeung, and B.C. McInnis. Solution of state-space equations via block-pulse functions. *International Journal of Control*, 29(3):383–392, 1978.

[76] A. Deb, G. Sarkar, S. K. Sen, and A. K. Datta. A new set of pulse-width modulated generalised block pulse functions (pwm-gbpf) and its applications to cross-/auto-correlation of time-varying functions. *International Journal of Systems Science*, 26(1):65–89, 1995.

[77] S.V. Lapin and N.D. Egupov. Analysis of continuous time-varying non-linear systems using block-pulse expansions. *International Journal of Systems and Sience*, 23(7):1201–1212, 1992.

[78] W. Marszalek. On the nature of block-pulse operational matrices: Some further results. *International Journal of Systems Science*, 16(6):727–743, 1985.

[79] J.S. Gu and W.S. Jiang. The Haar wavelets operational matrix of integration. *International Journal of Systems Science*, 27(7):623–628, 1996.

[80] C. Hwang and Y.P. Shih. Laguerre operational matrices for fractional calculus and applicatons. *International Journal of Control*, 34(3):577–584, 1981.

[81] C. Hwang and Y.P. Shih. Parameter identification via Laguerre polynomials. *International Journal of Systems Science*, 13(2):209–217, 1982.

[82] C. Hwang and Y.P. Shih. Laguerre series solution of a functional differential equation. *International Journal of Systems Science*, 13(7):783–789, 1982.

[83] S.C. Tsay and T.T. Lee. Analysis and optimal control of linear time-varying functions. *International Journal of Systems Science*, 18(8):1579–1594, 1987.

[84] M.L. Wang, R.Y. Chang, and S.Y.Yang. Analysis and parameter estimation of bilinear systems via generalised orthogonal polynomials. *International Journal of Control*, 46(2):719–729, 1987.

[85] R.Y. Chang and M.L. Wang. Parameter identification via shifted Legendre polynomials. *International Journal of Systems Science*, 13(1):1125–1135, 1982.

[86] R.Y. Chang and M.L. Wang. Legendre polynomials approximation to dynamic linear state equations with initial or boundary value conditions. *International Journal of Control*, 40(10):215–232, 1984.

[87] C. C. Liu and Y.P. Shih. Analysis and optimal control of time-varying system via Chebyshev. *International Journal of Control*, 38(5):1003–1012, 1983.

[88] P.N. Paraskevopoulos. Chebyshev series approach to system identification and optimal control. *Journal of the Franklin Institute*, 316(1):135–157, 1983.

[89] T.T. Lee and S.C. Tsay. Analysis of linear time varying systems and bilinear systems via shifted chebyshev polynomials of the second kind. *International Journal of Systems Science*, 17(12):1757–1766, 1986.

[90] C.C. Liu and Y.P. Shih. System analysis, parameter estimation and optimal regulator design of linear system via Jacobi series. *International Journal of Control*, 42(1):211–224, 1985.

[91] T.T. Lee and S.C. Tsay. Analysis of linear time-varying systems and bilinear systems via taylor series. *International Journal of Systems Science*, 18(8):1569–1578, 1987.

[92] T. Kailath. *Linear Systems.* Information and System Science Series. Prentice-Hall, Englewood Cliffs, N.J., 1980.

[93] L. Chua, C. A. Desoer, and E. S. Kuh. *Linear and Non-linear Circuits.* Electrical Engineering. McGraw Hill, Singapore, 1987.

[94] G.T. Heydt, K.J. Olenjniczack, R. Spark, and E. Viscinto. Application of the hartley transform to the analysis of propagation of nonsinusoidal waveforms in power systems. *IEEE Transactions on Power Delivery*, 9(2):970–976, October 1991.

[95] P.F. Ribeiro. Wavelet transform: An advance tool for analysing non-stationary harmonic distortions in power systems. In *IEEE ICHPS*, pages 365–369, Bologna, Italy, September 1994.

[96] R. N. Bracewell. *The Hartley Transform.* Oford Engineering, science series 19. Oxford Science Publications, New York, 1986.

[97] O. K. Ersoy. A comparative review of real and complex fourier-related transforms. *Proceedings of the IEEE*, 82(3):429–447, March 1994.

[98] R. N. Bracewell. Aspects of the hartley transform. *Proceedings of the IEEE*, 82(3):381–387, March 1994.

[99] T. J. E. Miller, editor. *Reactive Power Control in Electric Systems.* Wiley-Interscince, New York 1982.

[100] CIGRE Working Group 03 of Study Committee 14(HVDC Links). AC harmonic filter and reactive compensation for HVDC: a general survey. *Electra*, (63):65–102, 1979.

[101] R. M. Mathur. A study of noncharacteristic harmonics generated by thyristor phase controlled reactors. *IEE Conference Publication 205*, pages 117–120, 1981.

[102] R. Yacamini and J. W. Resende. Thyristor controlled reactors as harmonic sources in HVDC converters stations and AC systems. *IEE Proceedings*, 133, Pt B(4):263–269, July 1986.

[103] W. Xu and H. W. Dommel. Computation of steady state harmonics of static var compensator. *Proceedings of the Third International Conference on harmonics in Power Systems*, Nashville, IN:239–245, October 1988.

[104] W. Xu, J. R. Marti, and H. W. Dommel. Harmonic interactions in thyristor cotrolled reactors circuits. *IEEE Transactions on Power Delivery*, 4(3):183–190, February 1991.

[105] L. Bohmann and R. H. Lasseter. Harmonic interactions in thyristor controlled reactor circuits. *IEEE Transactions on Power Delivery*, 4, No. 3(3):68–74, July 1989.

[106] E. Acha. Harmonic domain representation of thyristor controlled reactors. In *AC and DC Power Transmission*, London, UK, September 1991.

[107] E. Acha and J. Rico. Harmonic domain modelling of non-linear power plant components. *Proceedings of the IEEE ICHPS VI,Bologna, Italy*, pages 206–213, September 1994.

[108] A. Medina, J. Arrillaga, and E. Acha. Sparsity-oriented hybrid formulation of linear multiports and application to harmonic analysis. *IEEE Transactions on Power Delivery*, 5, No. 3(3):1453–1458, July 1990.

[109] M. Dominguez, I. D. Coope, J. Arrillaga, and N. R. Watson. An adaptive scheme for the derivation of harmonic impedance contours. *IEEE Transactions on Power Delivery*, 9(2):879–886, April 1994.

[110] E. Acha and J. Rico. A critical review of multiconductor transmission line models at harmonic frequencies. In *Proceedings of the 29th Universities Power Engineering Conference*, number 1, pages 890–894, Galway, Irland, September 1994.

[111] J. M. D. Ferreira de Jesus. *D.C. Transmission System Harmonic Analysis and Stability Using Describing Functions.* PhD thesis, Imperial College of Science and Technology, University of London, 1982.

[112] G. H. Robinson. Harmonic phenomena associated with Benmore-Haywards HVDC transmission scheme. *New Zeland Engineering*, 21(1):16–29, January 1966.

[113] J. Arrillaga and C. P. Arnold. *Computer Analysis of Power Systems.* John Wiley and Sons, 1990.

[114] IEEE Industry Applications Society/Power Egineering Society. IEEE recomended practices and requirements for harmonic control in electrical power systems. Technical report, April 1993.

[115] F. De Leon and A. Semlyen. Complete transformer model for electromagnetic transients. *IEEE Transactions on Power Delivery*, 9(1):231–239, January 1994.

[116] C. Cherry. The duality between interlinked electric and magnetic circuits and the formation of transformer equivalent circuits. *Proceedings of the Physical Society B*, 62:101–111, 1949.

[117] G. R. Slemon. Equivalent circuits for transformers and machines including non-linear effects. *Proceedings of the IEE*, Part IV(100):129–143, July 1953.

[118] C. M. Arturi. Transient simulation and analysis of a three-phase five-limb step-up transformer following and out-of-phase synchronization. *IEEE Transaction on Power Delivery*, 6(1):196, January 1991.

[119] A. Narang and R. H. Brierley. Topologically based magnetic model for steady-state and transient studies for three-phase core type transformers. *IEEE Transactions on Power Delivery*, 9(3):1337–1349, August 1994.

[120] B. A. Mork and D. L. Stuehm. Application of non-linear dynamics and chaos to ferroresonace in distributions systems. *IEEE Transactions on Power Delivery*, 9(2):1009–1017, April 1994.

[121] F. de Leon and A. Semlyen. Efficient calculation of elementary parameters of transformers. *IEEE Transactions on Power Delivery*, 7(1):376–383, January 1992.

[122] M. A. Laughton. Analysis of unbalanced polyphase networks by the method of phase co-ordinates. *Proceedings of the IEE*, 115(8):1163–1172, August 1968.

[123] Mo-Shing Chen and W. E. Dillon. Power system modelling. *Proceedings of the IEEE*, 62(7):901–915, July 1974.

[124] V. Brandwajn, H. W. Dommel, and I. I. Dommel. Matrix representation of three-phase n-winding transformers for steady-state and transient studies. *IEEE Transaction on Power Appratus and Systems*, PAS -101(6):1369, June 1982.

[125] D. Hatziargyriou, M. Prosaliodis, and C. Papadias. Generalised transformer model based on the analysis of its magnetic core circuit. *Proceeding of the IEE, Part C*, 140(4):269–278, July 1993.

[126] A. Semlyen and N. Rajakovic. Harmonic domain medelling of laminated iron core. *IEEE Transactions on Power Delivery*, 4(1):382–390, January 1989.

[127] N. Rajakovic and A. Semlyen. Harmonic domain of field variables related to eddy currents and hysteresis losses in satrurated laminations. *IEEE Transactions on Power Delivery*, 4(2):1111–1116, April 1989.

[128] N. Rajakovic and A. Semlyen. Investigation of the inrush phenomenon: A quasi-stationary approach in the harmonic domain. *IEEE Transactions on Power Delivery*, 4(4):2114–2120, October 1989.

[129] E. Acha, J. Arrillaga, A. Medina, and A. Semlyen. General frame of reference for analysis of harmonic distortion in systems with multiple transformer non-linearities. *Proceedings of the IEE*, 136, Pt. C,(5):271–278, September 1989.

[130] C. Hatziantoniu, G. D. Galanos, and J. Millas-Argiatis. An incremental transformer model for the study of harmonic overvoltages in weak AC/DC systems. *IEEE Transactions on Power Delivery*, 3:1111–1121, July 1988.

[131] A. Medina and J. Arrillaga. Generalised modelling of power transformers in the harmonic domain. *IEEE Transactions on Power Delivery*, 7(3):1458–1465, July 1992.

[132] F. de Leon. *Transformer Model for the Study of Electromagnetic Transients.* PhD thesis, University of Toronto, 1992.

[133] H.F. Harmuth. *Transmission of Information by Orthonormal Functions.* Springer Verlag, New York, 1969.

[134] K. G. Beauchamp. *Walsh Functions and Their Applications.* Academic Press, London, 1975.

[135] M.S. Corrington and R. N. Adams. Applications of Walsh functions to nonlinear analysis. Contract AF30(602)2484 AD-277-942, Rome Air Development Center, Griffis Air Force base, N.Y., April 1962.

[136] P. Sharma, S.I. Ahson, and J. Henry. Microprocessor implementation of fast Walsh-Hadamard transform for calculation f symmetrical components. *Proceedings of the IEEE*, 76(10):1385–1388, October 1988.

[137] A. Haar. Zur theorie der orthogonalen funktionensysteme. *Mathematical Annals*, 69(1):331–371, 1910.

[138] J. L. Walsh. A close set of normal orthogonal functions. *American Journal of Mathematics*, 45(1):5–24, 1923.

[139] H. Rademacher. Einige satze von allgemeinen orthogonalfunktionen. *Mathematical Annals*, 87(1):112–138, 1922.

[140] W.A. Evans. Sine-wave synthesis using Walsh functions. *Proceedings of the IEE*, 134, Pt.G.(1):1–6, February 1987.

[141] D.F. Elliott and K.R. Rao. *Fast Transforms: Algorithms, Analyses, Applications.* Academic Press, New York, 1982.

[142] J.J. Rico, E. Acha, and T.J.E Miller. Harmonic domain modelling of three phase thyristor controlled reactors by means of switching functions and discrete convolutions. *IEEE Transactions on Power Delivery*, 11(3):1678–1684, July 1996.

[143] A. Semlyen and M.H. Abdel-Rahman. Transmission line modelling by rational transfer functions. *IEEE Transactions on Power Apparatus and Systems*, PAS-101(9):3576–3584, September 1982.

Appendix A

Parameters of the South Island Reduced System

The data of the test system used in Chapter 5 are as follows:

A.1 Transmission lines:

Earth resistivity: 100 S-m.

The phase conductors of the first three transmission lines are arranged in a double circuit configuration; symmetrically placed with respect to the tower vertical axis. There are two conductor per phase and the coordinates, given for one of the circuits, are taken form the center of the tower at the ground level. The fourth trasmission line is a two single-circuit line of flat configuration with one conductor per phase. The coordinates, given for the two circuits, are taken from the extreme left conductor at the ground level.

A.1.1 Invercagill220-Manapouri220

Line length: 152.9 km

Conductor type: GOAT(30/3.71+7/3.71 ACSR)

Earth-wire type: (7/3.05 Gehss)

Conductor coordinates (in meters):

Phase a	4.80	12.50
Phase b	06.34	18.00
Phase c	4.42	23.50
Earth-wire	0.00	29.00

A.1.2 Manapouri220-Tiwai220.

Line length:175.60 km

Type and coordinates of earth-wire and phase conductots are identical to those of line Invercagill220-Manapouri220.

A.1.3 Invercagill220-Tiwai220.

Line length:24.3 km

Conductor type: GOAT(30/371+7/3.71 ACSR)

Earth-wire type: (7/3.05 Gehss)

Conductor coordinates of circuit one (in meters):

Phase a	0.00	12.50
Phase b	6.47	12.50
Phase c	12.94	12.50
Earth-wire	1.86	18.41
Earth-wire	11.08	18.41

Conductor coordinates of circuit two (in meters):

Phase a	22.94	12.50
Phase b	30.14	12.50
Phase c	37.34	12.50

A.2 Generators:

Generator	X''_d	X''_0
Manapouri1014	0.0370	0.0197
Manapouri2014	0.1480	0.0788
Manapouri3014	0.1480	0.0788
Roxburgh1011	0.0620	0.0323

A.3 Transformers:

Transformers	X_l
Manapouri220 Manapouri1014	0.0269
Manapouri220 Manapouri2014	0.1072
Manapouri220 Manapouri3014	0.0269
Invercagill033 Invercagill220	0.1029
Invercagill033 Invercagill220	0.1029
Roxburgh220 Roxburgh1011	0.0382
Roxburgh011 Roxburgh220	0.07632
Roxburgh011 Roxburgh220	0.0382

A.4 Loads:

Load	P(MW)	Q(MVAR)
Roxburgh011	90.0	54.0
Manapouri2014	135.0	36.0

A.5 System parameters:

Base frequency: 50.0Hz
Base power: 100.0 MVA
Base voltage:220.0 kV

Appendix B

Parameters of the Jaguara Taquaril System

B.1 System data

Base frequency $f = 60Hz$ Base power $P_B = 100MVA$ Base voltage,$Kv_B = 345KV$

B.2 Transformers

$X_{PS} = 0.117p.u.$ $X_{PT} = 0.115p.u.$ $X_{ST} = 0.241p.u.$

B.3 Generators

$x''_d = 0.1385p.u.$ $X_0 = 0.047$

B.4 Shunt reactor

91 MVAR $X_0 = 0.35$

B.5 Transmission line

Earth resistivity: 100 $\Omega - m$ Phase conductors arranged in a horizontal configuration with two 954 MCM-ACSR conductors per phase and two $\frac{3''}{8}$ galvanised steel earth-wires. line length: 398 km Conductor type: 954 MCM-ACSR Phase conductor height: 13.18 m Phase spacing: 8.5 m Earth wires height: 22.97 m Earth wires spacing: 12.5

Appendix C

Power-Invariant Transformation for Transformer Connections

The following transformation matrices can be used to enable the admittance matrix of any transformer to be found in a systematic manner.

Delta-Delta connection:

$$\begin{pmatrix} v_1 \\ v_2 \\ v_3 \\ v_4 \\ v_5 \\ v_6 \end{pmatrix} = \frac{1}{\sqrt{3}} \begin{pmatrix} 1 & & & -1 & & \\ & 1 & & & -1 & \\ & & 1 & & & -1 \\ & & & 1 & & -1 \\ -1 & & & & 1 & \\ & -1 & & & & 1 \end{pmatrix} \begin{pmatrix} v_A \\ v_b \\ v_B \\ v_b \\ v_C \\ v_c \end{pmatrix} \tag{C.1}$$

Star-Star connection:

$$\begin{pmatrix} v_1 \\ v_2 \\ v_3 \\ v_4 \\ v_5 \\ v_6 \end{pmatrix} = \begin{pmatrix} 1 & & & & & -1 \\ & 1 & & & & & -1 \\ & & 1 & & & -1 & \\ & & & 1 & & & -1 \\ & & & & 1 & -1 & \\ & & & & & 1 & -1 \end{pmatrix} \begin{pmatrix} v_A \\ v_b \\ v_B \\ v_b \\ v_C \\ v_c \\ v_N \\ v_n \end{pmatrix} \tag{C.2}$$

GLASGOW
UNIVERSITY
LIBRARY